Obesity Induced Microglial Activation and its Role in Hippocampal Dysfunction

by

Rosemary E. Henn

A dissertation submitted in partial fulfillment
of the requirements for the degree of
Doctor of Philosophy
(Cellular and Molecular Biology)
at the University of Michigan
2022

Doctoral Committee:

Professor Eva Feldman, Chair
Professor Anuska Andjelkovic-Zochowska
Professor Carey Lumeng
Professor Geoffrey Murphy
Professor Martin Myers

Rosemary E. Henn
hennr@med.umich.edu
ORCID iD: 0000-0002-7392-1607

Dedication

This dissertation is dedicated to my sisters, Margaret and Alice Henn, who keep me grounded through challenging times.

Acknowledgements

The work presented here would not have been accomplished without the tireless help of numerous individuals. I am endlessly grateful to Dr. Eva Feldman and the entire Feldman Laboratory for their immense dedication to my success. Dr. Feldman's investment in my work and career training is immeasurable, and I will take so much of what I have learned on with me as I continue my training. Special thanks to Masha Savelieff for her mentorship and her contributions to the writing and editing process for this dissertation work. I would like to thank Sarah Elzinga, Junguk Hur, Kai Guo and Mohamed Noureldein for their collaboration and mentorship in the lab. I express my extreme gratitude to Crystal Pacut, Faye Mendelson, John Hayes, Bhumsoo Kim, Ian Webber-Davis, and Diana Rigan for their technical assistance and guidance, without which we could not have accomplished our goals. In addition to those who have already been mentioned, I also thank the other authors of the manuscripts within this dissertation: Jacquelin Kwentus, Evan Reynolds, Emily Glass, Rachel Parent, Adam Allouch, and Geoff Murphy. Additionally, I am so thankful for the mentorship and guidance of Dr. Steve Lentz. Finally, I thank my committee members for providing critical feedback and direction to my dissertation work, and the members of the Murphy lab for collaborating and performing animal behavior studies.

The following acknowledgements have been adapted from chapter manuscripts to acknowledge the funding and contributions within this thesis: *Funding:* NIH

(U01AG057562, U24DK115255, R01DK130913), the Michigan Alzheimer's Disease Research Center Early Career Investigator Mentorship Program (supported by the NIH/NIA funded by the Michigan Alzheimer's Disease Research Center (P30AG072931) and the University of Michigan Alzheimer's Disease Center, Berger Endowment), the NIDDK (T32DK007245), the JDRF (JDRF 5COE-2019-861-S-B), the Edith S. Briskin/SKS Foundation NeuroNetwork Emerging Scholar Fund, the Robert E. Nederlander Sr. Program for Alzheimer's Research, the Andrea and Lawrence A. Wolfe Brain Health Initiative Fund, the A. Alfred Taubman Medical Research Institute, and the NeuroNetwork for Emerging Therapies. *Support:* We thank the University of Michigan Microscopy, Imaging, and Cellular Physiology Core (MICPC) and Steve Lentz, PhD, for guidance and support in developing and implementing methods of microglial morphology analysis. We thank the following research cores and labs for their support: Michigan Diabetes Research Center (MDRC) Chemistry Lab (grant number P30DK020572 NIDDK); Immune Monitoring Core of the Rogel Cancer Center; Mouse Metabolic Phenotyping Core (grant number U2CDK110768); the University of Michigan's Advanced Genomics Core, Michigan State University's Genomics Core, the University of Michigan *in vivo* animal core, the University of Michigan Unit for Laboratory Animal Medicine, University of Michigan Flow Cytometry Core, the University of Cincinnati Mouse Metabolic Phenotyping Core. We thank Dr. Takao Iwawaki (Kanazawa Medical University) and Dr. Zu-Hang Sheng (NINDs) for providing the ERAI-Venus mouse strain.

My friends and community within the Medical Scientist Training Program have been vital to my success as a graduate student. I thank my family for their support and

motivation, and for troubleshooting MATLAB. The work presented here was a collaborative effort, relying on the skills, expertise, and hard work of so many people.

Table of Contents

List of Tables

List of Figures

Abstract

The prevalence of global obesity has rapidly risen over the past several decades. Management of obesity and its co-morbidities place an immense burden on patients and healthcare systems. Clinical studies show an association between mid-life obesity and late-life cognitive impairment and dementia, and childhood obesity is associated with cognitive deficits as well. A better understanding of mechanisms mediating cognitive dysfunction in obesity across the lifespan will be critical for developing appropriate therapeutic interventions.

Rodent models of high-diet diet (HFD)-induced obesity demonstrate HFD induced inflammation in the hippocampus, a brain region involved in declarative memory. The immune response contributes to complications of obesity and may play a role in obesity-associated hippocampal-dependent cognitive impairment. Hippocampal microglia, the resident innate immune cells of the central nervous system, are activated in obese mice, and are proposed to contribute to cognitive deficits by excessive pruning of neuronal dendritic spines. Mechanisms responsible for this microglial activation are unclear. The goal of this dissertation was to determine the temporal progression and distinct activation phenotype of hippocampal microglia and to identify potential mechanisms mediating activation, focusing on young, adolescent mice.

To address this goal, we proposed four aims. For Aim 1, we fed adolescent mice control or HFD longitudinally for 2 wk, 1 mo, or 3 mo and used three-dimensional

morphology measures to quantify microglial morphology as an indicator of activation state. HFD feeding induced obesity and metabolic dysfunction, which both increased in severity over time. Unexpectedly, in the hippocampal CA1 region, HFD did not alter microglia morphology metrics at any duration of diet, suggesting that effects on activation state may be subtle. Given potentially subtle effects, and because microglia manifest a heterogenous population of cells, we moved beyond morphology measures for Aim 2 and performed single-cell RNA-sequencing to investigate the activation phenotype of hippocampal microglia after 1 mo and 3 mo of control or HFD. Our work, to our knowledge, is the first scRNA-seq study of microglia in obesity, and transcriptomics revealed that HFD feeding alters intercellular immune signaling among microglia and dysregulates endoplasmic reticulum homeostasis.

To investigate the effect of age, in Aim 3 we determined the impact of HFD on cognitive function and hippocampal inflammation in young and middle-aged mice. We found that obese mice are cognitively impaired using the fear conditioning task, which measures associative learning, and that older age exacerbates performance deficits in this task. Our final set of ongoing experiments in Aim 4 seek to determine the role of endoplasmic reticulum stress in microglial activation in obesity.

In summary, our data demonstrate that diet-induced obesity in young mice alters the hippocampal microglial transcriptome but does not change microglial morphology in the CA1 region. We identified endoplasmic reticulum dysregulation as a potential mechanism mediating the microglia response. Future work is required to determine whether a potential ER stress response plays a protective or injurious role in microglial activation and subsequent cognitive impairment. Further, we found that older obese

mice display more severe cognitive deficits, suggesting that young age may protect against pathology. This dissertation builds a foundation to better understand critical periods across the lifespan for tackling cognitive deficits in obesity.

Chapter 1 Introduction

1.1 Obesity and its complications throughout the lifespan

The prevalence of obesity in the United States (US) and globally has grown over the past several decades, reaching pandemic levels [1]. According to the World Health Organization, obesity prevalence in 2016 was three times that of 1975 [2]. This uptrend in obesity continues and affects both adults and children. The predicted trajectory of obesity rates in the US suggests that 48.9% of adults will be obese by the year 2030 [3]. A 2017-18 survey found that 19.3% of US children were obese [4]. Globally, the World Obesity Atlas predicts that one billion people and 13% of children and adolescents will be obese by 2030 [5]. Overweight and obesity occur on a spectrum with overweight defined as a BMI over 25, obesity a BMI over 30, and morbid obesity a BMI over 35 (www.cdc.gov). A complex interplay of genetic predisposition and environmental factors contribute to the development of obesity [1,6]. Which factors are driving the global obesity pandemic are debated, but include the advent of the western diet, high in sugar and fat, and modernization, which is associated with a sedentary lifestyle [1,7]. While addressing the root cause of obesity would help to reverse and prevent the growing global burden, worldwide campaigns targeting obesity have largely failed [1,8]. Therefore, the complications of obesity must be understood and mitigated as the world faces the predicted trajectory of overweight and obesity.

Obesity increases the risk for multiple systemic complications at the individual level, that place a significant burden on both healthcare systems and national

economies. Obesity is associated with chronic, low-grade systemic inflammation as well as metabolic dysfunction, both of which negatively impact multiple organ systems. The metabolic dysfunction associated with obesity can progress to prediabetes and type 2 diabetes, which confers additional risk for complications, some of which is independent of the obesity-associated risk. Systemic complications of obesity include increased risk for cardiovascular disease, renal disease, cancer, and stroke [9,10]. Further, quality of life in adults and children is diminished [11,12], and obesity negatively impacts mental health [13,14]. Complications of the central nervous system beyond stroke and psychiatric pathology, include an increased risk for cognitive impairment and dementia [15–17]. In particular, obesity in middle-age is associated with dementia later in life [17–20], and central abdominal obesity is especially predictive of this risk [15] (**Figure 1.1**[15,17–23]).

Obesity also negatively impacts cognition in children [24]. Given the high rates of childhood obesity and potential complications, it is crucial to understand how being overweight or obese can impact the developing brain and its subsequent function throughout the lifespan. One study found that abdominal fat is associated with poorer hippocampal dependent memory in overweight and obese children [22], and increased adiposity is also associated with deficits in cognitive control and academic achievement [21]. Obesity is also associated with structural brain changes in adolescents [25]. A systematic review reports clear relationships between childhood obesity and deficits in executive function and attention, and contradictory results on the association with memory and learning impairment [24]. More research is needed to fully understand the

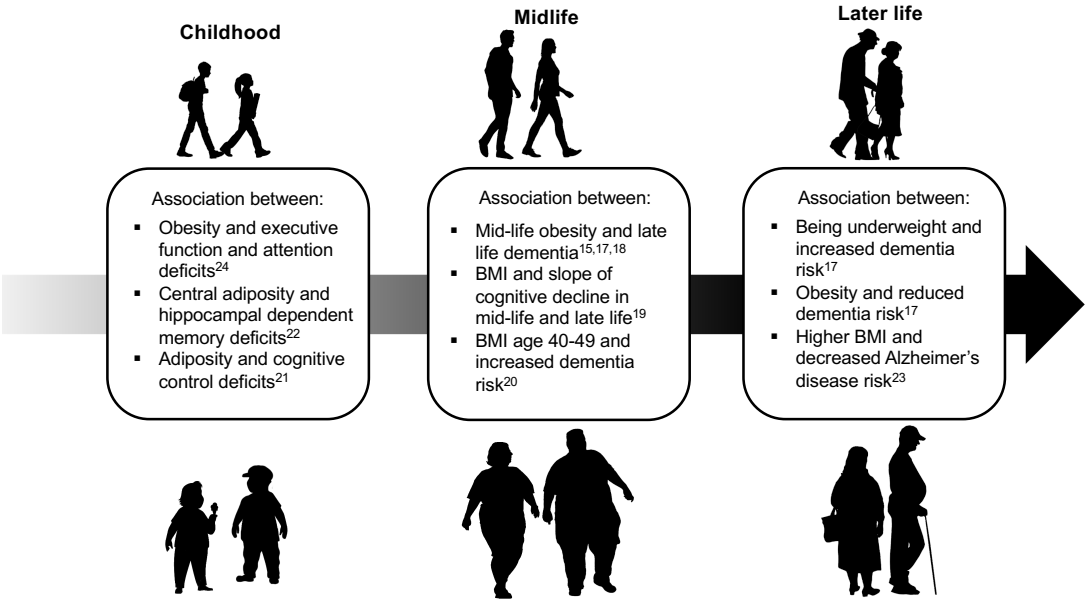

Figure 1.1 Summary of effects of obesity on cognitive function across the lifespan.

Review of associations reported in clinical studies between obesity, BMI, or adiposity and cognitive function in childhood (left), and dementia in mid-life (center) and late-life (right) individuals. Overall, studies of obesity in children demonstrate deficits in multiple cognitive domains. A focus on dementia and Alzheimer's disease risk later in life reveals an association between mid-life obesity and dementia late in life. Obesity in late life his associated with decreased risk for dementia and Alzheimer's disease.

effects of being overweight or obese on childhood and adolescent brain development and function. What is clear is that negative effects on the brain are not limited to adulthood dementia risk. Therefore, studies, such as the work presented in this doctoral thesis, must investigate the impact of obesity in the context of the young brain to begin to develop strategies to prevent or reverse consequent pathology and adverse health outcomes.

1.2 The economics of obesity

Given the numerous complications across organ systems, and on mental health and cognitive performance, it is unsurprising that a large economic burden accompanies the obesity pandemic. According to a 2018 report by the Milken Institute, 1.72 trillion US dollars was spent in the US on chronic diseases resulting from overweight and obesity in 2016 [10]. This price tag made up 47.1% of the cost of chronic diseases [10]. Over 100 billion of this 1.72 trillion US dollars was spent on Alzheimer's disease and vascular dementia. The prevalence of childhood obesity will contribute to a generation of adults with potential life-long chronic sequelae, further growing this healthcare and economic burden. Currently treatment of dementia is limited to pharmacologic and lifestyle interventions for management of symptoms, and no therapy effectively addresses the underlying pathology. Even less is available for managing central nervous system (CNS) consequences of childhood obesity, as the deficits themselves are not well understood or recognized. For this reason, it is critical to understand the pathological drivers of obesity-induced cognitive deficits throughout the lifespan, so that targeted therapies and lifestyle interventions can be developed.

1.3 Inflammation and its role in obesity related pathology: systemic and CNS

The immune system response may serve as one critical driver of CNS complications associated with obesity, as inflammation is a known consequence of and contributor to obesity associated pathology. Obesity induces inflammation throughout the body in both humans and animal models, characterized by increased pro-inflammatory cytokines as well as tissue recruitment and activation of immune cells [26–30]. While innate immune cells, including macrophages, are well-studied actors in this inflammatory response, cells of the adaptive immune system, such as T cells and B cells, have also been implicated in the response [26,27,29]. Adipose tissue inflammation and its role in contributing to metabolic dysfunction in obesity is well established [26,29]. In obesity, macrophages are recruited to adipose tissue where they make up the largest proportion of stromal immune cells [26]. The macrophage activation state in adipose tissue shifts to a pro-inflammatory phenotype in obesity [26,27].

Numerous mouse studies, including those using transgenic knock-outs of inflammatory genes, have demonstrated that inflammation, particularly driven by macrophages, contributes to the development of insulin resistance and metabolic dysfunction in obesity [27,29,31–33]. Although human obesity findings on adipose tissue macrophages do not align exactly with murine findings [34], evidence consistently demonstrates adipose tissue inflammation. Macrophages are activated in human adipose tissue [35], and BMI positively correlates with adipose expression of the pro-inflammatory cytokine tumor necrosis factor alpha (TNF-α) [36]. Further, obesity results in systemic inflammation in humans, including increased circulating cytokines [28] and complement protein C3, which correlates with insulin resistance [37].

Inflammation is not limited to adipose tissue and occurs in multiple organ systems, including skeletal muscle, liver, and the CNS [29]. In the brain of rodent models of diet-induced obesity, inflammatory sequalae depend on region and temporal progression of high-fat diet (HFD) feeding or obesity. Although the mechanisms responsible for brain inflammation are not well characterized, evidence suggests both a local inflammatory response from resident glial cells [38,39], as well as infiltration of immune cells from the systemic circulation [40]. An acute inflammatory response to HFD feeding has been identified in the hypothalamus, hippocampus [41], and amygdala [42]. In the hypothalamus [39], where the blood-brain barrier has increased permeability, HFD elevates expression of pro-inflammatory genes such as TNF-α within 1 day of feeding [43], and treatment with enteric gavage of saturated fatty acids results in microglial activation within a few days [39]. In the hippocampus, a brain region involved in learning and declarative memory, inflammation also occurs acutely. In the hippocampus of rats fed HFD for only three days, expression of the inflammasome protein nod-like receptor pyrin domain containing 3 (NLRP3) is elevated [44]. Another study showed elevated protein levels of pro-inflammatory cytokines TNF-α and interleukin 1 beta (IL-1β) in the hippocampus of mice fed a HFD for three, seven, and ten days [41].

Studies have also addressed the effects of chronic HFD feeding in the CNS. This paradigm results in the development of obesity and also induces hippocampal inflammation, characterized by elevated pro-inflammatory cytokines and morphological activation of microglia, the macrophage-like resident innate immune cells of the CNS. Examining a longer-term HFD feeding from P21 to P60 in adolescent mice, Vinuesa et al. similarly identified elevation of TNF-α and IL-1β mRNA in the hippocampus of HFD-

fed mice. Further, they found that the HFD-fed mice displayed altered ionized calcium binding adaptor molecule 1 (Iba1)+ microglial morphology with larger cell soma area [45]. In a longer-term feeding paradigm of three months of HFD, Hao et al. detected elevated hippocampal IL-1β protein, but not after one or two months HFD [46]. Additionally, they found that three months HFD induces an activated hippocampal microglial morphology, which can be reversed by dietary switch to a low-fat diet [46]. As the resident innate immune cells of the CNS, microglia play a role in mediating neuroinflammation in response to HFD and obesity, and this role will be examined in detail in subsequent sections **1.6** and **1.7**.

1.4 Microglia in the healthy developing and adult brain

As immune cells, microglia are responsible for responding to pathogens and tissue injury, but it is now understood that they play numerous roles beyond the immune response [47,48]. Microglia are hematopoietic derived cells that originate in the yolk sac in embryogenesis and migrate to the CNS in mice [49,50]. Glial cells, which include microglia, oligodendrocytes, and astrocytes, are considered the supporting cells of the brain. Microglia utilize their extensive branching processes to surveil their environment, they respond to secreted cytokines and neurotransmitters via cell surface receptors [51–53], and they also take part in contact-dependent communication with neurons [54]. Functionally, microglia are involved in development and maintenance of brain homeostasis during organismal development and adulthood. In the developing brain, microglia serve a variety of regulatory functions that contribute to neuronal development. Microglia can

induce neuronal death and clear apoptotic neurons during developmental programmed cell death, and promote neuronal survival, proliferation, and differentiation [55,56].

Microglia not only regulate the neuronal cell population, but also contribute to synaptic wiring during development [55,56]. They prune developing synapses in an activity-dependent manner, including in the hippocampus [47,57]. Interestingly, the microglial contribution to neuronal function is not limited to development but continues into adulthood. In adulthood, microglia also modulate synaptic plasticity [58–60]. In the adult neurogenic niche of the hippocampal dentate gyrus subgranular zone, microglia are responsible for phagocytosing apoptotic cells derived from neural precursors [61]. Given the proposed function of synaptic plasticity in learning and memory [62–64], and the role of adult neurogenesis in cognitive function [65], microglia are poised to contribute to cognitive health throughout the lifespan. Indeed, partial pharmacological microglial depletion in young and aged rats reduces hippocampal synaptic transmission and impairs hippocampal-dependent cognitive function in both age groups [66]. Because microglia play an essential role in neuronal and synaptic development and maintenance of homeostasis in adulthood, it is not surprising that they are implicated in responding to and driving neuropathology in CNS disease states.

1.5 Microglia in Alzheimer's disease

Microglia are implicated in disease pathology of neurodegenerative diseases, including Alzheimer's disease (AD) [67], amyotrophic lateral sclerosis (ALS) [68], and Parkinson's disease [69]. Extensive investigation of the role of microglia in neurodegenerative disease pathology has revealed complex and context-dependent

functions in both mitigating and driving pathology [67,70]. For decades, studies of mechanisms mediating AD focused on neurons and neurotoxicity driven by amyloid beta and tau protein aggregate pathology. However, recent focus has shifted to the contribution of microglia, in part due to the discovery of human AD risk allele variants in genes expressed by microglia, including within the gene encoding triggering receptor expressed on myeloid cells 2 (TREM2) [67,70–72]. Research on microglial function in mouse models of AD demonstrates that microglia can be both protective and detrimental over the course of disease progression [73,74]. Both *in vitro* and *in vivo* studies have begun to elucidate the function of microglial TREM2 sensing in AD, and the consequence of the TREM2 R47H allele variant. TREM2 directly binds amyloid beta oligomers, and TREM2 signaling mediates microglial degradation of amyloid beta *in vitro* [75]. TREM2 R47H is thought to be a loss-of-function variant [76], and microglia from AD patients with this allele variant display greater inflammatory phenotypes than microglia from wild type TREM2 samples [77]. Studies utilizing genetic manipulation of the TREM2 gene in mouse models of AD generally demonstrate a protective function for microglial TREM2, although some studies contradict this role [67,70,74]. As highlighted in a recent review by Leng and Edison (2020), TREM2 deficiency in two separate mouse models of AD yield conflicting outcomes [74,78,79]. In the 5XFAD AD mouse model, TREM2 deficiency results in increased amyloid beta burden and reduced microglia association with plaques [78], along with increased damage to neurons [80]. In contrast, TREM2 deficiency in the APP/PS1 AD mouse model yields decreased hippocampal amyloid beta load [79].

Ambiguity regarding whether microglia drive pathology or protect against disease progression is not limited to studies of TREM2. In addition to their established protective role of surrounding and containing amyloid plaques, and clearing amyloid beta [67], microglia can contribute to AD pathology by secreting proinflammatory and neurotoxic mediators such as cytokines and reactive oxygen species [74]. Further, they engage in aberrant and excessive complement-mediated synaptic pruning, which is suggested to reflect a re-activation of a developmental program [81]. Contradictory findings on the role of microglia in AD are likely affected by context-dependent factors such as differences in mouse models (*e.g.,* amyloid or tau pathology) or stage of disease, leaving many questions unanswered [70,73,74]. Further complicating translation of findings in mouse models to the treatment of human AD are differences in human and mouse microglial genes [74]. While the understanding of microglial function in AD remains an active area of ongoing research, the existing data could yield insights into mechanisms of microglia mediated cognitive dysfunction in other disease states, such as in obesity.

1.6 Microglia in obesity: hypothalamus, amygdala, and cortex

As discussed earlier, acute HFD or chronic obesity induce inflammation in multiple brain regions including the hypothalamus, amygdala, cortex, and hippocampus, and this inflammatory response is characterized by microglial activation (overview in **Figure 1.2, A-C**). The role of microglia in hypothalamic neuronal injury and subsequent systemic metabolic dysfunction in response to HFD is well established [82,83]. The hypothalamus is a region of the brain responsible for maintaining systemic homeostasis, including metabolic homeostasis, and distinct regions of the hypothalamus have

enhanced blood-brain barrier permeability and are exposed to components of the systemic circulation [84]. In a series of fundamental studies, Valdearcos et al. demonstrated that microglia play a pivotal role in the hypothalamic response to saturated fatty acids (SFAs). First, they showed that SFA-enriched HFD causes SFA accumulation in the mediobasal hypothalamus, alongside microglial pro-inflammatory activation, characterized by increased cell counts and cell size, elevated TNF-α co-localization, and increased pro-inflammatory mediator expression [39]. Further, using enteric short-term administration of SFAs, they found that SFAs alone induce this microglial activation along with neuronal stress, measured by expression of heat-shock protein 72 [39]. Next, they demonstrated that depletion of microglia via diphtheria toxin treatment reduces inflammation and neuronal stress in response to SFAs, suggesting a harmful role for microglia in response to saturated fatty acids [39]. Further, when microglia were pharmacologically depleted using a colony-stimulating factor 1 receptor (CSF1R) antagonist, not only were neuronal responses to leptin, a hormone that mediates satiety, restored, but HFD-fed mice also had decreased consumption of chow. In a later study, these same investigators utilized a microglial-specific knock-out of the master pro-inflammatory transcription factor nuclear factor-kappa B (NF-κB) to demonstrate that NF-κB mediated microglial signaling contributes to microgliosis, hyperphagia, and obesity in a model of HFD-induced obesity [85]. Similar research by another group using an antimitotic agent to prevent microglial proliferation also demonstrated reduced HFD chow consumption, weight gain, and adiposity, alongside decreases in microglial TNF-α expression in the arcuate nucleus of the hypothalamus [86].

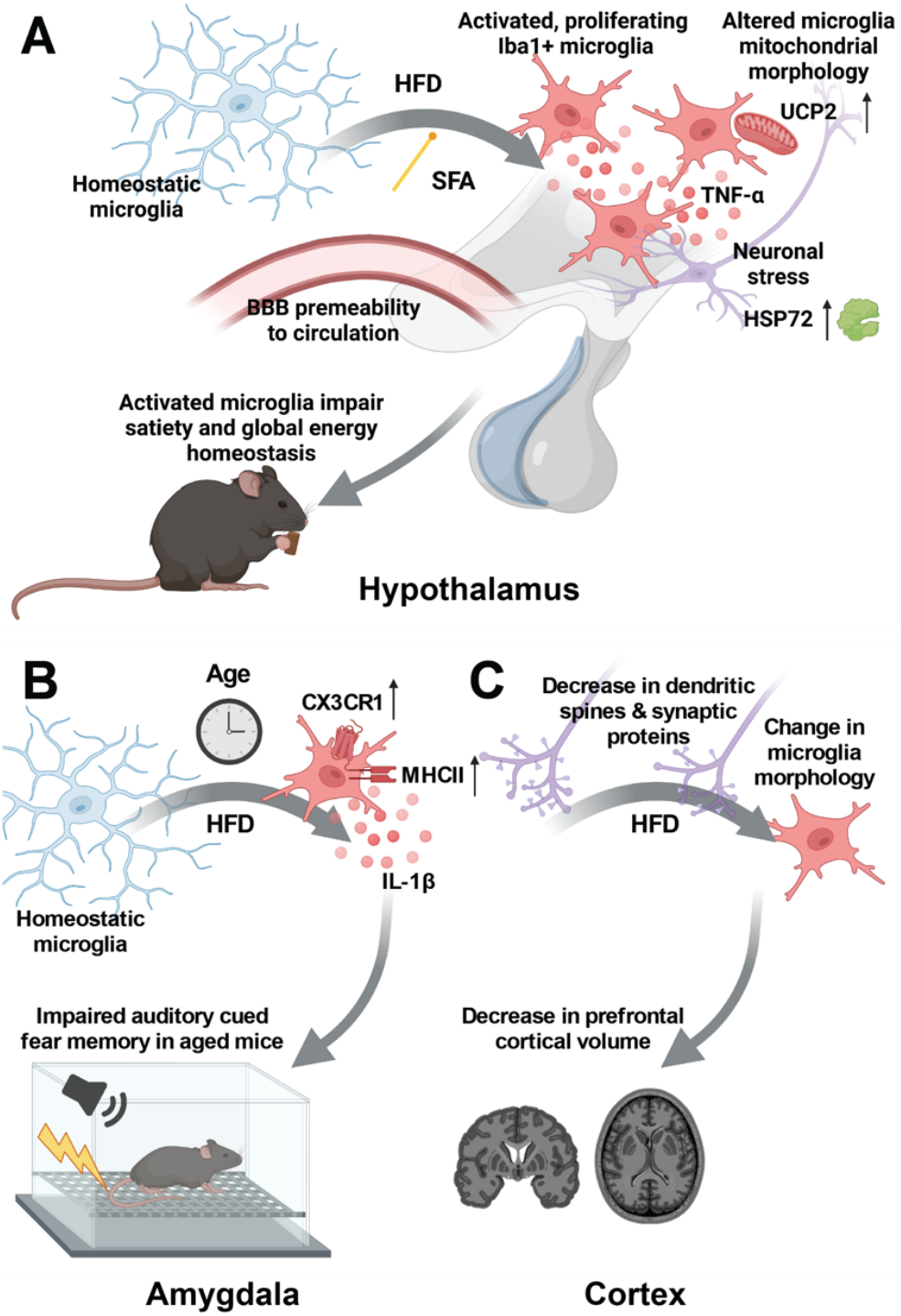

Figure 1.2 Effects of HFD and obesity on microglia in the brain.

Overview of literature for HFD-induced microglial activation in (A) the hypothalamus, (B) the amygdala, and (C) the cortex. In the hypothalamus, saturated fatty acids (SFA) and high-fat diet (HFD) induce an inflammatory microglial activation state, contributing to feeding behaviors and obesity. (B) In the amygdala, 3 days of HFD induces cognitive deficits in aged mice and exacerbates the effect of aging on microglia. (C) In the cortex, data is lacking, but changes in microglial morphology have been identified.

Microglial mitochondrial function plays a potential role in mediating these responses to HFD. The mitochondrial uncoupling protein 2 (UCP2) mRNA is transiently upregulated in microglia after three days of HFD, and microglia-specific UCP2 knockout not only restores mitochondrial morphology and reduces microglial activation in the arcuate nucleus, but also inhibits obesity in HFD-fed mice [87]. Intriguingly, microglia themselves express the leptin receptor, and microglial-specific leptin receptor deficiency in mice fed a standard control chow induces microglial morphological activation in the paraventricular nucleus, increases food consumption and weight gain, and alters hypothalamic neuronal circuitry [88]. Collectively, these studies suggest that hypothalamic microglia play a pivotal role in sensing nutrient status, and they negatively impact neuronal function and contribute to obesity in the setting of HFD.

In the amygdala, a brain region that regulates fear and emotional responses, the microglial response to HFD and obesity is less well characterized. Multiple studies led by the Barrientos laboratory have investigated the differential effects of HFD on hippocampal versus amygdalar cognitive deficits, inflammation, and microglial activation in both young and aged rats. They find that three days of HFD impairs amygdala-dependent long-term auditory cued fear memory in aged rats relative to control fed animals, and elevates levels of the pro-inflammatory cytokine IL-1β [42]. Long-term cued fear memory deficits were not observed in young HFD mice. Gene expression of major histocompatibility complex class II (MHCII), Iba1, and cluster of differentiation molecule 11b (Cd11b), which are associated with microglial activation, increased with age but not HFD in the amygdala. However, when microglia were isolated from the amygdala of young and aged rats, expression of MHCII and C-X3-C motif chemokine receptor 1

(CX3CR1) were elevated in microglia in both young and aged HFD animals relative to controls [89]. In a follow-up study, this same group demonstrated that three days of HFD in aged rats exacerbates aging-associated microglial priming, characterized by decreased morphological ramification, in the amygdala, and decreases microglial phagocytosis *ex vivo* [90]. While these three-day studies demonstrate that the amygdala is not shielded from the effects of SFA-enriched HFD, they do not investigate microglial activation over time, or with chronic obesity, and the contribution of microglial activation to amygdalar function remains unclear.

Short-term HFD and obesity induce deficits in multiple cognitive domains, driven by pathology in brain regions beyond the amygdala. Rats fed HFD for eight weeks demonstrate deficits in cognitive function dependent on the prefrontal and perirhinal cortices [91]. In addition to cognitive impairment, these rats have decreased dendritic spine density and decreased synaptic proteins in the aforementioned cortical regions, suggesting synaptic dysfunction. Further, obesity reduced prefrontal cortical volumes and increased microglial process length. The effect of obesity on the hippocampal microglial response and subsequent effects on hippocampal-dependent cognitive function will be examined in the following section.

1.7 Hippocampal microglia in obesity: what is known?

As mentioned in the opening section, obesity is associated with an increased risk for developing dementia in humans [15,18]. The hippocampus, a limbic structure involved in learning and memory, is particularly affected in dementias, such as AD, the most common type of dementia. Given the role of the hippocampus in AD pathology [92],

researchers have asked how obesity impacts hippocampal function. Indeed, murine models of HFD-induced obesity demonstrate cognitive deficits in hippocampal-dependent function. Hippocampal microglial pro-inflammatory activation is present in these cognitively impaired models of obesity, suggesting a potential role for microglia in disease pathology. Findings on the effects of HFD and obesity on hippocampal-dependent cognition and microglial activation in multiple hippocampal subregions, including the dentate gyrus and cornu ammonis 1 (CA1), will be reviewed here (summary in **Figure 1.3**).

We, and others, have shown that mice fed a SFA-enriched HFD for several months develop obesity and have deficits in hippocampal-dependent memory. Using the novel-object recognition task, we found that HFD-fed mice begun diet at four weeks of age (*i.e.*, adolescence) have deficits in short-term memory after two, six, and 24 weeks of diet [93]. Additionally, Morris water maze testing performed at the study endpoint demonstrated that obese mice have impaired long-term memory after 24 weeks of HFD. One experimental group was switched from HFD back to control chow after 16 weeks of HFD, rescuing both the short-term and long-term hippocampal-dependent memory deficits. In line with these findings, a study in six week old mice fed HFD for three months demonstrated impaired hippocampal-dependent function in spatial memory using the Y-maze task and also in the novel object recognition task [94]. Further, hippocampal IL-1β protein was elevated after three months HFD, but not after one or two months. The number of hippocampal dentate gyrus microglia, identified by immunostaining for Iba1, with morphology characteristic of activated microglia increased in obese mice. The authors defined activated microglia as those with ‘simple’ branching

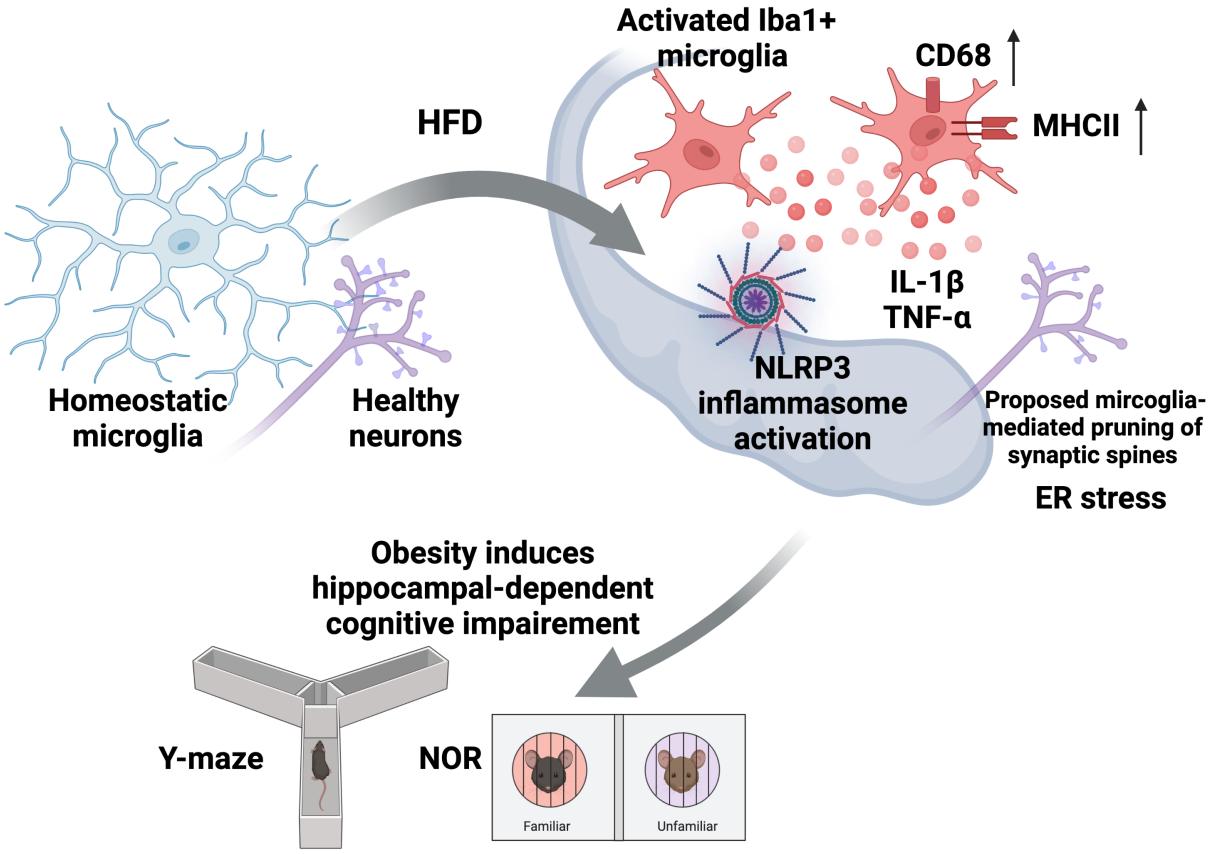

Figure 1.3 Hippocampal microglia are activated in rodent models of diet-induced obesity.

In the hippocampus, microglial activation has been reported after chronic HFD using measures of morphology and measures of MHCII and CD68 surface markers. Upregulation of inflammasome expression and ER stress proteins also occurs in response to HFD in the hippocampus. Evidence suggests that microglia likely excessively prune neuronal synapses, contributing to hippocampal-dependent cognitive dysfunction.

patterns, *i.e.*, one to two primary processes, versus 'complex' cells, with three or more primary processes. Additionally, HFD-fed mice had an increase in percentage of simple microglia co-staining for major histocompatibility complex II (MHC-II), an antigen presentation protein used as a marker of activation. HFD-feeding decreased dendritic spine density, decreased staining for the synaptic protein post-synaptic density protein 95 (PSD95) and altered microglial spatial relationships with PSD95 in the molecular layer of the dentate gyrus. Further, isolated microglia from HFD-fed mice demonstrated increased uptake of synaptosomes *in vitro,* suggesting that HFD microglia are potentially phagocytosing synaptic spines. HFD feeding during adolescence in slightly younger mice, P21 to P60 (age three weeks to ~ two months), similarly causes impairments in the novel object location recognition task, a measure of hippocampal-dependent spatial memory [95]. Additionally, in this study, HFD reduced hippocampal neurogenesis in the subgranular zone of the dentate gyrus, and altered Iba1+ microglia by increasing the area covered by cell somas in the hilus and CA1 stratum radiatum of the hippocampus [95]. Although the total hippocampal PSD95 protein levels and the CA1 neuronal dendritic spine density were not affected by HFD, HFD did reduce mature dendritic spines.

In older eight week old mice, fed HFD for 12 weeks, Cope et al. identified hippocampal deficits using the object location task and the Barnes maze task to test spatial memory and learning [38]. Again, obesity reduced dendritic spine density, both in dentate gyrus and CA1 neurons. However, immature, newborn neurons in the dentate gyrus were not reduced by obesity in this study. Obesity activated microglia in both the dentate gyrus molecular layer and the CA1 stratum radiatum, with microglia activation

defined based on the following parameters: decreased primary process number, increased cell body area, and increased cluster of differentiation 68 (CD68) co-expression. Further, Cope et al., utilized pharmacological inhibition of microglial activation and microglial phagocytosis to demonstrate that microglia contribute to cognitive deficits, likely by phagocytosing synaptic spines. The aforementioned studies were performed in male mice, and it is important to note that sex differences have been identified in obesity induced hippocampal pathology and associated microglial activation [96].

Studies of acute HFD feeding have also demonstrated hippocampal-dependent cognitive deficits. However, results are mixed, with some experimental designs only yielding inflammation and deficits after chronic feeding. For example, as discussed above, Hao et al. did not find elevated hippocampal IL-1β after one or two months of HFD [46], and Cope et al. found no difference between HFD and control mice in cognition after only two weeks diet [38]. Contrary to these findings, deficits in episodic, spatial, and contextual memory occur in adult mice 12 weeks of age, after a single day of HFD [97]. HFD feeding for three days in rats impairs hippocampal dependent long-term contextual memory in aged, but not young, animals [42]. Although some studies report elevated protein or mRNA levels of inflammatory mediators with acute HFD feeding [41,42,44], reports of acute microglial activation in the hippocampus are lacking. It is likely that the animal model, age, and diet formulation play a role in these contradictory outcomes. While there is strong evidence for hippocampal microglial activation, defined by morphology changes and co-expression of inflammatory phenotypic markers, after chronic HFD, the mechanisms mediating this activation remain poorly understood.

1.8 Potential mechanisms of hippocampal microglial activation

Although acute HFD induces a pro-inflammatory activation state in hypothalamic microglia, the evolution of hippocampal microglial activation is unclear. Because immune cells are poised to respond acutely and adapt with chronic stimulation, it is possible that hippocampal microglia become activated earlier in response to HFD, prior to the development of obesity. The permeability of the blood brain barrier in the hypothalamus may mediate more acute exposure to the systemic circulation compared to the hippocampus, however, acute hippocampal inflammation in response to HFD is reported in some studies [41,42,44]. Further, elevated saturated fatty acid and decreased monounsaturated fatty acid content of neutral lipids in the hippocampus occurs after only three days HFD in rats, suggesting that the hippocampus is not protected from systemic fatty acid perturbations [89]. A variety of local and systemic signals may mediate acute and/or chronic, sustained microglial activation [98]. Existing data suggest a pro-inflammatory microglial activation state in obesity, however, it is possible that some subtypes of microglia manifest a protective phenotype over the course of systemic challenge, as occurs in other CNS disease [73].

Systemic circulatory signals that may stimulate a microglial response include nutrients, such as saturated fatty acids, or inflammatory mediators, including circulating cytokines or recruited immune cells [40,98]. Palmitate, the most abundant saturated fatty acid in humans, is not only increased in the cerebrospinal fluid (CSF) of overweight and obese humans with mild cognitive impairment, but CSF palmitate concentrations inversely correlate with cognitive function [99]. Palmitate activates the toll-like receptor 4

(TLR4) innate immune pro-inflammatory signaling cascade [100]. In microglia, palmitate stimulates a pro-inflammatory phenotype characterized by increased IL-1β expression following lipopolysaccharide priming *in vitro* [101]. Microglia are the resident macrophage-like cell type of the CNS, and peripheral macrophage activation in obesity may provide insight into mechanisms mediating microglial activation. In macrophages, SFAs activate the inositol requiring enzyme 1 (IRE1α)-X-box binding protein 1 (XBP1) endoplasmic reticulum (ER) stress response, yielding a downstream inflammatory response [102]. IRE1α activation also promotes insulin resistance, secondary to IRE1α-mediated phosphorylation of c-Jun N-terminal kinase (JNK) and insulin receptor substrate 1 (IRS1) [103,104]. IRE1α activity in macrophages has been to shown to alter the macrophage activation phenotype in a mouse model of obesity [105]. Thus, the ER serves an immunometabolic function, whereby metabolic dysregulation triggers ER stress, which then contributes to inflammation in obesity [106,107]. The ER stress response may play a role in microglial activation, as it does in peripheral macrophages.

Saturated fatty acids stimulate the macrophage nod-like receptor pyrin domain containing 3 (NLRP3) inflammasome via activation of the endoplasmic reticulum stress response [102], and peripheral NLRP3 and downstream IL-1β signaling may contribute to CNS microglial activation. Inflammasome activation promotes insulin resistance in obesity [108,109]. NLRP3 knockout mice are protected from obesity induced hippocampal-dependent cognitive impairment [110]. Visceral adipose tissue (VAT) NLRP3 contributes to this impairment [110]. Transplantation of VAT from obese WT, but not from obese NLRP3 KO, mice into lean mice induces cognitive deficits and microglial activation [110]. Further, an inducible CX3CR1 IL-β receptor knockout mouse confirms that IL-β

signaling in microglia contributes to these effects. IL-1β cytokine signaling from the systemic circulation thus represents a potential mediator of hippocampal microglial activation in obesity. In addition to systemic cytokine stimulation, peripheral immune cell infiltration [40,111] may contribute to microglial activation in obesity. Indeed, the blood-brain barrier is disrupted in obesity, allowing for greater systemic exposure, including to the hippocampus [112], and increased peripheral cell trafficking occurs in obesity [40]. In addition to direct activation by nutrient or inflammatory signals, microglia could respond to signals of neuronal stress. The complex interplay between the systemic circulatory signals, local CNS cells, and microglial activation remains to be elucidated.

1.9 Overview of aims

HFD effects on the acute hippocampal microglial response, and the progression of activation over time, are largely unexplored, including in younger animal models. Further, mechanisms mediating hippocampal microglial activation in obesity remain unclear. Thus, in this dissertation project we aimed to, (**1**), identify effects of acute and chronic HFD on hippocampal microglial pro-inflammatory activation by quantifying morphological measures of activation with an emphasis on adolescent animals. Expanding beyond morphological measures, we (**2**), defined the effects of HFD on microglial activation using single-cell RNA-seq on animals fed a HFD for 12 weeks starting at five weeks age, simulating adolescent obesity. Single-cell sequencing enabled us to interrogate the heterogenous population of microglial subtypes and to determine the effects of HFD on microglial inflammatory signaling at the level of the transcriptome. We (**3**) next investigated the impact of age on obesity-induced

hippocampal inflammation and cognitive impairment, and are currently (**4**) determining the role of endoplasmic reticulum stress in microglial activation. These aims are reviewed in **Figures 1.4** through **1.7**.

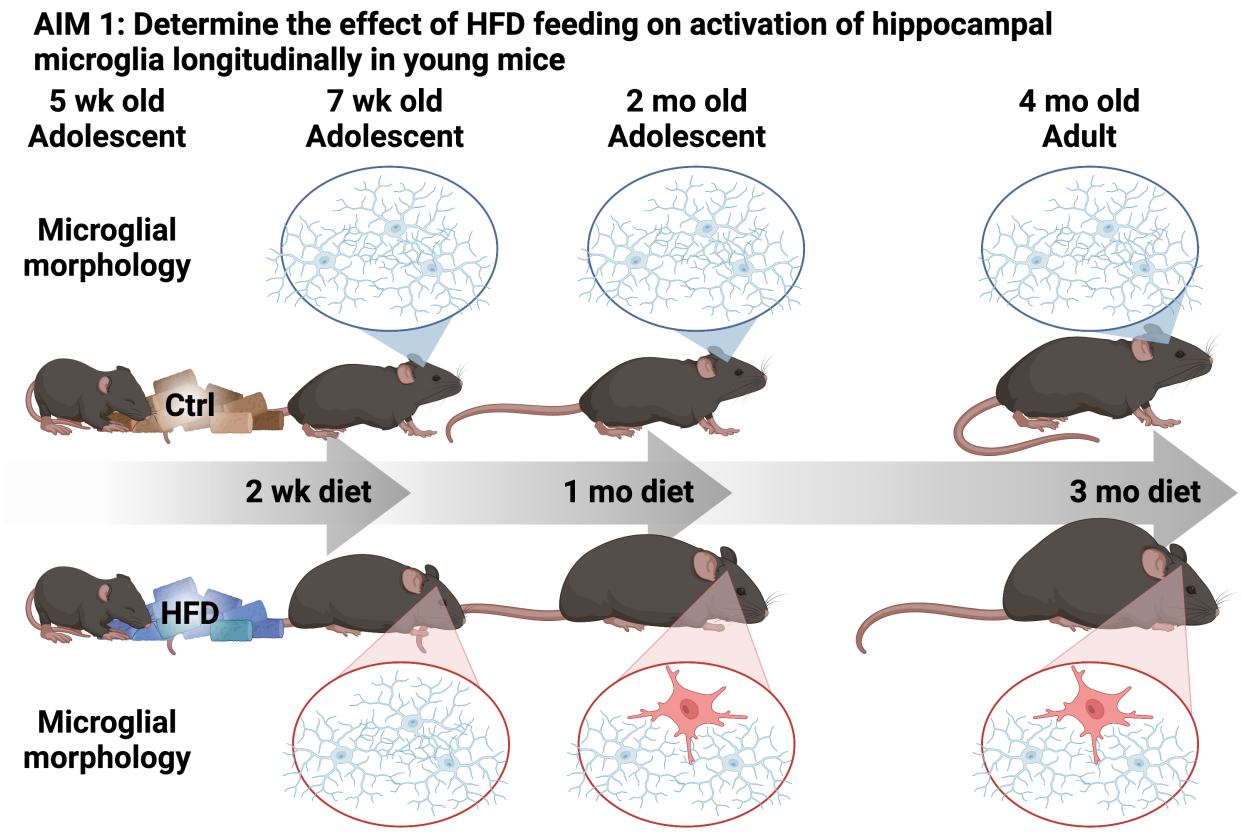

Figure 1.4 Aim 1.

For the first aim, we sought to identify effects of HFD longitudinally on hippocampal microglial pro-inflammatory activation by quantifying morphological measures of activation, with an emphasis on adolescent animals. To address this aim, we started mice on control or HFD at 5 wk of age using a longitudinal paradigm of 2 wk, 1mo, and 3 mo of feeding. We quantified microglial morphology measures using metrics in three-dimensions to infer activation state.

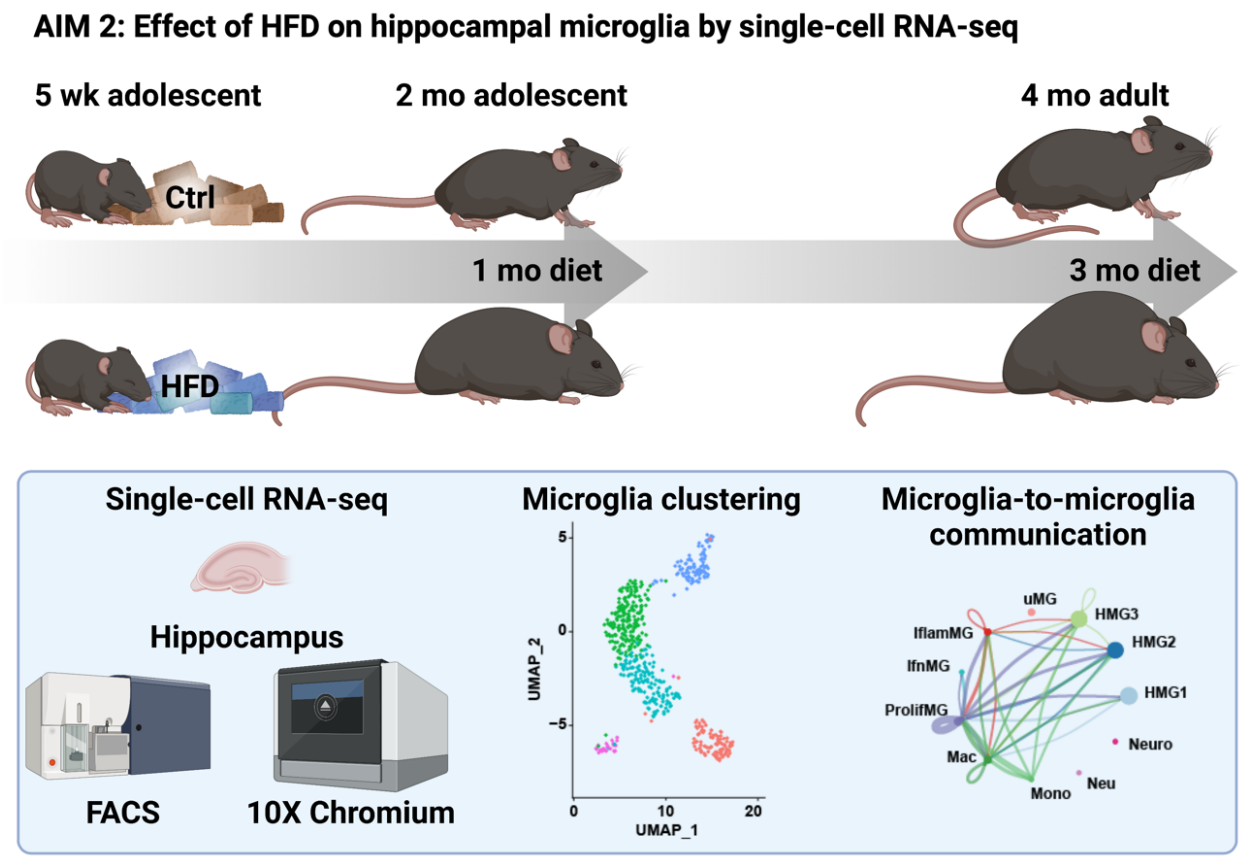

Figure 1.5 Aim 2.

Expanding beyond morphological measures, we defined the effects of HFD on microglial activation using single-cell RNA-seq on animals fed a HFD for 12 wk starting at 5 wk age, simulating adolescent obesity. Single-cell sequencing allowed us to interrogate microglial heterogeneity and to determine how HFD alters the microglial transcriptome.

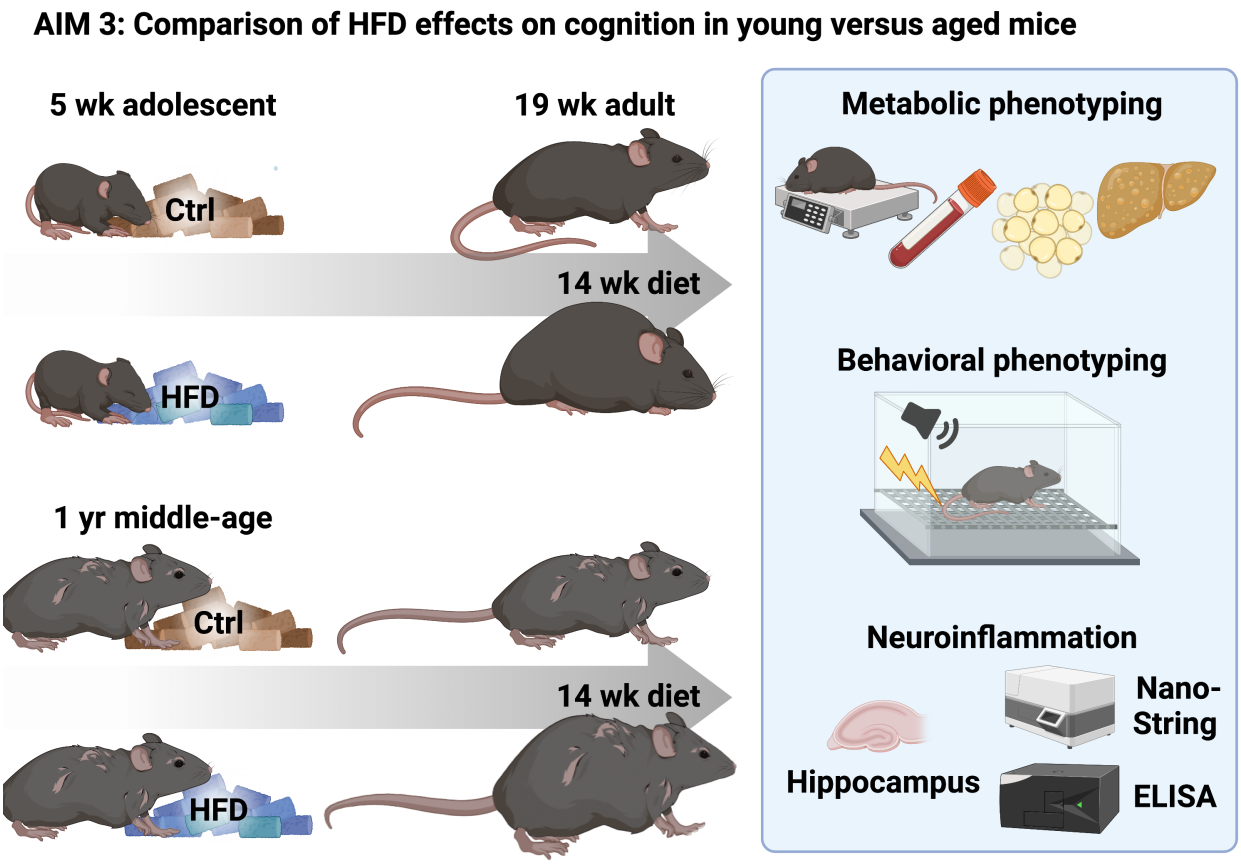

Figure 1.6 Aim 3.

We next investigated the impact of age on obesity-induced hippocampal inflammation and cognitive impairment. Young (5 wk of age) and mature adult (1 yr of age) mice were fed control or HFD for 14 wk and underwent cognitive testing using the fear condition task, which measures associative learning. NanoString gene expression profiling and ELISAs were performed to determine the impact of age on inflammatory response to HFD.

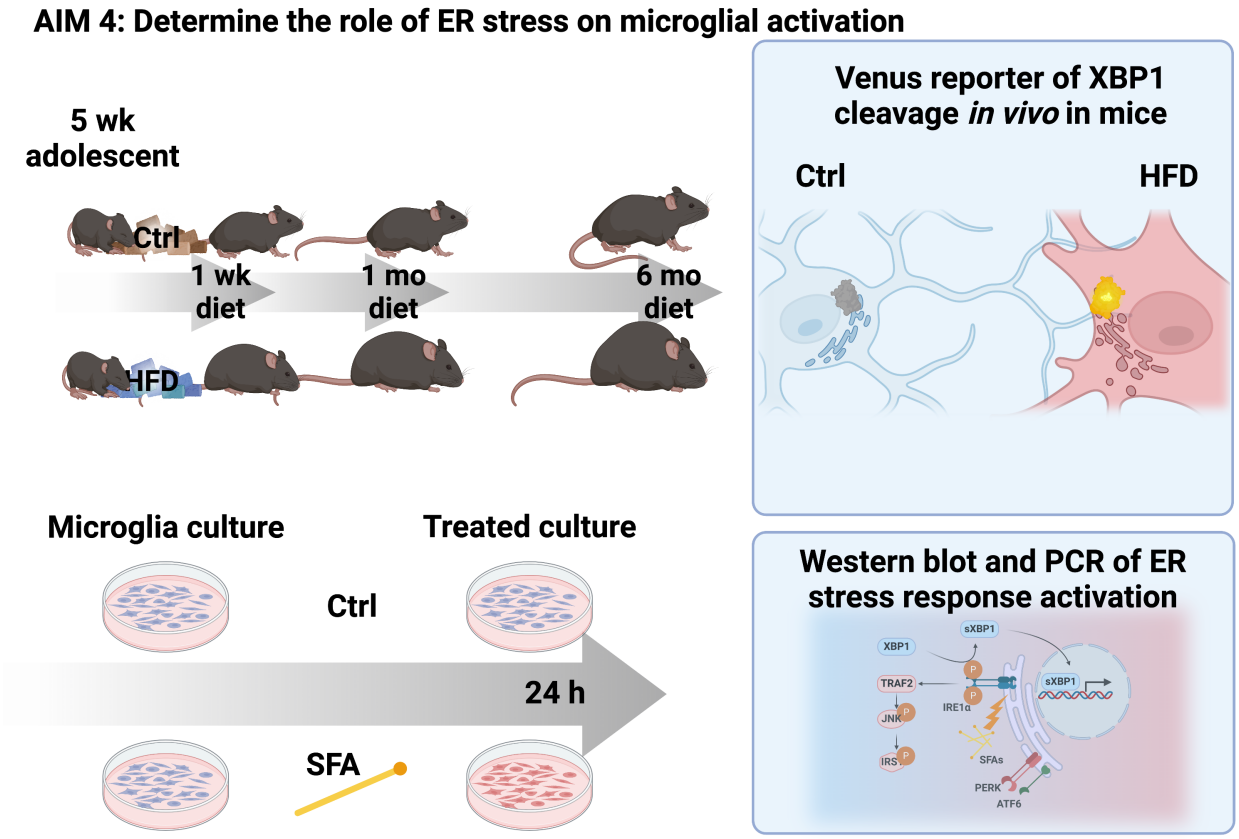

Figure 1.7 Aim 4.

The goal of this ongoing and future work is to determine the role of endoplasmic reticulum stress in microglial activation. To address this aim, we performed preliminary in vitro studies to determine whether the saturated fatty acid (SFA) palmitate activates the microglial IRE1α -XBP1 endoplasmic reticulum stress response. We also tested insulin responsiveness, because insulin resistance can occur downstream of IRE1α activation. In vivo studies using a transgenic reporter of XBP1 splicing will determine if HFD induces the IRE1a/XBP1 pathway in microglia, and if activation of this pathway associates with measures of inflammatory activation. Future directions include inhibition of this ER stress response to determine its role in microglial activation and cognitive impairment in obesity.

1.10 Bibliography

1. Blüher M. Obesity: global epidemiology and pathogenesis. *Nat Rev Endocrinol 2019 155*. 2019;15(5):288-298. doi:10.1038/s41574-019-0176-8

2. Obesity and overweight. Accessed March 8, 2022. https://www.who.int/news-room/fact-sheets/detail/obesity-and-overweight

3. Ward ZJ, Bleich SN, Cradock AL, et al. Projected U.S. state-level prevalence of adult obesity and severe obesity. *N Engl J Med*. 2019;381(25):2440-2450. doi:10.1056/NEJMsa1909301

4. The State of Childhood Obesity - Helping All Children Grow Up Healthy. Accessed April 1, 2021. https://stateofchildhoodobesity.org/

5. Policy Makers | World Obesity Day. Accessed July 10, 2022. https://www.worldobesityday.org/policy-makers

6. Causes of Obesity | Overweight & Obesity | CDC. Accessed August 6, 2022. https://www.cdc.gov/obesity/basics/causes.html?CDC_AA_refVal=https%3A%2F%2Fwww.cdc.gov%2Fobesity%2Fadult%2Fcauses.html

7. Davis RAH, Plaisance EP, Allison DB. Complementary Hypotheses on Contributors to the Obesity Epidemic. *Obesity*. 2018;26(1):17-21. doi:10.1002/OBY.22071

8. Roberto CA, Swinburn B, Hawkes C, et al. Patchy progress on obesity prevention: emerging examples, entrenched barriers, and new thinking. *Lancet*. 2015;385(9985):2400-2409. doi:10.1016/S0140-6736(14)61744-X

9. Hruby A, Manson JAE, Qi L, et al. Determinants and consequences of obesity. *Am J Public Health*. 2016;106(9):1656-1662. doi:10.2105/AJPH.2016.303326

10. Hugh Waters B, Graf M. AMERICA'S OBESITY CRISIS THE HEALTH AND ECONOMIC COSTS OF EXCESS WEIGHT. Published online 2018.

11. Friedlander SL, Larkin EK, Rosen CL, Palermo TM, Redline S. Decreased Quality of Life Associated With Obesity in School-aged Children. *Arch Pediatr Adolesc Med*. 2003;157(12):1206-1211. doi:10.1001/ARCHPEDI.157.12.1206

12. Stephenson J, Smith CM, Kearns B, Haywood A, Bissell P. The association between obesity and quality of life: a retrospective analysis of a large-scale population-based cohort study. *BMC Public Health*. 2021;21(1):1-9. doi:10.1186/S12889-021-12009-8/TABLES/5

13. Scott K, Bruffaerts R, Simon G, et al. (No Title). *Int J Obes*. 2008;32:192-200. doi:10.1038/sj.ijo.0803701

14. Luppino FS, De Wit LM, Bouvy PF, et al. Overweight, obesity, and depression: a systematic review and meta-analysis of longitudinal studies. *Arch Gen Psychiatry*. 2010;67(3):220-229. doi:10.1001/ARCHGENPSYCHIATRY.2010.2

15. Whitmer RA, Gustafson DR, Barrett-Connor E, Haan MN, Gunderson EP, Yaffe K. Central obesity and increased risk of dementia more than three decades later. *Neurology*. 2008;71(14):1057-1064. doi:10.1212/01.wnl.0000306313.89165.ef

16. Callaghan BC, Reynolds EL, Banerjee M, et al. The prevalence and determinants of cognitive deficits and traditional diabetic complications in the severely obese. *Diabetes Care*. 2020;43(3):683-690. doi:10.2337/dc19-1642

17. Fitzpatrick AL, Kuller LH, Lopez OL, et al. Midlife and late-life obesity and the risk of dementia: Cardiovascular health study. *Arch Neurol*. 2009;66(3):336-342. doi:10.1001/archneurol.2008.582

18. Pedditizi E, Peters R, Beckett N. The risk of overweight/obesity in mid-life and late life for the development of dementia: a systematic review and meta-analysis of longitudinal studies. *Age Ageing*. 2016;45(1):14-21. doi:10.1093/AGEING/AFV151

19. Karlsson IK, Gatz M, Arpawong TE, Dahl Aslan AK, Reynolds CA. The dynamic association between body mass index and cognition from midlife through late-life, and the effect of sex and genetic influences. *Sci Reports 2021 111*. 2021;11(1):1-15. doi:10.1038/s41598-021-86667-4

20. Li J, Joshi P, Ang TFA, et al. Mid- to Late-Life Body Mass Index and Dementia Risk: 38 Years of Follow-up of the Framingham Study. *Am J Epidemiol*. 2021;190(12):2503-2510. doi:10.1093/AJE/KWAB096

21. Kamijo K, Khan NA, Pontifex MB, et al. The relation of adiposity to cognitive control and scholastic achievement in preadolescent children. *Obesity (Silver Spring)*. 2012;20(12):2406-2411. doi:10.1038/OBY.2012.112

22. Khan NA, Baym CL, Monti JM, et al. Central adiposity is negatively associated with hippocampal-dependent relational memory among overweight and obese children. *J Pediatr*. 2015;166(2):302-308.e1. doi:10.1016/J.JPEDS.2014.10.008

23. Hughes TF, Borenstein AR, Schofield E, Wu Y, Larson EB. Association between late-life body mass index and dementia. *Neurology*. 2009;72(20):1741-1746. doi:10.1212/WNL.0B013E3181A60A58

24. Liang J, Matheson BE, Kaye WH, Boutelle KN. Neurocognitive correlates of obesity and obesity-related behaviors in children and adolescents. *Int J Obes 2014 384*. 2013;38(4):494-506. doi:10.1038/ijo.2013.142

25. Yau PL, Kang EH, Javier DC, Convit A. Preliminary Evidence of Cognitive and Brain Abnormalities in Uncomplicated Adolescent Obesity. *Obesity (Silver Spring)*. 2014;22(8):1865. doi:10.1002/OBY.20801

26. Mclaughlin T, Ackerman SE, Shen L, Engleman E. Role of innate and adaptive immunity in obesity-associated metabolic disease. *J Clin Invest*. 2017;127(1):5-13. doi:10.1172/JCI88876

27. Lumeng CN. Innate immune activation in obesity. *Mol Aspects Med*. 2013;34(1):12-29. doi:10.1016/J.MAM.2012.10.002

28. Schmidt FM, Weschenfelder J, Sander C, et al. Inflammatory Cytokines in General and Central Obesity and Modulating Effects of Physical Activity. *PLoS One*. 2015;10(3):121971. doi:10.1371/JOURNAL.PONE.0121971

29. Wu H, Ballantyne CM. Metabolic Inflammation and Insulin Resistance in Obesity. *Circ Res*. Published online 2020:1549-1564. doi:10.1161/CIRCRESAHA.119.315896/FORMAT/EPUB

30. Rohm T V., Meier DT, Olefsky JM, Donath MY. Inflammation in obesity, diabetes, and related disorders. *Immunity*. 2022;55(1):31-55. doi:10.1016/J.IMMUNI.2021.12.013

31. Mamane Y, Chan CC, Lavallee G, et al. The C3a Anaphylatoxin Receptor Is a Key Mediator of Insulin Resistance and Functions by Modulating Adipose Tissue Macrophage Infiltration and Activation. *Diabetes*. 2009;58(9):2006-2017. doi:10.2337/DB09-0323

32. Shin KC, Hwang I, Choe SS, et al. Macrophage VLDLR mediates obesity-induced insulin resistance with adipose tissue inflammation. *Nat Commun 2017 81*. 2017;8(1):1-14. doi:10.1038/s41467-017-01232-w

33. Weisberg SP, Hunter D, Huber R, et al. CCR2 modulates inflammatory and metabolic effects of high-fat feeding. *J Clin Invest*. 2006;116(1):115. doi:10.1172/JCI24335

34. Blaszczak AM, Jalilvand A, Hsueh WA. Adipocytes, Innate Immunity and Obesity: A Mini-Review. *Front Immunol*. 2021;12:1778. doi:10.3389/FIMMU.2021.650768/BIBTEX

35. Weisberg SP, McCann D, Desai M, Rosenbaum M, Leibel RL, Ferrante AW. Obesity is associated with macrophage accumulation in adipose tissue. *J Clin Invest*. 2003;112(12):1796-1808. doi:10.1172/JCI19246

36. Kern PA, Saghizadeh M, Ong JM, Bosch RJ, Deem R, Simsolo RB. The expression of tumor necrosis factor in human adipose tissue. Regulation by obesity, weight loss, and relationship to lipoprotein lipase. *J Clin Invest*. 1995;95(5):2111-2119. doi:10.1172/JCI117899

37. van Greevenbroek MMJ, Jacobs M, van der Kallen CJH, et al. The cross-sectional association between insulin resistance and circulating complement C3 is partly explained by plasma alanine aminotransferase, independent of central obesity and general inflammation (the CODAM study). *Eur J Clin Invest*. 2011;41(4):372-379. doi:10.1111/J.1365-2362.2010.02418.X

38. Cope EC, LaMarca EA, Monari PK, et al. Microglia Play an Active Role in Obesity-Associated Cognitive Decline. *J Neurosci*. 2018;38(41):8889-8904. doi:10.1523/JNEUROSCI.0789-18.2018

39. Valdearcos M, Robblee MM, Benjamin DI, Nomura DK, Xu AW, Koliwad SK. Microglia Dictate the Impact of Saturated Fat Consumption on Hypothalamic Inflammation and Neuronal Function. *Cell Rep*. 2014;9(6):2124-2138.

doi:10.1016/j.celrep.2014.11.018

40. Buckman LB, Hasty AH, Flaherty DK, et al. Obesity induced by a high-fat diet is associated with increased immune cell entry into the central nervous system. *Brain Behav Immun*. 2014;35:33-42. doi:10.1016/J.BBI.2013.06.007

41. Nakandakari SCBR, Muñoz VR, Kuga GK, et al. Short-term high-fat diet modulates several inflammatory, ER stress, and apoptosis markers in the hippocampus of young mice. *Brain Behav Immun*. 2019;79:284-293. doi:10.1016/j.bbi.2019.02.016

42. Spencer SJ, D'Angelo H, Soch A, Watkins LR, Maier SF, Barrientos RM. High-fat diet and aging interact to produce neuroinflammation and impair hippocampal- and amygdalar-dependent memory. *Neurobiol Aging*. 2017;58:88-101. doi:10.1016/J.NEUROBIOLAGING.2017.06.014

43. Thaler JP, Yi CX, Schur EA, et al. Obesity is associated with hypothalamic injury in rodents and humans. *J Clin Invest*. 2012;122(1):153-162. doi:10.1172/JCI59660

44. Sobesky JL, D'Angelo HM, Weber MD, et al. Glucocorticoids Mediate Short-Term High-Fat Diet Induction of Neuroinflammatory Priming, the NLRP3 Inflammasome, and the Danger Signal HMGB1. *eNeuro*. 2016;3(4):ENEURO.0113-16.2016. doi:10.1523/ENEURO.0113-16.2016

45. Vinuesa A, Bentivegna M, Calfa G, et al. Early Exposure to a High-Fat Diet Impacts on Hippocampal Plasticity: Implication of Microglia-Derived Exosome-like Extracellular Vesicles. *Mol Neurobiol*. 2019;56(7):5075-5094. doi:10.1007/s12035-018-1435-8

46. Hao S, Dey A, Yu X, Stranahan AM. Dietary obesity reversibly induces synaptic stripping by microglia and impairs hippocampal plasticity. *Brain Behav Immun*. 2016;51:230-239. doi:10.1016/j.bbi.2015.08.023

47. Schafer DP, Lehrman EK, Kautzman AG, et al. Microglia Sculpt Postnatal Neural Circuits in an Activity and Complement-Dependent Manner. *Neuron*. 2012;74(4):691-705. doi:10.1016/J.NEURON.2012.03.026

48. Wright-Jin EC, Gutmann DH. Microglia as Dynamic Cellular Mediators of Brain Function. *Trends Mol Med*. 2019;25(11):967-979. doi:10.1016/J.MOLMED.2019.08.013

49. Ginhoux F, Greter M, Leboeuf M, et al. Fate mapping analysis reveals that adult microglia derive from primitive macrophages. *Science (80-)*. 2010;330(6005):841-845. doi:10.1126/SCIENCE.1194637/SUPPL_FILE/GINHOUX.SOM.PDF

50. Saijo K, Glass CK. Microglial cell origin and phenotypes in health and disease. *Nat Rev Immunol*. Published online 2011. doi:10.1038/nri3086

51. Nimmerjahn A, Kirchhoff F, Helmchen F. Resting microglial cells are highly dynamic surveillants of brain parenchyma in vivo. *Science*. 2005;308(5726):1314-1318. doi:10.1126/SCIENCE.1110647

52. El Ali A, Rivest S. Microglia ontology and signaling. *Front Cell Dev Biol*. 2016;4(JUN):72. doi:10.3389/FCELL.2016.00072/BIBTEX

53. Marinelli S, Basilico B, Marrone MC, Ragozzino D. Microglia-neuron crosstalk: Signaling mechanism and control of synaptic transmission. *Semin Cell Dev Biol*. 2019;94:138-151. doi:10.1016/J.SEMCDB.2019.05.017

54. Cserép C, Pósfai B, Dénes Á. Shaping Neuronal Fate: Functional Heterogeneity of Direct Microglia-Neuron Interactions. *Neuron*. 2021;109(2):222-240. doi:10.1016/J.NEURON.2020.11.007

55. Mosser CA, Baptista S, Arnoux I, Audinat E. Microglia in CNS development: Shaping the brain for the future. *Prog Neurobiol*. 2017;149-150:1-20. doi:10.1016/j.pneurobio.2017.01.002

56. Schafer DP, Stevens B. Microglia Function in Central Nervous System Development and Plasticity. *Cold Spring Harb Perspect Biol*. 2015;7(10):a020545. doi:10.1101/CSHPERSPECT.A020545

57. Paolicelli RC, Bolasco G, Pagani F, et al. Synaptic pruning by microglia is necessary for normal brain development. *Science (80-)*. 2011;333(6048):1456-1458. doi:10.1126/SCIENCE.1202529/SUPPL_FILE/PAOLICELLI.SOM.PDF

58. Wu Y, Dissing-Olesen L, MacVicar BA, Stevens B. Microglia: Dynamic Mediators of Synapse Development and Plasticity. *Trends Immunol*. 2015;36(10):605-613. doi:10.1016/j.it.2015.08.008

59. Parkhurst CN, Yang G, Ninan I, et al. Microglia Promote Learning-Dependent Synapse Formation through Brain-Derived Neurotrophic Factor. *Cell*. 2013;155:1596-1609. doi:10.1016/j.cell.2013.11.030

60. Nguyen PT, Dorman LC, Pan S, et al. Microglial Remodeling of the Extracellular Matrix Promotes Synapse Plasticity. *Cell*. 2020;182(2):388-403.e15. doi:10.1016/J.CELL.2020.05.050

61. Sierra A, Encinas JM, Deudero JJP, et al. Microglia Shape Adult Hippocampal Neurogenesis through Apoptosis-Coupled Phagocytosis. *Cell Stem Cell*. 2010;7(4):483-495. doi:10.1016/j.stem.2010.08.014

62. Humeau Y, Choquet D. The next generation of approaches to investigate the link between synaptic plasticity and learning. *Nat Neurosci 2019 2210*. 2019;22(10):1536-1543. doi:10.1038/s41593-019-0480-6

63. Amtul Z, Atta-Ur-Rahman. Neural plasticity and memory: Molecular mechanism. *Rev Neurosci*. 2015;26(3):253-268. doi:10.1515/REVNEURO-2014-0075/ASSET/GRAPHIC/REVNEURO-2014-0075_FIG2.JPG

64. Basu J, Siegelbaum SA. The Corticohippocampal Circuit, Synaptic Plasticity, and Memory. *Cold Spring Harb Perspect Biol*. 2015;7(11):a021733. doi:10.1101/CSHPERSPECT.A021733

65. Aimone JB, Li Y, Lee SW, Clemenson GD, Deng W, Gage FH. Regulation and

function of adult neurogenesis: from genes to cognition. *Physiol Rev*. 2014;94(4):991-1026. doi:10.1152/PHYSREV.00004.2014/ASSET/IMAGES/LARGE/Z9J004142701000 7.JPEG

66. Yegla B, Boles J, Kumar | Ashok, Foster TC. Partial microglial depletion is associated with impaired hippocampal synaptic and cognitive function in young and aged rats. Published online 2021. doi:10.1002/glia.23975

67. Hansen D V, Hanson JE, Sheng M. Microglia in Alzheimer's disease. *J Cell Biol*. 2018;217(2):459-472. doi:10.1083/jcb.201709069

68. Geloso MC, Corvino V, Marchese E, Serrano A, Michetti F, D'Ambrosi N. The Dual Role of Microglia in ALS: Mechanisms and Therapeutic Approaches. *Front Aging Neurosci*. 2017;9(JUL). doi:10.3389/FNAGI.2017.00242

69. Lecours C, Bordeleau M, Cantin L, Parent M, di Paolo T, Tremblay MÈ. Microglial Implication in Parkinson's Disease: Loss of Beneficial Physiological Roles or Gain of Inflammatory Functions? *Front Cell Neurosci*. 2018;12. doi:10.3389/FNCEL.2018.00282

70. Li Q, Barres BA. Microglia and macrophages in brain homeostasis and disease. *Nat Rev Immunol*. 2018;18(4):225-242. doi:10.1038/NRI.2017.125

71. Jonsson T, Stefansson H, Steinberg S, et al. Variant of *TREM2* Associated with the Risk of Alzheimer's Disease. *N Engl J Med*. 2013;368(2):107-116. doi:10.1056/NEJMoa1211103

72. Guerreiro R, Wojtas A, Bras J, et al. TREM2 variants in Alzheimer's disease. *N Engl J Med*. 2013;368(2):117-127. doi:10.1056/NEJMoa1211851

73. Onuska KM. The Dual Role of Microglia in the Progression of Alzheimer's Disease. *J Neurosci*. 2020;40(8):1608-1610. doi:10.1523/JNEUROSCI.2594-19.2020

74. Leng F, Edison P. Neuroinflammation and microglial activation in Alzheimer disease: where do we go from here? *Nat Rev Neurol 2020 173*. 2020;17(3):157-172. doi:10.1038/s41582-020-00435-y

75. Chen X, Zhu B, Wu X, et al. TREM2 Is a Receptor for β-Amyloid that Mediates Microglial Function. *Neuron*. 2018;97(5):1023-1031.e7. doi:10.1016/j.neuron.2018.01.031

76. Sudom A, Talreja S, Danao J, et al. Molecular basis for the loss-of-function effects of the Alzheimer's disease–associated R47H variant of the immune receptor TREM2. *J Biol Chem*. 2018;293(32):12634-12646. doi:10.1074/JBC.RA118.002352

77. Sayed FA, Kodama L, Fan L, et al. AD-linked R47H-TREM2 mutation induces disease-enhancing microglial states via AKT hyperactivation. *Sci Transl Med*. 2021;13(622):eabe3947. doi:10.1126/SCITRANSLMED.ABE3947

78. Wang Y, Cella M, Mallinson K, et al. TREM2 lipid sensing sustains the microglial response in an Alzheimer's disease model. *Cell*. 2015;160(6):1061-1071. doi:10.1016/j.cell.2015.01.049

79. Jay TR, Miller CM, Cheng PJ, et al. TREM2 deficiency eliminates TREM2+ inflammatory macrophages and ameliorates pathology in Alzheimer's disease mouse models. *J Exp Med*. 2015;212(3):287-295. doi:10.1084/JEM.20142322

80. Wang Y, Ulland TK, Ulrich JD, et al. TREM2-mediated early microglial response limits diffusion and toxicity of amyloid plaques. *J Exp Med*. 2016;213(5):667-675. doi:10.1084/JEM.20151948

81. Hong S, Beja-Glasser VF, Nfonoyim BM, et al. Complement and microglia mediate early synapse loss in Alzheimer mouse models. *Science (80-)*. 2016;352(6286):712-716. doi:10.1126/SCIENCE.AAD8373/SUPPL_FILE/HONG.SM.PDF

82. Folick A, Cheang RT, Valdearcos M, Koliwad SK. Metabolic factors in the regulation of hypothalamic innate immune responses in obesity. *Exp Mol Med*. 2022;54(4):393-402. doi:10.1038/s12276-021-00666-z

83. Valdearcos M, Myers MG, Koliwad SK. Hypothalamic microglia as potential regulators of metabolic physiology. *Nat Metab 2019 13*. 2019;1(3):314-320. doi:10.1038/s42255-019-0040-0

84. Haddad-Tóvolli R, Dragano NRV, Ramalho AFS, Velloso LA. Development and function of the blood-brain barrier in the context of metabolic control. *Front Neurosci*. 2017;11(APR):224. doi:10.3389/FNINS.2017.00224/BIBTEX

85. Valdearcos M, Douglass JD, Robblee MM, et al. Microglial Inflammatory Signaling Orchestrates the Hypothalamic Immune Response to Dietary Excess and Mediates Obesity Susceptibility. *Cell Metab*. 2017;26(1):185-197.e3. doi:10.1016/j.cmet.2017.05.015

86. André C, Quevedo OG, Rey C, et al. Inhibiting Microglia Expansion Prevents Diet-Induced Hypothalamic and Peripheral Inflammation. *Diabetes*. 2016;66(4):908-919. doi:10.2337/DB16-0586

87. Kim JD, Yoon NA, Jin S, Diano S. Microglial UCP2 Mediates Inflammation and Obesity Induced by High-Fat Feeding. *Cell Metab*. 2019;30(5):952-962.e5. doi:10.1016/j.cmet.2019.08.010

88. Gao Y, Vidal-Itriago A, Milanova I, et al. Deficiency of leptin receptor in myeloid cells disrupts hypothalamic metabolic circuits and causes body weight increase. *Mol Metab*. 2018;7:155-160. doi:10.1016/J.MOLMET.2017.11.003

89. Butler MJ, Cole RM, Deems NP, Belury MA, Barrientos RM. Fatty food, fatty acids, and microglial priming in the adult and aged hippocampus and amygdala. *Brain Behav Immun*. 2020;89:145-158. doi:10.1016/J.BBI.2020.06.010

90. Spencer SJ, Basri B, Sominsky L, et al. High-fat diet worsens the impact of aging on microglial function and morphology in a region-specific manner. *Neurobiol*

Aging. 2019;74:121-134. doi:10.1016/J.NEUROBIOLAGING.2018.10.018

91. Bocarsly ME, Fasolino M, Kane GA, et al. Obesity diminishes synaptic markers, alters Microglial morphology, and impairs cognitive function. *Proc Natl Acad Sci U S A*. 2015;112(51):15731-15736. doi:10.1073/PNAS.1511593112/SUPPL_FILE/PNAS.1511593112.SAPP.PDF

92. Maruszak A, Thuret S. Why looking at the whole hippocampus is not enough-a critical role for anteroposterior axis, subfield and activation analyses to enhance predictive value of hippocampal changes for Alzheimer's disease diagnosis. *Front Cell Neurosci*. 2014;8(MAR):95. doi:10.3389/FNCEL.2014.00095/BIBTEX

93. Sims-Robinson C, Bakeman A, Bruno E, et al. Dietary reversal ameliorates short- and long-term memory deficits induced by high-fat diet early in life. *PLoS One*. 2016;11(9). doi:10.1371/journal.pone.0163883

94. Hao S, Dey A, Yu X, Stranahan AM. Dietary obesity reversibly induces synaptic stripping by microglia and impairs hippocampal plasticity HHS Public Access. doi:10.1016/j.bbi.2015.08.023

95. Vinuesa A, Bentivegna M, Calfa G, et al. Early Exposure to a High-Fat Diet Impacts on Hippocampal Plasticity: Implication of Microglia-Derived Exosome-like Extracellular Vesicles. *Mol Neurobiol*. Published online November 24, 2018:1-20. doi:10.1007/s12035-018-1435-8

96. Robison LS, Albert NM, Camargo LA, et al. High-Fat Diet-Induced Obesity Causes Sex-Specific Deficits in Adult Hippocampal Neurogenesis in Mice. *eNeuro*. 2020;7(1):391-410. doi:10.1523/ENEURO.0391-19.2019

97. McLean FH, Grant C, Morris AC, et al. Rapid and reversible impairment of episodic memory by a high-fat diet in mice. *Sci Rep*. 2018;8(1). doi:10.1038/s41598-018-30265-4

98. Alexaki VI. cells The Impact of Obesity on Microglial Function: Immune, Metabolic and Endocrine Perspectives. Published online 2021. doi:10.3390/cells10071584

99. Melo HM, Seixas da Silva G da S, Sant'Ana MR, et al. Palmitate Is Increased in the Cerebrospinal Fluid of Humans with Obesity and Induces Memory Impairment in Mice via Pro-inflammatory TNF-α. *Cell Rep*. 2020;30(7):2180-2194.e8. doi:10.1016/j.celrep.2020.01.072

100. Nicholas DA, Zhang K, Hung C, et al. Palmitic acid is a toll-like receptor 4 ligand that induces human dendritic cell secretion of IL-1β. *PLoS One*. 2017;12(5). doi:10.1371/JOURNAL.PONE.0176793

101. Tracy LM, Bergqvist F, Ivanova E V., Jacobsen KT, Iverfeldt K. Exposure to the Saturated Free Fatty Acid Palmitate Alters BV-2 Microglia Inflammatory Response. *J Mol Neurosci*. 2013;51(3):805-812. doi:10.1007/s12031-013-0068-7

102. Robblee MM, Kim CC, Abate JP, et al. Saturated Fatty Acids Engage an IRE1α-Dependent Pathway to Activate the NLRP3 Inflammasome in Myeloid Cells. *Cell Rep*. 2016;14(11):2611-2623. doi:10.1016/j.celrep.2016.02.053

103. Salvadó L, Palomer X, Barroso E, Vá Zquez-Carrera M. Targeting endoplasmic reticulum stress in insulin resistance. doi:10.1016/j.tem.2015.05.007

104. Zcan UO¨, Cao Q, Yilmaz E, et al. *Endoplasmic Reticulum Stress Links Obesity, Insulin Action, and Type 2 Diabetes*. Accessed April 4, 2021. http://science.sciencemag.org/

105. Shan B, Wang X, Wu Y, et al. The metabolic ER stress sensor IRE1α suppresses alternative activation of macrophages and impairs energy expenditure in obesity. *Nat Immunol 2017 185*. 2017;18(5):519-529. doi:10.1038/ni.3709

106. Hotamisligil GS. Endoplasmic Reticulum Stress and the Inflammatory Basis of Metabolic Disease. *Cell*. 2010;140(6):900-917. doi:10.1016/J.CELL.2010.02.034

107. Hummasti S, Hotamisligil GS. Endoplasmic reticulum stress and inflammation in obesity and diabetes. *Circ Res*. 2010;107(5):579-591. doi:10.1161/CIRCRESAHA.110.225698/FORMAT/EPUB

108. Wen H, Gris D, Lei Y, et al. Fatty acid-induced NLRP3-ASC inflammasome activation interferes with insulin signaling. *Nat Immunol*. 2011;12(5):408-415. doi:10.1038/ni.2022

109. Vandanmagsar B, Youm Y-H, Ravussin A, et al. The NLRP3 inflammasome instigates obesity-induced inflammation and insulin resistance. *Nat Med*. 2011;17(2):179-188. doi:10.1038/nm.2279

110. Guo DH, Yamamoto M, Hernandez CM, Khodadadi H, Baban B, Stranahan AM. Visceral adipose NLRP3 impairs cognition in obesity via IL-1R1 on CX3CR1+ cells. *J Clin Invest*. 2020;130(4):1961-1976. doi:10.1172/JCI126078

111. Butler MJ. The role of Western diets and obesity in peripheral immune cell recruitment and inflammation in the central nervous system. *Brain, Behav Immun - Heal*. 2021;16:100298. doi:10.1016/J.BBIH.2021.100298

112. Salameh TS, Mortell WG, Logsdon AF, Butterfield DA, Banks WA. Disruption of the hippocampal and hypothalamic blood-brain barrier in a diet-induced obese model of type II diabetes: Prevention and treatment by the mitochondrial carbonic anhydrase inhibitor, topiramate. *Fluids Barriers CNS*. 2019;16(1):1-17. doi:10.1186/S12987-018-0121-6/FIGURES/7

Chapter 2 Longitudinal Evolution of Hippocampal Microglial Activation in a Murine Model of Adolescent Obesity

2.1 Abstract

The global human population faces an obesity pandemic, affecting both children and adults. Clinical studies establish midlife obesity as a risk factor for dementia, and studies in children demonstrate cognitive deficits in varying domains. The precise mechanism of obesity-induced cognitive impairment remains incompletely understood but may involve activation of microglia, the resident innate immune cells of the brain. Activated microglia are proposed to contribute to cognitive impairment by phagocytosing neuronal synaptic spines. Thus, targeting microglial activation could constitute a potential therapeutic avenue. However, the progression of microglial activation over time from acute to chronic exposure to obesogenic diets remains unclear, including in youth. High-fat diet (HFD) rodent models, which develop metabolic dysfunction and cognitive impairment mirroring humans, offer an opportunity to investigate evolution in microglial activation during adolescent brain development. We investigated hippocampal microglial activation longitudinally by cellular morphology following acute (2 weeks), intermediate (1 month [mo]), and chronic (3 mo) HFD beginning at 5 weeks of age. We found that HFD did not significantly alter microglial morphology in the CA1 region of the hippocampus.

2.2 Introduction

The global prevalence of obesity has dramatically increased in the past several decades [1,2]. Alongside obesity comes the burden of numerous systemic complications that arise from obesity and associated metabolic dysfunction. In the central nervous system, obesity increases the risk of stroke, psychiatric disease, and dementia [3–6]. Indeed, several clinical studies demonstrate that midlife obesity predisposes individuals to cognitive impairment and dementia in later life [5,7,8]. Unfortunately, the rising obesity rates are not limited to adults, as childhood obesity is also on the rise [9,10]. Given that the developing brain manifests a unique and especially plastic physiological state [11] compared to the adult brain, the effect of obesity on cognition may be distinct in different phases of the lifespan. Several investigations demonstrate that obesity adversely impacts cognitive performance in children [12–14]. Unfortunately, mechanisms mediating obesity-induced cognitive deficits are poorly understood. To develop preventative strategies, or therapeutics to reverse or slow cognitive deficits, we must better understand these mechanisms. Further, we must elucidate how age interacts with the effects of obesity on the brain, to appropriately target interventions to the developing, adult, or aging brain.

In the brain, the hippocampus plays a role in learning and memory, and the hippocampus is particularly affected by pathology in Alzheimer's disease [15], the most common type of dementia. Hippocampal cognitive deficits associated with human obesity are mirrored in animal models of obesity. Rodents fed a high-fat diet (HFD) enriched in saturated-fatty acids develop obesity and exhibit hippocampal-dependent cognitive impairment [16,17]. Rodent models have facilitated investigations into the

pathophysiology of obesity-induced cognitive impairment. The presence of systemic inflammation in obesity is a well-studied phenomenon, and inflammation has been implicated in driving complications such as insulin resistance and cardiovascular disease [18–21]. An inflammatory response to HFD also occurs in the brain, where microglia, the macrophage-like innate immune cells of the central nervous system, take on a pro-inflammatory activation state [16,17,22]. Like other complications of obesity, evidence suggests that the immune response may play a role in driving the pathology responsible for cognitive deficits

The role of HFD induced hypothalamic microglial activation in mediating eating behaviors and obesity has been well characterized [22–25]. Like in the hypothalamus, studies report that HFD activates hippocampal microglia in animal models. However, many questions remain regarding the role of microglial activation in obesity-induced hippocampal-dependent cognitive impairment. Acute HFD ingestion of only a few days activates innate immune inflammatory pathways in the hippocampus, including upregulated hippocampal pro-inflammatory cytokines and NLRP3 inflammasome expression [26,27]. Longer-term HFD feeding, including in young adolescent mice [28], has been shown to activate microglia in the hippocampus [16,17], and microglial activation contributes to cognitive impairment [16].

Whether hippocampal microglia become activated earlier on, and how this activation may change over time is not clear. An understanding of obesity-induced temporal changes in hippocampal microglia can shed insight into disease mechanisms and suggest possible windows for therapeutic intervention. Microglia are a heterogenous population of cells [29], manifesting a range of phenotypic states depending on context.

Research has relied heavily on measures of morphology to indicate activation state, because morphology can transition from ramified (homeostatic morphology), to other states including hyper-ramified, hypo-ramified, or amoeboid in response to stimuli [30,31]. The highly ramified, complex processes in homeostatic microglia characteristically retract when microglia are reacting to a pathological insult [30,32]. In addition to de-ramification [33], cell somas increase in size in reactive microglia [34]. Herein, we investigated hippocampal microglial activation longitudinally in young animals through changes in cellular morphology following a paradigm of subacute (2 weeks), intermediate (1 month), and chronic (3 months) HFD beginning at 5 weeks of age. Employing an adapted 3D Morph protocol [35], we analyzed the three-dimensional morphology of individual microglia in a relatively high throughput manner, characterizing over 1,800 cells. We found that HFD induced obesity and metabolic dysfunction after only 2 weeks HFD, both of which increased in severity over time by 3 months. Our results show that despite metabolic impairment, HFD-fed mice do not display hippocampal microglial morphological differences compared to control-fed mice. These findings suggest that the effect of obesity on hippocampal microglia may be subtle in young, adolescent mice, and that more sensitive techniques than morphology measures alone are required to define the impact on microglial activation.

2.3 Results

2.3.1 HFD induces obesity and systemic metabolic dysfunction

Herein, we employed our HFD-induced mouse model of obesity [36,37] and cognitive impairment [38], which mirrors obesity and associated cognitive impairment in humans. In this model, wild-type mice fed HFD, a diet enriched in saturated fatty acids, develop obesity, glucose intolerance, dyslipidemia, and hyperinsulinemia. Mice aged 5 weeks (wk), were fed HFD or control diet for 2 wk (subacute), 1 mo (intermediate), and 3 mo (chronic) (**Fig 2.1A**). As anticipated, HFD mice weighed significantly more than their control-fed counterparts at all durations of diet (**Fig 2.1B**). Subacute 2-wk HFD duration already increased the weight of mice versus control diet (P=0.0013, Sidak's multiple comparisons test for mixed effects model). At all time points, HFD also induced glucose tolerance deficits, characterized by elevated peak glucose following glucose bolus challenge (**Fig 2.2A**). Although HFD mice were glucose intolerant within 2 wk, they did not develop hyperinsulinemia until 3 mo had elapsed (P<0.0001, Sidak's multiple comparisons test for ordinary two-way ANOVA) (**Fig 2.2B**). We also noted that HFD induced dyslipidemia in mice, evidenced by elevated levels of both total cholesterol (P<0.0001, Sidak's multiple comparisons test for ordinary two-way ANOVA) and high-density lipoprotein (HDL) (P<0.0001, Sidak's multiple comparisons test for ordinary two-way ANOVA) after 3 mo (**Fig 2.2D-E**).

2.3.2 HFD does not significantly alter hippocampal microglial volumes

Next, to determine whether HFD affects hippocampal microglial activation over time, we quantified three-dimensional (3-D) cellular morphology measures as indicators of activation state. Under homeostatic conditions, microglia surveil their environment by extending highly branched processes; however, in response to pathological conditions,

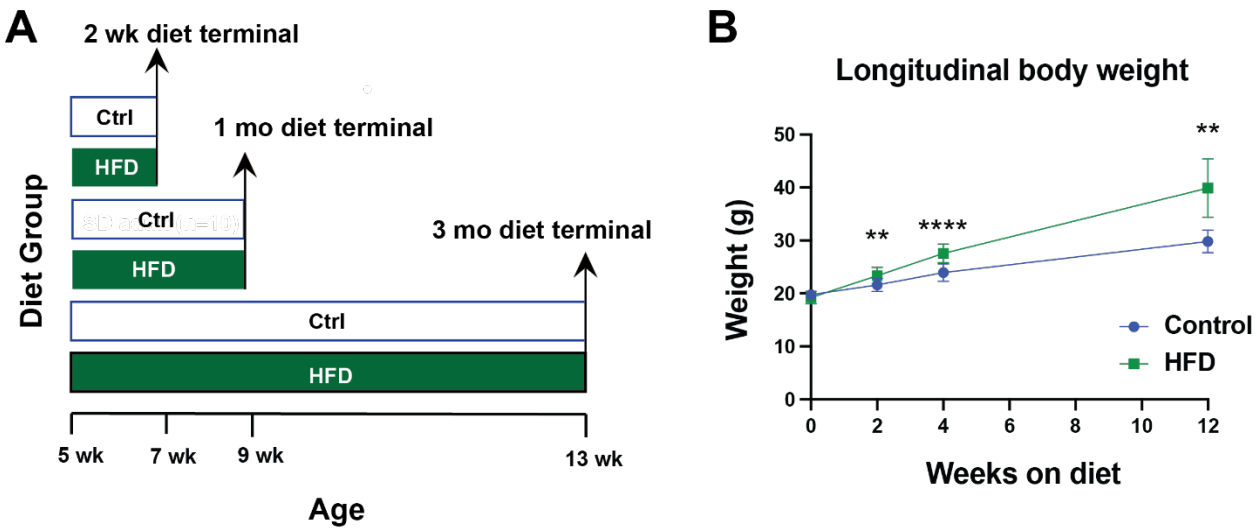

Figure 2.1 HFD induces obesity in adolescent mice.

(A) Study scheme: 5-wk old mice were fed high-fat diet (HFD) or control standard diet (ctrl) for 2 wk, 1 mo, and 3 mo. At each terminal point, brains were collected for microglial morphology and plasma for measures of metabolic health. (B) Longitudinal body weight for control (blue, circles) and HFD (green, squares) mice from baseline to study termination for 2 wk, 1 mo, and 3 mo cohorts combined. **P<0.01, ****P<0.0001 by Sidak's multiple comparisons test for mixed effects model; n=21 per group at 0 and 2 wk, n=14 per group at 4 wk, and n=7 per group at 12 wk.

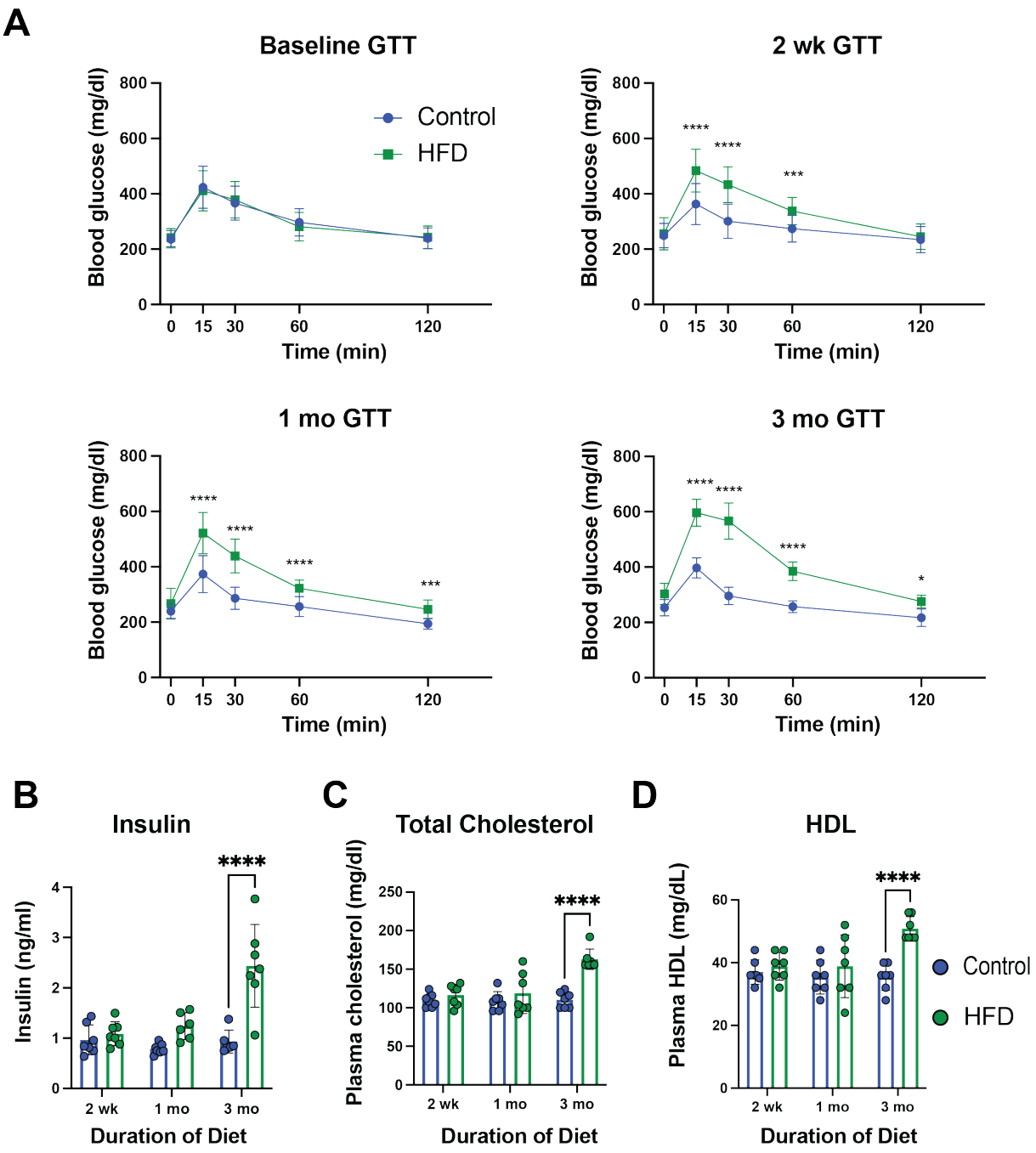

Figure 2.2 HFD induces systemic metabolic dysfunction at as early as 2 weeks.

(A) Baseline and terminal glucose tolerance tests (GTTs) for control and HFD mice at 0 wk, 2 wk, 1 mo, and 3 mo of diet. Glucose levels were measured from one drop of tail blood at 0, 15, 30, 60, and 120 minutes (min) after a bolus of 1 g glucose/1 kg body weight. Values exceeding the upper threshold of the glucometer were set at that threshold, 750 mg/dl. Terminal fasting plasma (B) insulin, (C) total cholesterol, (D) high density lipoprotein (HDL) for control and HFD mice at 2 wk, 1 mo, and 3 mo terminal time points. *P<0.05, ***P<0.001, ****P<0.0001 by Sidak's multiple comparisons test for repeated measures two-way ANOVA for GTTs and Sidak's multiple comparisons test for ordinary two-way ANOVA for insulin, cholesterol, and HDL; n=21 mice per group for baseline GTT, n=19-21 per group for 2 wk GTT, n=14 per

group for 1 mo GTT, and n=7 per group for 3 mo GTT; n=7 per group for total cholesterol and HDL and n=6-7 per group for insulin. Error bars represent mean ± standard deviation.

microglia shift their morphology by retracting processes, reducing branching, and covering less territory [30,33,35]. The microglial marker ionized calcium binding adaptor molecule 1 (Iba1) was used for immunohistochemistry to identify microglia. Brain sections were imaged by confocal microscopy and 3-D z-stacks of the hippocampus were analyzed using a modified 3D-Morph protocol [35], which relies on methods such as convex hull analysis and skeletonization to measure territorial volume, cell volume, ramification complexity, number of endpoints per cell, number of branchpoints per cell, and average, minimum, and maximum branch length for every individual cell. We analyzed microglia in the CA1 region (three z-stacks per animal; **Fig 2.3A**) of the hippocampus, focusing on the stratum radiatum, where effects of obesity on microglial morphology have been reported [16,28].

Territorial volume comprises the 3-D space occupied by the microglia itself and the space trapped within extended microglia processes, outlined by a polygonal convex hull. Cell volume is the volume of the cell itself, and complexity is measured using the ramification index, which is the ratio of territorial volume to cell volume. There were no differences in territorial volume or cell volume between HFD and control microglia at any duration of diet (by nested t-test **Fig 2.3B-C**). As expected, given that the ramification index is a ratio of territorial volume to cell volume, there were also no differences in complexity between HFD and control microglia (**Fig 2.3D**).

2.3.3 HFD does not induce de-ramification in CA1 hippocampal microglia

Next, the 3D-Morph pipeline skeletonizes each individual cell and counts endpoints, branchpoints, and branch lengths (**Fig 2.4A**). The number of branchpoints and endpoints would be expected to decrease if microglia are manifesting a reactive or pro-inflammatory state. We found that number of endpoints per cell (**Fig 2.4B**) and number of branchpoints per cell (**Fig 2.4C**) did not differ between control and HFD microglia at 2 wk, 1 mo, or 3 mos (by nested t-test). Additionally, the average branch length per cell (**Fig 2.4D**) as well as the minimum (**Fig 2.5A**) and maximum (**Fig 2.5B**) did not differ by diet group at any time point (by nested t-test).

2.3.4 Hippocampal CA1 microglia decrease in size from adolescence to adulthood

There were no detected differences in microglial morphology between HFD and control microglia when compared at each duration of diet, but we next wanted to determine whether there was an effect of time or time by diet interaction on morphology. We, therefore, performed linear mixed effects regression modeling [36]. We found that cell volume decreased in the HFD group from 2 wk to 3 mo (P=0.0318) (**Fig 2.6A**). However, there was no significant difference in this reduction between HFD and control, suggesting that microglial volume reduces over time independent of diet. Additionally, this model demonstrated a significant reduction in minimum branch length in HFD versus control microglia at 2 wk (P=0.0472) (**Fig 2.6B**). Aligning with the within time point comparisons by nested t-test above, the majority of the comparisons demonstrated non-significant differences (data not shown).

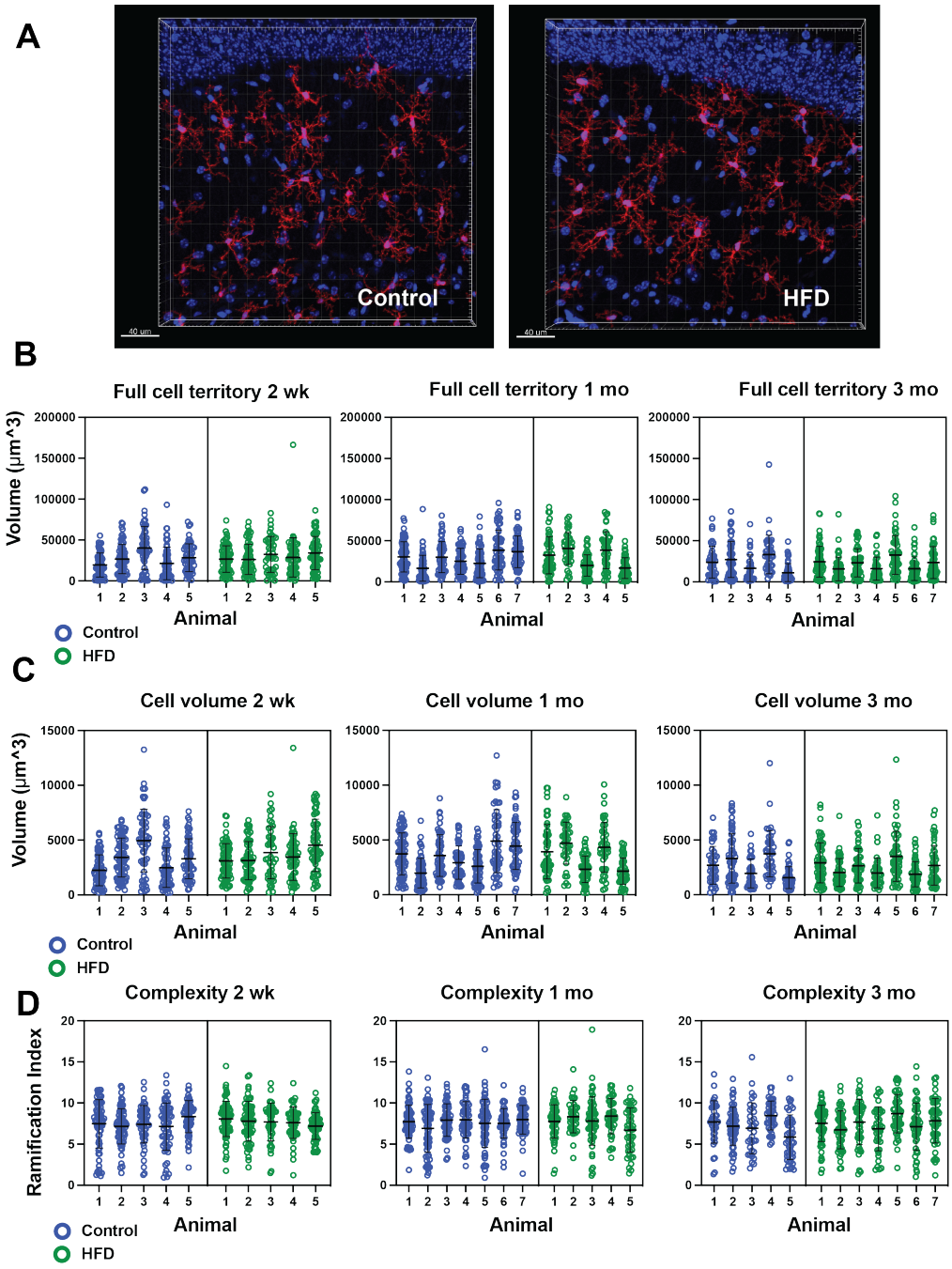

Figure 2.3 HFD does not alter microglial territory or volume in the hippocampal CA1 region of adolescent mice.

(A) Representative images of 3-D rendering of z-stacks for Iba1-stained microglia in the hippocampal CA1 for control (left) and high-fat diet (HFD) mice. Hoescht nuclear fluorescence signal in blue and Iba1 signal in red. Red channel represents pre-processed z-stacks for extraction of intact microglia cells. (B) Full cell territory for control (blue) and HFD (green) microglia at 2 wk (left), 1 mo (center), and 3 mo (right). Cell territory is the three-dimensional space encompassed within a polygon surrounding the outermost branches of the cell. Each point represents a single cell and individual animals are plotted along the x-

axis. (C) Cell volume for control and HFD microglia at 2 wk (left), 1 mo (center), and 3 mo (right). Cell volume is the volume of the cell body and branches of the cell itself, and is calculated by scaling image voxels to micron units. (D) Cell complexity measured by the ramification index (ratio of cell territory to cell volume) for control and HFD microglia at 2 wk (left), 1 mo (center), and 3 mo (right). No significant differences in HFD versus control group by nested t-test. n=5-7 mice per group, three CA1 z-stacks analyzed per mouse, 39 to 75 microglia analyzed per mouse. Error bars represent mean ± standard deviation.

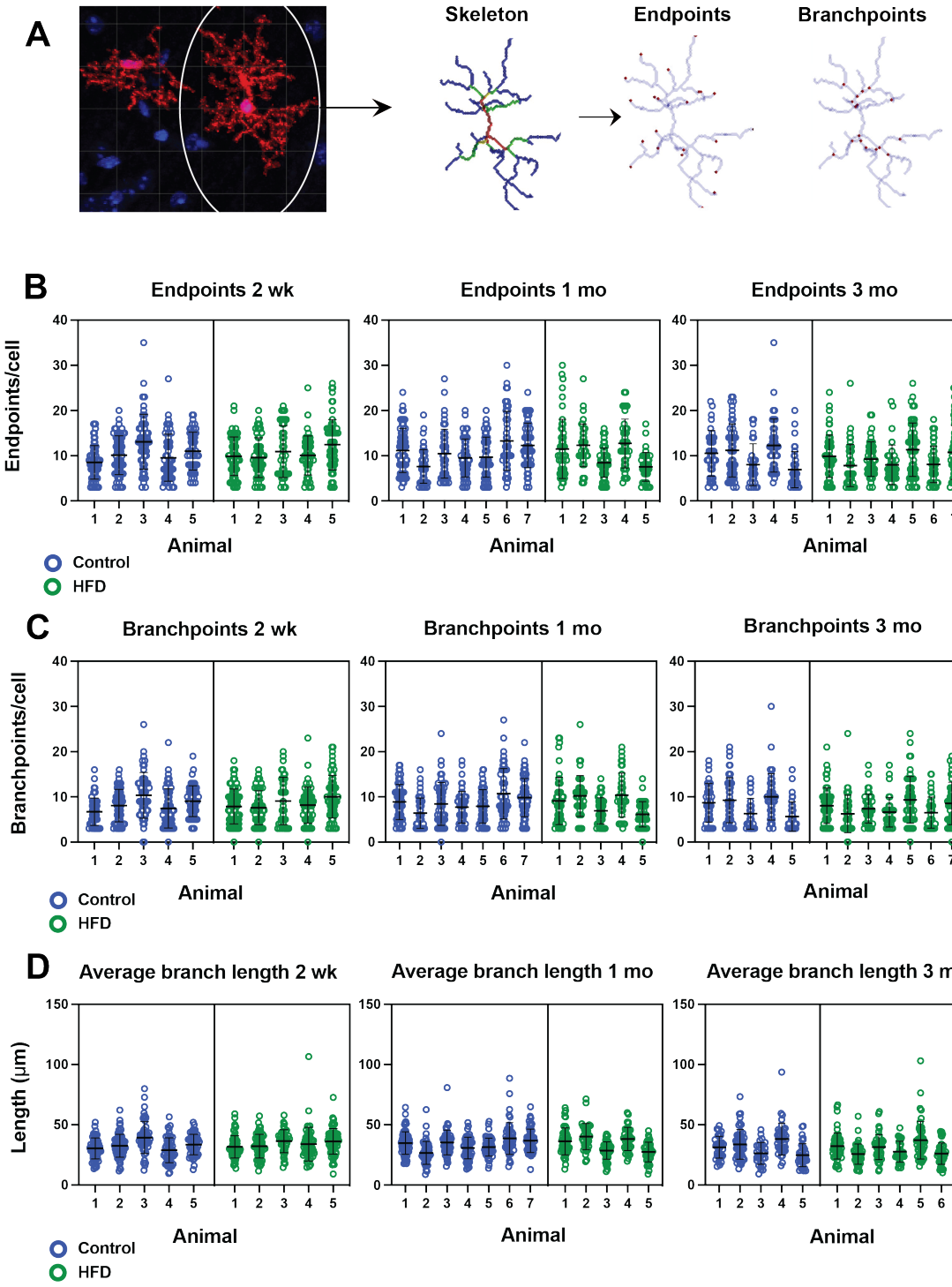

Figure 2.4 HFD does not alter microglial ramification in the CA1 of adolescent mice.

(A) Example of skeletonization (center) from Iba1 stained 3-D microglia (left). Running the 3DMorph pipeline in MATLAB yields endpoints per cell and branchpoints per cell (right). (B) Endpoints per cell for control (blue) and HFD (green) microglia at 2 wk (left), 1 mo (center), and 3 mo (right). Each point represents a value for a single cell and individual animals are plotted along the x-axis. (C) Branchpoints per cell for control (blue) and HFD (green) microglia at 2 wk (left), 1 mo (center), and 3 mo (right). (D) Average branch length per cell for control (blue) and HFD (green) microglia at 2 wk (left), 1 mo (center), and 3 mo (right). No significant differences in HFD versus control group by nested t-test. n=5-7 mice per group, three CA1 z-stacks analyzed per mouse. Error bars represent mean ± standard deviation.

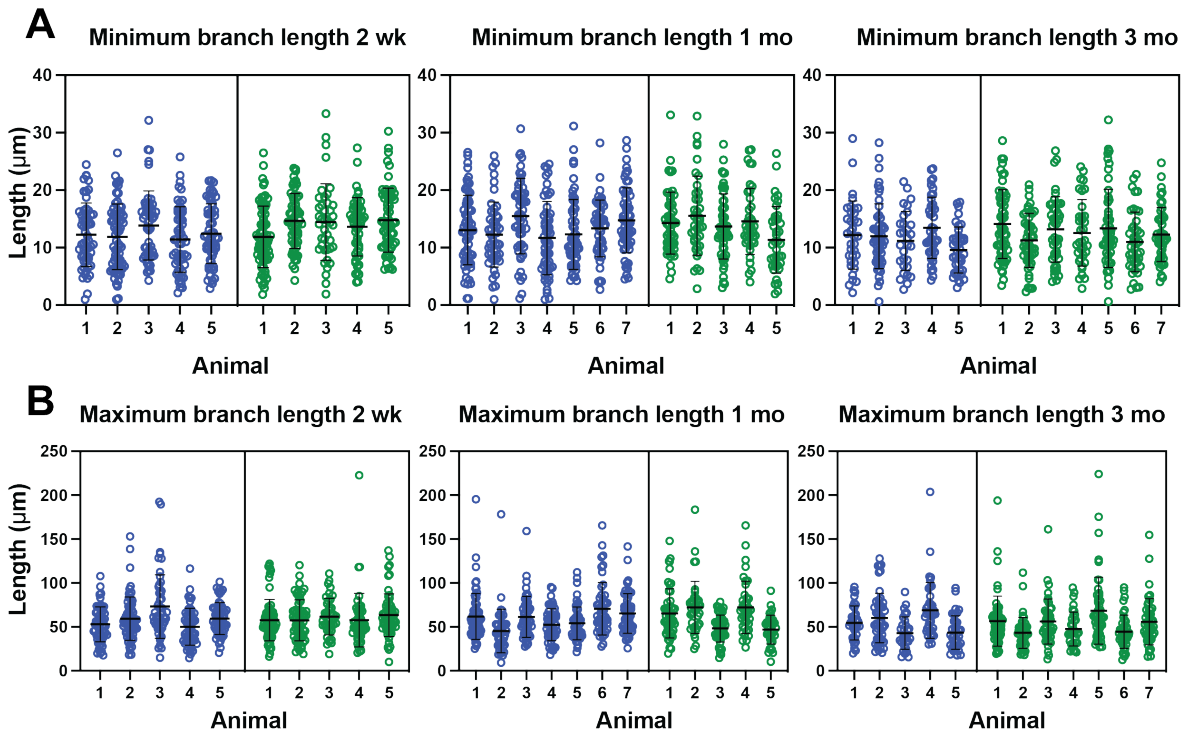

Figure 2.5 HFD does not alter microglial minimum or maximum branch length.

Minimum (A) and maximum (B) branch length per cell for control (blue) and HFD (green) microglia at 2 wk (left), 1 mo (center), and 3 mo (right). Each point represents a value for a single cell and individual animals are plotted along the x-axis. No significant differences in HFD versus control group by nested t-test. n=5-7 mice per group, three CA1 z-stacks analyzed per mouse. Error bars represent mean ± standard deviation.

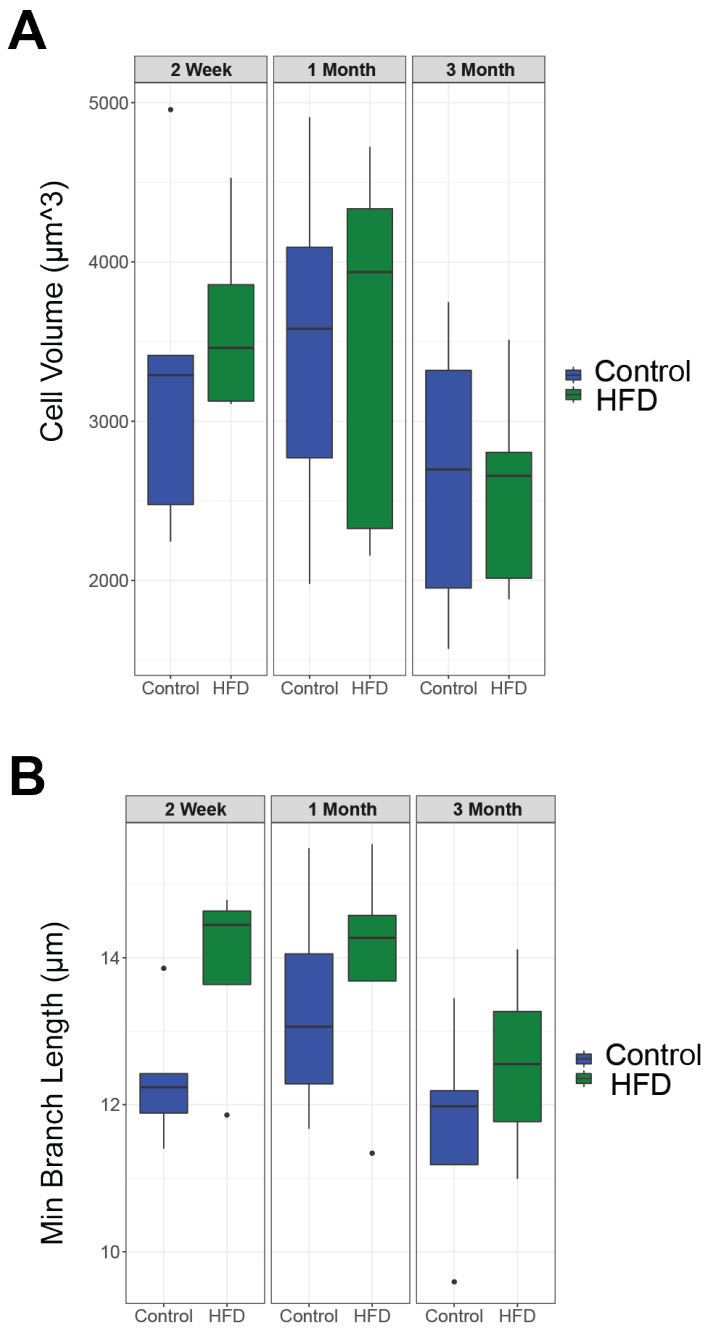

Figure 2.6 Linear mixed effects model results of cell volume and minimum branch length.

(A) Boxplot of cell volume at 2 wk (left), 1 mo (center), and 3 mo (right) and (B) boxplot of minimum branch length at 2 wk (left), 1 mo (center), and 3 mo (right). The boxplots display 5 summary statistics: The box represents the 25th percentile, median, and 75th percentile of the data. The whispers extend to 1.5 times the interquartile range (IQR) above the 75th percentile and below the 25th percentile, where IQR = 75th percentile - 25th percentile. Data Points beyond 1.5 times the IQR are plotted individually. Each datapoint represents the mean value across cell measurements for each animal individually. Control in blue and HFD in green.

2.3.5 Microglial morphological measures associate with metabolic function

By examining each cell morphology measures plotted by animal on the x-axis (**Figs 2.3B-D**, **2.4B-D**, and **2.5A-B**), we noticed a considerable degree of variation between animals, even within the same diet group (**Fig 2.3B-D**, **Fig 2.4B-D**, and **Fig 2.5A-B**). Although we did not find differences between HFD and control morphology measures in the aggregate data based on the means of each experimental group, we asked whether measures of metabolic function might associate with morphology. We, therefore, again used a linear mixed effects regression model [36] to examine the association between each morphology measure (cell territory, cell volume, complexity, number of endpoints, number of branchpoints, average branch length, minimum branch length, and maximum branch length) and terminal measures of metabolic health (weight, plasma insulin, plasma cholesterol, plasma HDL). Significant associations included an association between decreased cell volume (**Fig 2.7A**) and decreased cell territory (**Fig 2.7B**) with increased cholesterol in the HFD group. The association between cholesterol and cell volume/cell territory was not significantly different between HFD and control groups, suggesting that the relationship between cholesterol and these outcomes was not unique to specific ranges of actual cholesterol levels, high (HFD group) or normal (control group).

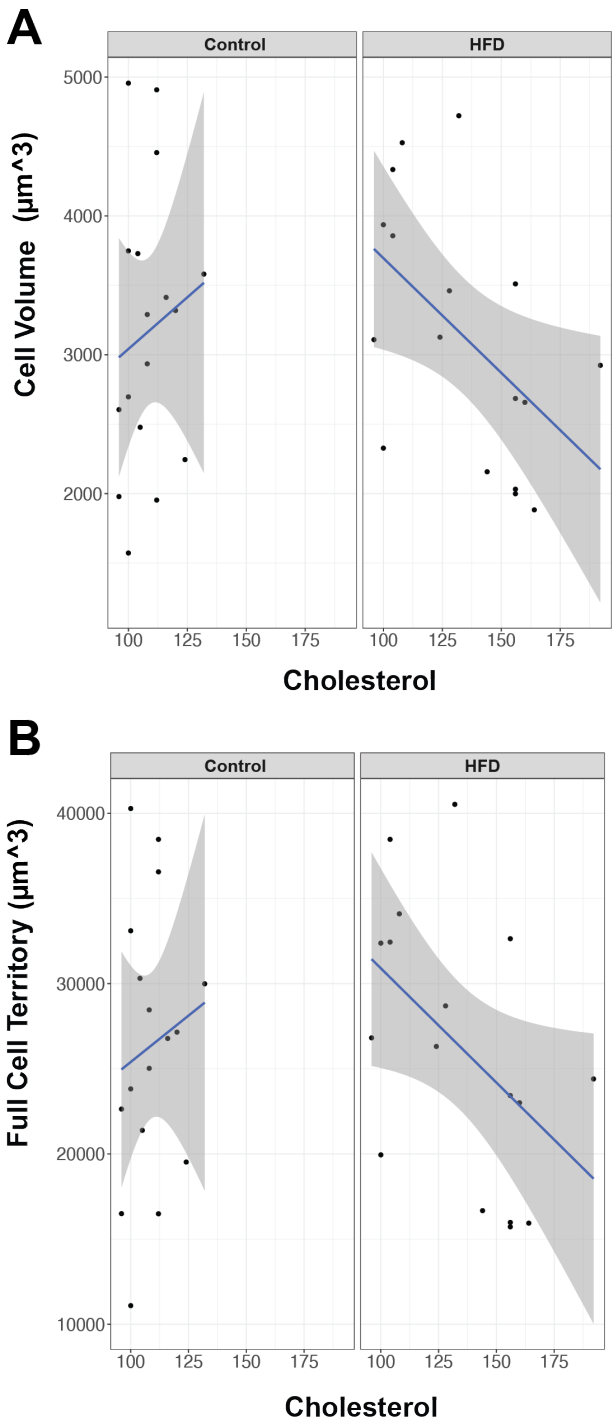

Figure 2.7 Association between cholesterol and cell volume or cell territory.

(A) Scatterplot of terminal cholesterol (x-axis) and cell volume (y-axis), across all time points, and (B) scatterplot of terminal cholesterol (x-axis) and full cell territory (y-axis), across all time points. Each datapoint represents the mean value across cell measurements for each animal individually. Plotted line represents results from a linear regression model fit between each outcome and cholesterol, stratified by diet. Shaded area represents a 95% confidence interval corresponding to the fitted linear regression line.

2.4 Discussion

Activated microglia are proposed to contribute to obesity-induced cognitive impairment by aberrantly over phagocytosing dendritic spines [16]. However, evolution and drivers of hippocampal microglial activation in obesity remain unknown. Immune responses occur in acute and chronic phases, so investigating the evolution of microglial activation in obesity is critical both for generating insight into potential disease mechanisms, and for suggesting optimal windows for intervention. Indeed, studies in HFD rodent models have reported acute pro-inflammatory responses in the hippocampus [27,39] and activation of microglia after long-term exposure to HFD [16,17]. However, studies of microglial activation have generally reported only a single time point following intermediate to chronic HFD, *e.g.*, after diet duration of 6 wk [28], 3 mo [16,17], and even longer [40]. Reports examining hippocampal microglial activation at acute time points, *e.g.*, a few days to a couple of weeks, are sparse [41,42]. Here, to address this gap, we assessed hippocampal microglial activation longitudinally, using metrics of 3-D cellular morphology as indicators of activation state. We followed a paradigm of 2 wk, 1 mo, and 3 mo of HFD duration to model subacute, intermediate, and chronic exposure, respectively starting in mice at 5 wk of age, and continuing throughout adolescence. Using our HFD model, we found that HFD did not significantly alter any measure of hippocampal CA1 region microglial morphology at any duration of diet examined in the current study.

We found that mice developed obesity and progressively poorer metabolism. HFD caused obesity in mice, characterized by weight gain. Metabolic dysfunction became gradually worse with time; by 3 mo of diet, HFD mice exhibited

hyperinsulinemia, elevated total cholesterol, and elevated HDL. These observations align with our previous work [37,43,44] and work by others [45–48], including after acute HFD exposure. Indeed, only 3 days of HFD already impairs glucose homeostasis in mice without changes to body weight or adipocyte size [49]. This model robustly and consistently develops obesity along with other features of metabolic dysfunction reflective of obese humans.

Next, we examined the influence of HFD on microglia morphology in the hippocampus. We focused on the CA1 stratum radiatum, where microglial morphology changes have been reported in HFD-fed mice [16,28]. We found that HFD, at early and chronic durations of diet, did not alter territorial volume, cell volume, or complexity of microglia in the hippocampal CA1 region. Further, we detected no differences in number of endpoints or branchpoints per cell, or in branch lengths. No reports, to our knowledge, demonstrate hippocampal microglial activation in response to HFD after durations of diet as short as 2 wk. Our findings at the more chronic time points of 1 mo and 3 mo diet parallel a study that reported no effect of prolonged HFD on hippocampal microglial morphology [50]. However, they do not align with other reports of HFD-induced hippocampal microglial morphological activation [16,17,28,51].

Due to the unique physiology of the developing, adolescent brain [52], we expected that age of diet onset may play a critical role in microglial responses. Thus, we compared our results to studies using a diet-induced obesity model in more similarly aged, adolescent mice. In mice started on diet at 6 wk of age and fed for 3 mo, obesity increased the number of ‘simple’ microglia, with 1 or 2 primary processes, and increased the proportion of ‘simple’ microglia co-staining for MHCII in the dentate gyrus,

[17]. Perhaps the difference in hippocampal region examined (dentate gyrus versus CA1) could help explain the differences between this study and our results reported here, although morphological measures of activation occurred in both the dentate gyrus and CA1 in the study of 8 wk old mice described above [16]. In a study of adolescent mice begun at 3 wk age and fed HFD until around 2 mo age, the researchers found morphological activation of CA1 stratum radiatum and dentate gyrus hilus microglia by quantifying an increase in area covered by cell somas [28]. In an earlier study they found that HFD administered for 4 mo starting at 4 wk age also increased Iba1+ cell soma area in the stratum radiatum and hilus [51]. It is difficult to directly compare these results to our findings in the CA1 region, given that metrics for morphological activation differed. We are currently quantifying cell soma volume in the CA1, which will allow us a more direct comparison to the metric of cell soma area.

Although not directly comparable to our adolescent paradigm, beginning diet at 5 wk age, reports on hippocampal microglia morphology in mice started on diet at 8 wk of age and fed for 12 to 24 wk, demonstrate mixed findings and our results parallel one such study. A study feeding HFD for 24 wk did not alter CA1, CA3, or dentate gyrus microglial morphology, based on measures including skeleton length, soma area, convex hull area, and cell perimeter [50]. However, in another study, 12 weeks of HFD increases the activation score of microglia in the dentate gyrus and CA1 stratum radiatum [16]. The activation measure in this study represented a score of morphology metrics (primary process counts, cell body area) and CD68 co-expression (marker of phagocytic activity) [16]. At 8 wk (2 mo) of age, mice from these two studies were further

through adolescence at the initiation of HFD, as 3 mo is considered the beginning of mature adulthood in mice.

Differences in morphology metrics (soma area versus branching patterns) may contribute to the differences in findings. Variation in results using morphological measures of activation might also suggest the limitation of relying heavily on morphology to infer microglial phenotype state, and the need to supplement with additional approaches such as transcriptomics, particularly if changes in phenotype are subtle. While the differences in choice of morphology metrics reported in studies may help explain variability in conclusions, it is also likely that changes in hippocampal microglia morphology are subtle in the young, adolescent age group. The immune system becomes dysfunctional in the normal aging process [53,54], and microglia might be more susceptible to diet-induced perturbations in older animals. For example, when aged and young rats were fed HFD for only 3 days, HFD impaired hippocampal and amygdalar dependent cognition and elevated MHCII expression in hippocampi in old, but not young animals [42]. In a follow-up study the research group found an effect of advanced age on microglial morphology, but no additional effect of HFD after 3 days [41]. In summary, our findings raise important questions regarding the nature of obesity-induced hippocampal microglial activation that require further study. Future work is needed to clarify the hippocampal microglial response to HFD, and a particular focus on the impact of age and technical approach are required to elucidate effects on the microglial activation phenotype that might prove subtle in nature.

2.5 Methods

2.5.1 Animals and study design

Wild-type C57BL/6J male mice aged 4 wk (Jackson Laboratory, cat# 000664) were housed in cages with littermates in a specific-pathogen-free facility kept at 20 ± 2 °C with a 12/12-h light/dark maintained by the Unit for Laboratory Animal Medicine (ULAM) at the University of Michigan. ULAM veterinary staff monitored the health of the animals daily. When mice had acclimated for 1 wk following arrival to the facility, *i.e*., were 5 wk of age, they were randomized to two dietary groups, control and HFD, for three possible regimen durations, 2 wk, 4 wk (1 mo), and 12 wk (3 mo). Thus, the study comprised 6 groups of 7 mice each, for a total of 42 animals. Diets were provided *ad libitum* along with free access to water. Control diet comprised 10% kcal derived from fat (Research Diets, cat# D12450J), and HFD was composed of 60% kcal derived from fat (Research Diets, cat# D12492). Animals were sacrificed at study termination at 2 wk, 1 mo, and 3 mo by intraperitoneal pentobarbital injection (Fatal-Plus, Vortech Pharmaceuticals) followed by perfusion with phosphate buffered saline. The study and all procedures (see sections below) were approved by the University of Michigan's Institutional Animal Care and Use Committee (IACUC; protocol numbers PRO00010039 and PRO00010247).

2.5.2 Metabolic phenotyping

Metabolic phenotyping included baseline, longitudinal, and terminal body weights, and baseline and terminal glucose tolerance tests, and were performed as

previously described [37]. Terminal plasma insulin, total cholesterol, HDL, and triglycerides were measured. Baseline glucose tolerance tests (GTTs) were performed just prior to diet initiation for all animals, *i.e.*, when aged 5 wk. Terminal GTTs were performed at study termination just prior to sacrifice at 2 wk, 1 mo, and 3 mo. For GTTs, mice were fasted for a minimum of 4 hours (h) and administered an intraperitoneal injection of 1 g glucose /kg body mass in normal saline. Blood glucose levels were measured by glucometer (AlphaTrak, Abbott Laboratories) from one drop of tail blood at baseline and 15, 30, 60, and 120 minutes (min) after glucose injection. Terminal plasma insulin (ELISA), total cholesterol, HDL, and triglycerides (lipid profiles measured on the Randox RX Daytona+) were quantified following established protocols by the Michigan Diabetes Research Center Chemistry Laboratory.

2.5.3 Microglial immunohistochemistry

One brain hemisphere from each mouse was dissected at study termination at 2 wk, 1 mo, and 3 mo just following sacrifice. Brain hemispheres were fixed in 4% paraformaldehyde for ~ 48 h followed by serial 10%, 20%, and 30% sucrose for ~24 h at each concentration. Hemibrains were sectioned to 45 μm thickness and floating sections were stained by immunohistochemistry in rabbit anti-Iba1 (1:1000; Wako, cat# 019-19741) at 4 °C overnight. Next, sections were incubated in goat-anti rabbit secondary antibody (1:2000, Alexa fluor Plus 594; Invitrogen, cat# A32740) for 2 h at room temperature followed by a Hoechst nuclear stain (1 mg/ml; Sigma-Aldrich, cat# 861405) for 8 min. Sections were mounted using ProLong Gold Antifade Mountant (Thermo Fisher Scientific, cat# P36930).

2.5.4 Microglial morphological analysis

Iba1-stained sections were imaged and z-stacks captured using a 40X objective with oil immersion on a Nikon A1 confocal microscope. Z-stacks 27 μm in thickness were pre-processed using Imaris Software (Oxford Instruments). Intact microglia (containing overlap of nuclear staining with Iba1 staining) were identified via the surface rendering tool and a mask was generated to isolate their fluorescence signal from the raw data and exclude branches not associated with cell somas. Cells with somas within the CA1 pyramidal layer were deleted prior to MATLAB processing. Pre-processed z-stacks were saved as open microscopy environment TIF files, which were analyzed by an adapted 3DMorph script using MATLAB [35]. Cells touching the X-Y border of the z-stack were eliminated as partial cells. Partial cells on the edge of the z-stack were included, but required to have nuclear Hoescht signal overlapping with Iba1 fluorescence. Results were then curated manually to eliminate objects misidentified as cells (or cell objects containing 2 nuclei) from the final dataset. The CA1 regions of the hippocampus from each animal was analyzed by 3 consecutive images centered around the stratum radiatum of CA1. A total of 35 to 75 cells per animal at each time point were included in the final analysis for a total of 1,857 cells analyzed. Cells that 3DMorph failed to skeletonize in MATLAB were included in territorial volume, cell volume, and complexity results, but excluded from branch and endpoint results.

2.5.5 Statistical methods

Statistical analyses were performed in Prism (GraphPad) and R software version 4.1.1. Body weights were analyzed by mixed effects model, GTTs by two-way ANOVA with repeated measures, insulin, cholesterol, HDL, and triglycerides by ordinary two-way ANOVA, all with Sidak's multiple comparisons test. Linear mixed effects models with random animal-specific intercepts were used to determine the association between microglial cell morphology measures, treatment group (HFD vs control), duration of diet (2 weeks, 1 month, 3 months), and individual terminal metabolic factors (weight, cholesterol, HDL, insulin, triglycerides). The mixed effects models were fit using the lmerTest package in R and model parameter estimates were determined using the maximum likelihood method [55]. T-tests performed using Satterthwaite's degrees of freedom method were evaluated to assess differences in morphology measurements between treatment groups and diet duration groups. To visually confirm assumptions of normality, histograms were used.

2.6 Bibliography

1. Blüher M. Obesity: global epidemiology and pathogenesis. *Nat Rev Endocrinol 2019 155*. 2019;15(5):288-298. doi:10.1038/s41574-019-0176-8
2. Di Cesare M, Bentham J, Stevens GA, et al. Trends in adult body-mass index in 200 countries from 1975 to 2014: a pooled analysis of 1698 population-based measurement studies with 19·2 million participants. *Lancet (London, England)*. 2016;387(10026):1377-1396. doi:10.1016/S0140-6736(16)30054-X
3. Luppino FS, De Wit LM, Bouvy PF, et al. Overweight, obesity, and depression: a systematic review and meta-analysis of longitudinal studies. *Arch Gen Psychiatry*. 2010;67(3):220-229. doi:10.1001/ARCHGENPSYCHIATRY.2010.2
4. Scott KM, Bruffaerts R, Simon GE, et al. Obesity and mental disorders in the general population: Results from the world mental health surveys. *Int J Obes*. 2008;32(1):192-200. doi:10.1038/SJ.IJO.0803701
5. Fitzpatrick AL, Kuller LH, Lopez OL, et al. Mid- and Late-Life Obesity: Risk of Dementia in the Cardiovascular Health Cognition Study. *Arch Neurol*. 2009;66(3):336. doi:10.1001/ARCHNEUROL.2008.582
6. Hruby A, Manson JAE, Qi L, et al. Determinants and consequences of obesity. *Am J Public Health*. 2016;106(9):1656-1662. doi:10.2105/AJPH.2016.303326
7. Pedditizi E, Peters R, Beckett N. The risk of overweight/obesity in mid-life and late life for the development of dementia: a systematic review and meta-analysis of longitudinal studies. *Age Ageing*. 2016;45(1):14-21. doi:10.1093/AGEING/AFV151
8. Whitmer RA, Gustafson DR, Barrett-Connor E, Haan MN, Gunderson EP, Yaffe K. Central obesity and increased risk of dementia more than three decades later. *Neurology*. 2008;71(14):1057-1064. doi:10.1212/01.wnl.0000306313.89165.ef
9. Anderson PM, Butcher KF, Schanzenbach DW. Understanding recent trends in childhood obesity in the United States. *Econ Hum Biol*. 2019;34:16-25. doi:10.1016/J.EHB.2019.02.002
10. Wang Y, Lim H. The global childhood obesity epidemic and the association between socio-economic status and childhood obesity. *Int Rev Psychiatry*. 2012;24(3):176. doi:10.3109/09540261.2012.688195
11. Kolb B, Harker A, Gibb R. Principles of plasticity in the developing brain. *Dev Med Child Neurol*. 2017;59(12):1218-1223. doi:10.1111/DMCN.13546/ABSTRACT
12. Yau PL, Kang EH, Javier DC, Convit A. Preliminary Evidence of Cognitive and Brain Abnormalities in Uncomplicated Adolescent Obesity. *Obesity (Silver Spring)*. 2014;22(8):1865. doi:10.1002/OBY.20801
13. Kamijo K, Khan NA, Pontifex MB, et al. The relation of adiposity to cognitive control and scholastic achievement in preadolescent children. *Obesity (Silver Spring)*. 2012;20(12):2406-2411. doi:10.1038/OBY.2012.112
14. Khan NA, Baym CL, Monti JM, et al. Central adiposity is negatively associated

with hippocampal-dependent relational memory among overweight and obese children. *J Pediatr*. 2015;166(2):302-308.e1. doi:10.1016/J.JPEDS.2014.10.008

15. Maruszak A, Thuret S. Why looking at the whole hippocampus is not enough-a critical role for anteroposterior axis, subfield and activation analyses to enhance predictive value of hippocampal changes for Alzheimer's disease diagnosis. *Front Cell Neurosci*. 2014;8(MAR):95. doi:10.3389/FNCEL.2014.00095/BIBTEX

16. Cope EC, LaMarca EA, Monari PK, et al. Microglia Play an Active Role in Obesity-Associated Cognitive Decline. *J Neurosci*. 2018;38(41):8889-8904. doi:10.1523/JNEUROSCI.0789-18.2018

17. Hao S, Dey A, Yu X, Stranahan AM. Dietary obesity reversibly induces synaptic stripping by microglia and impairs hippocampal plasticity. *Brain Behav Immun*. 2016;51:230-239. doi:10.1016/J.BBI.2015.08.023

18. Lumeng CN. Innate immune activation in obesity. *Mol Aspects Med*. 2013;34(1):12-29. doi:10.1016/J.MAM.2012.10.002

19. Mclaughlin T, Ackerman SE, Shen L, Engleman E. Role of innate and adaptive immunity in obesity-associated metabolic disease. *J Clin Invest*. 2017;127(1):5-13. doi:10.1172/JCI88876

20. Andrae J, Gallini R, Betsholtz C. Role of platelet-derived growth factors in physiology and medicine. *Genes Dev*. 2008;22(10):1276-1312. doi:10.1101/GAD.1653708

21. Khafagy R, Dash S. Obesity and Cardiovascular Disease: The Emerging Role of Inflammation. *Front Cardiovasc Med*. 2021;8:768119. doi:10.3389/FCVM.2021.768119

22. Valdearcos M, Douglass JD, Robblee MM, et al. Microglial Inflammatory Signaling Orchestrates the Hypothalamic Immune Response to Dietary Excess and Mediates Obesity Susceptibility. *Cell Metab*. 2017;26(1):185-197.e3. doi:10.1016/j.cmet.2017.05.015

23. Valdearcos M, Robblee MM, Benjamin DI, Nomura DK, Xu AW, Koliwad SK. Microglia dictate the impact of saturated fat consumption on hypothalamic inflammation and neuronal function. *Cell Rep*. 2014;9(6):2124-2138. doi:10.1016/j.celrep.2014.11.018

24. Folick A, Cheang RT, Valdearcos M, Koliwad SK. Metabolic factors in the regulation of hypothalamic innate immune responses in obesity. *Exp Mol Med*. 2022;54(4):393-402. doi:10.1038/s12276-021-00666-z

25. André C, Quevedo OG, Rey C, et al. Inhibiting Microglia Expansion Prevents Diet-Induced Hypothalamic and Peripheral Inflammation. *Diabetes*. 2016;66(4):908-919. doi:10.2337/DB16-0586

26. Nakandakari SCBR, Muñoz VR, Kuga GK, et al. Short-term high-fat diet modulates several inflammatory, ER stress, and apoptosis markers in the hippocampus of young mice. *Brain Behav Immun*. 2019;79:284-293. doi:10.1016/j.bbi.2019.02.016

27. Sobesky JL, D'Angelo HM, Weber MD, et al. Glucocorticoids Mediate Short-Term High-Fat Diet Induction of Neuroinflammatory Priming, the NLRP3 Inflammasome, and the Danger Signal HMGB1. *eNeuro*. 2016;3(4):ENEURO.0113-16.2016. doi:10.1523/ENEURO.0113-16.2016

28. Vinuesa A, Bentivegna M, Calfa G, et al. Early Exposure to a High-Fat Diet Impacts on Hippocampal Plasticity: Implication of Microglia-Derived Exosome-like Extracellular Vesicles. *Mol Neurobiol*. Published online November 24, 2018:1-20. doi:10.1007/s12035-018-1435-8

29. Masuda T, Sankowski R, Staszewski O, et al. Spatial and temporal heterogeneity of mouse and human microglia at single-cell resolution. *Nat 2019 5667744*. 2019;566(7744):388-392. doi:10.1038/s41586-019-0924-x

30. Walker F, Nilsson M, Jones K. Acute and Chronic Stress-Induced Disturbances of Microglial Plasticity, Phenotype and Function. *Curr Drug Targets*. 2013;14(11):1262-1276. doi:10.2174/13894501113149990208

31. Smith KL, Kassem MS, Clarke DJ, et al. Microglial cell hyper-ramification and neuronal dendritic spine loss in the hippocampus and medial prefrontal cortex in a mouse model of PTSD. *Brain Behav Immun*. 2019;80:889-899. doi:10.1016/J.BBI.2019.05.042

32. Fernández-Arjona M del M, Grondona JM, Fernández-Llebrez P, López-Ávalos MD. Microglial Morphometric Parameters Correlate With the Expression Level of IL-1β, and Allow Identifying Different Activated Morphotypes. *Front Cell Neurosci*. 2019;13. doi:10.3389/FNCEL.2019.00472/FULL

33. Morrison H, Young K, Qureshi M, Rowe RK, Lifshitz J. Quantitative microglia analyses reveal diverse morphologic responses in the rat cortex after diffuse brain injury. *Sci Reports 2017 71*. 2017;7(1):1-12. doi:10.1038/s41598-017-13581-z

34. Kozlowski C, Weimer RM. An Automated Method to Quantify Microglia Morphology and Application to Monitor Activation State Longitudinally In Vivo. *PLoS One*. 2012;7(2):e31814. doi:10.1371/JOURNAL.PONE.0031814

35. York EM, Ledue JM, Bernier LP, Macvicar BA. 3dmorph automatic analysis of microglial morphology in three dimensions from ex vivo and in vivo imaging. *eNeuro*. 2018;5(6). doi:10.1523/ENEURO.0266-18.2018

36. O'Brien PD, Guo K, Eid SA, et al. Integrated lipidomic and transcriptomic analyses identify altered nerve triglycerides in mouse models of prediabetes and type 2 diabetes. *DMM Dis Model Mech*. 2020;13(2). doi:10.1242/dmm.042101

37. O'Brien PD, Hinder LM, Rumora AE, et al. Juvenile murine models of prediabetes and type 2 diabetes develop neuropathy. *Dis Model Mech*. 2018;11(12). doi:10.1242/dmm.037374

38. Sims-Robinson C, Bakeman A, Bruno E, et al. Dietary reversal ameliorates short- and long-term memory deficits induced by high-fat diet early in life. *PLoS One*. 2016;11(9). doi:10.1371/journal.pone.0163883

39. Nakandakari SCBR, Muñoz VR, Kuga GK, et al. Short-term high-fat diet

modulates several inflammatory, ER stress, and apoptosis markers in the hippocampus of young mice. *Brain Behav Immun*. 2019;79:284-293. doi:10.1016/j.bbi.2019.02.016

40. Wang Q, Yuan J, Yu Z, et al. FGF21 Attenuates High-Fat Diet-Induced Cognitive Impairment via Metabolic Regulation and Anti-inflammation of Obese Mice HHS Public Access Author manuscript. *Mol Neurobiol*. 2018;55(6):4702-4717. doi:10.1007/s12035-017-0663-7

41. Spencer SJ, Basri B, Sominsky L, et al. High-fat diet worsens the impact of aging on microglial function and morphology in a region-specific manner. *Neurobiol Aging*. 2019;74:121-134. doi:10.1016/J.NEUROBIOLAGING.2018.10.018

42. Spencer SJ, D'Angelo H, Soch A, Watkins LR, Maier SF, Barrientos RM. High-fat diet and aging interact to produce neuroinflammation and impair hippocampal- and amygdalar-dependent memory. *Neurobiol Aging*. 2017;58:88-101. doi:10.1016/J.NEUROBIOLAGING.2017.06.014

43. Hinder LM, Park M, Rumora AE, et al. Comparative RNA-Seq transcriptome analyses reveal distinct metabolic pathways in diabetic nerve and kidney disease. *J Cell Mol Med*. 2017;21(9):2140-2152. doi:10.1111/jcmm.13136

44. O'Brien PD, Guo K, Eid SA, et al. Integrated lipidomic and transcriptomic analyses identify altered nerve triglycerides in mouse models of prediabetes and type 2 diabetes. *DMM Dis Model Mech*. 2020;13(2). doi:10.1242/dmm.042101

45. Talley S, Bonomo R, Gavini C, et al. Monitoring of inflammation using novel biosensor mouse model reveals tissue- and sex-specific responses to Western diet. *Dis Model Mech*. 2022;15(6). doi:10.1242/DMM.049313

46. Medrikova D, Jilkova ZM, Bardova K, Janovska P, Rossmeisl M, Kopecky J. Sex differences during the course of diet-induced obesity in mice: adipose tissue expandability and glycemic control. *Int J Obes*. 2012;36:262-272. doi:10.1038/ijo.2011.87

47. Lamping KG, Nuno DW, Coppey LJ, et al. Modification of high saturated fat diet with n-3 polyunsaturated fat improves glucose intolerance and vascular dysfunction. *Diabetes, Obes Metab*. 2013;15(2):144-152. doi:10.1111/DOM.12004

48. Wong SK, Chin KY, Suhaimi FH, Fairus A, Ima-Nirwana S. Animal models of metabolic syndrome: a review. *Nutr Metab 2016 131*. 2016;13(1):1-12. doi:10.1186/S12986-016-0123-9

49. Haley MJ, Krishnan S, Burrows D, et al. Acute high-fat feeding leads to disruptions in glucose homeostasis and worsens stroke outcome. *J Cereb Blood Flow Metab*. 2019;39(6):1026. doi:10.1177/0271678X17744718

50. Leyh J, Winter K, Reinicke M, Ceglarek U, Bechmann I, Landmann J. Long-term diet-induced obesity does not lead to learning and memory impairment in adult mice. *PLoS One*. 2021;16(9):e0257921. doi:10.1371/JOURNAL.PONE.0257921

51. Vinuesa A, Pomilio C, Menafra M, et al. Juvenile exposure to a high fat diet

promotes behavioral and limbic alterations in the absence of obesity. *Psychoneuroendocrinology*. 2016;72:22-33. doi:10.1016/J.PSYNEUEN.2016.06.004

52. Fuhrmann D, Knoll LJ, Blakemore SJ. Adolescence as a Sensitive Period of Brain Development. *Trends Cogn Sci*. 2015;19(10):558-566. doi:10.1016/J.TICS.2015.07.008

53. Franceschi C, Garagnani P, Parini P, Giuliani C, Santoro A. Inflammaging: a new immune-metabolic viewpoint for age-related diseases. *Nat Rev Endocrinol*. 2018;14(10):576-590. doi:10.1038/S41574-018-0059-4

54. Weyand CM, Goronzy JJ. Aging of the immune system: Mechanisms and therapeutic targets. *Ann Am Thorac Soc*. 2016;13(Suppl 5):S422-S428. doi:10.1513/ANNALSATS.201602-095AW/SUPPL_FILE/DISCLOSURES.PDF

55. Kuznetsova A, Brockhoff PB, Christensen RHB. lmerTest Package: Tests in Linear Mixed Effects Models. *J Stat Softw*. 2017;82(13):1-26. doi:10.18637/JSS.V082.I13

Chapter 3 Single-cell RNA Sequencing Identifies Hippocampal Microglial Dysregulation in Diet-induced Obesity

3.1 Abstract

Obesity is a growing global concern in adults and youth along with a parallel rise in associated complications, including cognitive impairment. Obesity induces brain inflammation and activates microglia, which contribute to cognitive impairment likely by aberrantly phagocytosing synaptic spines. Local and systemic signals, such as inflammatory cytokines and metabolites likely participate in obesity-induced microglial activation. However, the precise mechanisms mediating microglial activation during obesity remain incompletely understood. Herein, we leveraged our mouse model of high-fat diet (HFD)-induced obesity, which mirrors human obesity, and develops hippocampal-dependent cognitive impairment. We assessed hippocampal microglial activation by morphological and single-cell transcriptomic analysis to evaluate this heterogeneous, functionally diverse, and dynamic class of cells over time after 1 and 3 months of HFD. HFD altered cell-to-cell communication, particularly immune modulation and cellular adhesion signaling, and induced a differential gene expression signature of protein processing in the endoplasmic reticulum in a time-dependent manner.

3.2 Introduction

The global prevalence of obesity continues to rise. The World Health

Organization estimates that global obesity rates tripled from 1975 to 2016, including an increase from 4% to 16% of overweight or obese children and teens ([WHO 2021]). This steep rise is concerning as the complications of obesity place an immense strain on patients and healthcare systems. Obesity is associated with cognitive impairment and structural brain changes in adults [2,3] and children and adolescents [4–6]. Midlife obesity also raises the risk of future dementia [7,8]. Currently, dementia management is limited to pharmacological and lifestyle interventions, which address only symptoms, not disease pathology. There is a critical need to understand the mechanisms underlying obesity-associated cognitive impairment across the lifespan. Obesity activates microglia, the resident macrophage-like central nervous system (CNS) immune cells, which contribute to this impairment [9], and thus constitute a potential target for intervention.

In the healthy developing and adult hippocampus, a limbic brain structure involved in memory and learning, microglia serve a variety of homeostatic roles, including regulating synaptic function [10,11]. Consequently, changes in microglial inflammatory status can lead to pathological states, which may impact cognition. Murine models of diet-induced obesity exhibit hippocampal inflammation after both acute [12,13] and chronic periods of high-fat diet (HFD) feeding [9,14,15]. Indeed, obese mice suffer from hippocampal-dependent cognitive deficits [9,14,16], along with hippocampal microglial morphology changes characteristic of pro-inflammatory activation after chronic HFD [9,14].

Microglia are thought to contribute to cognitive impairment in obesity by aberrantly phagocytosing synaptic spines [9]. Obesity increases brain inflammation and levels of hippocampal pro-inflammatory cytokines [17], *e.g.* interleukin 1 beta (IL-1β) [14] and tumor necrosis factor alpha (TNFα) [18]. Inflammatory cytokines may activate

microglia [19], along with a variety of other local or systemic signals such as dysregulated metabolites [20], *e.g.* saturated fatty acids from HFD. Additionally, endoplasmic reticulum (ER) stress drives peripheral macrophage activation in obesity [21]. We [22], and others [12], have shown that obesity induces hippocampal ER stress, which may similarly activate microglia as in peripheral macrophages. Moreover, obesity increases peripheral immune cell recruitment [23], and impairs blood-brain barrier function, facilitating entry of systemic inflammatory mediators [24].

The impact of activated microglia on neuronal dysfunction and subsequent systemic metabolism and obesity has been well defined in the hypothalamus [25–27]. However, less is understood about microglial activation in the hippocampus, and the precise mechanisms mediating this activation are unknown. Further, there is a need to address microglial heterogeneity, as a class of functionally diverse cells, as well as clarify the evolution of microglial activation over time to determine the appropriate temporal window for intervention. Currently, existing studies in the obesity field are limited by bulk hippocampal tissue analysis, which likely masks microglial-specific findings. By harnessing the power of single-cell RNA sequencing (scRNA-seq), we, for the first time, characterize the hippocampal microglial transcriptomic landscape at fine-grained single-cell resolution in the context of diet-induced obesity. We identified obesity-associated dysregulated inflammatory pathways in microglia after 1 or 3 months (mo) of HFD in wild-type C57B/L6J mice as they transitioned from adolescence to adulthood. Additionally, we leveraged our single-cell dataset to investigate the dynamic immune cell-to-cell interplay, which is crucial for understanding subtle differences in microglial behavior in obesity. Our characterization of microglial activation states

provides the foundation necessary to elucidate the role of microglia in hippocampal pathology in obesity.

3.3 Results

3.3.1 HFD induces obesity but not early hippocampal microglial morphological activation

To determine the effect of obesity on hippocampal microglial activation, we utilized our previously established mouse model of diet-induced obesity [28]. We fed 5-wk-old male C57BL/6J mice (n=10/group) either a 60% HFD enriched with saturated fatty acids or a control diet containing 10% fat (**Figure 3.1A**). To determine time-dependent changes in microglia in response to HFD, mice were divided into two cohorts and fed for 1 mo or 3 mo. At the study endpoints, we isolated hippocampal microglia and performed scRNA-seq. HFD fed mice were heavier than control fed mice as early as after 2 wk of diet (**Figure 3.1B**). After 1 mo and 3 mo, HFD mice had deficits in glucose homeostasis versus control mice, characterized by elevated peak blood glucose levels upon glucose challenge, alongside a delayed return to baseline (**Figure 3.1C**). Baseline, *i.e.*, at 5 wk of age, GTTs were indistinguishable between HFD and control groups (**Figure 3.2A**). Although glucose homeostasis was disrupted after 1 mo of HFD, fasting plasma insulin did not increase in HFD mice relative to controls until 3 mo (**Figure 3.1D**; P=0.0003), recapitulating hyperinsulinemia in humans with chronic obesity.

We also examined basic plasma lipid profiles for cholesterol, triglycerides, phospholipids, and non-esterified fatty acids (NEFAs). Total plasma cholesterol was elevated in HFD mice after 1 mo and 3 mo diet (**Figure 3.1E**; P=0.0474, P=0.0021,

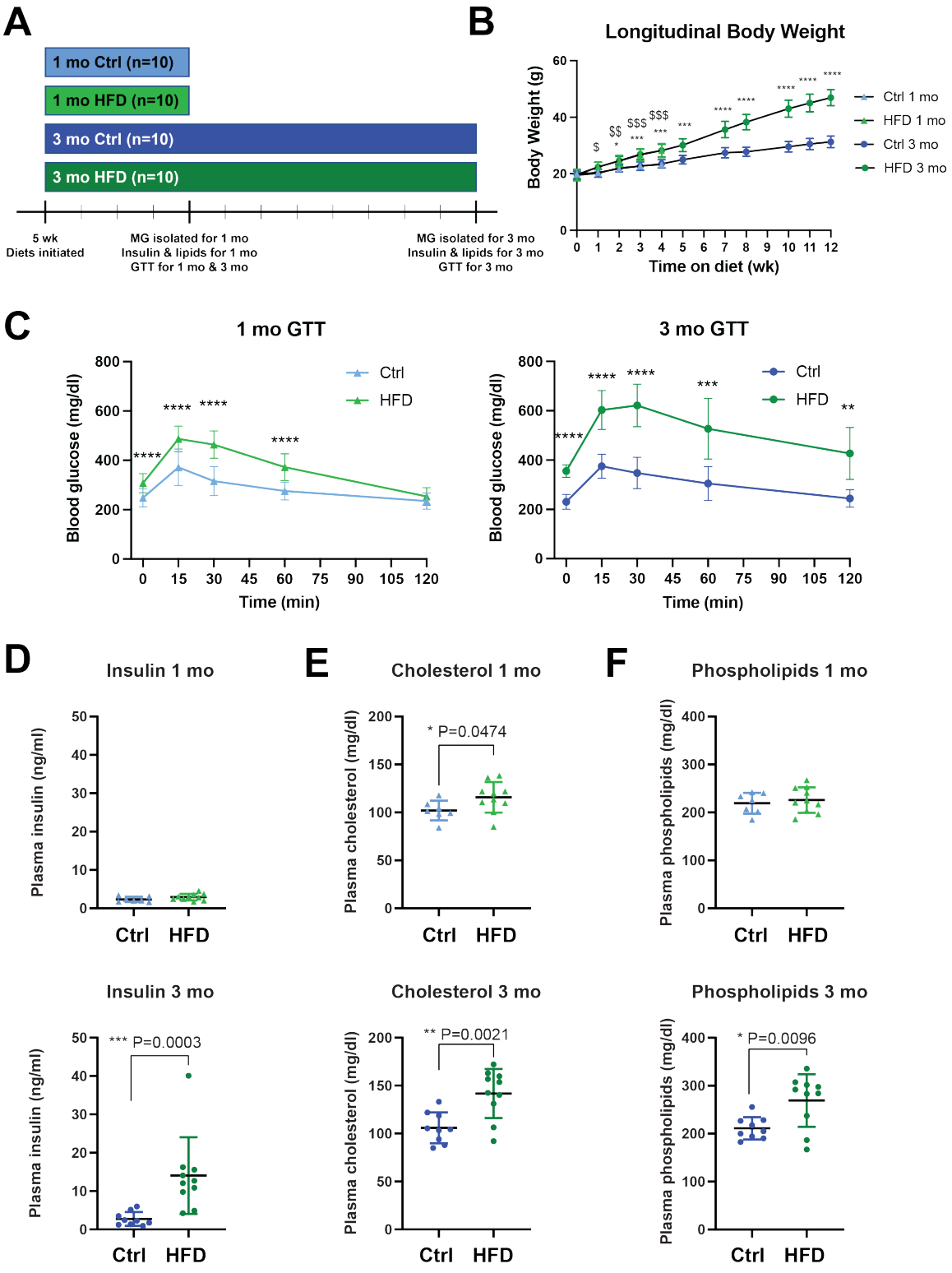

Figure 3.1 HFD induces obesity and dyslipidemia in mice.

(A) Study design. Wild-type C57BL/6J mice aged 5 weeks were randomized to a high-fat diet (HFD) or control standard diet (ctrl). After 1 month (mo) or 3 (mo) of diet, HFD and control mice were sacrificed for

microglial isolation and metabolic phenotyping (n=10 per diet per time point). (B) Longitudinal body mass; from 0 to 4 wk (i.e., 1 mo time point) n=20 per diet per time point (HFD, green; ctrl, blue); from 5 wk onward, n=10 per diet (HFD, green; ctrl, blue). $P<0.05, $$P<0.01, $$$P<0.001, for HFD versus ctrl 1 mo cohort; *P<0.05, ***P<0.001, ****P<0.0001 for HFD versus ctrl 3 mo cohort; Sidak's multiple comparisons test for repeated measures two-way ANOVA. (C) Glucose tolerance test (GTT); left panel for HFD (n=20; light green) versus control (n=20; light blue) at 1 mo (triangles); right panel for HFD (n=10; dark green) versus control (n=10; dark blue) at 3 mo (circles). Measures above the glucometer's upper threshold were set to the threshold, 750 mg/dl. Plasma (D) insulin, (E) cholesterol, and (F) phospholipids; top panels for HFD (n=10; light green) versus control (n=7; light blue) at 1 mo (triangles); bottom panels for HFD (n=10; dark green) versus control (n=9; dark blue) at 3 mo (circles). C to F, *P<0.05, **P<0.01, ***P<0.001, ****P<0.0001 for HFD versus control, by Sidak's multiple comparisons test for repeated measures two-way ANOVA for GTTs, by Welch's t-test for insulin, cholesterol, and phospholipids, except for insulin 3 mo by Mann-Whitney test as data were not normally distributed.

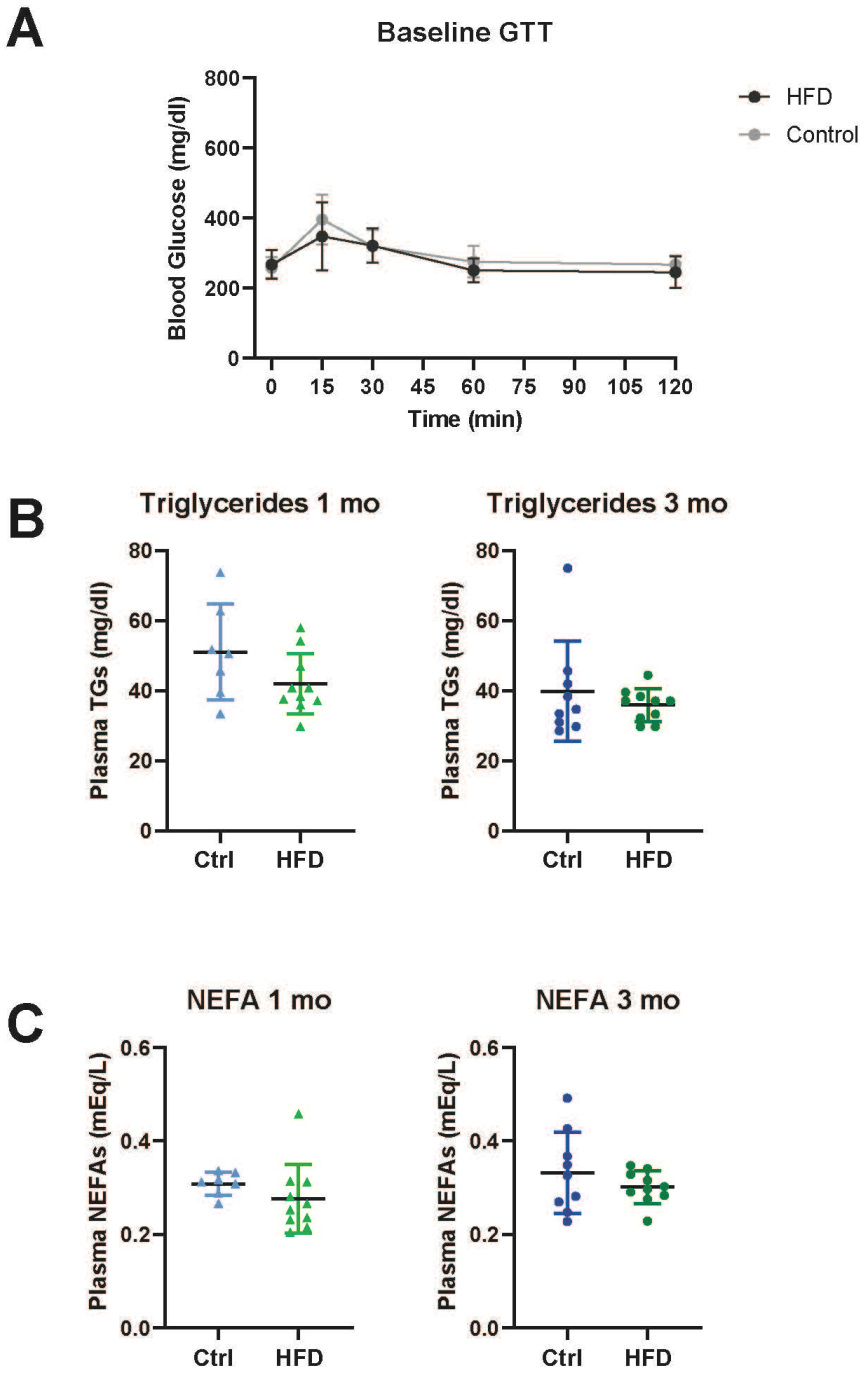

Figure 3.2 Metabolic parameters in HFD and control mice.

(A) Baseline glucose tolerance test (GTT) for HFD (1 mo and 3 mo combined; n=20; dark grey) versus control (ctrl; 1 mo and 3 mo combined; n=20; light grey) mice. Plasma (B) triglycerides (TGs) and (C) non-esterified fatty acids (NEFAs); left panels for HFD (n=10; light green) versus control (n=7; light blue) at 1 mo (triangles); right panels for HFD (n=10; dark green) versus control (n=9; dark blue) at 3 mo (circles). No significant difference between HFD and control in (A) by Sidak's multiple comparisons test for repeated measures two-way ANOVA for GTT, and in (B,C) by Welch's t-test except for NEFA 1 mo and triglycerides 3 mo by Mann-Whitney test as data were not normally distributed.

respectively) and phospholipids after 3 mo (**Figure 3.1F**; P=0.0096). Diet did not affect triglyceride (**Figure 3.2B**) or NEFA (**Figure 3.2C**) levels. Collectively, these metabolic data demonstrate that HFD mice are obese and develop systemic metabolic dysfunction after just 1 mo (*e.g.*, glucose intolerance, elevated cholesterol), which becomes more severe after 3 mo (*i.e.*, hyperinsulinemia, elevated phospholipids).

We previously reported hippocampal dependent cognitive deficits in short-term memory in a mouse model after 2 wk, 6 wk, and 24 wk of HFD using a novel object recognition task [16]. Obesity activates hippocampal microglia, assessed by morphological activation [9,14] after 3 mo of chronic HFD feeding. To address if hippocampal microglial changes occur earlier, like cognitive deficits, we quantified 3-dimensional (3D) microglial morphology after 1 mo. Homeostatic microglia display complex branching patterns to surveil their environment, but environmental challenges trigger morphology shifts, characterized by smaller territorial volume and simpler branching patterns.

We performed 3D analyses on tissue sections stained by immunohistochemistry for the microglial marker ionized calcium binding adaptor molecule 1 (Iba1) using a modified 3D-Morph protocol [29]. 3D z-stack images of hippocampal tissue sections were acquired by confocal microscopy. After pre-processing in Imaris, images were run through 3D-Morph in MATLAB to measure territorial volume, cell volume, and branching parameters based on convex hull analyses and skeletonization [29] (representative cells, **Figure 3.3A-B**). After 1 mo diet, microglia in the CA1 region of the hippocampus from HFD-fed mice were not morphologically distinct from control microglia. Territorial volume (P=0.16), the 3D space taken up by the cell body and all its branches, cell

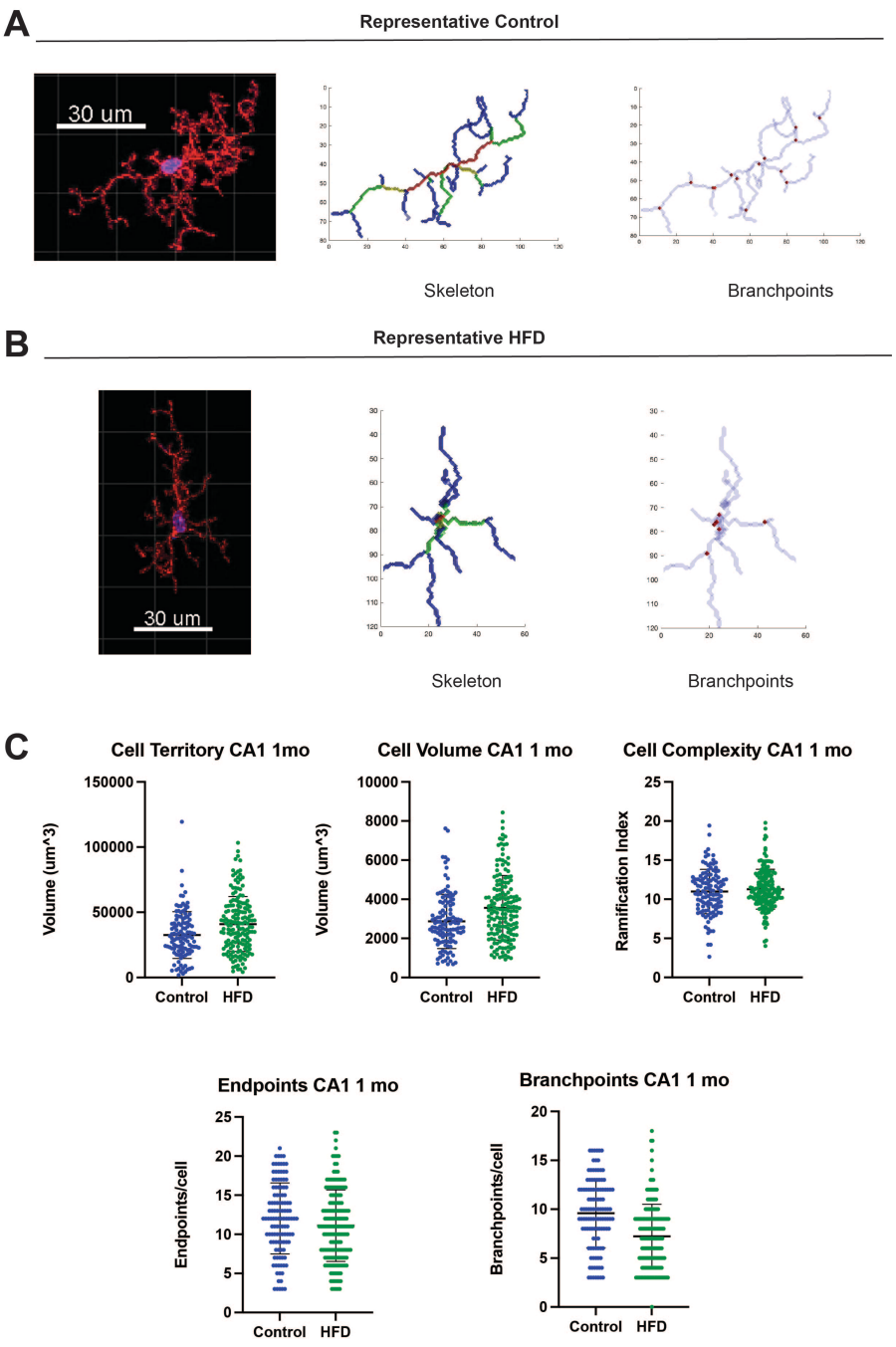

Figure 3.3 Obesity does not alter hippocampal microglial morphology at 1 mo.

(A) Representative 3D Morph[29] analysis for a control microglia from the hippocampal CA1 region, confocal microscopy (left), skeletonization (center), and branchpoints (right). (B) Representative 3D Morph analysis for a HFD microglia from the hippocampal CA1 region. Sections were stained for microglial Iba1 (594 nm, red channel) and with Hoechst nuclear staining (blue channel). Scale bar is 30 µm. Microglial (C) territorial volume, (D) cell volume, (E) ramification index, and (F) branchpoint number per cell; left panels for control (ctrl; n=3 animals, 3 images/animal; blue) versus HFD (n=4 animals, 3 images/animal; green), each circle represents an individual cell. There were no significant differences in HFD versus control by linear mixed effects models with random animal-specific intercepts with t-test.

volume (P=0.26), defined as the volume of the soma and branches themselves, and ramification index (P=0.52), defined as the territorial volume divided by the cell volume, did not differ by diet. There was also no difference in the number of endpoints (P=0.42) and branchpoints (P=0.08); however, there was a trend towards fewer branchpoints per cell in HFD microglia.

3.3.2 Microglial heterogeneity remains constant in HFD and control mice

Next, we investigated the microglial single-cell transcriptome to understand how hippocampal microglia are activated to contribute to obesity associated cognitive impairment. To characterize transcriptomic heterogeneity of the microglial landscape, we performed scRNA-seq on microglia isolated from the hippocampi of HFD and control mice (n=6/group) after 1 mo and 3 mo (**Figure 3.4A**). We performed a papain enzymatic digestion followed by serial trituration to prepare a single cell suspension from the hippocampus. We enriched for microglia by applying a 40% Percoll centrifugation to our cells and collecting the cell pellet, and further purified by fluorescence activated cell sorting (FACS). We sorted $CD11b^{+}/CD45^{low}$ double positive cells, representing microglia, rather than $CD11b^{+}/CD45^{high}$ cell surface markers, which represent macrophages. Sorted cells were sequenced on the 10X Chromium platform and RNA reads were quality filtered before mapping to the mouse reference genome. We used CellRanger Count to prepare sample files, which were read into Seurat. Cells were excluded from downstream analysis based on criteria outlined in the **Methods** (section 3.5). In total, 4,555 HFD and 4,945 control cells were included in analysis at 1 mo, and 1,292 HFD and 1,255 control cells at 3 mo. To determine the success of FACS, we

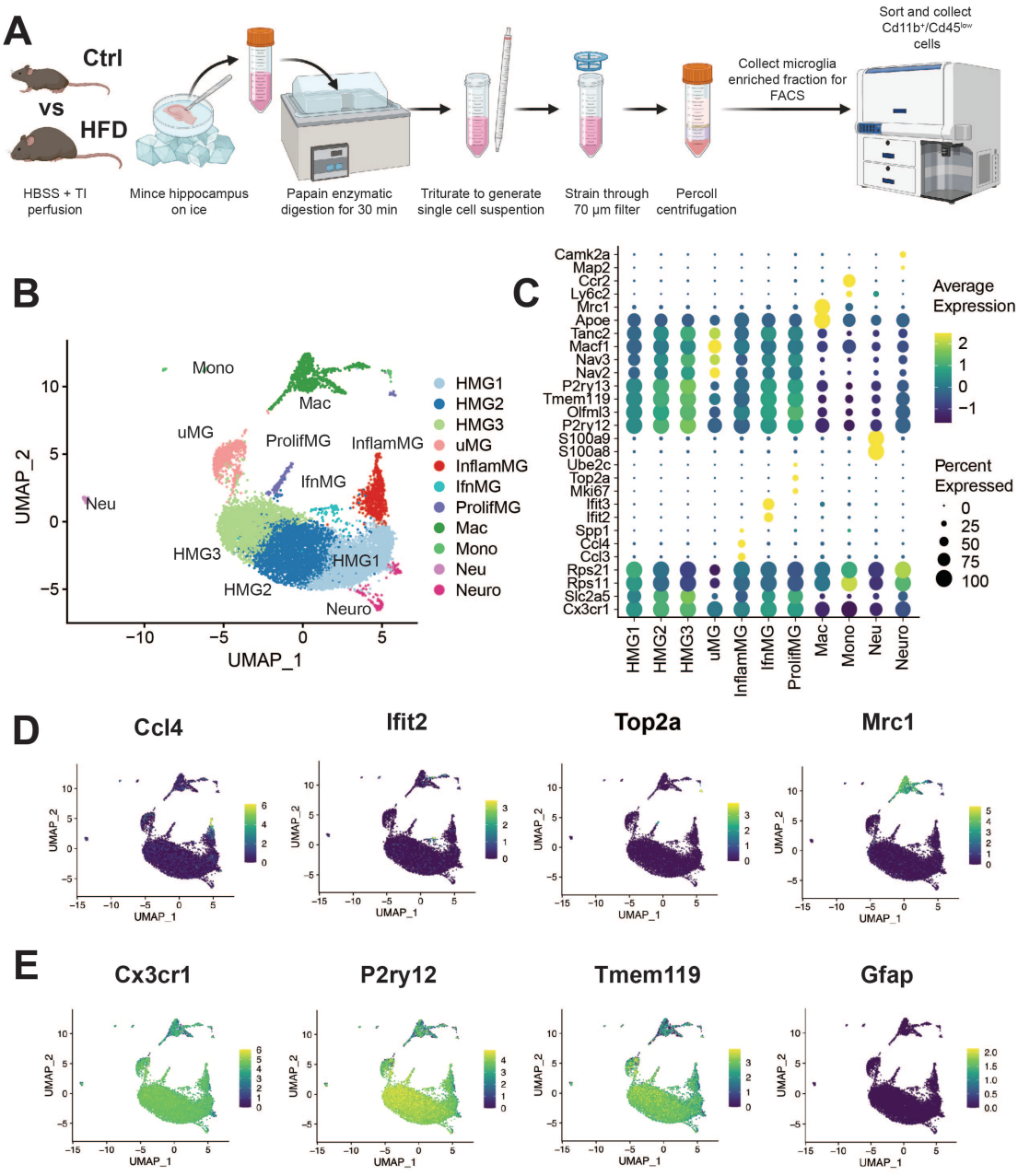

Figure 3.4 Isolated cells cluster into eleven distinct populations.

(A) Diagram of microglial isolation protocol. (B) Uniform Manifold Approximation and Projection (UMAP) shows 11clusters, which represent homeostatic microglia 1 (HMG1), HMG2, HMG3, macrophages (Mac), uMG (uknown, functionally undescribed), inflammatory microglia (InflamMG), proliferating microglia (ProlifMG), neurons (Neuro), interferon-related microglia (IfnMG), neutrophils (Neu), and monocytes (Mono). (D) Dot plot of markers used to assign cluster identity. Dot size represents the percentage of cells from a given cluster expressing the marker, dot color represents average expression relative to all other clusters. (E) UMAP plots by markers that differentiated various clusters, InflamMG by chemokine Ccl4 (C-C motif chemokine ligand 4), IfnMG by interferon-induced Ifit2 (interferon induced protein with tetratricopeptide repeats 2), ProlifMG by DNA topoisomerase Top2a (DNA topoisomerase II alpha), and macrophages by immunomodulating Mrc1 (mannose receptor C-type 1). (F) UMAP plots with expression of microglial (Cx3cr1, CX3C chemokine receptor 1; P2ry12, purinergic receptor P2Y12; Tmem119,

transmembrane protein 119) versus astrocytic (Gfap, glial fibrillary acidic protein) markers shows a relatively pure microglia isolation. UMAP plot for another microglial marker, Aif1 (allograft inflammatory factor 1), the gene encoding Iba1 protein, is shown in Figure 3.5.

examined expression of the CD11b gene, *Itgam*, and the CD45 gene, *Ptprc*, which were expressed by most cells, suggesting a successful cell sort (**Figure 3.5A**).

Next, we performed principal component analysis to reduce data dimensionality and then analyzed and visualized clusters using Uniform Manifold Approximation and Projection (UMAP). We identified eleven cell clusters (**Figure 3.4B**), which were characterized by cell-specific markers found using the FindAllMarkers function in Seurat (**Figure 3.4C**). We reviewed previously published data sets and leveraged the CellMarker and PanglaoDB databases to assign cell type identities to each cluster. As anticipated, most clusters, seven out of eleven, were microglial subtypes, of which three were homeostatic microglia (HMG), HMG1, 2, 3. The remaining microglial subtypes were inflammatory microglia (InflamMG, expressing C-C motif chemokine ligand 4 [Ccl4] and Ccl3, **Figure 3.4D**), interferon-related microglia (IfnMG, expressing interferon induced protein with tetratricopeptide repeats 2 [Ifit2] and Ifit3, **Figure 3.4D**), proliferating microglia (ProlifMG, expressing DNA topoisomerase II alpha [Top2a], **Figure 3.4D**, and marker of proliferation Ki-67 [Mki67]), and a functionally undescribed subtype labeled “uMG” for ‘undescribed microglia’ (**Table 3.1**).

In addition to the microglia subtypes, we also identified macrophages (Mac, expressing mannose receptor C-type 1 [Mrc1], **Figure 3.4D**), monocytes (Mono, expressing C-C motif chemokine receptor 2 [Ccr2] and lymphocyte antigen 6 complex, locus C2 [Ly6c2], UMAP not shown, features in **Figure 3.4C**), neutrophils (Neu, expressing S100 calcium binding protein A8 [S100a8] and S100a9, UMAP not shown,

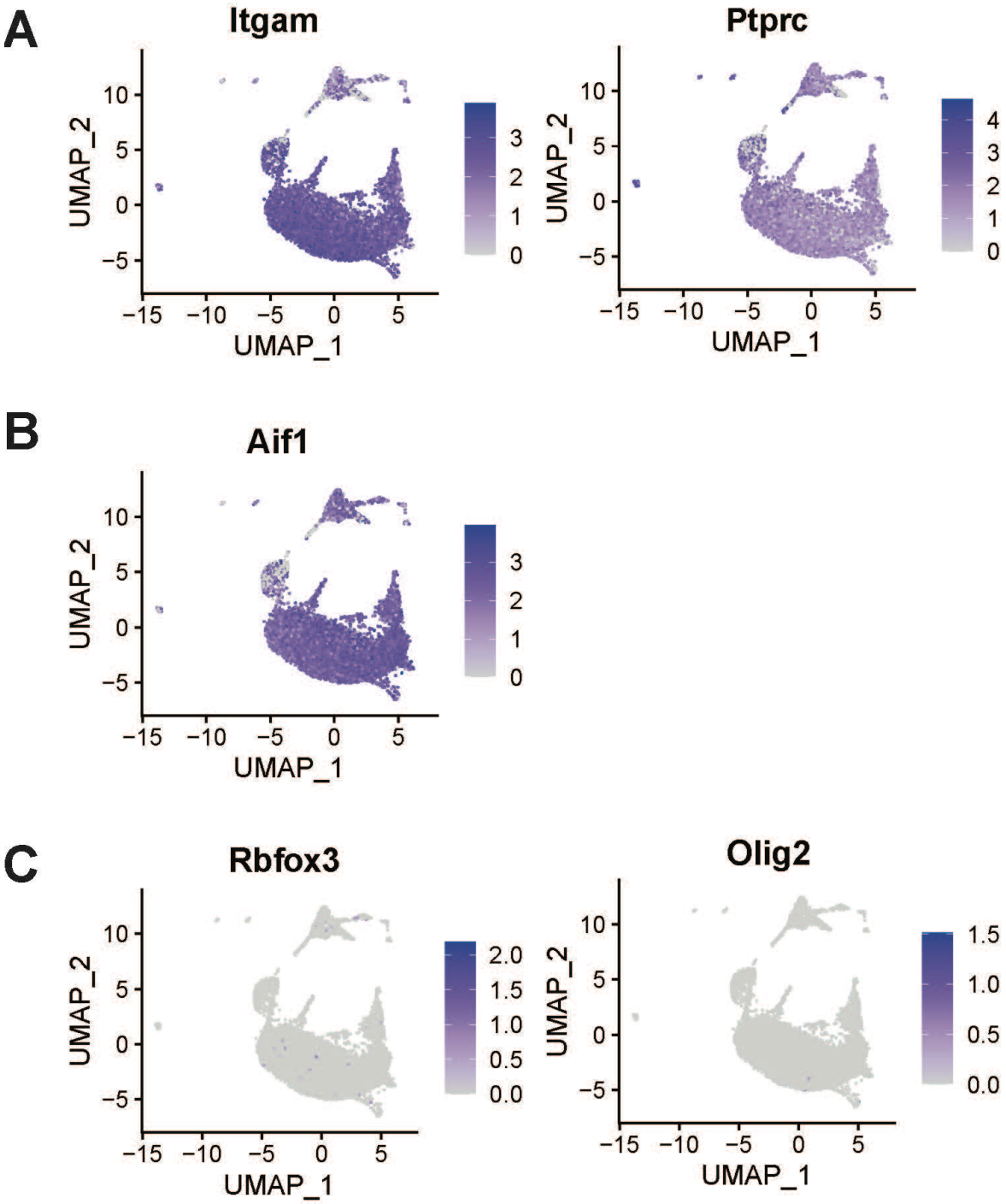

Figure 3.5 UMAP shows purity of microglial isolation and successful FACS sort.

(A) UMAP plots of gene expression for antigens used in FACS sorting, CD11b and CD45. Almost all cells express Itgam (integrin subunit alpha M; left panel), the gene encoding CD11b (cluster of differentiation 11b), and Ptprc (protein tyrosine phosphatase receptor type C; right panel), the gene encoding CD45. (B) UMAP plot with expression of Aif1 (allograft inflammatory factor 1), the gene encoding Iba1 protein, a microglial marker. (C) UMAP plot with expression of Rbfox3 (RNA binding fox-1 homolog 3; left panel), the gene encoding NeuN protein, a neuronal marker, and for Olig2 (oligodendrocyte transcription factor 2; right panel), an oligodendrocyte marker.

Table 3.1 Cluster-specific marker genes.

Gene markers used to cluster cells into homeostatic microglia (HMG), HMG1, 2, and 3, inflammatory microglia (InflamMG), interferon-related (IfnMG,), proliferating microglia (ProlifMG), functionally undescribed microglia (uMG), macrophages (Mac), monocytes (Mono), neutrophils (Neu), and neurons (Neuro). Entries arranged by nominal P-value. Adjusted P-value (Padj) based on Bonferroni correction using all features in the dataset. FC, fold-change; pct.1, percentage of cells where the feature is detected in the first group; pct.2, percentage of cells where the feature is detected in the second group. Only the top 10 genes for each cluster are listed below; the complete dataset will be available at the time of publication or upon request.

Gene	Cluster	P-value	avg Log_2FC	pct.1	pct.2	Padj
Rps4x	HMG1	0.00E+00	0.859	1.000	0.956	0.00E+00
Rpl39	HMG1	0.00E+00	0.831	1.000	0.962	0.00E+00
Rpl21	HMG1	0.00E+00	0.825	1.000	0.962	0.00E+00
Rps21	HMG1	0.00E+00	0.825	1.000	0.965	0.00E+00
Rps3a1	HMG1	0.00E+00	0.824	1.000	0.956	0.00E+00
Rpl30	HMG1	0.00E+00	0.824	1.000	0.961	0.00E+00
Rps7	HMG1	0.00E+00	0.813	1.000	0.941	0.00E+00
Rpl37a	HMG1	0.00E+00	0.801	1.000	0.965	0.00E+00
Rps15a	HMG1	0.00E+00	0.799	1.000	0.950	0.00E+00
Fau	HMG1	0.00E+00	0.797	1.000	0.976	0.00E+00
P2ry12	HMG2	2.28E-178	0.387	1.000	0.962	7.36E-174
Cx3cr1	HMG2	4.08E-158	0.328	1.000	0.980	1.32E-153
Selplg	HMG2	1.73E-138	0.330	1.000	0.943	5.59E-134
Tmem119	HMG2	7.58E-119	0.336	0.997	0.890	2.45E-114
Sparc1	HMG2	2.06E-118	0.332	1.000	0.933	6.66E-114
Hexb	HMG2	4.14E-118	0.290	1.000	0.987	1.34E-113
Slc2a5	HMG2	5.78E-100	0.333	0.921	0.732	1.86E-95
Cd164	HMG2	7.10E-93	0.280	0.989	0.905	2.29E-88
P2ry13	HMG2	5.56E-92	0.284	0.995	0.890	1.79E-87
Gpr34	HMG2	7.11E-92	0.278	0.999	0.939	2.30E-87
P2ry121	HMG3	0.00E+00	0.679	1.000	0.963	0.00E+00
Rhob1	HMG3	0.00E+00	0.666	0.986	0.876	0.00E+00
Tgfbr1	HMG3	0.00E+00	0.616	0.999	0.931	0.00E+00
Hexb1	HMG3	0.00E+00	0.435	1.000	0.987	0.00E+00
Arhgap5	HMG3	1.65E-298	0.600	0.995	0.903	5.34E-294
Gpr341	HMG3	4.81E-282	0.542	1.000	0.941	1.55E-277
P2ry131	HMG3	1.41E-279	0.591	0.993	0.894	4.55E-275
Selplg1	HMG3	9.46E-273	0.486	1.000	0.945	3.05E-268
Mef2a	HMG3	5.48E-272	0.518	0.991	0.937	1.77E-267
Nrip1	HMG3	2.72E-256	0.631	0.952	0.822	8.78E-252
Itgax	InflamMG	6.91E-307	0.660	0.365	0.034	2.23E-302
Cd9	InflamMG	5.54E-270	1.424	1.000	0.907	1.79E-265
Cst7	InflamMG	4.75E-257	1.084	0.487	0.081	1.53E-252
Lpl	InflamMG	8.56E-251	1.355	0.466	0.075	2.76E-246
Ctsz	InflamMG	3.52E-243	1.119	1.000	0.951	1.14E-238
Cd63	InflamMG	9.55E-243	1.825	0.983	0.748	3.08E-238
Gas2l3	InflamMG	1.12E-240	0.636	0.293	0.028	3.63E-236
Ctsb	InflamMG	2.98E-240	1.152	1.000	0.976	9.62E-236
Csf1	InflamMG	5.74E-223	1.249	0.464	0.085	1.85E-218
Lgals3	InflamMG	7.05E-199	0.843	0.239	0.022	2.28E-194
Ifit2	IfnMG	6.67E-225	1.760	0.525	0.022	2.15E-220
Ifit3	IfnMG	1.74E-203	2.496	0.673	0.042	5.62E-199
Ifit3b	IfnMG	6.88E-203	1.362	0.386	0.012	2.22E-198
Usp18	IfnMG	1.48E-174	1.124	0.495	0.025	4.77E-170
Ifit1	IfnMG	2.51E-151	1.157	0.317	0.011	8.10E-147
Rtp4	IfnMG	8.18E-151	1.535	0.802	0.082	2.64E-146
Irf7	IfnMG	1.63E-138	0.773	0.376	0.018	5.25E-134
Oasl2	IfnMG	6.75E-115	1.219	0.475	0.036	2.18E-110
Isg15	IfnMG	1.04E-109	1.699	0.535	0.049	3.36E-105
Rsad2	IfnMG	1.09E-93	0.672	0.248	0.011	3.52E-89
Mki67	ProlifMG	0.00E+00	2.181	0.264	0.004	0.00E+00

Nusap1	ProlifMG	0.00E+00	1.242	0.214	0.002	0.00E+00
Birc5	ProlifMG	0.00E+00	1.162	0.242	0.003	0.00E+00
Pbk	ProlifMG	0.00E+00	1.140	0.220	0.001	0.00E+00
Tpx2	ProlifMG	0.00E+00	0.967	0.242	0.004	0.00E+00
Knl1	ProlifMG	0.00E+00	0.900	0.220	0.001	0.00E+00
Lockd	ProlifMG	0.00E+00	0.731	0.220	0.002	0.00E+00
Nuf2	ProlifMG	0.00E+00	0.707	0.264	0.003	0.00E+00
Aspm	ProlifMG	0.00E+00	0.649	0.165	0.001	0.00E+00
Fignl1	ProlifMG	0.00E+00	0.590	0.341	0.006	0.00E+00
mt-Cytb	uMG	5.15E-225	1.991	0.982	0.997	1.66E-220
mt-Atp6	uMG	4.93E-222	1.975	0.982	0.997	1.59E-217
mt-Nd4	uMG	1.79E-214	1.964	0.967	0.993	5.79E-210
mt-Nd2	uMG	3.01E-213	2.074	0.958	0.989	9.71E-209
mt-Nd1	uMG	4.00E-213	2.021	0.956	0.991	1.29E-208
mt-Co3	uMG	4.93E-210	1.914	0.982	0.998	1.59E-205
mt-Co2	uMG	1.12E-205	1.902	0.977	0.996	3.61E-201
Malat11	uMG	1.48E-198	1.084	0.998	0.994	4.77E-194
mt-Co1	uMG	3.03E-180	1.739	0.979	0.997	9.79E-176
Ivns1abp1	uMG	1.65E-106	1.237	0.866	0.952	5.33E-102
Apoe	Mac	0.00E+00	5.384	0.998	0.760	0.00E+00
Pf4	Mac	0.00E+00	5.062	0.949	0.108	0.00E+00
Mrc1	Mac	0.00E+00	4.890	0.965	0.149	0.00E+00
Wfdc17	Mac	0.00E+00	4.144	0.798	0.074	0.00E+00
Ms4a7	Mac	0.00E+00	4.013	0.932	0.034	0.00E+00
Dab2	Mac	0.00E+00	3.984	0.959	0.185	0.00E+00
Lyz2	Mac	0.00E+00	3.910	0.995	0.773	0.00E+00
F13a1	Mac	0.00E+00	3.770	0.883	0.035	0.00E+00
Cd163	Mac	0.00E+00	3.285	0.684	0.018	0.00E+00
Pla2g7	Mac	0.00E+00	2.895	0.849	0.032	0.00E+00
S100a4	Mono	0.00E+00	4.131	0.795	0.028	0.00E+00
S100a6	Mono	0.00E+00	3.921	0.880	0.027	0.00E+00
Ahnak1	Mono	0.00E+00	3.332	0.932	0.020	0.00E+00
Vim	Mono	0.00E+00	2.910	0.855	0.027	0.00E+00
Ly6c2	Mono	0.00E+00	2.716	0.308	0.004	0.00E+00
Lgals31	Mono	0.00E+00	2.557	0.821	0.026	0.00E+00
Gzmb	Mono	0.00E+00	2.539	0.145	0.000	0.00E+00
Napsa	Mono	0.00E+00	2.454	0.829	0.004	0.00E+00
Anxa2	Mono	0.00E+00	2.304	0.897	0.024	0.00E+00
Itgal	Mono	0.00E+00	2.264	0.641	0.012	0.00E+00
Retnlg	Neu	0.00E+00	6.026	0.960	0.009	0.00E+00
Il1b1	Neu	0.00E+00	5.448	0.949	0.022	0.00E+00
S100a61	Neu	0.00E+00	5.355	0.970	0.028	0.00E+00
Slpi	Neu	0.00E+00	4.685	0.919	0.005	0.00E+00
Cxcr2	Neu	0.00E+00	4.184	0.960	0.005	0.00E+00
Dusp1	Neu	0.00E+00	3.890	0.909	0.018	0.00E+00
Mmp9	Neu	0.00E+00	3.859	0.939	0.005	0.00E+00
Ifitm1	Neu	0.00E+00	3.822	0.677	0.006	0.00E+00
Lcn2	Neu	0.00E+00	3.812	0.606	0.006	0.00E+00
Wfdc21	Neu	0.00E+00	3.692	0.717	0.003	0.00E+00
Cpe	Neuro	1.96E-134	1.251	0.368	0.026	6.34E-130
Slc1a2	Neuro	1.65E-116	2.127	0.349	0.027	5.32E-112
Ptprz1	Neuro	1.93E-115	0.801	0.112	0.002	6.24E-111
Ddn	Neuro	2.68E-106	0.792	0.184	0.008	8.64E-102
Mt3	Neuro	2.80E-105	1.832	0.441	0.050	9.03E-101
Sparcl1	Neuro	1.96E-103	1.646	0.250	0.015	6.34E-99
Clu	Neuro	3.78E-92	1.344	0.204	0.011	1.22E-87
Sptbn2	Neuro	1.08E-90	0.432	0.105	0.003	3.48E-86
Cnih2	Neuro	4.01E-74	0.373	0.105	0.003	1.29E-69
Pcsk1n	Neuro	1.26E-69	0.591	0.145	0.007	4.06E-65

features in **Figure 3.4C**), and neurons (Neuro, expressing calcium/calmodulin dependent protein kinase II alpha [Camk2a] and microtubule associated protein 2 [Map2], UMAP not shown, features in **Figure 3.4C**). Most sequenced cells expressed microglial markers *Cx3cr1*, *P2ry12* (**Figure 3.4E**), and *Aif1* (gene coding for Iba1; **Figure 3.5B**) and the microglial-specific gene *Tmem119* (**Figure 3.4E**), as expected, since we enriched for microglia. Further, the analyzed cells expressed only low levels of the astrocyte specific gene *Gfap* (**Figure 3.4E**) neuronal specific gene *Rbfox3*, and oligodendrocyte specific gene *Olig2* (**Figure 3.5C**).

All seven microglial and four additional cell type clusters were present in both HFD and control groups (**Figure 3.6A**), and at both 1 mo and 3 mo. Although all cell clusters were represented in all experimental groups, we assessed the proportion of each cell cluster by diet or age. Cluster proportions were similar between HFD and control groups at 1 mo and 3 mo (**Figure 3.6B**). In all experimental groups, the largest proportion of cells comprised homeostatic microglia, HMG1, 2, and 3 at both 1 mo (HFD 77.8% versus control 76.9%) and 3 mo (HFD 69.4% versus control 65.3%). Macrophages were the second most abundant cell type after HMGs at 1 mo (HFD 7.1% versus control 7.5%) and 3 mo (HFD 12.2% versus control 12.4%). Other microglial subtypes (uMG, InflamMG, ProlifMG, and IfnMG) ranged from 0.8% to 8.6% of all cells in HFD and control conditions at 1 mo and 3 mo.

3.3.3 Obesity dysregulates microglial inflammatory cell-to-cell signaling

Microglia are immune cells that constantly survey the CNS environment and respond to external signals [30–32]. Thus, we examined the effect of obesity on cell-to-cell

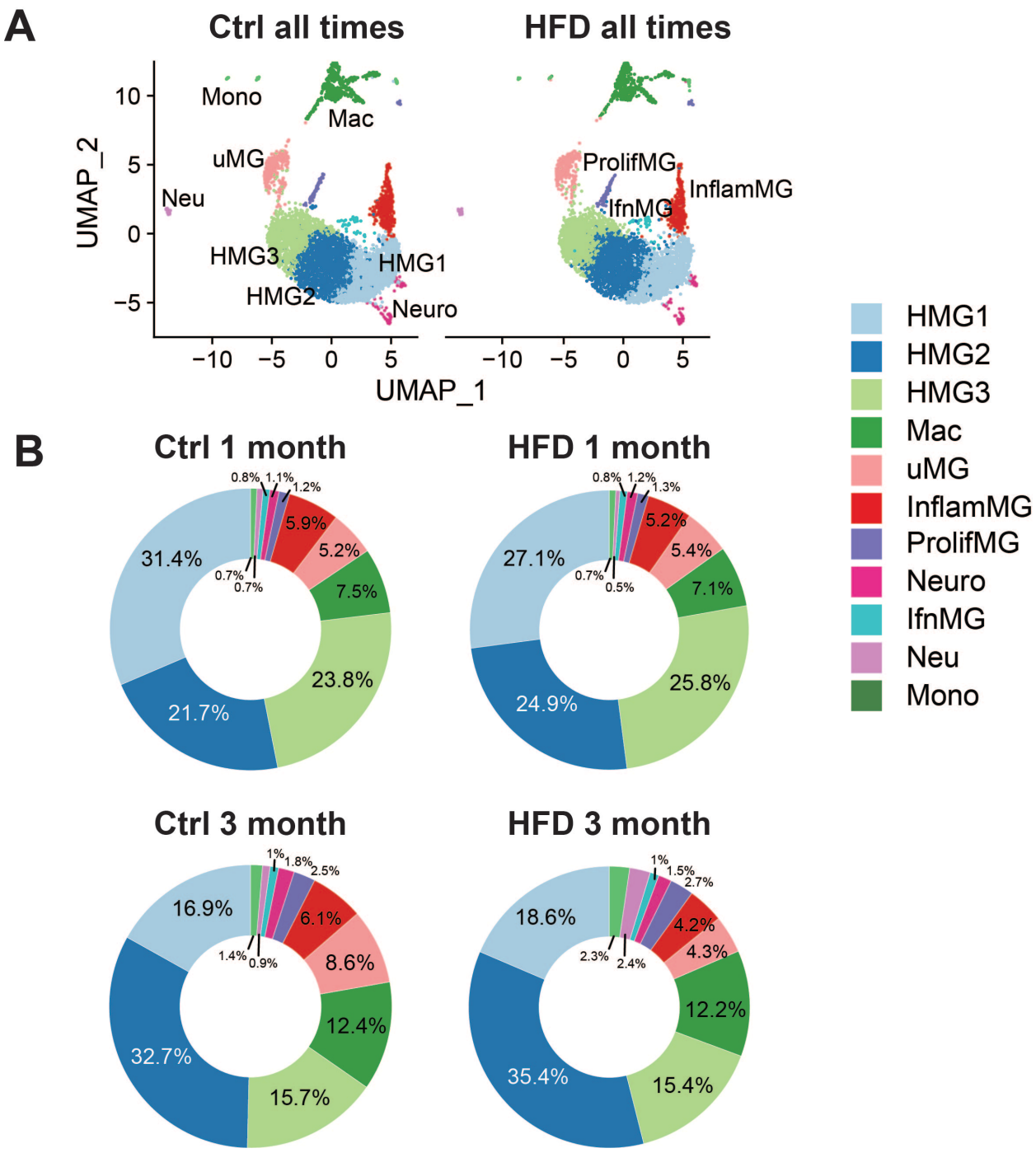

Figure 3.6 Microglial heterogeneity remains constant in HFD versus control mice.

(A) UMAP of HFD versus control (ctrl) at both time points. (B) Top panel: Circle chart of all 11 cell types by percentage at 1 mo for HFD (left) versus control (right). Bottom panel: Circle chart of all 12 cell types by percentage at 3 mo for HFD (left) versus control (right).

communication within our single-cell dataset. To do so, we utilized CellChat [33], a tool that leverages a database of over 2,000 ligand and receptor pairs and scRNA-seq data to infer intercellular communication. We first looked at information flow of intercellular signaling pathways in HFD and control conditions at 1 mo and 3 mo (**Figures 3.7A, 3.7D**), which is based on a summation of probabilities of pathway communication for all cell type pairs. For each pathway, CellChat also identifies the ligand-receptor gene pairs contributing to pathway signaling, which is visualized in circle plots of cell types that send and receive signals for the given pathway (**Figures 3.7B-C, 3.7E-F**).

Information flow at the 1 mo time point was higher in 23 pathways in HFD versus control cells and 12 pathways in control versus HFD cells (**Figure 3.7A**). In some instances, signaling pathways were only detected in cells of one diet group, *e.g.*, type-1 interferon (IFN-I) signaling at 1 mo in HFD cells. The pathways with microglia-to-microglia signaling that were elevated in HFD at 1 mo fell into a few broad categories. 'CDH', 'ICAM1,' 'PECAM1', 'HSPG, and 'CD200' ligands are cell surface glycoproteins with various immune regulatory roles, including cellular adhesion [34], T-cell co-stimulation [35], microglial pro-inflammatory activation [36–38], as well as inhibition of microglial activation in the case of CD200 [39]. The 'IFN-I' ligand is a cytokine involved in canonical pro-inflammatory signaling. 'EGF', 'GRN', and 'TGFb' ligands are growth factors, and loss of microglial progranulin and granulin signaling has been extensively studied in frontotemporal dementia [40] and neurodegeneration [41]. Finally, the 'SEMA6' ligand is a transmembrane protein with a known role in axon guidance [42].

'HSPG' and 'IFN-I' were the sole pathways driven by microglia-to-microglia signaling with information flow turned on in HFD cells at 1 mo (**Figures 3.7B-C**). For

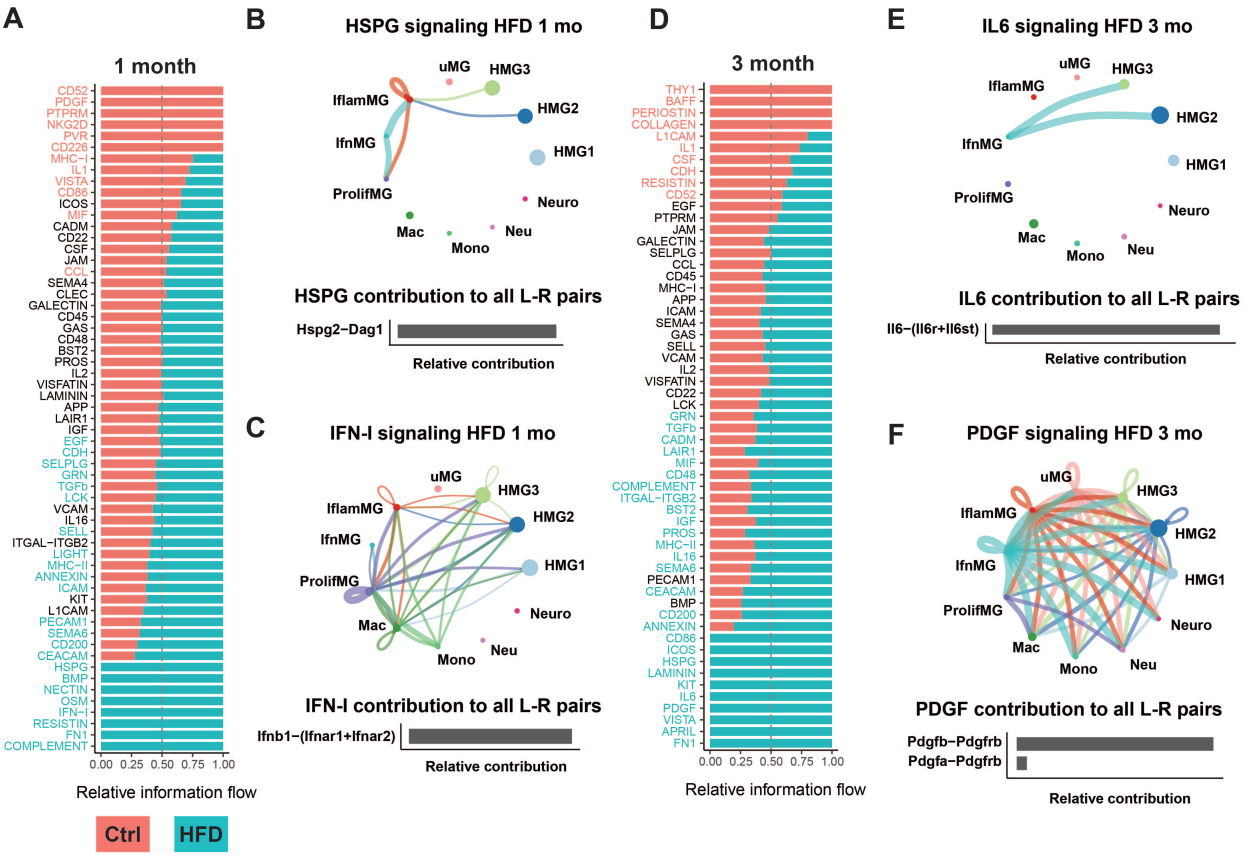

Figure 3.7 Cell-to-cell communication analyses reveal HFD specific intercellular communication pathways.

(A) Information flow charts at 1 mo for HFD (blue) versus control (ctrl; red) generated by CellChat. Teal bars represent information flow in HFD cells, red bars represent information flow in control cells. Signaling pathways in teal text have significantly higher information flow in HFD cells relative to control, signaling pathways in red text have significantly higher information flow in control cells, and signaling pathways in black text are not significantly different between groups; vertical dashed lines represent information flow equal in both HFD and control. (B-C) Circle plots of cellular signaling interactions (top) and their top contributing ligand-receptor (L-R) pairs (bottom) for pathway networks involving (B) HSPG for HFD at 1 mo and (C) IFN-I for HFD at 1 mo. Dots in circle plots represent cell populations with color codes matching UMAP clusters; strokes represent communication between distinct cell populations and loops represent signaling within cell populations. Stroke and loop colors reflect the cluster sending the signal, and thickness reflects strength of the signaling pair. (D) Information flow chart at 3 mo for HFD (blue) versus control (ctrl; red). (E-F) Circle plots (top) and top contributing L-R pairs (bottom) for pathway networks involving (E) IL6 for HFD at 3 mo and (F) PDGF for HFD at 3 mo.

‘HSPG’ signaling, InflamMG signaled to HMG3, HMG2, and ProlifMG, with autocrine signaling to itself, and IfnMG cells signaled to InflamMG and ProlifMG (**Figure 3.7B; top**). Signaling was mediated between the ligand heparan sulfate proteoglycan 2 (Hspg2) and its receptor, dystroglycan 1 (Dag1) (**Figure 3.7B; bottom**). The interferon (‘IFN-I’) signaling pathway network in HFD cells at 1 mo was more complex and involved connections among multiple cell types, including non-microglia cells. ‘IFN-I’ signaling originated from ProlifMG, Mac, Mono, IfnMG, InflamMG, HMG3, HMG2, and HMG1) (**Figure 3.7C**). Since we enriched for microglia using $CD11b^{+}/CD45^{low}$ FACS, the non-microglial immune cells we isolated may comprise a biased sampling of the true populations. Due to this potential bias and the likelihood that they do not represent the full diversity of monocytes, neutrophils, macrophages, and neurons, it is difficult to draw firm conclusions regarding signaling networks involving these cell types as the senders and/or receivers. However, we can determine that IFN-I signaling involves a dynamic interplay between multiple cell types, highlighting the value of cell-to-cell communication analysis in the context of microglial mediated pathology.

Information flow at the 3 mo time point was higher in 27 pathways in HFD versus control cells and 10 pathways in control versus HFD cells (**Figure 3.7D**). Again, in some cases, signaling pathways were only detected in cells of one diet group, *e.g.*, ‘IL6’ signaling at 3 mo in HFD cells. At 3 mo, HFD turned on microglia-to-microglia signaling of ‘IL6’, ‘PDGF’ (**Figures 3.7E-F**), ‘KIT’, ‘VISTA’ (**Figure 3.8A**), ‘HSPG’, and ‘LAMININ’ pathways. The pathways elevated in HFD cells relative to controls containing microglia-to-microglia network signaling included ‘CD86’, ‘ICOS’, ‘CD200’, ‘SEMA6’, ‘PROS’, ‘CD48’, ‘CADM’ (**Figure 3.8B-C**), ‘TGFb’, and ‘GRN’. Like at 1 mo, signaling pathways

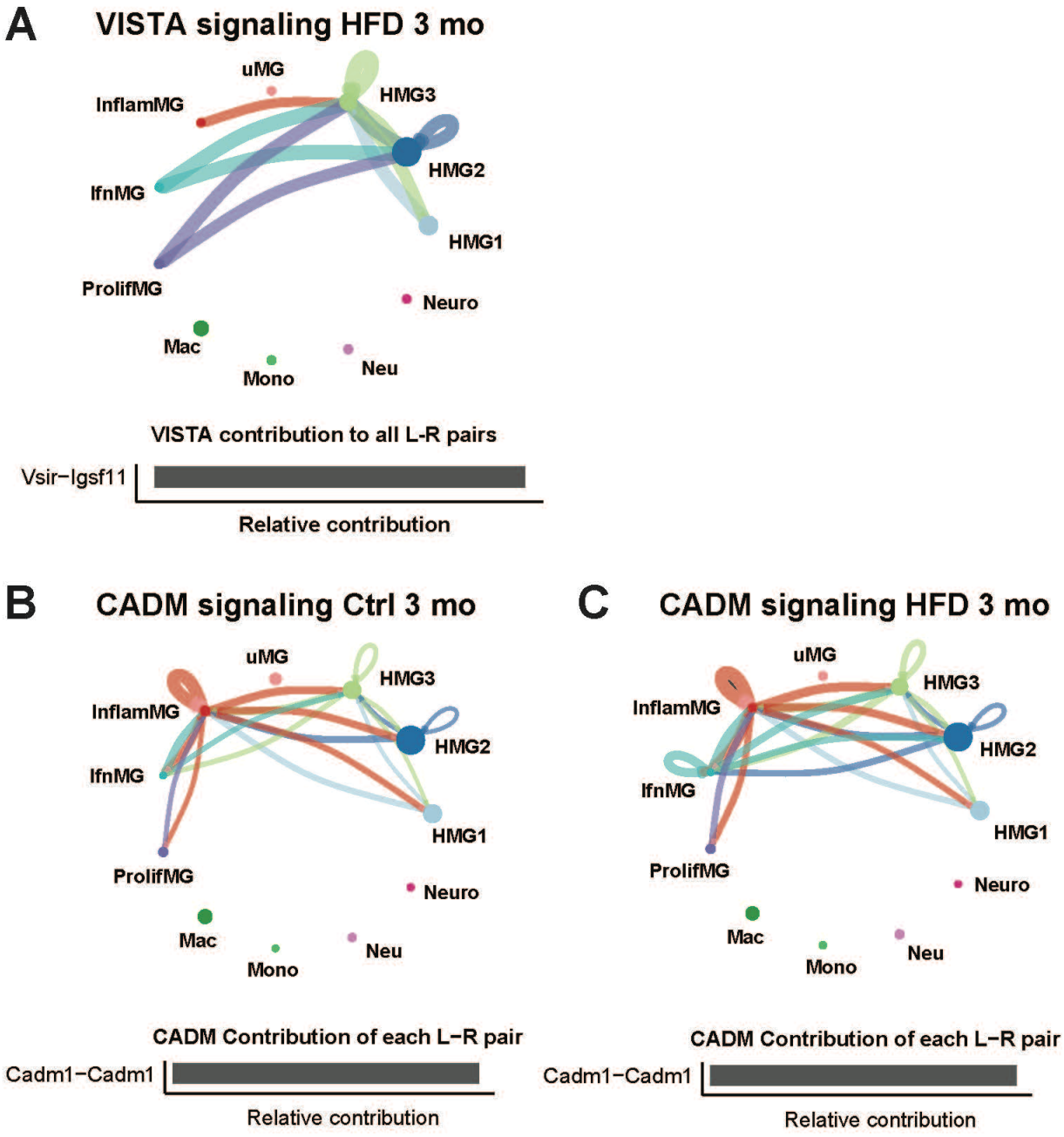

Figure 3.8 Cell-to-cell communication analyses.

Circle plots of cellular signaling interactions (top) and their top contributing ligand-receptor (L-R) pairs (bottom) for pathway networks involving (A) VISTA for HFD at 3 mo, (B) CADM for control (Ctrl) at 3 mo, (C) CADM for HFD at 3 mo. Dots in circle plots represent cell populations with color codes matching UMAP clusters; strokes represent communication between distinct cell populations and loops represent signaling within cell populations. Stroke and loop colors reflect the cluster sending the signal, thickness reflects strength of the signaling pair.

ligands included growth factors, *e.g.,* 'PDGF', 'KIT', 'TGFb', and 'GRN', and glycoproteins with immunomodulatory functions, *e.g.*, 'HSPG' and 'CD200'. 'IL6' and 'KIT' ligands are cytokines, and other ligands are cell surface immunomodulatory antigens, *e.g.*, 'CD86', 'ICOS', 'CD48', and 'VISTA'. IL-6, a cytokine with context-dependent pro- or anti-inflammatory effects [43], was expressed by IfnMG and its receptor by HMG2 and HMG3 (**Figure 3.7E**). We found obesity turned on PDGF signaling at 3 mo (**Figure 3.7F**). Several microglia subtypes (InflamMG, HMG1, HMG2, HMG3, ProlifMG, IfnMG, uMG) expressed the platelet derived growth factor (PDGF) ligand and signaled to other microglia, as well as to macrophages, neutrophils, monocytes, and neurons. PDGF is a mitogen with well-studied roles in development and wound healing, yet has detrimental effects in various disease contexts, such as cancer and atherosclerosis [44,45].

3.3.4 Obesity dysregulates microglial ER homeostasis

The results from CellChat yielded insight into the effects of obesity on microglial cell-to-cell communication. However, we were also interested in the dysregulated intracellular processes to identify potential drivers of an activated state. To accomplish this goal, we performed differentially expressed gene (DEG) analysis for all microglia types combined in HFD versus control using DESeq2. There were 89 DEGs after 1 mo HFD, and 46 DEGs after 3 mo (adjusted P-value <0.05) (**Figure 3.9A**, **Table 3.2**). To identify the biological significance of these DEGs, we performed Kyoto Encyclopedia of Genes and Genomes (KEGG) enrichment analysis (**Figure 3.9B**). Five pathways were identified at 1 mo; 'ribosome' and 'Covid-19' contained the same genes, which were all

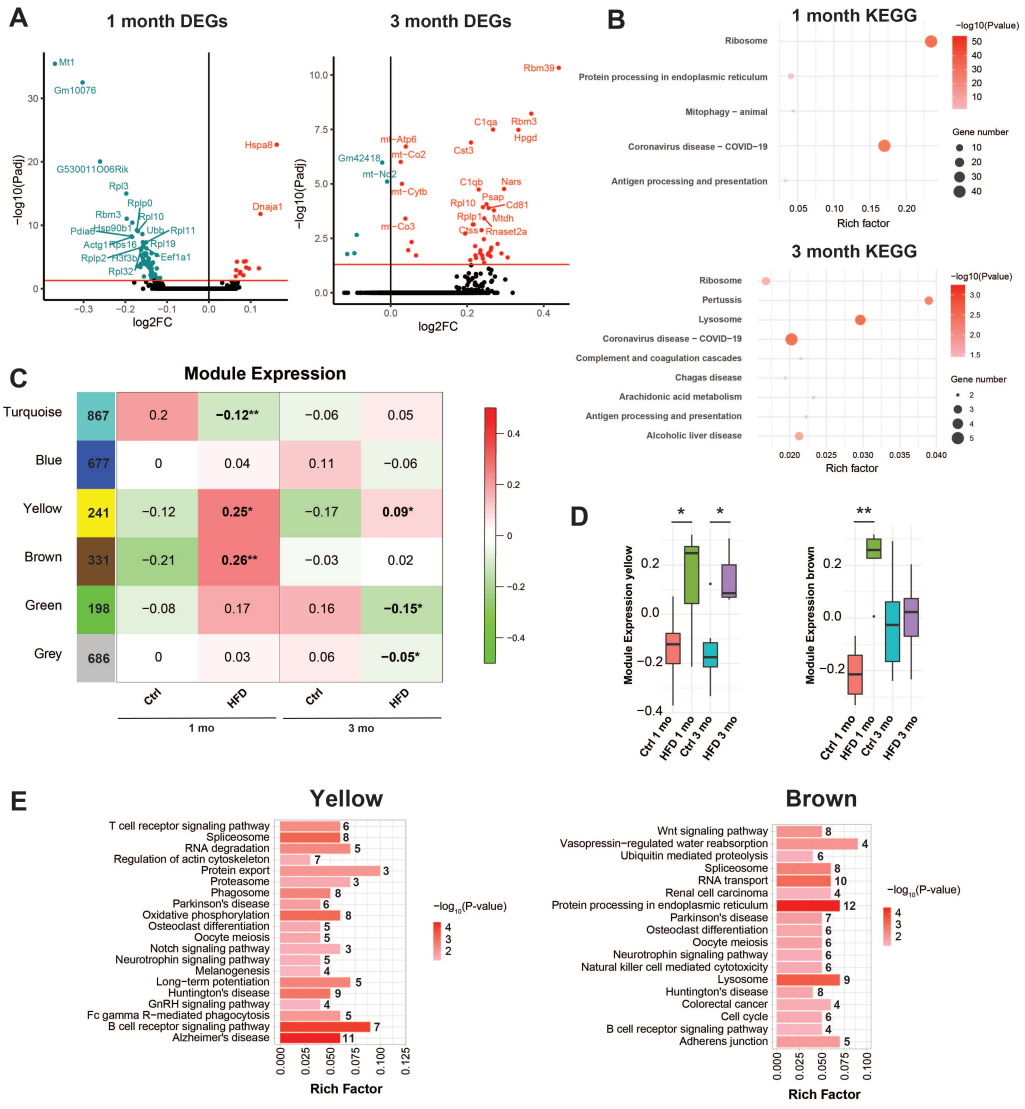

Figure 3.9 HFD dysregulates protein processing in the ER across microglial subtypes.

(A) Volcano plots of differentially expressed genes (DEGs) in HFD versus control (ctrl) at 1 mo (left) and 3 mo (right) for all microglia subtypes combined with top 20 annotated DEGs. Significant DEGs above the horizontal red line based on P-adjusted <0.05, blue dots represent significantly downregulated in HFD, red dots represent significantly upregulated in HFD. FC, fold-change. (B) KEGG pathway analysis of DEGs in HFD versus control at 1 mo (top) and 3 mo (bottom). Dot color represents -log10(P-value) from least significant (light pink) to most significant (red); dot size represents gene number, the number of significant DEGs in the KEGG pathway; rich factor represents the fraction of significant DEGs among all genes in the KEGG pathway. (C) WGCNA modules by color, turquoise, yellow, brown, green, blue, with number of genes assigned to each module (column 1), and corresponding heatmap of median module expression by condition. The grey module comprises genes not clustered into a co-expression module. Significant differences in expression of genes in modules between experimental groups by Kruskal-Wallis, *P<0.05, **P<0.01. (D) Boxplots of yellow and brown module expression. Significant differences by Kruskal-Wallis, *P<0.05, **P<0.01. (E) KEGG pathway analysis of genes in HFD versus control from the yellow (left) and brown (right) modules. Bar color represents -log10(P-value) from least significant (light pink) to most significant (red); bar length represents the number of genes in the KEGG pathway, annotated with a number; rich factor represents the fraction of genes among all genes in the KEGG pathway.

Table 3.2 Microglia DEGs.

Differentially expressed genes (DEGs) of all microglia clusters combined from HFD versus control mice at 1 mo (white) and 3 mo (grey) meeting the criteria of nominal P-value>0.05. Entries arranged by nominal P-value. Adjusted P-value based on Bonferroni correction using all features in the dataset. FC, fold-change; pct.1, percentage of cells where the feature is detected in the first group; pct.2, percentage of cells where the feature is detected in the second group. Only the top 50 genes for each timepoint are included below; the complete dataset will be available at the time of publication or upon request.

Gene	p_val	avg_log2FC	pct.1	pct.2	p_val_adj
Mt1	1.12E-40	-0.36863	0.564	0.692	3.63E-36
Gm10076	9.99E-38	-0.30252	0.528	0.651	3.22E-33
Hspa8	6.32E-28	0.162455	0.936	0.917	2.04E-23
G530011O06Rik	2.82E-25	-0.26056	0.477	0.584	9.09E-21
Rpl3	3.14E-20	-0.19781	0.934	0.947	1.01E-15
Dnaja1	5.11E-17	0.123507	0.697	0.646	1.65E-12
Rbm3	2.85E-16	-0.19676	0.509	0.605	9.19E-12
Hsp90b1	1.19E-15	-0.18333	0.975	0.98	3.83E-11
Rplp0	1.86E-14	-0.17252	0.932	0.946	6.02E-10
Rpl10	2.70E-14	-0.1699	0.964	0.971	8.73E-10
Ubb	7.56E-14	-0.15925	0.958	0.966	2.44E-09
Pdia6	1.70E-13	-0.18534	0.842	0.876	5.48E-09
Actg1	2.11E-13	-0.18381	0.898	0.93	6.82E-09
Rps16	1.42E-12	-0.1581	0.96	0.969	4.60E-08
Rpl11	1.54E-12	-0.15044	0.964	0.974	4.97E-08
Rpl19	3.53E-12	-0.15649	0.962	0.97	1.14E-07
Rplp2	7.75E-12	-0.15791	0.961	0.97	2.50E-07
Eef1a1	1.34E-11	-0.14966	0.983	0.989	4.31E-07
H3f3b	1.43E-11	-0.16161	0.945	0.955	4.61E-07
Rpl32	2.40E-11	-0.1626	0.968	0.974	7.75E-07
Trem2	7.97E-11	-0.13733	0.975	0.982	2.57E-06
Lamtor4	8.24E-11	-0.15449	0.695	0.748	2.66E-06
Zeb2os	8.65E-11	-0.15022	0.506	0.571	2.79E-06
Rack1	1.21E-10	-0.15145	0.927	0.936	3.89E-06
Fcer1g	1.48E-10	-0.12497	0.983	0.985	4.78E-06
Rps20	1.62E-10	-0.16168	0.963	0.963	5.24E-06
Rps7	1.91E-10	-0.15009	0.96	0.969	6.16E-06
Eef1b2	4.82E-10	-0.15831	0.918	0.922	1.56E-05
Rps9	5.30E-10	-0.14391	0.971	0.975	1.71E-05
Naca	1.38E-09	-0.14461	0.908	0.918	4.45E-05
Zeb2	1.43E-09	0.088121	0.927	0.905	4.63E-05
Gapdh	1.46E-09	-0.15731	0.898	0.918	4.72E-05
Fau	1.51E-09	-0.14693	0.983	0.987	4.89E-05
Rpsa	1.61E-09	-0.15303	0.946	0.95	5.21E-05
Rps18	1.62E-09	-0.15134	0.944	0.946	5.21E-05
Fam91a1	1.66E-09	0.083871	0.752	0.728	5.35E-05
Hpgd	1.73E-09	0.067212	0.917	0.908	5.60E-05
Rpl5	1.99E-09	-0.14716	0.96	0.962	6.43E-05
Uba52	2.11E-09	-0.14924	0.936	0.942	6.82E-05
Rpl8	2.24E-09	-0.1339	0.94	0.951	7.22E-05
Rpl12	2.34E-09	-0.14569	0.942	0.952	7.56E-05
Fth1	2.98E-09	-0.14554	0.981	0.986	9.63E-05
Rpl21	3.10E-09	-0.13779	0.973	0.98	0.0001
Rpl17	3.35E-09	-0.14847	0.963	0.971	0.000108
Rpl35	3.76E-09	-0.16315	0.946	0.949	0.000121
Rpl15	3.79E-09	-0.1365	0.943	0.95	0.000122
Calr	3.88E-09	-0.15554	0.954	0.959	0.000125
Ppib	4.68E-09	-0.13976	0.937	0.945	0.000151
Rpl30	4.70E-09	-0.1398	0.972	0.978	0.000152
Rps5	6.94E-09	-0.14728	0.939	0.947	0.000224
Rbm39	1.45E-15	0.439514	0.954	0.913	4.68E-11
Rbm3	1.85E-13	0.367636	0.712	0.608	5.97E-09
C1qa	9.92E-13	0.267721	0.992	0.985	3.20E-08
Hpgd	1.03E-12	0.333976	0.933	0.868	3.31E-08
Cst3	3.90E-12	0.20993	1	1	1.26E-07
mt-Atp6	6.00E-12	0.039408	0.999	1	1.94E-07
mt-Co2	3.03E-11	0.026206	1	0.997	9.77E-07

Gm42418	3.25E-11	-0.02227	1	1	1.05E-06
mt-Nd2	2.42E-10	-0.00951	0.996	0.997	7.83E-06
mt-Cytb	3.09E-10	0.029253	0.998	0.999	9.98E-06
Nars	5.28E-10	0.296505	0.913	0.84	1.71E-05
C1qb	5.61E-10	0.230102	0.992	0.983	1.81E-05
Psap	2.68E-09	0.250591	0.985	0.97	8.65E-05
Rpl10	3.63E-09	0.241252	0.966	0.935	0.000117
Cd81	4.01E-09	0.256155	0.976	0.949	0.00013
Mtdh	5.08E-09	0.269967	0.966	0.931	0.000164
Rnaset2a	1.19E-08	0.244693	0.945	0.888	0.000384
mt-Co3	1.21E-08	0.038341	0.999	0.998	0.000391
Rplp1	2.26E-08	0.216809	0.979	0.958	0.000729
Ctss	2.28E-08	0.21476	0.994	0.99	0.000737
Laptm4a	4.13E-08	0.237581	0.948	0.924	0.001334
Itm2b	5.90E-08	0.194612	0.991	0.976	0.001905
Hsp90ab1	6.83E-08	-0.08903	0.96	0.937	0.002204
Trem2	1.07E-07	0.24371	0.981	0.964	0.003449
mt-Nd4	1.44E-07	0.054547	0.996	0.995	0.004657
Ighm	1.76E-07	0.279486	0.845	0.779	0.005675
Laptm5	2.23E-07	0.220742	0.986	0.964	0.007194
Ptgs1	2.61E-07	0.263238	0.968	0.952	0.008423
Siglech	3.40E-07	0.261664	0.991	0.985	0.010975
mt-Nd1	3.42E-07	0.045724	0.994	0.999	0.011038
Fth1	3.48E-07	0.234793	0.979	0.961	0.011248
Tpm3	4.65E-07	0.256175	0.961	0.932	0.015004
Tpt1	4.67E-07	0.233878	0.977	0.951	0.015091
AY036118	4.72E-07	-0.09499	0.971	0.955	0.015231
Txnip	4.82E-07	0.289599	0.882	0.815	0.015571
P4ha1	5.15E-07	-0.11377	0.822	0.81	0.01662
Ltc4s	5.55E-07	0.254251	0.951	0.905	0.017924
Clic1	5.89E-07	0.238995	0.954	0.923	0.01902
Tmem50a	5.91E-07	0.221639	0.954	0.9	0.019096
mt-Co1	5.96E-07	0.066076	0.999	0.999	0.019251
Tra2b	6.54E-07	0.261272	0.83	0.72	0.021102
Rapgef6	7.41E-07	0.305789	0.717	0.605	0.023925
Cfl1	7.80E-07	0.223134	0.947	0.901	0.025176
Abhd12	8.28E-07	0.240939	0.962	0.921	0.026743
Rps23	9.79E-07	0.208066	0.966	0.944	0.031613
Cx3cr1	1.28E-06	0.244314	0.998	0.993	0.041441
Rpl7a	1.68E-06	0.210422	0.954	0.906	0.054168
Cd37	2.44E-06	0.256471	0.948	0.914	0.078924
Btg1	2.78E-06	0.263299	0.882	0.802	0.089777
Rpl18a	3.93E-06	0.204247	0.967	0.948	0.127018

ribosomal and included *Rpl3*, *Rplp0*, *Rpl10*, *Rps16*, *Rpl11*, among others. 'Protein processing in the endoplasmic reticulum' (ER) contained *Hspa8*, *Dnaja1*, *Hsp90b1*, *Pdia6*, *Calr*, *Hspa5*, and *Dnajb1*. 'Mitophagy-animal' and 'antigen processing and presentation' contained only three genes each. Performing KEGG analysis for 3 mo was less informative, due to few DEGs, only 46, KEGG enrichment analysis at 3 mo yielded 'lysosome,' 'Covid-19,' 'pertussis,' 'alcoholic liver disease,' 'ribosome,' 'arachidonic acid metabolism,' 'antigen processing and presentation,' 'complement and coagulation cascades,' and 'chagas disease.' However, there were no more than five genes in each KEGG pathway, including *C1qa* and *C1qb* complement genes, which were present in five of the nine pathways.

Next, we identified DEGs in HFD versus control for each of the 11 cell types at both 1 mo and 3 mo. Overall, few DEGs (adjusted P-value <0.05) were identified, with 0 DEGs for most comparisons (**Table 3.3**). DEGs for HFD versus control were identified for HMG1 (18 DEGs), HMG2 (8 DEGs), HMG3 (8 DEGs), and Mac (3 DEGs) at 1 mo. At 3 mo, DEGs were identified for HMG1 (1 DEGs), HMG2 (8 DEGs), and HMG3 (1 DEG). For both the cluster specific and all microglia combined analyses, there were more DEGs at 1 mo than 3 mo. The cluster specific analysis detected DEGs in HFD versus control only in HMG populations and macrophages. Although there were too few genes to perform KEGG on cluster specific DEGs, we found again, that protein processing in the ER genes were represented. At 1 mo, ER related DEGs included *Hspa8*, *Hsp90b1*, and *Dnaja1* for HMG1, *Hspa8* and *Calr* for HMG2, and *Hspa8*, *Dnaja1*, and *Pdia6* for HMG3. The DEGs in the macrophage group were *H3f3b*, *Ucp2*, and *Gm10076*. At 3 mo, *Hsp90ab1* and *Hsp90aa1* were DEGs in HMG2.

Table 3.3 Cluster-specific DEGs.

(A) Summary of the number of significant differentially expressed genes (DEGs) in each cell cluster in HFD versus control mice at 1 mo (white) and 3 mo (grey). (B) DEGs in each cell cluster in HFD versus control mice at 1 mo (white) and 3 mo (grey) meeting the criteria of adjusted P-value (Padj)>0.05 based on Bonferroni correction using all features in the dataset. FC, fold-change; pct.1, percentage of cells where the feature is detected in the first group; pct.2, percentage of cells where the feature is detected in the second group. HMG1, 2, 3, homeostatic microglia 1, 2, 3; InflamMG, inflammatory microglia; IfnMG, interferon-related; ProlifMG, proliferating microglia; uMG, functionally undescribed microglia; Mac, macrophages; Mono, monocytes; Neu, neutrophils; Neuro, neurons.

3.3A

Cluster	1 mo	3 mo
HMG1	18	1
HMG2	8	8
HMG3	8	1
InflamMG	0	0
IfnMG	0	0
ProlifMG	0	0
Mono	0	0
Neuro	0	0
Neu	0	0
Mac	3	0
uMG	0	0

3.3B

Cluster, time point	Gene	P-value	avg Log_2FC	pct.1	pct.2	Padj
HMG1, 1 mo	Hspa8	1.29E-13	0.149	0.975	0.955	4.17E-09
HMG1, 1 mo	Gm10076	2.27E-13	-0.294	0.694	0.819	7.33E-09
HMG1, 1 mo	Mt1	1.70E-12	-0.329	0.653	0.766	5.50E-08
HMG1, 1 mo	Rbm39	1.90E-11	0.121	0.959	0.943	6.13E-07
HMG1, 1 mo	Actg1	5.17E-11	-0.247	0.936	0.968	1.67E-06
HMG1, 1 mo	G530011O06Rik	3.57E-10	-0.255	0.469	0.570	1.15E-05
HMG1, 1 mo	Rpl3	6.86E-10	-0.174	0.996	0.999	2.22E-05
HMG1, 1 mo	H3f3b	1.82E-08	-0.211	0.986	0.992	5.86E-04
HMG1, 1 mo	AY036118	2.68E-08	0.159	0.935	0.925	8.64E-04
HMG1, 1 mo	Pmepa1	3.81E-08	-0.250	0.959	0.962	1.23E-03
HMG1, 1 mo	Arid1a	5.13E-08	0.116	0.804	0.754	1.66E-03
HMG1, 1 mo	Hpgd	7.94E-08	0.082	0.958	0.955	2.56E-03
HMG1, 1 mo	Hsp90b1	9.66E-08	-0.204	0.997	0.999	3.12E-03
HMG1, 1 mo	Ubb	1.50E-07	-0.191	0.998	0.999	4.83E-03
HMG1, 1 mo	Dnaja1	2.12E-07	0.113	0.730	0.687	6.83E-03
HMG1, 1 mo	Wdr44	4.68E-07	0.120	0.493	0.425	1.51E-02
HMG1, 1 mo	Rbm3	4.98E-07	-0.193	0.605	0.687	1.61E-02
HMG1, 1 mo	Cirbp	1.52E-06	-0.186	0.321	0.402	4.91E-02
HMG1, 3 mo	Rbm3	1.17E-06	0.428	0.796	0.698	3.77E-02
HMG2, 1 mo	G530011O06Rik	4.89E-22	-0.417	0.486	0.636	1.58E-17
HMG2, 1 mo	Hspa8	1.11E-16	0.191	0.971	0.937	3.59E-12
HMG2, 1 mo	Mt1	1.73E-12	-0.350	0.585	0.706	5.59E-08
HMG2, 1 mo	Gm10076	3.81E-11	-0.292	0.513	0.625	1.23E-06
HMG2, 1 mo	Rbm3	3.68E-09	-0.241	0.517	0.640	1.19E-04
HMG2, 1 mo	Calr	7.08E-07	-0.213	0.986	0.987	2.28E-02
HMG2, 1 mo	Pmepa1	7.88E-07	-0.222	0.963	0.979	2.54E-02
HMG2, 1 mo	I830077J02Rik	1.26E-06	-0.199	0.496	0.601	4.07E-02
HMG2, 3 mo	Rbm39	8.62E-18	0.470	0.985	0.951	2.78E-13
HMG2, 3 mo	Hsp90ab1	1.68E-15	-0.216	0.989	0.995	5.43E-11
HMG2, 3 mo	Hsp90aa1	7.59E-08	-0.178	0.899	0.922	2.45E-03
HMG2, 3 mo	Rbm3	1.34E-07	0.348	0.746	0.650	4.31E-03
HMG2, 3 mo	Rapgef6	5.14E-07	0.370	0.788	0.689	1.66E-02
HMG2, 3 mo	Arid5b	1.06E-06	0.377	0.626	0.496	3.41E-02
HMG2, 3 mo	C1qa	1.24E-06	0.219	1.000	1.000	3.99E-02
HMG2, 3 mo	Nars	1.45E-06	0.309	0.969	0.927	4.69E-02
HMG3, 1 mo	Mt1	1.04E-23	-0.412	0.460	0.619	3.36E-19
HMG3, 1 mo	Hspa8	9.12E-20	0.285	0.978	0.956	2.95E-15
HMG3, 1 mo	Dnaja1	3.55E-13	0.251	0.730	0.607	1.15E-08

HMG3, 1 mo	Zeb2	1.31E-07	0.169	0.939	0.924	4.22E-03
HMG3, 1 mo	Ywhah	3.70E-07	0.141	0.958	0.938	1.19E-02
HMG3, 1 mo	Gm10076	6.65E-07	-0.170	0.431	0.524	2.15E-02
HMG3, 1 mo	Fam91a1	1.20E-06	0.149	0.805	0.775	3.86E-02
HMG3, 1 mo	Pdia6	1.25E-06	-0.158	0.876	0.914	4.03E-02
HMG3, 3 mo	Rbm39	8.62E-18	0.470	0.985	0.951	2.78E-13
HMG3, 3 mo	Hsp90ab1	1.68E-15	-0.216	0.989	0.995	5.43E-11
HMG3, 3 mo	Hsp90aa1	7.59E-08	-0.178	0.899	0.922	2.45E-03
HMG3, 3 mo	Rbm3	1.34E-07	0.348	0.746	0.650	4.31E-03
HMG3, 3 mo	Rapgef6	5.14E-07	0.370	0.788	0.689	1.66E-02
HMG3, 3 mo	Arid5b	1.06E-06	0.377	0.626	0.496	3.41E-02
HMG3, 3 mo	C1qa	1.24E-06	0.219	1.000	1.000	3.99E-02
HMG3, 3 mo	Nars	1.45E-06	0.309	0.969	0.927	4.69E-02
Mac, 1 mo	H3f3b	8.30E-13	-0.595	0.929	0.927	2.68E-08
Mac, 1 mo	Ucp2	1.67E-09	-0.647	0.851	0.889	5.39E-05
Mac, 1 mo	Gm10076	8.78E-08	-0.538	0.447	0.639	2.83E-03

Due to the similarity among UMAP clustered HMG subtypes, and because most cluster specific DEGs were identified in HMGs, we next considered the three homeostatic microglia subtypes as a single cluster and performed DESeq2 analysis. We identified 96 DEGs at 1 mo and 12 DEGs at 3 mo in all three homeostatic microglia subtypes combined (**Table 3.4**). KEGG analysis at 1 mo in this subset of HMGs again showed enrichment in 'ribosome,' 'covid-19,' and 'protein processing in the endoplasmic reticulum,' as well as in 'prostate cancer' and 'salmonella infection.' Homeostatic microglia make up the largest proportion of all microglia, so it is expected that HMG DEGs reflect the DEGs for the combined microglia analysis.

Since few DEGs were identified between HFD and control groups, we implemented an additional approach to examine differences between groups and infer potential biological significance. We performed weighted gene co-expression network analysis (WGCNA), an unsupervised correlation analysis, to identify co-expressed gene modules across all samples, including genes for all cell types. Analysis of 1 mo and 3 mo samples yielded five co-expression modules and 1 module of genes (grey module) that were not assigned to a co-expression module (**Figure 3.9C;** module dendrogram, **Figure 3.10A**). Four modules, turquoise, yellow, brown, and green, differed significantly between HFD and control groups. The turquoise module, containing 867 genes, had reduced expression in HFD at 1 mo (P=0.0087), the yellow module, containing 241 genes, had elevated expression in HFD at 1 mo (P=0.041) and 3 mo (P=0.026), the brown module, containing 331 genes, had elevated expression in HFD after 1 mo (P=0.0022), and the green module, containing 198 genes, had reduced expression in HFD at 3 mo (P=0.041) (**Figure 3.9D; Figure 3.10B**). We next performed KEGG

Table 3.4 HMG DEGs.

Differentially expressed genes (DEGs) of all homeostatic microglia (HMG) clusters combined from HFD versus control mice at 1 mo (white) and 3 mo (grey) meeting the criteria of nominal P-value>0.05. Entries arranged by nominal P-value. Adjusted P-value (Padj) based on Bonferroni correction using all features in the dataset. FC, fold-change; pct.1, percentage of cells where the feature is detected in the first group; pct.2, percentage of cells where the feature is detected in the second group. Only the top 50 genes are included below; the complete dataset will be available at the time of publication or upon request.

HFD versus control at 1 month						HFD versus control at 3 month					
Gene	**P-value**	**avg Log_2FC**	**pct.1**	**pct.2**	**Padj**	**Gene**	**P-value**	**avg Log_2FC**	**pct.1**	**pct.2**	**Padj**
Hspa8	9.60E-52	0.207	0.975	0.950	3.10E-47	Rbm39	2.01E-19	0.452	0.971	0.932	6.50E-15
Mt1	5.84E-43	-0.377	0.567	0.704	1.89E-38	Hsp90ab1	3.32E-19	-0.136	0.990	0.994	1.07E-14
Gm10076	4.90E-33	-0.303	0.549	0.673	1.58E-28	P4ha1	3.05E-12	-0.160	0.852	0.874	9.83E-08
G530011O06Rik	1.60E-27	-0.272	0.492	0.606	5.15E-23	Rbm3	4.08E-12	0.363	0.728	0.641	1.32E-07
Dnaja1	1.73E-21	0.138	0.722	0.664	5.58E-17	Hsp90aa1	1.20E-11	-0.135	0.887	0.909	3.88E-07
Rbm3	5.02E-20	-0.211	0.515	0.617	1.62E-15	Gm42418	7.10E-08	-0.088	1.000	1.000	2.29E-03
Rpl3	8.69E-18	-0.207	0.972	0.980	2.81E-13	Fth1	2.44E-07	0.262	1.000	0.999	7.87E-03
Rbm39	1.15E-14	0.071	0.961	0.949	3.72E-10	AY036118	4.50E-07	-0.137	0.996	0.995	1.45E-02
Dleu2	1.27E-14	0.131	0.737	0.688	4.09E-10	Hspa8	6.28E-07	-0.024	0.984	0.977	2.03E-02
Actg1	2.00E-14	-0.188	0.935	0.964	6.47E-10	Lars2	7.10E-07	-0.092	0.968	0.973	2.29E-02
Fam91a1	1.78E-13	0.089	0.789	0.759	5.76E-09	Rapgef6	1.18E-06	0.324	0.747	0.637	3.81E-02
Zeb2	6.57E-13	0.078	0.938	0.917	2.12E-08	Cbfa2t3	1.43E-06	0.298	0.546	0.449	4.61E-02
Hpgd	1.63E-12	0.060	0.959	0.947	5.26E-08	Arid5b	2.66E-06	0.309	0.579	0.472	8.57E-02
Serinc3	2.99E-12	-0.005	1.000	1.000	9.66E-08	Slc6a6	2.76E-06	0.285	0.718	0.621	8.92E-02
AY036118	4.14E-12	0.101	0.914	0.896	1.34E-07	Hpgd	3.21E-06	0.289	0.970	0.948	1.04E-01
Arid1a	4.29E-12	0.077	0.822	0.791	1.39E-07	Fus	1.08E-05	0.334	0.945	0.893	3.49E-01
Ubb	8.92E-12	-0.160	0.993	0.996	2.88E-07	Fkbp5	1.82E-05	0.260	0.463	0.339	5.87E-01
Rpl10	1.00E-11	-0.176	0.998	0.998	3.24E-07	Rbm25	2.12E-05	0.295	0.898	0.851	6.85E-01
Rplp0	1.14E-11	-0.176	0.970	0.980	3.69E-07	Gm47283	2.56E-05	0.252	0.397	0.267	8.27E-01
Gls	2.48E-11	0.096	0.462	0.417	8.01E-07	Ttc14	2.94E-05	0.280	0.677	0.612	9.50E-01
Dynll1	3.65E-11	0.079	0.644	0.608	1.18E-06	Pfkl	4.27E-05	-0.125	0.258	0.334	1.00E+00
Btg1	8.38E-11	0.070	0.840	0.834	2.70E-06	Nars	4.39E-05	0.263	0.946	0.901	1.00E+00
Hsp90b1	8.69E-11	-0.160	0.998	0.999	2.81E-06	Chsy1	4.80E-05	-0.107	0.525	0.561	1.00E+00
Pdia6	1.21E-10	-0.173	0.873	0.904	3.92E-06	Srsf3	7.19E-05	0.255	0.911	0.849	1.00E+00
Cirbp	1.59E-10	-0.154	0.316	0.396	5.14E-06	Acox3	7.74E-05	0.233	0.592	0.470	1.00E+00
Rhob	3.83E-10	0.054	0.972	0.970	1.24E-05	Slc38a2	1.06E-04	0.261	0.718	0.604	1.00E+00
Rps20	4.38E-10	-0.172	0.997	0.996	1.41E-05	Abcg1	1.37E-04	0.249	0.665	0.605	1.00E+00

Rplp2	7.19E-10	-0.167	0.996	0.999	2.32E-05	mt-Nd2	1.50E-04	-0.003	0.999	1.000	1.00E+00
Dnajb1	7.95E-10	0.088	0.383	0.332	2.57E-05	H3f3b	1.54E-04	0.008	0.992	0.988	1.00E+00
H3f3b	8.32E-10	-0.160	0.983	0.989	2.68E-05	Tspo	1.57E-04	0.219	0.537	0.427	1.00E+00
Eef1a1	1.58E-09	-0.157	1.000	1.000	5.10E-05	Tcf25	1.62E-04	0.244	0.765	0.693	1.00E+00
Rpl32	1.76E-09	-0.170	0.997	0.999	5.68E-05	Ccnt2	1.66E-04	0.225	0.619	0.533	1.00E+00
Zeb2os	1.87E-09	-0.148	0.531	0.594	6.04E-05	Arrb2	1.83E-04	0.242	0.831	0.777	1.00E+00
Rps9	1.90E-09	-0.158	0.999	0.999	6.14E-05	Pabpn1	1.94E-04	0.215	0.502	0.395	1.00E+00
Slc15a4	1.95E-09	0.089	0.412	0.354	6.29E-05	Brox	1.95E-04	0.216	0.547	0.437	1.00E+00
Rps16	2.10E-09	-0.164	0.997	0.997	6.80E-05	Atf7ip	2.02E-04	0.258	0.670	0.602	1.00E+00
Lamtor4	2.24E-09	-0.153	0.730	0.782	7.24E-05	Mtr	2.18E-04	0.219	0.521	0.429	1.00E+00
Rack1	2.98E-09	-0.162	0.963	0.970	9.62E-05	Pcyox1	2.59E-04	0.221	0.440	0.338	1.00E+00
Ywhah	4.82E-09	0.037	0.943	0.931	1.56E-04	Rcsd1	2.88E-04	0.237	0.677	0.589	1.00E+00
Rpl19	5.65E-09	-0.159	0.994	0.998	1.82E-04	Arpc5l	3.10E-04	0.217	0.535	0.462	1.00E+00
Rpl11	8.22E-09	-0.155	0.997	0.999	2.65E-04	Hsp90b1	3.30E-04	0.025	1.000	0.999	1.00E+00
Maf	8.57E-09	0.034	0.994	0.992	2.77E-04	Psmd7	3.65E-04	0.222	0.567	0.478	1.00E+00
Marcks	1.55E-08	-0.003	1.000	0.999	4.99E-04	Snrnp70	3.67E-04	0.271	0.910	0.838	1.00E+00
Mat2a	1.71E-08	0.072	0.574	0.543	5.52E-04	Actg1	4.08E-04	0.005	0.974	0.966	1.00E+00
Zfp36l2	1.92E-08	0.054	0.851	0.834	6.21E-04	Zfp207	4.32E-04	0.221	0.625	0.532	1.00E+00
Ep300	2.59E-08	0.066	0.702	0.659	8.36E-04	Srsf11	4.44E-04	0.243	0.762	0.691	1.00E+00
Fau	2.78E-08	-0.156	1.000	1.000	8.98E-04	Ccng2	5.22E-04	0.234	0.635	0.548	1.00E+00
Eef1b2	2.99E-08	-0.169	0.962	0.958	9.64E-04	Rpl10	5.25E-04	0.194	1.000	0.998	1.00E+00
Nrip1	2.99E-08	0.055	0.921	0.910	9.65E-04	Tmem63a	5.39E-04	0.220	0.643	0.594	1.00E+00

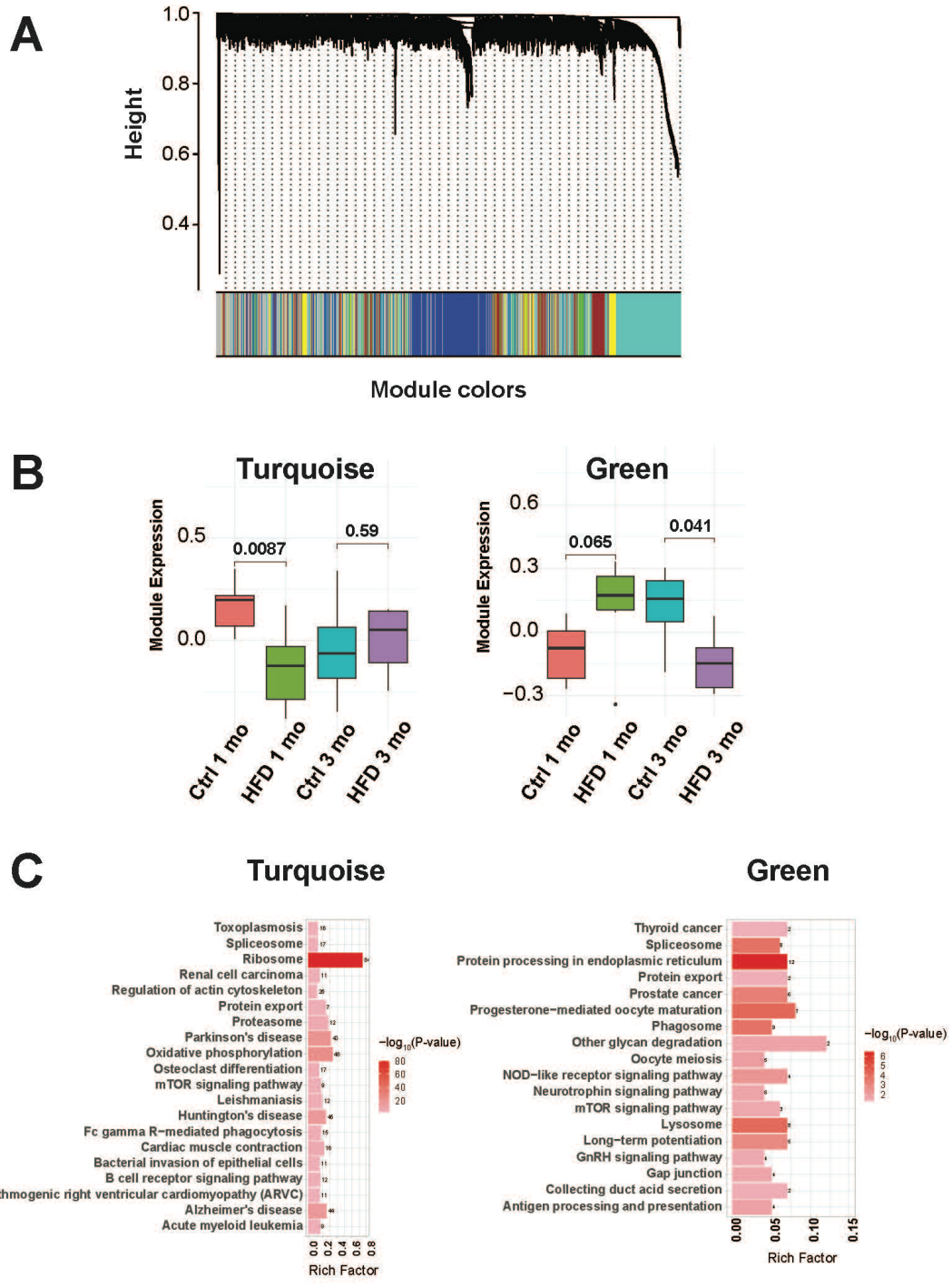

Figure 3.10 WGCNA modules.

(A) WGCNA cluster dendrogram arranges genes from all cell types into 6 modules: grey, turquoise, yellow, brown, green, blue. (B) Significant differences in expression of genes in turquoise and green modules between experimental groups by Kruskal-Wallis, *P<0.05, **P<0.01. (C) KEGG pathway analysis of genes in HFD versus control from the turquoise (left) and green (right) modules. Bar color represents -log10(P-value) from least significant (light pink) to most significant (red); bar length represents the number of genes in the KEGG pathway, annotated with a number; rich factor represents the fraction of genes among all genes in the KEGG pathway.

enrichment analysis on each module. The yellow module was enriched for genes in a variety of biological pathways, including 'Alzheimer's disease', containing the genes *Psenen*, *Ndufb5*, *Atp5o*, *Gnaq*, *Ndufs8*, *Ndufa5*, *Mapk3*, *Ndufs4*, *Atp5g3*, *Ppp3r1*, and *Psen1* (**Table 3.5**), and 'B cell receptor signaling pathway' (**Figure 3.9E**). The brown module was enriched for 'protein processing in the endoplasmic reticulum,' containing *Hspa8*, *Nfe2l2*, *Selenos*, *P4hb*, *Dnaja1*, *Ssr1*, *Edem1*, *Man1c1*, *Eif2s1*, *Ube2j1*, *Erlec1, and Dnajb1* (**Table 3.5**). The turquoise module was most significantly enriched in 'ribosome' and 'oxidative phosphorylation' genes, and the green module in 'protein processing in the endoplasmic reticulum' genes (**Figure 3.10C-D**).

3.4 Discussion

Rates of obesity are climbing ([WHO 2021]), alongside rises in associated complications, such as cognitive impairment [2,8]. Thus, there is a need to understand the pathophysiology of cognitive deficits secondary to obesity to intervene. Through their contribution to cognitive impairment in obesity [9], microglia serve as a potential therapeutic target, although the mechanisms of microglial activation in this context remain incompletely understood. In this study, we used scRNA-seq to determine the effect of obesity over time on the hippocampal microglial transcriptome. scRNA-seq allowed us to probe the heterogeneity of microglial populations and identify unique cellular processes and inflammatory pathways that are dysregulated in obesity. We, for the first time in the adolescent and adult C57BL/6J hippocampus, identified seven microglial subtypes, along with three other immune cell types and neurons. All cell types were present in HFD and control groups at 1 mo and 3 mo diet, and diet did not affect

Table 3.5 WGCNA module gene enrichment.

Unsupervised weighted gene co-expression network analysis (WGCNA) of 1 mo and 3 mo samples identified two significant modules, yellow and brown. KEGG pathway analysis shown in table of yellow (top) and brown (bottom) module. Padj, adjusted P-value. 'Annot,' KEGG pathway identification number; 'Annotated,' number of genes annotated in KEGG pathway; 'Significant,' number of genes in the module that are represented in the KEGG term annotation; 'Gene,' gene names for each significant gene.

Yellow module

Annot	Term	Annotated	Significant	P-value	Padj	Gene
5010	Alzheimer's disease	178	11	2.88E-05	3.45E-03	Psenen, Ndufb5, Atp5o, Gnaq, Ndufs8, Ndufa5, Mapk3, Ndufs4, Atp5g3, Ppp3r1, Psen1
4662	B cell receptor signaling pathway	76	7	7.49E-05	4.50E-03	Fcgr2b, Pik3ap1, Vav1, Mapk3, Nfatc1, Bcl10, Ppp3r1
3040	Spliceosome	133	8	4.54E-04	1.74E-02	Hnrnpk, Srsf3, Prpf40a, Pcbp1, Snu13, Srsf6, Snrnp27, Cdc40
190	Oxidative phosphorylation	138	8	5.81E-04	1.74E-02	Atp6v1e1, Ndufb5, Atp5o, Ndufs8, Ndufa5, Atp6v0d1, Ndufs4, Atp5g3
5016	Huntington's disease	188	9	1.05E-03	2.53E-02	Ndufb5, Atp5o, Gnaq, Ndufs8, Ndufa5, Ap2b1, Ndufs4, Atp5g3, Hdac1
4720	Long-term potentiation	69	5	2.48E-03	4.29E-02	Camk2d, Gnaq, Mapk3, Prkacb, Ppp3r1
4145	Phagosome	173	8	2.50E-03	4.29E-02	Ctsl, Calr, Fcgr1, Fcgr2b, Ncf2, Atp6v1e1, Atp6v0d1, Eea1
3018	RNA degradation	74	5	3.37E-03	5.00E-02	Btg2, Cnot4, Cnot6l, Cnot3, Dhx36
4660	T cell receptor signaling pathway	109	6	3.75E-03	5.00E-02	Vav1, Mapk3, Nfatc1, Bcl10, Pdk1, Ppp3r1
3060	Protein export	29	3	7.11E-03	8.46E-02	Sec11c, Sec11a, Spcs3
4666	Fc gamma R-mediated phagocytosis	90	5	7.75E-03	8.46E-02	Fcgr1, Fcgr2b, Arpc5, Vav1, Mapk3
5012	Parkinson's disease	139	6	1.20E-02	1.20E-01	Ndufb5, Atp5o, Ndufs8, Ndufa5, Ndufs4, Atp5g3
4114	Oocyte meiosis	112	5	1.87E-02	1.73E-01	Camk2d, Ywhaq, Mapk3, Prkacb, Ppp3r1
4380	Osteoclast differentiation	118	5	2.29E-02	1.89E-01	Fcgr1, Fcgr2b, Ncf2, Mapk3, Nfatc1
3050	Proteasome	45	3	2.36E-02	1.89E-01	Psma6, Psmd1, Psmd7
4810	Regulation of actin cytoskeleton	215	7	2.81E-02	2.11E-01	Pfn1, Nckap1l, Arpc5, Myl12a, Gna13, Vav1, Mapk3
4330	Notch signaling pathway	50	3	3.10E-02	2.19E-01	Psenen, Hdac1, Psen1
4722	Neurotrophin signaling pathway	131	5	3.40E-02	2.26E-01	Camk2d, Ywhaq, Mapk3, Pdk1, Psen1
4912	GnRH signaling pathway	99	4	4.70E-02	2.77E-01	Camk2d, Gnaq, Mapk3, Prkacb
4916	Melanogenesis	100	4	4.85E-02	2.77E-01	Camk2d, Gnaq, Mapk3, Prkacb

Brown module

Annot	Term	Annotated	Significant	P-value	Padj	Gene

4141	Protein processing in endoplasmic reticulum	166	12	3.58E-05	4.37E-03	Hspa8, Nfe2l2, Selenos, P4hb, Dnaja1, Ssr1, Edem1, Man1c1, Eif2s1, Ube2j1, Erlec1, Dnajb1
4142	Lysosome	122	9	3.04E-04	1.86E-02	Lgmn, Ctsa, Atp6v0b, Gns, Tpp1, Arsb, Ppt1, Npc1, Ap1g1
3013	RNA transport	164	10	6.51E-04	2.65E-02	Eif4g2, Eif3a, Acin1, Eif1b, Ube2i, Eif2s1, Ranbp2, Upf2, Eif3d, Eif3b
3040	Spliceosome	133	8	2.48E-03	7.58E-02	Hspa8, Srsf5, Hnrnpu, Srsf7, Hnrnpm, Acin1, Tra2a, Cdc5l
4310	Wnt signaling pathway	153	8	5.84E-03	1.41E-01	Rac1, Ppp3ca, Csnk1a1, Csnk1e, Rock1, Ep300, Apc, Cacybp
4962	Vasopressin-regulated water reabsorption	43	4	6.96E-03	1.41E-01	Arhgdib, Dynll1, Creb1, Rab5a
4520	Adherens junction	74	5	1.01E-02	1.75E-01	Actg1, Rac1, Ptpn6, Ep300, Ctnna1
5012	Parkinson's disease	139	7	1.19E-02	1.81E-01	Vdac2, Ndufb3, Slc25a4, Sdhc, Ube2j1, Ndufa8, Ppid
4114	Oocyte meiosis	112	6	1.47E-02	1.99E-01	Ywhae, Ywhah, Ppp3ca, Ywhab, Ppp1cc, Pttg1
4380	Osteoclast differentiation	118	6	1.86E-02	2.09E-01	Csf1r, Rac1, Ppp3ca, Ifnar2, Creb1, Akt1
5016	Huntington's disease	188	8	1.88E-02	2.09E-01	Vdac2, Ndufb3, Ep300, Slc25a4, Creb1, Sdhc, Ndufa8, Ppid
4110	Cell cycle	125	6	2.39E-02	2.24E-01	Ywhae, Ywhah, Ywhab, Ep300, Cdk6, Pttg1
4650	Natural killer cell mediated cytotoxicity	125	6	2.39E-02	2.24E-01	Rac1, Ppp3ca, Ptpn6, Ifnar2, Pak1, Hcst
5210	Colorectal cancer	65	4	2.83E-02	2.38E-01	Rac1, Apc, Akt1, Appl1
4722	Neurotrophin signaling pathway	131	6	2.93E-02	2.38E-01	Ywhae, Ywhah, Rac1, Arhgdib, Ywhab, Akt1
4120	Ubiquitin mediated proteolysis	138	6	3.64E-02	2.69E-01	Ube2b, Ube2i, Trip12, Ube2k, Ube2q1, Ube2j1
5211	Renal cell carcinoma	71	4	3.75E-02	2.69E-01	Rac1, Ep300, Pak1, Akt1
4662	B cell receptor signaling pathway	76	4	4.63E-02	3.14E-01	Rac1, Ppp3ca, Ptpn6, Akt1

Turquoise module

Annot	Term	Annotated	Significant	P-value	Padj	Gene
3010	Ribosome	112	84	3.23E-81	6.04E-79	Rps29,Rplp1,Fau,Rps24,Rps21,Rpl39,Rps27,Rpl35a,Rpl37a,Rpl37,Rps12,Rpl30,Rps27a,Rpl23,Rps8,Rps28,Rpl21,Rps4x,Rps9,Rps11,Rpl41,Rps23,Rps3a1,Rpl10,Rpl34,Rpl26,Rpl32,Rps15a,Rpl18a,Rplp2,Rps14,Rpl38,Rpl17,Rpl27a,Rpl9,Rps16,Rpl6,Rps7,Rpl19,Rps20,Rpl11,Rpl13a,Rps25,Rpl28,Rpl13,Rps10,Rps3,Rpl35,Rpl7,Rps15,Rpl5,Rpl36,Rps13,Rpl24,Rpl23a,Rps19,Rpl22,Rpl27,Rps26,Rpsa,Rps18,Rpl12,Uba52,Rpl18,Rpl3,Rps5,Rps6,Rplp0,Rpl15,Rpl36a,Rpl8,Rpl14,Rpl29,Rps17,Rpl10a,Rpl7a,Rpl31,Rpl4,Rpl36al,Rps2,Rpl22l1,Rps27l,Rps27rt,Rsl24d1
190	Oxidative phosphorylation	138	46	4.84E-23	4.53E-21	Atp6v0c,Atp5e,Cox4i1,Atp5g2,Cox6c,Uqcrh,Ndufa4,Cox8a,Cox6b1,Cox7a2l,Atp5l,Atp5h,Atp5j2,Ndufa3,Cox7a2,Atp6v1g1,Ndufa2,Uqcrb,Atp5b,Ndufa13,Ndufa7,Uqcr11,Atp5k,Atp5c1,Uqcrq,Cox7b,Atp5g1,

						Ndufa1,Cox17,Ndufb11,Ndufb4,Ndufa6,Ndufc1,Ndufv3,Cox6a1,Ndufs7,Atp6v0a1,Cox5b,Uqcrc2,Ndufs5,Ndufa11,Atp5d,Sdhb,Ndufs6,Ndufb8,Ndufv2
5012	Parkinson's disease	139	43	3.75E-20	2.34E-18	Ubb,Atp5e,Cox4i1,Atp5g2,Cox6c,Uqcrh,Slc25a5,Ndufa4,Cox8a,Cox6b1,Cox7a2l,Atp5h,Ndufa3,Cox7a2,Ndufa2,Uqcrb,Atp5b,Ndufa13,Ndufa7,Uqcr11,Atp5c1,Uqcrq,Cox7b,Atp5g1,Park7,Ndufa1,Ube2l3,Ndufb11,Ndufb4,Ndufa6,Ndufc1,Ndufv3,Cox6a1,Ndufs7,Cox5b,Uqcrc2,Ndufs5,Ndufa11,Atp5d,Sdhb,Ndufs6,Ndufb8,Ndufv2
5010	Alzheimer's disease	178	44	1.85E-16	8.66E-15	Gapdh,Atp5e,Cox4i1,Atp5g2,Cox6c,Uqcrh,Ndufa4,Cox8a,Cox6b1,Cox7a2l,Atp5h,Ndufa3,Cox7a2,Ndufa2,Uqcrb,Atp5b,Ndufa13,Ndufa7,Uqcr11,Atp5c1,Uqcrq,Cox7b,Gsk3b,Atp5g1,Ndufa1,Atp2a2,Ndufb11,Ndufb4,Ndufa6,Ndufc1,Ndufv3,Cox6a1,Ndufs7,Cox5b,Uqcrc2,Ndufs5,Ndufa11,Atp5d,Sdhb,Ndufs6,Ndufb8,Mapk1,Aph1a,Ndufv2
5016	Huntington's disease	188	45	3.08E-16	1.15E-14	Atp5e,Cox4i1,Atp5g2,Cox6c,Uqcrh,Slc25a5,Ndufa4,Cox8a,Cox6b1,Cox7a2l,Atp5h,Ndufa3,Cox7a2,Ndufa2,Uqcrb,Atp5b,Ndufa13,Ndufa7,Uqcr11,Atp5c1,Uqcrq,Cox7b,Atp5g1,Ndufa1,Ndufb11,Crebbp,Ndufb4,Ndufa6,Ndufc1,Ndufv3,Cox6a1,Ndufs7,Cox5b,Uqcrc2,Ndufs5,Ndufa11,Atp5d,Sdhb,Ndufs6,Ndufb8,Trp53,Sp1,Creb3l2,Ndufv2,Polr2f
3050	Proteasome	45	12	9.44E-06	0.0002866	Pomp,Psme1,Psma3,Psmb1,Psma2,Psmc3,Psmb2,Psmc6,Psme2,Psma5,Psmd8,Psmb9
4260	Cardiac muscle contraction	77	16	1.07E-05	0.0002866	Cox4i1,Cox6c,Uqcrh,Cox8a,Cox6b1,Cox7a2l,Cox7a2,Uqcrb,Uqcr11,Uqcrq,Cox7b,Atp2a2,Cox6a1,Slc8a1,Cox5b,Uqcrc2
4666	Fc gamma R-mediated phagocytosis	90	15	0.0002847	0.0066558	Cdc42,Lyn,Cfl1,Arpc3,Arpc4,Ncf1,Pik3r1,Pik3cg,Syk,Pld1,Pla2g4a,Plcg2,Mapk1,Was,Arpc5l
5140	Leishmaniasis	64	12	0.0003779	0.0078526	Cyba,Ifngr1,Itgb1,Ncf1,H2-DMa,Ifngr2,Nfkb1,Mapk14,H2-DMb1,Mapk1,Jun,Tlr4
4810	Regulation of actin cytoskeleton	215	26	0.0005089	0.0095172	Tmsb4x,Actb,Cdc42,Cfl1,Ssh2,Arpc3,Brk1,Itgb1,Arpc4,Itga6,Pik3r1,Pip4k2a,Myl12b,Myh9,Rdx,Pik3cg,Nras,Itgav,Gna12,Ppp1cb,Mapk1,Itgb3,Itga9,Was,Arpc5l,Actn4
4380	Osteoclast differentiation	118	17	0.0006758	0.0114882	Tyrobp,Trem2,Cyba,Ifngr1,Ncf1,Pik3r1,Pik3cg,Spi1,Ifngr2,Nfkb1,Syk,Mapk14,Plcg2,Cyld,Mapk1,Itgb3,Jun
3060	Protein export	29	7	0.0013723	0.0213846	Hspa5,Sec62,Sec61g,Spcs1,Srp14,Srp9,Srp19
4662	B cell receptor signaling pathway	76	12	0.0018488	0.0265937	Lyn,Pik3r1,Pik3cg,Gsk3b,Nras,Nfkb1,Syk,Dapp1,Plcg2,Nfat5,Mapk1,Jun
3040	Spliceosome	133	17	0.0025854	0.0345329	Ddx5,Sf3b1,Snrpg,Sf3b2,Hnrnpa1,Snrpe,Cwc15,Lsm6,Zmat2,Dhx15,Snrpd2,Snrpf,Rbm22,Ddx42,Bcas2,Slu7,Sf3b3
5100	Bacterial invasion of epithelial cells	71	11	0.0032976	0.0385411	Actb,Cdc42,Arpc3,Itgb1,Arpc4,Pik3r1,Hcls1,Cbl,Pik3cg,Was,Arpc5l
5211	Renal cell carcinoma	71	11	0.0032976	0.0385411	Cdc42,Rap1b,Pik3r1,Elob,Rbx1,Pik3cg,Nras,Crebbp,Hif1a,Mapk1,Jun
5145	Toxoplasmosis	127	16	0.0039554	0.0423607	Gnai2,Ifngr1,Itgb1,Itga6,Pik3r1,H2-DMa,Pik3cg,Xiap,Ifngr2,Nfkb1,Mapk14,Pla2g4a,Stat3,H2-DMb1,Mapk1,Tlr4

4150	mTOR signaling pathway	53	9	0.0040775	0.0423607	Rps6,Pik3r1,Pik3cg,Hif1a,Ulk2,Eif4e2,Cab39,Mapk1,Rictor
5412	Arrhythmogenic right ventricular cardiomyopathy (ARVC)	74	11	0.004575	0.0450274	Actb,Itgb1,Itga6,Atp2a2,Itgav,Slc8a1,Tcf7l2,Itgb3,Itga9,Emd,Actn4
5221	Acute myeloid leukemia	57	9	0.0066876	0.0625294	Pik3r1,Pik3cg,Nras,Spi1,Nfkb1,Runx1,Tcf7l2,Stat3,Mapk1
4120	Ubiquitin mediated proteolysis	138	16	0.0088292	0.0756918	Herc2,Elob,Rbx1,Cbl,Ube2d3,Rnf7,Ube2l3,Itch,Xiap,Cul1,Ube3a,Anapc13,Klhl9,Herc1,Pias1,Ube4a
5212	Pancreatic cancer	70	10	0.0089049	0.0756918	Cdc42,Pik3r1,Pik3cg,Nfkb1,Ralbp1,Pld1,Stat3,Mapk1,Trp53,Rala
5213	Endometrial cancer	52	8	0.0120494	0.097967	Pik3r1,Pik3cg,Gsk3b,Pten,Nras,Tcf7l2,Mapk1,Trp53
4142	Lysosome	122	14	0.0150401	0.1171873	Ctsd,Ctsz,Npc2,Cd68,Cd164,Atp6v0c,Asah1,Gm2a,Pla2g15,Scarb2,Gusb,Fuca1,Atp6v0a1,Ap3d1
5142	Chagas disease (American trypanosomiasis)	100	12	0.0169749	0.1269721	Gnai2,Ifngr1,Gnas,Pik3r1,Pik3cg,Ifngr2,Nfkb1,Mapk14,Mapk1,Ppp2r1a,Jun,Tlr4
5215	Prostate cancer	89	11	0.0178	0.1280231	Pik3r1,Pik3cg,Gsk3b,Pten,Nras,Crebbp,Nfkb1,Tcf7l2,Mapk1,Trp53,Creb3l2
4664	Fc epsilon RI signaling pathway	80	10	0.0216689	0.1500775	Fcer1g,Lyn,Pik3r1,Pik3cg,Nras,Syk,Mapk14,Pla2g4a,Plcg2,Mapk1
4722	Neurotrophin signaling pathway	131	14	0.0263654	0.176083	Cdc42,Ywhaz,Rap1b,Pik3r1,Pik3cg,Gsk3b,Nras,Nfkb1,Sh2b3,Mapk14,Plcg2,Mapk1,Trp53,Jun
4670	Leukocyte transendothelial migration	120	13	0.0287114	0.185139	Actb,Cdc42,Cyba,Gnai2,Itgb1,Ncf1,Rap1b,Pik3r1,Myl12b,Pik3cg,Mapk14,Plcg2,Actn4
4510	Focal adhesion	200	19	0.0329588	0.2006686	Actb,Cdc42,Tln1,Itgb1,Itga6,Rap1b,Pik3r1,Myl12b,Pik3cg,Gsk3b,Pten,Xiap,Itgav,Ppp1cb,Mapk1,Itgb3,Itga9,Jun,Actn4
5222	Small cell lung cancer	86	10	0.0338927	0.2006686	Itgb1,Itga6,Pik3r1,Pik3cg,Pten,Xiap,Itgav,Nfkb1,Pias1,Trp53
5200	Pathways in cancer	324	28	0.034339	0.2006686	Cdc42,Itgb1,Itga6,Pik3r1,Elob,Rbx1,Cbl,Pik3cg,Gsk3b,Pten,Xiap,Nras,Crebbp,Itgav,Hif1a,Spi1,Nfkb1,Runx1,Stk4,Ralbp1,Tcf7l2,Plcg2,Stat3,Pias1,Mapk1,Trp53,Jun,Rala
4370	VEGF signaling pathway	76	9	0.0388204	0.219982	Cdc42,Pik3r1,Pik3cg,Nras,Mapk14,Pla2g4a,Plcg2,Nfat5,Mapk1
5414	Dilated cardiomyopathy	89	10	0.0415334	0.2280216	Actb,Gnas,Itgb1,Itga6,Atp2a2,Itgav,Slc8a1,Itgb3,Itga9,Emd
5223	Non-small cell lung cancer	54	7	0.0426778	0.2280216	Pik3r1,Pik3cg,Nras,Stk4,Plcg2,Mapk1,Trp53

Green module

Annot	Term	Annotated	Significant	P-value	Padj	Gene
4141	Protein processing in endoplasmic reticulum	166	12	3.76E-07	4.40E-05	Hsp90b1,Hsp90ab1,Pdia3,Canx,Pdia6,Hsp90aa1,Pdia4,Ube2d2a,Derl2,Atf4,Sec61a1,Sar1a
4914	Progesterone-mediated oocyte maturation	87	7	6.11E-05	0.0030214	Hsp90ab1,Hsp90aa1,Rps6ka1,Adcy7,Kras,Rps6ka3,Gnai3
4142	Lysosome	122	8	7.75E-05	0.0030214	Laptm5,Psap,Lamp1,Man2b1,Ctsh,Clta,Aga,Naga

3040	Spliceosome	133	8	0.0001423	0.0038175	Rbm25,Hnrnpc,Sf3b6,Snrpd3,Sf3b5,Srsf1,Phf5a,Lsm3
4145	Phagosome	173	9	0.0001631	0.0038175	Fcgr3,Canx,Lamp1,Itgb2,Stx7,Tuba1a,Atp6v1c1,Atp6v1d,Sec61a1
5215	Prostate cancer	89	6	0.0005532	0.0107878	Hsp90b1,Hsp90ab1,Hsp90aa1,Ccnd1,Atf4,Kras
4720	Long-term potentiation	69	5	0.0011809	0.0197384	Rps6ka1,Ppp1ca,Atf4,Kras,Rps6ka3
4621	NOD-like receptor signaling pathway	57	4	0.0042105	0.0615788	Hsp90b1,Hsp90ab1,Hsp90aa1,Naip2
4114	Oocyte meiosis	112	5	0.009574	0.1244622	Rps6ka1,Ppp1ca,Adcy7,Ywhag,Rps6ka3
4612	Antigen processing and presentation	78	4	0.0126598	0.1481198	Hsp90ab1,Pdia3,Canx,Hsp90aa1
511	Other glycan degradation	17	2	0.0162582	0.1707797	Man2b1,Aga
4722	Neurotrophin signaling pathway	131	5	0.0179207	0.1707797	Rps6ka1,Atf4,Ywhag,Kras,Rps6ka3
4540	Gap junction	88	4	0.0189755	0.1707797	Tuba1a,Adcy7,Kras,Gnai3
4150	mTOR signaling pathway	53	3	0.0234552	0.1960185	Rps6ka1,Eif4e,Rps6ka3
4912	GnRH signaling pathway	99	4	0.0278525	0.2172491	Atf4,Adcy7,Kras,Cacna1d
4966	Collecting duct acid secretion	27	2	0.0389421	0.2847641	Atp6v1c1,Atp6v1d
3060	Protein export	29	2	0.0443801	0.3054398	Spcs2,Sec61a1
5216	Thyroid cancer	30	2	0.0471989	0.3067926	Ccnd1,Kras

cell type proportion. Conversely, cell-to-cell communication analysis revealed a functionally diverse set of signaling pathways, which differed significantly between diet groups. In particular, HFD dysregulated microglial signaling involved in immune modulation. DEG analysis along with KEGG pathway enrichment revealed a signature of dysregulated ER genes in HFD microglia, which was independently confirmed by a separate WGNCA analysis.

We studied the effect of obesity on microglial activation in our established mouse model of diet-induced obesity [28], which displays hippocampal-dependent cognitive impairment [16]. HFD mice were heavier than their control counterparts after only 2 wk of diet and went on to develop progressive metabolic dysfunction, including hyperinsulinemia and dyslipidemia, as occurs in human obesity. Since we expected that the immune response would evolve over time, we assessed morphological activation early on at 1 mo. We found that HFD did not alter microglial morphology in the hippocampal CA1 region at 1 mo. This finding is not unexpected at 1 mo, since previously published studies showed HFD-induced morphological activation of microglia, quantified in part by fewer primary cell processes, occurs later at 3 mo in the hippocampal dentate gyrus and CA1 [9,14]. Although there was no significant difference in branchpoints per cell between groups, there was a trend towards fewer branchpoints in HFD microglia. Further studies are required to determine whether this trend might represent the start of ramification reduction, which then continues over time.

Although we did not observe hippocampal microglial morphological activation, scRNA-seq enabled us to investigate early transcriptomic changes across diverse microglial subtypes. No studies, to our knowledge, had examined hippocampal

microglial heterogeneity in obesity, and no microglial scRNA-seq studies have focused on the healthy hippocampus in the C57BL/6J mouse. Thus, we performed scRNA-seq on microglia isolated from the hippocampi of obese and lean mice after 1 mo and 3 mo. We sought to determine the effect of obesity on microglial activation and its temporal evolution at the transcriptomic level. In our sequenced $CD11b^{+}/CD45^{low}$ cells, we identified seven microglial subtypes as well as small populations of monocytes, macrophages, neutrophils, and neurons. In addition to three homeostatic populations, other microglia subtypes included inflammatory microglia, interferon-related microglia, proliferative microglia, and a cluster with unknown function, which we termed uMG. As far as we are aware, this uMG cluster has not been previously described. It is characterized by upregulation of mitochondrial genes, and perhaps represents a dying subset, as seen in other scRNA-seq data [46].

We found that diet did not affect the cluster proportions. Homeostatic microglia comprised the largest cell population in all experimental groups. In line with our results, microglial scRNA-seq studies have similarly demonstrated that homeostatic microglia are the largest clusters in both healthy and disease contexts in the adolescent and adult brain [47–49]. The presence of the smaller clusters, InflamMG, IfnMG, ProlifMG, and uMG, is not uniform in the literature, and differs with various factors, including age, brain region, disease state, and study design or perhaps power. We found an InflamMG (*Ccl4/3* expressing) population, which has also been identified in small clusters in the healthy cortex at 2 mo and 4 mo and as a larger microglial percentage in a model of infectious disease [49]. This inflammatory population, as well as an interferon-related population like our IfnMG cluster (*Ifit3* expressing), are prevalent in the whole brain with

aging [47]. A proliferative microglia cluster like our ProlifMG (*Top2a*, *Mki67* expressing) are present in the healthy adult brain [50], prevalent in the early developing brain [47] and found in the cortex of an HIV infection model [49]. The lack of activated morphology at 1 mo aligns with our transcriptomic findings; HFD did not alter the proportion of InflamMG and IfnMG and homeostatic microglia dominated all experimental groups. The apparent trending increase in peripheral immune cell types (monocytes, neutrophils) in HFD versus control samples at 3 mo could potentially reflect obesity-induced recruitment of immune cells to the brain [23].

Our identified populations are unlikely an artifact of processing-associated *ex vivo* activation, because they have been identified with transcriptional inhibition, which we employed, in the roughly 3 mo old mouse brain [50]. Marsh et al. showed that transcriptional inhibition prevented a processing-associated cluster, which has appeared in other microglial scRNA-seq [51]. Overall, we showed, for the first time, that hippocampal microglia in the healthy adolescent and adult hippocampus are mostly homeostatic microglia, with small populations of inflammatory, proliferative, and interferon-related microglia. Future work is needed to determine whether young age and/or the chronic, low-grade nature of obesity-induced inflammation may have protected against changes in inflammatory microglia proportions, which are seen in microglial scRNA-seq studies in aging [47] and overt transgenic models of disease [49].

Immune cells function by sensing and responding to their environment, so cell-to-cell communication is an integral part of microglial function [52]. Obesity disrupts the inflammatory milieu in the brain [23,24], so we asked whether obesity alters intercellular microglial signaling. Thus, we next examined whether diet impacted cell-to-cell

interactions in the hippocampus by employing CellChat to infer intercellular communication among microglia. Of the signaling that differed by diet, the pathways driving microglia-to-microglia communication serve a diverse set of biological functions, many implicated in immune modulation of microglia or other immune cell types. These pathways contained glycoproteins with known immunomodulatory roles (*e.g.*, 'HSPG,' 'ICAM1) [35–38], growth factors (*e.g.*, 'TGFb,' 'PDGF'), and immune antigens (*e.g.*, 'CD86', 'ICOS', 'CD48', and 'VISTA'). Several pathways contained proteins with known pro-inflammatory (*e.g.*, 'HSPG,' 'IFN-I,' 'IL6') or anti-inflammatory properties (*e.g.*, 'VISTA,' 'CD200,' 'IL6'). Heparan sulfate proteoglycans (HSPGs) are immunomodulators [38] with pro-inflammatory effects on microglia. HSPGs stimulate tumor necrosis factor alpha cytokine production [37] and are involved in the microglial lipopolysaccharide-induced toll-like receptor 4 response [53]. V-domain immunoglobulin-containing suppressor of T-cell activation (Vista), plays an immune checkpoint role as a negative regulator of T-cells, and is involved in other myeloid cell functions, such as phagocytosis, but its role in microglia is not well characterized [54]. Both Vista and cell adhesion molecule 1 (*Cadm1*), the ligand and receptor for 'CADM' signaling, are differentially expressed in Alzheimer's disease-associated microglia [48,54].

Further studies are needed to understand the role of these signaling pathways in modulating microglial behavior in obesity. HFD upregulated more microglial immune and inflammatory signaling at 3 mo versus 1 mo, which supports the hypothesis that chronic HFD enhances immune responses to obesity. HFD pathways associated with homeostatic and protective microglia (*e.g.*, 'GRN,' 'TGFb,' 'CD200') [39,40,55] might reflect a failed attempt to maintain homeostasis under conditions of stress during obesity.

Regarding the involvement of signaling pathways related to adhesion molecules, it is possible to speculate these changes may reflect microglial migration as a component of the inflammatory response. Overall, the changes in intercellular microglia-to-microglia signaling revealed by CellChat suggest microglia respond early to an immune challenge, which ramps up over time, leading to a condition of chronic inflammation.

Next, we examined the effect of HFD on intracellular processes in hippocampal microglia by DEG analyses with KEGG enrichment. DEGs between HFD and control microglia at 1 mo were enriched in ribosome and protein processing in the ER KEGG pathways. We identified very few cell cluster specific DEGs, but heat shock proteins related to the protein processing in the ER pathway were dysregulated in HFD homeostatic microglia, particularly at 1 mo. There were so few DEGs overall at 3 mo that we could not infer much biological pathway significance from KEGG enrichment in HFD versus control microglia. However, at 3 mo, complement genes (*C1qa*, *C1qb*) were upregulated and among the top 20 most significant DEGs in HFD versus control microglia. Microglia upregulate C1q in response to insult such as ischemic injury [56] or in a model of Alzheimer's disease [57]. The complement cascade's canonical role is in immune response, but complement is also involved in microglial mediated synaptic pruning in brain development [58]. Hippocampal microglia are thought to excessively prune synapses in obesity [9], so it is possible that complement proteins contribute to this aberrant pruning. In support of this hypothesis, microglia contribute to aberrant complement mediated synaptic pruning in Alzheimer's disease [57]. HFD at 3 mo also upregulated genes such as *Trem2*, an Alzheimer's disease associated microglia gene

[48,59], as well as genes encoding enzymes for processing pro-inflammatory arachidonic acid derived mediators, prostaglandins (*Hpgd, Ptgs1*) and leukotrienes (*Ltc4s*).

Microglia DEG fold-changes were low, but relatively consistent with chronic challenge [60], including chronic HFD [61]. Since there were few total DEGs, we also performed WGNCA on all cells, which identified five gene co-expression modules, four of which differed by diet. KEGG analysis of the brown module, elevated at 1 mo in HFD versus control, and the green module, reduced at 3 mo in HFD, identified genes enriched in protein processing in the ER. The turquoise module, reduced at 1 mo in HFD, was enriched in ribosome genes, and the yellow module, elevated at 1 mo and 3 mo in HFD versus control, identified genes enriched in Alzheimer's disease and B cell receptor signaling pathways. Overall, gene expression in HFD microglia was characterized by an earlier ER response signature at 1 mo, followed by a more inflammatory signature at 3 mo.

Our DEG and WGNCA findings closely align with published bulk RNA-seq data of microglia after 8 wk of HFD [61]. The study found only 77 DEGs that differed in HFD versus control whole brain microglia and an upregulated WGNCA module containing heat shock protein genes, such as *Hspa8*, *Dnaja1*, *Dnajb1* [61], which were identified by our study. We also previously found that chronic HFD after 20 wk induces hippocampal ER stress, enhancing expression of heat shock protein 5 and a member of the canonical inositol requiring enzyme 1 ER stress response, spliced x-box binding protein 1 [62]. The link between ER stress and inflammation is a well-studied phenomenon in obesity [63,64]. Saturated fatty acids [65,66] activate the macrophage ER stress response, which contributes to a pro-inflammatory phenotype in obesity [21]. The heat shock

proteins upregulated in our study at 1 mo, *e.g.*, *Hspa8*, *Dnaja1*, and *Dnajb1,* are protein folding chaperones and co-chaperones, which work to maintain ER homeostasis. Brykczynska et al. [61] proposed that the increase in microglial ER heat shock proteins after 8 wk HFD might be a protective mechanism. By examining DEGs, we identified an inflammatory gene expression signature later at 3 mo, which aligns with enhanced immunomodulatory intercellular microglia-to-microglia driven signaling by CellChat. This inflammatory gene expression signature was characterized by HFD upregulated microglial genes, *e.g.*, *C1qa, C1qb*, *Trem2*, *Hpgd*, *Ptgs1,* and *Ltc4s*. Possibly, an early microglial ER heat shock protein response combats increased burden, which, if misfolded protein aggregates accumulate, may transition to an ER stress response capable of inducing inflammation.

Additional investigations are required to elucidate the mechanistic underpinnings in the evolving microglial response in obesity, which our findings suggest may be characterized by an earlier ER response, followed by a more chronic inflammatory state. Possibly obesity stressors trigger an adaptive ER response in attempt to maintain homeostatic function at 1 mo, which evolves to a more activated state by 3 mo. Indeed, rats pretreated with a mild ER stress inducer are protected from lipopolysaccharide-induced cognitive impairment and microglial pro-inflammatory activation, suggesting that mild ER stress may mitigate hippocampal sequela of inflammatory challenge [67]. Alternatively, obesity may trigger a cascade of processes with increased demand on the ER, followed by an injurious ER stress response, which activates inflammatory pathways, as occurs in macrophages in obesity [21]. ER stress has been implicated in microglial mediated inflammation in other disease contexts [68]. Further studies that

manipulate microglial ER stress are needed to determine whether it mitigates or contributes to microglial pro-inflammatory activation in obesity. Moreover, our findings indicate potential therapeutic targets for microglia-mediated cognitive impairment secondary to obesity. Targeting complement [57] and prostaglandin [69] in microglia or macrophages slows synapse loss and cognitive decline in aging and Alzheimer's disease models and may additionally constitute promising approaches in obesity-induced cognitive impairment.

In summary, we used morphological and scRNA-seq analyses to determine the effects of obesity on hippocampal microglial activation in mice transitioning from adolescence to adulthood. We found that HFD did not alter hippocampal CA1 microglial morphology after just 1 mo. We demonstrated, for the first time, the microglial landscape of the healthy adolescent and adult hippocampus in the C57BL/6J mouse. Although diet did not affect cluster proportions, HFD dysregulated intercellular inflammatory signaling pathways, an effect which was more pronounced at 3 mo. Analysis of gene expression revealed a microglial signature of dysregulated endoplasmic reticulum protein processing and ribosome pathways at 1 mo, which transitioned into an inflammatory response at 3 mo. Identifying these obesity-induced microglial intercellular and intracellular pathways sets the foundation for further studies to elucidate mechanisms of microglial mediated cognitive deficits in obesity.

3.5 Methods

3.5.1 Animals and study design

C57BL/6J mice were obtained (Jackson Laboratory, catalog # 000664) at 4 weeks (wk) of age (n=40) and housed in a specific-pathogen-free facility at the Unit for Laboratory Animal Medicine (ULAM) at the University of Michigan. Mice were housed in cages with littermates on paper bedding at 20 ± 2 °C and a 12/12-h light/dark cycle and were monitored daily by ULAM staff. Mice were acclimated for 1 wk, and at 5 wk of age were randomized to four groups: Control 1 month (mo) and 3 mo and HFD 1 mo and 3 mo (**Figure 3.1A**). Control diet (10% fat, 70% carbohydrates, 20% protein; Research Diets, catalog # D12450J) or HFD (60% fat, 20% carbohydrates, 20% protein; Research Diets, catalog # D12492) were provided *ad libitum,* and mice also had free access to water.

Mice were weighed weekly, except at weeks 6 and 9. Baseline glucose tolerance tests (GTTs) were performed for all animals at 5 wk of age. 1 mo control and HFD mice had GTTs at the 1 mo endpoint; 3 mo control and HFD mice had GTTs at both 1 mo and 3 mo endpoints. For GTTs, mice were fasted for 4 hours (h), and blood glucose levels were measured from one drop of tail blood using a glucometer (AlphaTrak, Abbott Laboratories) at baseline and at 15, 30, 60, and 120 minutes (min) after intraperitoneal injection of 1 g/kg body mass glucose in normal saline. Additional metabolic phenotyping included terminal plasma insulin, cholesterol, triglycerides, phospholipids, and non-esterified fatty acids performed by the Mouse Metabolic Phenotyping Center at the University of Cincinnati. All procedures were approved by the University of Michigan's Institutional Animal Care and Use Committee (IACUC; PRO00008116, approved 2 May 2018).

3.5.2 Microglial isolation, sorting, and scRNA-seq

Mice were euthanized using an IACUC approved protocol. Mice were injected with intraperitoneal pentobarbital (Fatal-Plus, Vortech Pharmaceuticals) and perfused with Hanks' balanced salt solution (HBSS; Thermo Fisher, catalog # 14175-145) supplemented with the transcription inhibitors actinomycin D (5 μg/ml; Sigma, catalog # A1410) and triptolide (10 μM; Sigma, catalog # T3652 or Cayman Chemical #11973), an approach described by Marsh et al.[50] All subsequent microglial isolation steps were performed on ice or at 4 °C when possible and in a laminar flow hood or biological safety cabinet. Transcription inhibitors and ice were used to minimize processing-associated microglial activation to preserve an *in-vivo* transcriptional state. Hippocampi were dissected from HFD and control mice (n=6/group) and minced on ice. A single cell suspension was prepared by a papain enzymatic digestion at 37 °C followed by trituration (1 mg/ml; Worthington catalog # LS003119) in Hibernate A -Calcium - Magnesium (BrainBits, catalog # HACAMG) media with Glutamax (~0.5 nM; Gibco, catalog # 35050061). Transcription inhibitors actinomycin D, triptolide, and anisomycin (27.1 μg/ml; Sigma, catalog # A9789) were used until the end of the enzymatic digestion step.

Digested tissue was serially triturated at room temperature with a fire-polished pipette twice followed by a smaller diameter salinized ~0.5 mm fire polished pipette twice (BrainBits, catalog # FPP). The cell suspension was passed through a wet 70 μm strainer on ice and then pelleted. Microglia were enriched by resuspending in 40% Percoll and centrifuging at 500*g* for 30 min at room temperature. The cell pellet was washed in ice-cold HBSS, centrifuged for 10 min at 300*g* at 4 °C, and resuspended in

ice-cold flow sorting buffer (1X PBS [phosphate buffered saline], 2% fetal bovine serum, 1 mM ethylenediaminetetraacetic acid). Cells were moved to a 96-well plate, blocked with TruStain FcX™ (anti-mouse CD16/32) (Biolegend, catalog # 101320) for 30 min on ice, and then incubated with APC-CD45 (Biolegend, catalog # 103112) and APC-Cy7-CD11b (Biolegend, catalog # 101226) at 1:50 in the presence of 1 µg/100 µl TotalSeq-B anti-mouse Hashtag antibodies (Biolegend, catalog #s 155831, 155833, 155835) for 30 min on ice.

After staining, cells were washed with 200 µl ice-cold flow sorting buffer for 10 min at 4 °C and resuspended for flow sorting on the Sony MA900 Cell Sorter by the University of Michigan Flow Cytometry Core. Tagged control and HFD samples were combined on 10X chips to mitigate batch effects. scRNA-seq was performed by the Advanced Genomics Core at the University of Michigan using the 10X Genomics Chromium system (10X Genomics): An automated counter (Countess II, Thermo Fisher) was used to quantify cells/µl. The single cell suspension was then diluted to a final concentration ranging from 700 to 1000 cells/µl. Using the Chromium Controller, 3' libraries of single cells were created leveraging 3' V3.1 chemistry using NextGEM Chip G reagents, according to the manufacturer's protocol (all from 10X Genomics). The quality of the final library was evaluated by Tapestation 4200 (Agilent) and Kapa qPCR (Roche) was used to quantify libraries. Pooled libraries were sequenced using 150 bp paired-end format (Illumina NovaSeq 6000). De-multiplexed Fastq files were generated (Bcl2fastq2 Conversion Software, Illumina) and reads were aligned and counted (CellRanger Pipeline, 10X Genomics).

3.5.3 scRNA-seq data alignment and sample aggregating

Low-quality reads were filtered out (quality less than Q30). Reads were then mapped to the GRCm38 mouse reference genome (CellRanger Pipeline [70] version 4.0.0, 10X Genomics). The individual sample output files from CellRanger Count were read into Seurat v3 [71]. The hashtag oligo (HTO) [72] raw counts of each cell were normalized using a centered log ratio transformation across cells. Cells were then demultiplexed by using the HTODemux function in Seurat, [71] and droplets with two cells (doublets), more than two cells, or no cell (empty droplet) were subsequently removed. Cells were excluded from downstream analysis based on filtering by the following criteria: unique molecular identifier counts per cell <200, gene count per cell >7500, and the fraction of transcripts mapped to mitochondrial genes >25%. Count data were then normalized using the NormalizeData function in Seurat with the default setting.

3.5.4 Dimension reduction, clustering, and visualization

Principal component analysis (PCA) was performed based on the top 2,000 most variable genes. The optimal principal component (PC) number was selected based on the point where the percent change in variation in consecutive PCs was lower than 0.1%. Then, Uniform Manifold Approximation and Projection (UMAP) was performed on the PCs to visualize cells, and graph-based clustering was performed on the PCA-reduced data.

3.5.5 Cell type annotation and differential expression analysis

To assign a cell type identity to each cluster, the cluster gene markers were identified using the FindAllMarkers function in Seurat. Cell types were assigned based on the cluster gene markers using the CellMarker [73] and PanglaoDB [74] databases and information available in the relevant literature. DESeq2 [75] was used to identify differentially expressed genes (DEGs) between control and HFD cells for all microglia cell types combined and for each cell type separately. Genes were considered differentially expressed if the adjusted P-value was lower than 0.05. Kyoto Encyclopedia of Genes and Genomes (KEGG) enrichment was performed using the richR package (https://github.com/hurlab/richR) and an adjusted P-value < 0.05 was chosen as the cutoff value to select significant KEGG pathways.

3.5.6 Cell-to-cell communication

CellChat [33] was used to examine communication among cells. CellChat uses network analysis and pattern recognition to predict major signaling inputs to cells and signaling outputs from cells. CellChat also predicts how these cells and input and output signals coordinate. First, the software identified the significant ligand-receptor pairs across cell clusters, which were classified into signaling pathways. Next, it predicted incoming signals to specific cell clusters and outgoing signals from specific cell clusters. The global communication pattern was also predicted by pattern recognition approaches. Signaling pathways were then organized by similarity measures and manifold learning from topological perspectives. Finally, CellChat calculated the

communication probability of a signaling pathway by summarizing the probabilities of its associated ligand-receptor pairs.

3.5.7 Weighted gene co-expression network analysis

Weighted gene co-expression network analysis (WGCNA) [76] was performed to build signed co-expression networks using the WGCNA R package. The co-expression network was built using the top 3,000 most variable genes selected using the “mostVar” function from the transcripTools R package. Batch correction was done using the “ComBat” function from the sva R package. Soft power 6 was chosen by WGCNA’s “pickSoftThreshold” function to calculate the adjacency matrix.

3.5.8 Immunohistochemistry and microglial morphology analysis

One brain hemisphere from each mouse was dissected at the time of sacrifice and fixed in 4% paraformaldehyde for ~48 h. Each brain was then placed in 10% sucrose for ~24 h, followed by 20% sucrose for ~24 h, and 30% sucrose for a minimum of 24 h. Sections (50 µm) were cut on a cryostat and immunohistochemistry was performed on floating tissue. Sections were stained with rabbit anti-Iba1 (1:1000; Wako, catalog # 019-19741) at 4 °C overnight, followed by goat-anti rabbit Alexa fluor Plus 594 secondary antibody (1:2000; Invitrogen, catalog # A32740) for 2 h at room temperature followed by a Hoechst nuclear stain for 8 min. Z-stack images were acquired at 40X objective with oil immersion on a Leica Stellaris 8 Falcon Confocal Microscope. Z-stacks (25.5 µm) were pre-processed using Imaris Software (Oxford Instruments). The surface

rendering tool was used to identify intact microglial cells, and a mask was created and manually edited to extract the fluorescent signal of full intact cells from the raw data, while eliminating cell branches not associated with cell somas. An open microscopy environment TIF file was then run through an adapted 3DMorph script using MATLAB [29]. Objects misidentified as cells and misrepresented cells were manually removed from the final data set. For each animal (HFD n=4, control n=3), 3 CA1 images were analyzed, and a total of 34 to 46 cells per animal were included in the final analysis.

3.5.9 Quantification and statistical analysis

Statistical analyses of mouse metabolic phenotyping was performed in Prism 9. For HFD versus control comparisons within timepoints, normality was tested using the Shapiro-Wilk test. Welch's t-test was performed to detect differences between groups for data with normal distributions, and the Mann-Whitney test performed for non-normally distributed data. For repeated measurements (GTTs, body mass) 2-way ANOVA was performed. For microglia morphology measures, linear mixed effects models with random animal-specific intercepts were used to detect differences between diet groups. The lmerTest package in R v4.1.1 was used to fit the mixed effects models and model parameter estimates were determined using the maximum likelihood method [77]. T-tests calculated using Satterthwaite's degrees of freedom method were performed to assess differences in morphology measurements between diet groups. Histograms provided visual confirmation of assumptions of normality. The significance cutoff for all comparisons was $P<0.05$.

3.6 Bibliography

1. Obesity and overweight. Accessed March 8, 2022. https://www.who.int/news-room/fact-sheets/detail/obesity-and-overweight
2. Callaghan BC, Reynolds EL, Banerjee M, et al. The prevalence and determinants of cognitive deficits and traditional diabetic complications in the severely obese. *Diabetes Care*. 2020;43(3):683-690. doi:10.2337/dc19-1642
3. Dekkers IA, Jansen PR, Lamb HJ. Obesity, brain volume, and white matter microstructure at MRI: A cross-sectional UK biobank study. *Radiology*. 2019;291(3):763-771. doi:10.1148/RADIOL.2019181012/ASSET/IMAGES/LARGE/RADIOL.2019181012.FIG4.JPEG
4. Black N, Johnston DW, Peeters A. Childhood Obesity and Cognitive Achievement. *Health Econ*. 2015;24(9):1082-1100. doi:10.1002/HEC.3211
5. Alosco ML, Stanek KM, Galioto R, et al. Body mass index and brain structure in healthy children and adolescents. *http://dx.doi.org/103109/002074542013817408*. 2013;124(1):49-55. doi:10.3109/00207454.2013.817408
6. Yau PL, Castro MG, Tagani A, Tsui WH, Convit A. Obesity and Metabolic Syndrome and Functional and Structural Brain Impairments in Adolescence. *Pediatrics*. 2012;130(4):e856. doi:10.1542/PEDS.2012-0324
7. Xu WL, Atti AR, Gatz M, Pedersen NL, Johansson B, Fratiglioni L. Midlife overweight and obesity increase late-life dementia risk A population-based twin study. Published online 2011.
8. Pedditizi E, Peters R, Beckett N. The risk of overweight/obesity in mid-life and late life for the development of dementia: a systematic review and meta-analysis of longitudinal studies. *Age Ageing*. 2016;45(1):14-21. doi:10.1093/AGEING/AFV151
9. Cope EC, LaMarca EA, Monari PK, et al. Microglia Play an Active Role in Obesity-Associated Cognitive Decline. *J Neurosci*. 2018;38(41):8889-8904. doi:10.1523/JNEUROSCI.0789-18.2018
10. Wu Y, Dissing-Olesen L, MacVicar BA, Stevens B. Microglia: Dynamic Mediators of Synapse Development and Plasticity. *Trends Immunol*. 2015;36(10):605-613. doi:10.1016/j.it.2015.08.008
11. Paolicelli RC, Bisht K, Tremblay M-Ã. Fractalkine regulation of microglial physiology and consequences on the brain and behavior. *Front Cell Neurosci*. 2014;8(May):1-10. doi:10.3389/fncel.2014.00129
12. Nakandakari SCBR, Muñoz VR, Kuga GK, et al. Short-term high-fat diet modulates several inflammatory, ER stress, and apoptosis markers in the hippocampus of young mice. *Brain Behav Immun*. 2019;79:284-293. doi:10.1016/j.bbi.2019.02.016
13. Sobesky JL, D'Angelo HM, Weber MD, et al. Glucocorticoids Mediate Short-Term High-Fat Diet Induction of Neuroinflammatory Priming, the NLRP3 Inflammasome,

and the Danger Signal HMGB1. *eNeuro*. 2016;3(4):ENEURO.0113-16.2016. doi:10.1523/ENEURO.0113-16.2016

14. Hao S, Dey A, Yu X, Stranahan AM. Dietary obesity reversibly induces synaptic stripping by microglia and impairs hippocampal plasticity. *Brain Behav Immun*. 2016;51:230-239. doi:10.1016/j.bbi.2015.08.023
15. Valcarcel-Ares MN, Tucsek Z, Kiss T, et al. Obesity in Aging Exacerbates Neuroinflammation, Dysregulating Synaptic Function-Related Genes and Altering Eicosanoid Synthesis in the Mouse Hippocampus: Potential Role in Impaired Synaptic Plasticity and Cognitive Decline. *Journals Gerontol Ser A*. 2019;74(3):290-298. doi:10.1093/GERONA/GLY127
16. Sims-Robinson C, Bakeman A, Bruno E, et al. Dietary reversal ameliorates short- and long-term memory deficits induced by high-fat diet early in life. *PLoS One*. 2016;11(9). doi:10.1371/journal.pone.0163883
17. Guillemot-Legris O, Muccioli GG. Obesity-Induced Neuroinflammation: Beyond the Hypothalamus. *Trends Neurosci*. 2017;40(4):237-253. doi:10.1016/J.TINS.2017.02.005
18. Kang EB, Koo JH, Jang YC, et al. Neuroprotective Effects of Endurance Exercise Against High-Fat Diet-Induced Hippocampal Neuroinflammation. *J Neuroendocrinol*. 2016;28(5). doi:10.1111/JNE.12385
19. Guo DH, Yamamoto M, Hernandez CM, Khodadadi H, Baban B, Stranahan AM. Visceral adipose NLRP3 impairs cognition in obesity via IL-1R1 on CX3CR1+ cells. *J Clin Invest*. 2020;130(4):1961-1976. doi:10.1172/JCI126078
20. Melo HM, Seixas da Silva G da S, Sant'Ana MR, et al. Palmitate Is Increased in the Cerebrospinal Fluid of Humans with Obesity and Induces Memory Impairment in Mice via Pro-inflammatory TNF-α. *Cell Rep*. 2020;30(7):2180-2194.e8. doi:10.1016/j.celrep.2020.01.072
21. Shan B, Wang X, Wu Y, et al. The metabolic ER stress sensor IRE1α suppresses alternative activation of macrophages and impairs energy expenditure in obesity. *Nat Immunol*. 2017;18(5):519-529. doi:10.1038/ni.3709
22. Sims-Robinson C, Zhao S, Hur J, Feldman EL. Central nervous system endoplasmic reticulum stress in a murine model of type 2 diabetes. *Diabetologia*. 2012;55(8):2276-2284. doi:10.1007/s00125-012-2573-6
23. Buckman LB, Hasty AH, Flaherty DK, et al. Obesity induced by a high-fat diet is associated with increased immune cell entry into the central nervous system. *Brain Behav Immun*. 2014;35:33-42. doi:10.1016/J.BBI.2013.06.007
24. Salas-Venegas V, Flores-Torres RP, Rodríguez-Cortés YM, et al. The Obese Brain: Mechanisms of Systemic and Local Inflammation, and Interventions to Reverse the Cognitive Deficit. *Front Integr Neurosci*. 2022;0:24. doi:10.3389/FNINT.2022.798995
25. Valdearcos M, Douglass JD, Robblee MM, et al. Microglial Inflammatory Signaling Orchestrates the Hypothalamic Immune Response to Dietary Excess and

Mediates Obesity Susceptibility. *Cell Metab*. 2017;26(1):185-197.e3. doi:10.1016/j.cmet.2017.05.015

26. Valdearcos M, Robblee MM, Benjamin DI, Nomura DK, Xu AW, Koliwad SK. Microglia Dictate the Impact of Saturated Fat Consumption on Hypothalamic Inflammation and Neuronal Function. *Cell Rep*. 2014;9(6):2124-2138. doi:10.1016/j.celrep.2014.11.018

27. Valdearcos M, Myers MG, Koliwad SK. Hypothalamic microglia as potential regulators of metabolic physiology. *Nat Metab 2019 13*. 2019;1(3):314-320. doi:10.1038/s42255-019-0040-0

28. O'Brien PD, Hinder LM, Rumora AE, et al. Juvenile murine models of prediabetes and type 2 diabetes develop neuropathy. *Dis Model Mech*. 2018;11(12). doi:10.1242/dmm.037374

29. York EM, Ledue JM, Bernier LP, Macvicar BA. 3dmorph automatic analysis of microglial morphology in three dimensions from ex vivo and in vivo imaging. *eNeuro*. 2018;5(6). doi:10.1523/ENEURO.0266-18.2018

30. Colonna M, Butovsky O. Microglia Function in the Central Nervous System During Health and Neurodegeneration. *https://doi.org/101146/annurev-immunol-051116-052358*. 2017;35:441-468. doi:10.1146/ANNUREV-IMMUNOL-051116-052358

31. ElAli A, Rivest S. Microglia Ontology and Signaling. *Front Cell Dev Biol*. 2016;4(June). doi:10.3389/fcell.2016.00072

32. Nimmerjahn A, Kirchhoff F, Helmchen F. Resting microglial cells are highly dynamic surveillants of brain parenchyma in vivo. *Science*. 2005;308(5726):1314-1318. doi:10.1126/SCIENCE.1110647

33. Jin S, Guerrero-Juarez CF, Zhang L, et al. Inference and analysis of cell-cell communication using CellChat. *Nat Commun 2021 121*. 2021;12(1):1-20. doi:10.1038/s41467-021-21246-9

34. Wimmer I, Tietz S, Nishihara H, et al. PECAM-1 stabilizes blood-brain barrier integrity and favors paracellular T-cell diapedesis across the blood-brain barrier during neuroinflammation. *Front Immunol*. 2019;10(APR):711. doi:10.3389/FIMMU.2019.00711/BIBTEX

35. Van De Stolpe A, Van Der Saag PT. Intercellular adhesion molecule-1. *J Mol Med (Berl)*. 1996;74(1):13-33. doi:10.1007/BF00202069

36. Werner A, Kloss CUA, Walter J, Kreutzberg GW, Raivich G. Intercellular adhesion molecule-1 (ICAM-1) in the mouse facial motor nucleus after axonal injury and during regeneration. *J Neurocytol*. 1998;27(4):219-232. doi:10.1023/A:1006928830251

37. Bussini S, Meda L, Scarpini E, et al. Heparan sulfate proteoglycan induces the production of NO and TNF-α by murine microglia. *Immun Ageing*. 2005;2(1):1-9. doi:10.1186/1742-4933-2-11/FIGURES/5

38. O'Callaghan P, Zhang X, Li JP. Heparan Sulfate Proteoglycans as Relays ofNeuroinflammation. *J Histochem Cytochem*. 2018;66(4):305.

doi:10.1369/0022155417742147

39. Lyons A, Downer EJ, Crotty S, Nolan YM, Mills KHG, Lynch MA. CD200 Ligand–Receptor Interaction Modulates Microglial Activation In Vivo and In Vitro: A Role for IL-4. *J Neurosci*. 2007;27(31):8309. doi:10.1523/JNEUROSCI.1781-07.2007

40. Telpoukhovskaia MA, Liu K, Sayed FA, et al. Discovery of small molecules that normalize the transcriptome and enhance cysteine cathepsin activity in progranulin-deficient microglia. *Sci Reports 2020 101*. 2020;10(1):1-12. doi:10.1038/s41598-020-70534-9

41. Rhinn H, Tatton N, McCaughey S, Kurnellas M, Rosenthal A. Progranulin as a therapeutic target in neurodegenerative diseases. *Trends Pharmacol Sci*. Published online January 15, 2022. doi:10.1016/J.TIPS.2021.11.015

42. Rünker AE, Little GE, Suto F, Fujisawa H, Mitchell KJ. Semaphorin-6A controls guidance of corticospinal tract axons at multiple choice points. *Neural Dev*. 2008;3(1):1-19. doi:10.1186/1749-8104-3-34/FIGURES/10

43. Rothaug M, Becker-Pauly C, Rose-John S. The role of interleukin-6 signaling in nervous tissue. *Biochim Biophys Acta - Mol Cell Res*. 2016;1863(6):1218-1227. doi:10.1016/J.BBAMCR.2016.03.018

44. Andrae J, Gallini R, Betsholtz C. Role of platelet-derived growth factors in physiology and medicine. *Genes Dev*. 2008;22(10):1276-1312. doi:10.1101/GAD.1653708

45. Pierce GF, Mustoe TA, Altrock BW, Deuel TF, Thomason A. Role of platelet-derived growth factor in wound healing. *J Cell Biochem*. 1991;45(4):319-326. doi:10.1002/JCB.240450403

46. Braeuer RR, Walker NM, Misumi K, et al. Transcription factor FOXF1 identifies compartmentally distinct mesenchymal cells with a role in lung allograft fibrogenesis. *J Clin Invest*. 2021;131(21). doi:10.1172/JCI147343

47. Hammond TR, Dufort C, Dissing-Olesen L, et al. Single-Cell RNA Sequencing of Microglia throughout the Mouse Lifespan and in the Injured Brain Reveals Complex Cell-State Changes. *Immunity*. 2019;50(1):253-271.e6. doi:10.1016/j.immuni.2018.11.004

48. Keren-Shaul H, Spinrad A, Weiner A, et al. A Unique Microglia Type Associated with Restricting Development of Alzheimer's Disease. *Cell*. 2017;169(7):1276-1290.e17. doi:10.1016/j.cell.2017.05.018

49. Zheng J, Ru W, Adolacion JR, et al. Single-cell RNA-seq analysis reveals compartment-specific heterogeneity and plasticity of microglia. *iScience*. 2021;24(3). doi:10.1016/J.ISCI.2021.102186

50. Marsh SE, Walker AJ, Kamath T, et al. Dissection of artifactual and confounding glial signatures by single-cell sequencing of mouse and human brain. *Nat Neurosci 2022 253*. 2022;25(3):306-316. doi:10.1038/s41593-022-01022-8

51. Li Q, Cheng Z, Zhou L, et al. Developmental Heterogeneity of Microglia and Brain Myeloid Cells Revealed by Deep Single-Cell RNA Sequencing. *Neuron*.

2019;101(2):207-223.e10. doi:10.1016/J.NEURON.2018.12.006

52. Borst K, Dumas AA, Prinz M. Microglia: Immune and non-immune functions. *Immunity*. 2021;54(10):2194-2208. doi:10.1016/J.IMMUNI.2021.09.014

53. O'Callaghan P, Li JP, Lannfelt L, Lindahl U, Zhang X. Microglial Heparan Sulfate Proteoglycans Facilitate the Cluster-of-Differentiation 14 (CD14)/Toll-like Receptor 4 (TLR4)-Dependent Inflammatory Response. *J Biol Chem*. 2015;290(24):14904. doi:10.1074/JBC.M114.634337

54. Borggrewe M, Kooistra SM, Noelle RJ, Eggen BJL, Laman JD. Exploring the VISTA of microglia: immune checkpoints in CNS inflammation. *J Mol Med*. 2020;98(10):1415-1430. doi:10.1007/S00109-020-01968-X/TABLES/1

55. Zöller T, Schneider A, Kleimeyer C, et al. Silencing of TGFβ signalling in microglia results in impaired homeostasis. *Nat Commun 2018 91*. 2018;9(1):1-13. doi:10.1038/s41467-018-06224-y

56. Schäfer MK-H, Schwaeble WJ, Post C, et al. Complement C1q Is Dramatically Up-Regulated in Brain Microglia in Response to Transient Global Cerebral Ischemia. *J Immunol*. 2000;164(10):5446-5452. doi:10.4049/JIMMUNOL.164.10.5446

57. Hong S, Beja-Glasser VF, Nfonoyim BM, et al. Complement and microglia mediate early synapse loss in Alzheimer mouse models. *Science (80-)*. 2016;352(6286):712-716. doi:10.1126/SCIENCE.AAD8373/SUPPL_FILE/HONG.SM.PDF

58. Schartz ND, Tenner AJ. The good, the bad, and the opportunities of the complement system in neurodegenerative disease. *J Neuroinflammation 2020 171*. 2020;17(1):1-25. doi:10.1186/S12974-020-02024-8

59. McQuade A, Kang YJ, Hasselmann J, et al. Gene expression and functional deficits underlie TREM2-knockout microglia responses in human models of Alzheimer's disease. *Nat Commun 2020 111*. 2020;11(1):1-17. doi:10.1038/s41467-020-19227-5

60. McCarthy GM, Farris SP, Blednov YA, Harris RA, Mayfield RD. Microglial-specific transcriptome changes following chronic alcohol consumption. *Neuropharmacology*. 2018;128:416-424. doi:10.1016/J.NEUROPHARM.2017.10.035

61. Brykczynska U, Geigges M, Wiedemann SJ, et al. Distinct Transcriptional Responses across Tissue-Resident Macrophages to Short-Term and Long-Term Metabolic Challenge. *Cell Rep*. 2020;30(5):1627-1643.e7. doi:10.1016/J.CELREP.2020.01.005

62. Sims-Robinson C, Bakeman A, Glasser R, Boggs J, Pacut C, Feldman EL. The role of endoplasmic reticulum stress in hippocampal insulin resistance. *Exp Neurol*. 2016;277:261-267. doi:10.1016/j.expneurol.2016.01.007

63. Hummasti S, Hotamisligil GS. Endoplasmic reticulum stress and inflammation in obesity and diabetes. *Circ Res*. 2010;107(5):579-591.

doi:10.1161/CIRCRESAHA.110.225698/FORMAT/EPUB

64. Hotamisligil GS. Endoplasmic Reticulum Stress and the Inflammatory Basis of Metabolic Disease. *Cell*. 2010;140(6):900-917. doi:10.1016/J.CELL.2010.02.034

65. Korbecki J, Bajdak-Rusinek K. The effect of palmitic acid on inflammatory response in macrophages: an overview of molecular mechanisms. *Inflamm Res 2019 6811*. 2019;68(11):915-932. doi:10.1007/S00011-019-01273-5

66. Robblee MM, Kim CC, Abate JP, et al. Saturated Fatty Acids Engage an IRE1α-Dependent Pathway to Activate the NLRP3 Inflammasome in Myeloid Cells. *Cell Rep*. 2016;14(11):2611-2623. doi:10.1016/j.celrep.2016.02.053

67. Wang Y, Zhou Q, Zhang X, et al. Mild endoplasmic reticulum stress ameliorates lipopolysaccharide-induced neuroinflammation and cognitive impairment via regulation of microglial polarization. doi:10.1186/s12974-017-1002-7

68. Shi M, Chai Y, Zhang J, Chen X. Endoplasmic Reticulum Stress-Associated Neuronal Death and Innate Immune Response in Neurological Diseases. *Front Immunol*. 2022;12:5796. doi:10.3389/FIMMU.2021.794580/BIBTEX

69. Minhas PS, Latif-Hernandez A, McReynolds MR, et al. Restoring metabolism of myeloid cells reverses cognitive decline in ageing. *Nature*. 2021;590(7844):122-128. doi:10.1038/S41586-020-03160-0

70. Zheng GXY, Terry JM, Belgrader P, et al. Massively parallel digital transcriptional profiling of single cells. *Nat Commun*. 2017;8. doi:10.1038/NCOMMS14049

71. T S, A B, P H, et al. Comprehensive Integration of Single-Cell Data. *Cell*. 2019;177(7):1888-1902.e21. doi:10.1016/J.CELL.2019.05.031

72. Stoeckius M, Zheng S, Houck-Loomis B, et al. Cell Hashing with barcoded antibodies enables multiplexing and doublet detection for single cell genomics. *Genome Biol*. 2018;19(1):1-12. doi:10.1186/S13059-018-1603-1/FIGURES/3

73. Zhang X, Lan Y, Xu J, et al. CellMarker: a manually curated resource of cell markers in human and mouse. *Nucleic Acids Res*. 2019;47(D1):D721-D728. doi:10.1093/NAR/GKY900

74. Franzén O, Gan LM, Björkegren JLM. PanglaoDB: a web server for exploration of mouse and human single-cell RNA sequencing data. *Database*. 2019;2019(1). doi:10.1093/DATABASE/BAZ046

75. Love MI, Huber W, Anders S. Moderated estimation of fold change and dispersion for RNA-seq data with DESeq2. *Genome Biol*. 2014;15(12):1-21. doi:10.1186/S13059-014-0550-8/FIGURES/9

76. Zhang B, Horvath S. A general framework for weighted gene co-expression network analysis. *Stat Appl Genet Mol Biol*. 2005;4(1). doi:10.2202/1544-6115.1128/MACHINEREADABLECITATION/RIS

77. Kuznetsova A, Brockhoff PB, Christensen RHB. lmerTest Package: Tests in Linear Mixed Effects Models. *J Stat Softw*. 2017;82(13):1-26. doi:10.18637/JSS.V082.I13

Chapter 4 Obesity-induced Neuroinflammation and Cognitive Impairment in Adult Versus Aged Mice

4.1 Abstract

Obesity rates are increasing worldwide. Obesity leads to many complications, including predisposing individuals to the development of cognitive impairment as they age. Immune dysregulation, including inflammaging (characterized by increased circulating cytokine levels) and immunosenescence (declining immune system function), commonly occur in obesity and aging and may impact cognitive impairment. As such, immune system changes across the lifespan may impact the effects of obesity on neuroinflammation and associated cognitive impairment. However, the role of age in obesity-induced neuroinflammation and cognitive impairment is unclear. To further define this putative relationship, the current study examined metabolic and neuroinflammatory profiles, along with cognitive changes using a high-fat diet (HFD) mouse model of obesity. First, HFD promoted age-related changes in hippocampal gene expression. Given this early HFD-induced aging phenotype, we fed HFD to young and middle-aged mice to determine the effect of age on inflammatory responses, metabolic profile, and cognitive function. As anticipated, HFD caused a dysmetabolic phenotype in both age groups. However, older age exacerbated HFD cognitive and neuroinflammatory changes, with a bi-directional regulation of hippocampal inflammatory gene expression. Collectively, these data indicate that HFD promotes an early aging phenotype in the brain suggestive of inflammaging and immunosenescence.

Furthermore, age significantly compounded the impact on cognitive outcomes and on the regulation of neuroinflammatory programs in the brain

4.2 Introduction

The obesity crisis is reaching pandemic levels [1]. According to the World Health Organization, in 2016 over 109 billion adults worldwide were overweight or obese. Not only does obesity significantly impact quality of life [2–4], it promotes a multitude of systemic complications. Obesity leads to comorbidities including type 2 diabetes, cardiovascular disease, cancer, stroke, and cognitive impairment [1,5–7]. Further, obesity is a risk factor for aging associated dementias, including Alzheimer's disease and Alzheimer's disease related dementias. Studies demonstrate that mid-life obesity in particular is a risk factor for developing dementia later in life [5,8]. However, obesity can occur throughout the lifespan, and its effects on cognition during adolescence and throughout adulthood are unclear. The impact of age on obesity-induced cognitive impairment requires better clarification. Further, the mechanistic link between obesity and cognitive impairment remains poorly characterized.

Immune dysregulation is a hallmark of both obesity [9] and Alzheimer's disease [10], and contributes to obesity induced cognitive impairment [11,12]. Obesity is associated with systemic [13] and central nervous system (CNS) inflammation, including in the hippocampus [11,12,14], a brain region contributing to learning and memory affected by Alzheimer's disease [15]. While it is evident that immune responses contribute to obesity-induced cognitive impairment, differential effects of age on this interaction are unclear. The immune system is profoundly impacted by aging, and effects of aging on both

innate and adaptive immune function have been extensively studied [16–18]. The aged immune system has reduced ability to effectively mount a response to challenge, a phenomenon termed ‘immunosenescence’ [18]. Yet, the innate arm of the immune system becomes aberrantly overactive, leading to chronic low level systemic inflammation, termed ‘inflammaging’ [16,17,19]. Due to these age-dependent changes in immune responses, age likely impacts the role of neuroinflammation in obesity-induced cognitive impairment.

Adolescent and adult murine models of diet-induced obesity demonstrate cognitive impairment [12,20,21], including increased anxiety-like behavior [22,23]. Equivalent studies in aged mice are lacking; some evidence suggests that obesity worsens age-related cognitive decline [24], while other studies show that consuming a high-fat diet (HFD) does not affect baseline aging deficits [23]. However, it is established that HFD promotes the aging process in the CNS. Not only does HFD accelerate Alzheimer’s disease pathology and associated cognitive impairment [25–27], but it also exacerbates neuroinflammation and microglial aging in the healthy brain [28,29]. Given this effect of HFD on CNS age-related inflammation, alongside the established role of the immune system in obesity-induced cognitive impairment, this study investigated potential differential effects of age on hippocampal neuroinflammation and cognitive function in obesity.

Herein, we initially employed our established model of HFD-induced obesity throughout adolescence and into adulthood to determine the effect of obesity on hippocampal transcriptomics. We found that obesity during earlier periods of the lifespan induced an ‘early-aging’ hippocampal phenotype. Therefore, we then used this

same model in young adult and middle-aged mice to determine the impact of age on obesity-induced neuroinflammation and associated cognitive impairment. We found that age exacerbated HFD effects on some metabolic parameters. However, age significantly impacted HFD effects on fear conditioning. Further, age differentially affected hippocampal inflammatory gene expression, indicating that age plays an important role in the regulation of inflammatory responses in obesity.

4.3 Results

4.3.1 Obesity promotes a premature aging transcriptomic signature in the hippocampus

First, our established mouse model of diet-induced obesity and cognitive decline [20,30,31] was used to determine the effect of chronic obesity on the hippocampal transcriptome in adolescent mice maturing into young adulthood. Hippocampi from a previously published study [30] using C57BL/6 mice (n=8-9 per group) fed HFD or SD from 5 week (wk) of age until either 16 or 24 wk of age (**Figure 4.1A**; cohort 1) were processed for RNA-sequencing (RNA-seq). Hippocampal gene expression analysis identified 886 differentially expressed genes (DEGs; adjusted P-value <0.05) between HFD and SD at 16 wk age, and 111 genes between HFD and SD at 24 wk (**Table 4.1**). Interestingly, HFD mice had similar gene expression at both ages, indicating that HFD-related changes likely occur early and are persistent. Next, Kyoto Encyclopedia of Genes and Genomes (KEGG) pathway enrichment analysis was performed to infer potential biological significance of the DEGs. The identified DEGs between HFD and SD

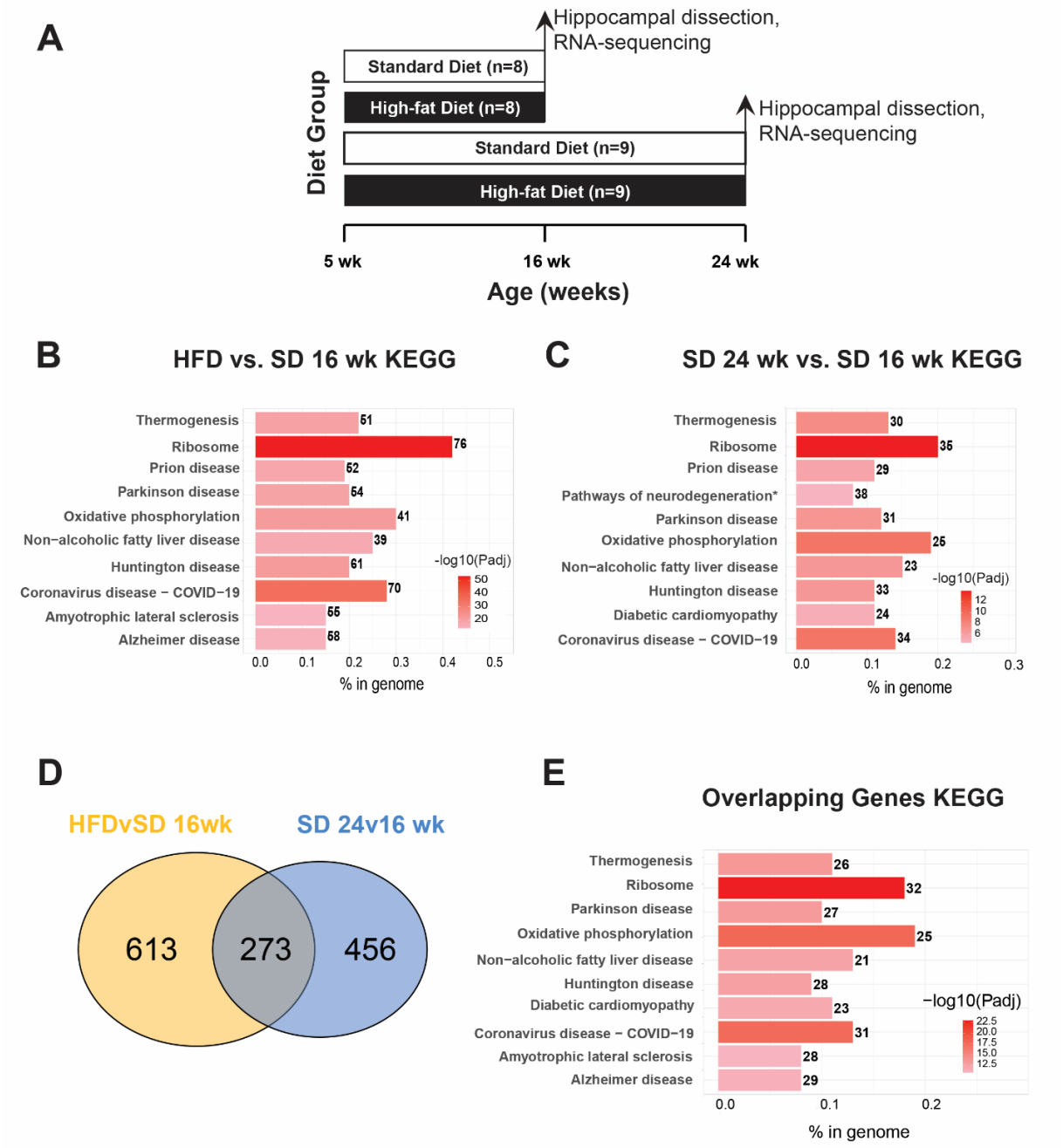

Figure 4.1 Obesity promotes a premature aging transcriptomic signature in the hippocampus.

(A) Study paradigm for cohort 1: mice aged 5 wk were fed high-fat diet (HFD) or standard diet (SD) for 11 wk (final age 16 wk) or 19 wk (final age 24 wk) and hippocampi were analyzed by RNA-sequencing. (B) Bar plot of KEGG enrichment analysis of differentially expressed genes (DEGs) in HFD 16 wk versus SD 16 wk. (C) Bar plot of KEGG enrichment analysis of DEGs in SD 24 wk versus SD 16 wk DEGs. (D) Venn diagram of overlapping DEGs (adjusted P-value<0.05) in HFD 16 wk versus SD 16 wk comparison (yellow) with SD 24 wk versus SD 16 wk comparison (light blue). (E) Bar plot of KEGG enrichment analysis of the 273 overlapping DEGs from (D). For (B), (C), and (E), bar color represents -log10(Padj), number to the right of the bar represents number of DEGs in the KEGG pathway, and bar length along the x-axis, '% in genome,' represents the fraction of DEGs relative to all KEGG pathway genes.

Table 4.1 Longitudinal hippocampal differentially expressed genes (DEGs) in high-fat diet (HFD) versus standard diet (SD).

DEGs (adjusted P-value<0.05) from hippocampal RNA-sequencing from cohort 1; HFD versus SD at 16 wk age, i.e., after 11 wk of diet (HFDvsSD16wk_DEG; sheet 1), HFD versus SD at 24 wk age i.e., after 19 wk of diet (HFDvsSD24wk_DEG; sheet 3), HFD at 24 wk age versus HFD at 16 wk age (HFD24wk_vs_HFD16wk_DEG; sheet 4), and SD at 24 wk age versus SD at 16 wk age (SD24wk_vs_SD16wk_DEG; sheet 2). Only the top 20 DEGs for each comparison are included below; the complete dataset will be available at the time of publication or upon request.

	Gene Name	baseMean	log2FoldChange	lfcSE	stat	pvalue	padj
HFD vs SD 16 wk	Bcorl1	1257.842	0.483792	0.092361	5.238067	1.62E-07	0.002068
	8430427H17Rik	3089.025	0.363976	0.074098	4.912096	9.01E-07	0.002872
	Chsy1	806.6382	0.282045	0.057064	4.942634	7.71E-07	0.002872
	Vprbp	1837.717	0.300465	0.06069	4.950845	7.39E-07	0.002872
	Neurl1b	2848.53	0.557649	0.115966	4.808743	1.52E-06	0.003024
	Sos1	3721.088	0.286577	0.059567	4.810969	1.50E-06	0.003024
	Yy1	2311.748	0.273283	0.057043	4.790864	1.66E-06	0.003024
	H2afz	1898.542	-0.3077	0.064642	-4.76004	1.94E-06	0.003084
	Cbfa2t3	2184.016	0.661251	0.141132	4.685323	2.80E-06	0.003871
	Fam126a	1563.839	0.297775	0.06398	4.654209	3.25E-06	0.003871
	Fktn	2121.238	0.32121	0.069097	4.648696	3.34E-06	0.003871
	Elovl6	3401.399	0.240276	0.05196	4.624274	3.76E-06	0.003993
	Ccser2	6670.338	0.190984	0.041898	4.558308	5.16E-06	0.005056
	Rpl10a	2048.479	-0.33502	0.073971	-4.52899	5.93E-06	0.005396
	Kdm2a	4894.105	0.272722	0.060997	4.47108	7.78E-06	0.0062
	N4bp1	3068.535	0.297929	0.066621	4.472023	7.75E-06	0.0062
	Cox7c	1423.063	-0.41568	0.094114	-4.41678	1.00E-05	0.006721
	Ifnar1	2242.115	0.18099	0.040846	4.431082	9.38E-06	0.006721
	Rpl32	4207.976	-0.41814	0.094448	-4.42722	9.55E-06	0.006721
	Ankrd11	12501.18	0.344385	0.078567	4.383329	1.17E-05	0.006834
SD 24 wk vs SD 16 wk	Nfya	1015.686	0.455303	0.073451	6.198719	5.69E-10	9.12E-06
	Elovl6	3401.399	0.291211	0.050374	5.780923	7.43E-09	5.95E-05
	Mlec	7501.257	0.376343	0.066197	5.685227	1.31E-08	6.97E-05
	Lcn2	64.58255	-4.83509	0.898711	-5.38003	7.45E-08	0.000298
	Cox7c	1423.063	-0.4745	0.091334	-5.19514	2.05E-07	0.000469
	Mir3091	8.542845	-1.79933	0.347577	-5.17679	2.26E-07	0.000469
	Phf23	1644.169	0.227955	0.044093	5.169829	2.34E-07	0.000469
	Tab2	3897.14	0.214211	0.041162	5.204037	1.95E-07	0.000469
	2610524H06Rik	385.3625	-0.40705	0.081058	-5.02178	5.12E-07	0.000581
	Ankib1	3234.375	0.235848	0.046981	5.020106	5.16E-07	0.000581
	Gm561	375.4641	-0.46951	0.093355	-5.02922	4.92E-07	0.000581
	Lars	2221	-0.2258	0.044642	-5.05802	4.24E-07	0.000581
	Mtmr4	4501.578	0.274359	0.054625	5.02261	5.10E-07	0.000581
	Nab1	1648.047	0.249803	0.04908	5.089684	3.59E-07	0.000581
	Snap29	1404.932	0.223004	0.044511	5.010124	5.44E-07	0.000581
	Ppm1f	3873.479	0.265356	0.05337	4.972057	6.62E-07	0.000663
	Rbl2	2960.98	0.211742	0.043324	4.887357	1.02E-06	0.000963
	Pkp4	17020.92	0.243454	0.049983	4.870793	1.11E-06	0.000989
	Fndc3b	1217.026	0.442273	0.09162	4.827249	1.38E-06	0.001167
	Fktn	2121.238	0.322476	0.067039	4.810272	1.51E-06	0.001207
HFD vs SD 24 wk	Creld2	618.2393	-0.65419	0.102665	-6.37211	1.86E-10	3.29E-06
	Xbp1	3291.223	-0.37372	0.068866	-5.42678	5.74E-08	0.000507
	Manf	2043.642	-0.46682	0.094055	-4.96329	6.93E-07	0.003535
	Sh3rf2	93.85328	-4.18006	0.846997	-4.93515	8.01E-07	0.003535
	Pdia4	2749.252	-0.51323	0.111292	-4.61158	4.00E-06	0.012536
	Rrbp1	2609.963	-0.34589	0.075221	-4.59826	4.26E-06	0.012536
	Bfsp2	193.5877	-0.78131	0.175412	-4.45415	8.42E-06	0.016202
	Dnajc3	4110.762	-0.36651	0.084791	-4.3225	1.54E-05	0.016202
	Fam46a	398.6578	-0.51925	0.119993	-4.32736	1.51E-05	0.016202
	Hspb1	148.0451	-0.93889	0.217493	-4.31686	1.58E-05	0.016202
	Klhl31	8.713686	-1.89323	0.439529	-4.3074	1.65E-05	0.016202
	Nexn	155.895	-2.31003	0.535165	-4.31648	1.59E-05	0.016202
	Parp12	462.937	-0.34423	0.077554	-4.43862	9.05E-06	0.016202
	Scarna9	8.56995	1.816351	0.408096	4.45079	8.56E-06	0.016202

	Sdf2l1	631.4646	-0.66616	0.150331	-4.43132	9.37E-06	0.016202
	Serpinh1	808.752	-0.65527	0.150708	-4.3479	1.37E-05	0.016202
	Slc16a6	692.5536	-0.71079	0.162875	-4.36403	1.28E-05	0.016202
	Sntg1	1538.537	0.322648	0.074432	4.334778	1.46E-05	0.016202
	Tmem179b	133.8246	-0.40496	0.094356	-4.29179	1.77E-05	0.016469
	Iqgap1	1458.886	-0.52556	0.123446	-4.25737	2.07E-05	0.018259
HFD 24 wk vs HFD 16 wk	Acss2	2364.382	-0.17651	0.033256	-5.30766	1.11E-07	0.001186
	Samd3	29.51401	3.603186	0.678277	5.312266	1.08E-07	0.001186

in 16 wk young adult mice were enriched in pathways related to metabolism (*e.g.,* 'oxidative phosphorylation,' 'non-alcoholic fatty liver disease') and neurodegenerative disease (*e.g.,* 'Parkinson disease,' 'Alzheimer disease') (**Figure 4.1B**, top 10 pathways).

There was also an effect of age on the hippocampal transcriptome. In SD mice, age (24 wk versus 16 wk) affected 729 genes. KEGG pathway analysis of age-related DEGs identified enrichment of pathways related to metabolic dysfunction (*e.g.,* 'oxidative phosphorylation,' and 'diabetic cardiomyopathy') and neurodegenerative disease (*e.g.,* 'Parkinson disease' and 'Huntington disease') (**Figure 4.1C,** top 10 enriched pathways). Because the KEGG pathways identified for HFD versus SD DEGs at 16 wk mirrored those for the age-associated DEG set in young versus mature adult SD mice, the impact of HFD on age related gene expression was assessed. Indeed, 273 genes overlapped between the 16 wk HFD versus SD DEGs and the SD 24 versus 16 wk DEGs (**Figure 4.1D**). KEGG pathway analysis for these 273 genes revealed enrichment similar to the diet- and age-dependent DEGs, including 'ribosome,' 'oxidative phosphorylation,' and 'Parkinson disease' (**Figure 4.1E,** top ten enriched pathways).

4.3.2 HFD induces obesity and metabolic dysfunction in adult and aged mice

Since obesity induced this premature aging hippocampal phenotype, we next investigated diet-induced obesity in young and aged mice to determine the effect of age on obesity-induced neuroinflammation and cognitive impairment (cohort 2). Young

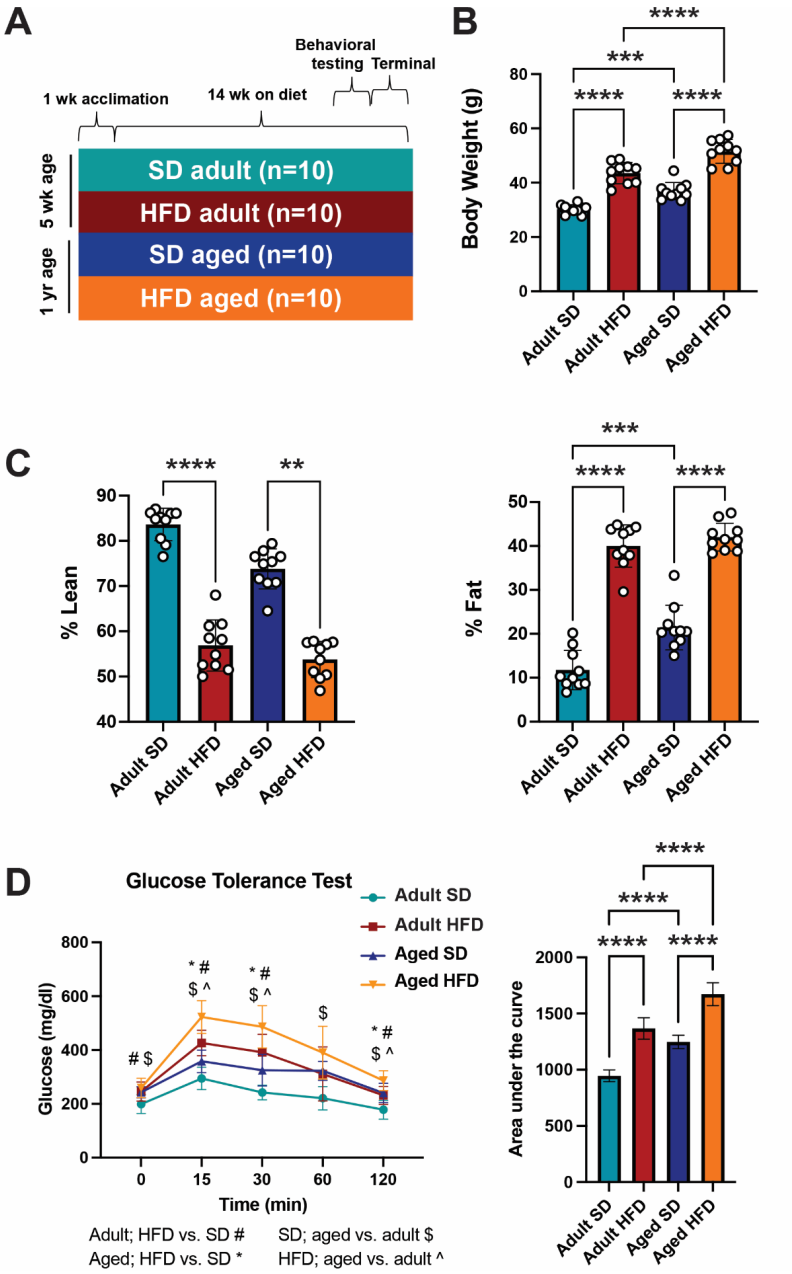

Figure 4.2 HFD induces obesity and metabolic dysfunction in adult and aged mice.

(A) Study design for cohort 2: mice aged 5 wk and 1 yr were fed high-fat diet (HFD) or standard diet (SD) for 14 wk; SD adult in teal, HFD adult in red, SD aged in blue, and HFD aged in orange. (B) Terminal body weights at study endpoint, ***P<0.001, ****P<0.0001 by Tukey's multiple comparisons test for ordinary one-way ANOVA. (C) Terminal body composition by percent lean and fat mass, **P<0.01, ***P<0.001, ****P<0.0001 by Dunn's or Tukey's multiple comparisons test for Kruskal-Wallis for non-normally distributed lean mass and for ordinary one-way ANOVA for fat mass. (D) Terminal glucose tolerance test, P<0.05 by Tukey's multiple comparisons test for repeated measures two-way ANOVA (*, #, $, ^; shown in legend); area under the curve for each experimental group, ****P<0.0001 by Tukey's multiple comparisons test for ordinary one-way ANOVA. n=10 per group for all measures. Data are presented as mean ± standard deviation.

(henceforth labeled ‘adult’) and middle-aged (labeled ‘aged’) mice were fed HFD or SD for 14 wk (**Figure 4.2A**). HFD mice had significantly higher terminal body weights than their SD counterparts, regardless of age (adult HFD versus adult SD and aged HFD versus aged SD; P<0.0001, one-way ANOVA) (**Figure 4.2B**). Further, older age was associated with increased body weight, regardless of diet (adult SD versus aged SD, P<0.001; adult HFD versus aged HFD, P<0.0001). Next, we measured terminal body composition, as percent lean and percent fat. Relative to their SD counterparts, both adult and aged HFD mice had lower percentage of lean body mass (adult HFD versus adult SD, P<0.0001; aged HFD versus aged SD, P=0.006, one-way ANOVA) and a higher percentage of fat mass (adult HFD versus adult SD, P<0.0001; aged HFD versus aged SD, P<0.0001) (**Figure 4.2C**). Further, aged SD mice had a higher percentage body fat than adult SD mice (P=0.0001), but there was no difference in percent fat between the adult and aged HFD groups. Terminal glucose tolerance tests were then performed to determine the effect of HFD on glucose homeostasis in adult and aged mice (**Figure 4.2D**). Both adult and aged HFD mice showed an impaired response to glucose challenge compared to SD counterparts, demonstrated by higher peak blood glucose levels at 15 min post glucose bolus and increased area under the curve (AUC). Older age was associated with a worse response to glucose challenge in both SD and HFD animals (AUC, adult SD versus aged SD, P<0.0001; adult HFD versus aged HFD, P<0.0001, one-way ANOVA).

Next, to further define the differential effect of obesity on the metabolic health of adult versus aged mice, we terminal epididymal adipocyte hypertrophy and fasting plasma insulin concentrations (**Figure 4.3**), and hepatic pathology (**Figure 4.4**) to

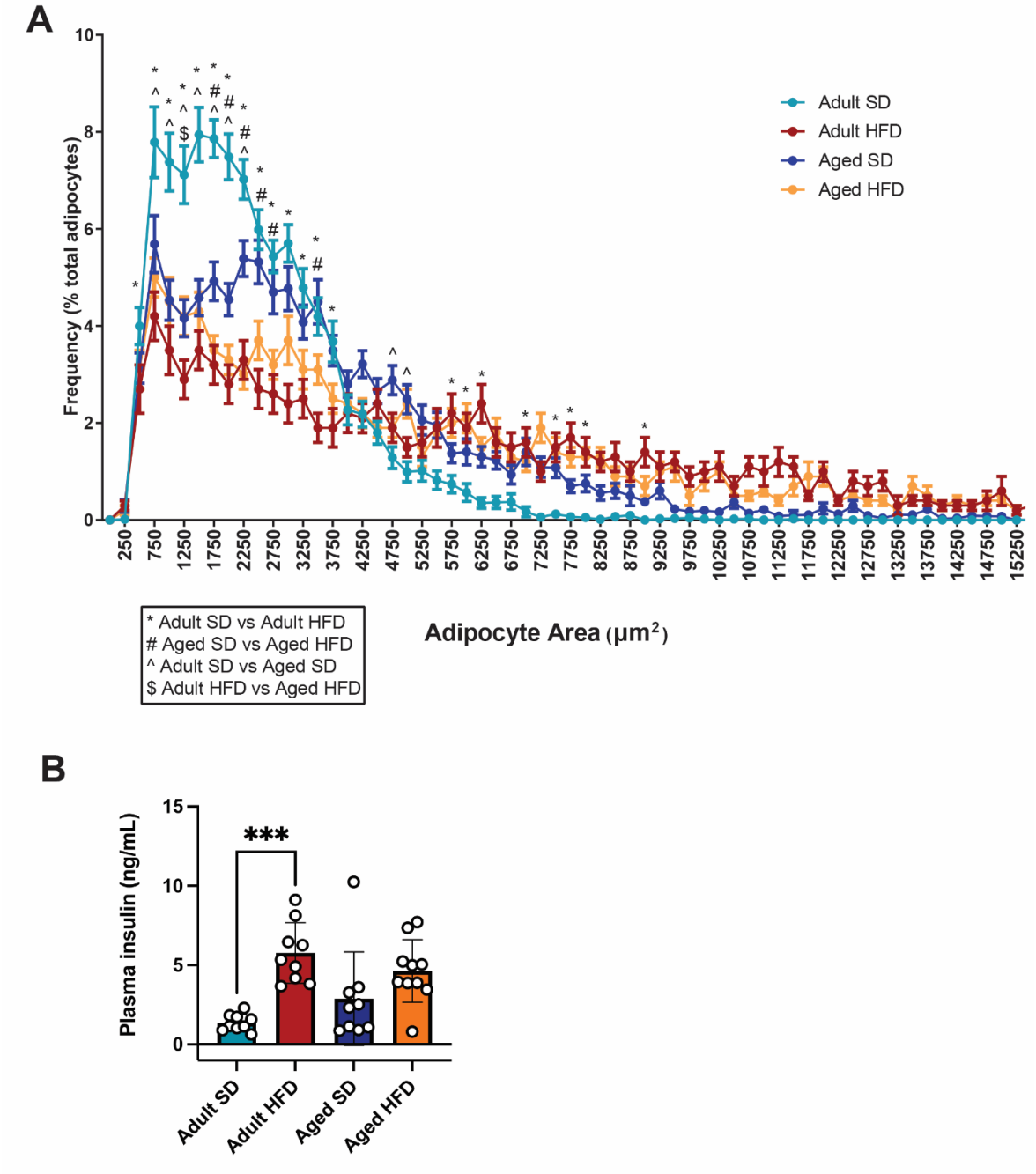

Figure 4.3 Terminal adipocyte hypertrophy and plasma insulin.

(A) Adipocyte size-frequency distribution in adult SD (teal), adult HFD (red), aged SD (blue), aged HFD (orange) in cohort 2. Data are presented as the percentage of total adipocytes per binned adipocyte (μm2). Adipocyte areas were placed into 250 μm^2 bins for analysis/representation. Bars represent mean ± standard error of the mean. Significant differences ($P<0.05$) between groups is per bin is represented by characters, * represents differences between adult SD and adult HFD mice, # represents differences between aged SD and aged HFD mice, ^ represents differences between adult SD and aged SD mice, and $ represents differences between adult HFD and aged HFD mice by two-way ANOVA, n=8-10 per group. (B) Fasting plasma insulin for cohort 2 mice; adult SD (teal), adult HFD (red), aged SD (blue), aged HFD (orange), ***$P<0.001$ by Dunn's multiple comparisons test for Kruskal-Wallis test, n=9-10 per group. Error bars represent mean ± standard deviation.

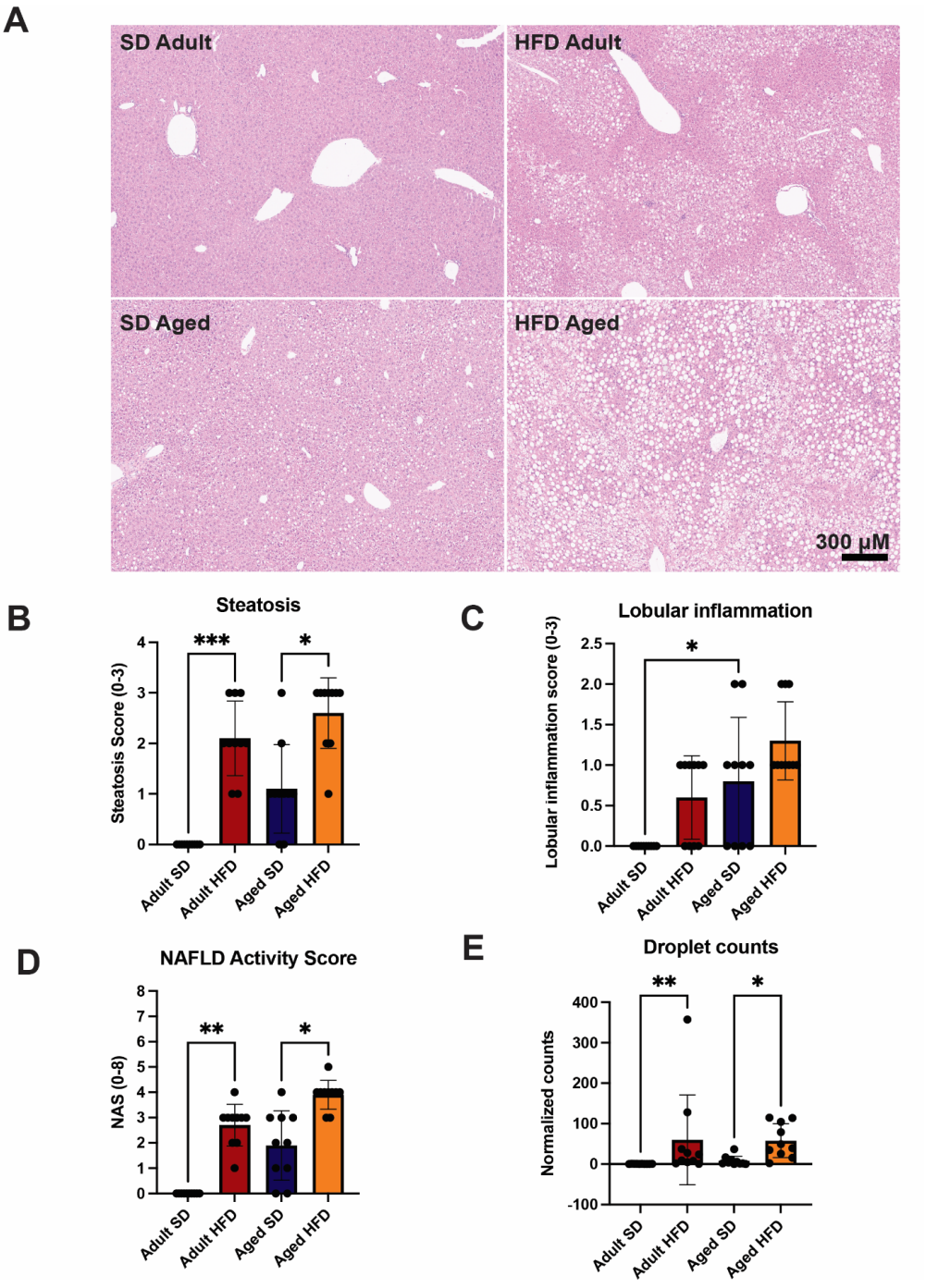

Figure 4.4 Terminal liver pathology.

(A) Representative images of adipose tissue stained with hematoxylin and eosin for adult SD (top left), adult HFD (top right), aged SD (bottom left) and aged HFD (bottom right) for cohort 2; 10X objective, scale bars are 300 μm. Kleiner scoring 32–34 of non-alcoholic fatty liver disease (NAFLD) components (B) steatosis (0-3), (C) lobular inflammation (0-3), and (D) summed NAFLD activity score (NAS; 0-8). NAS is a summation of steatosis, lobular inflammation, and ballooning degeneration (all measures for the latter were zero; data not shown). (E) Droplet counts for droplets within an area of 100-1000 μm^2, normalized to tissue area mm2. *P<0.05, **P<0.01, ***P<0.001 by Dunn's multiple comparisons test for Kruskal-Wallis test, error bars represent mean with standard deviation for (B)-(E).

assess the effect in multiple organs. HFD reduced the proportion of small adipocytes in both adult and aged mice (**Figure 4.3A**). Age also affected the distribution of adipocyte size in controls, with a lower proportion of small adipocytes in aged SD mice versus adult SD animals. However, older age did not compound the effects of HFD on adipocyte hypertrophy, suggesting a potential obesity 'ceiling effect' in response to HFD. HFD elevated plasma insulin concentrations in adults (P=0.0007, Kruskal-Wallis), but in HFD aged mice the increase relative to SD mice did not reach statistical significance (P=0.296) (**Figure 4.3B**). Kleiner scoring [32–34] for non-alcoholic fatty liver disease (NAFLD) pathology demonstrated that HFD increased steatosis in both adult (P=0.0004, Kruskal-Wallis) and aged (P=0.039) mice, but corresponding increases in lobular inflammation did not reach statistical significance (**Figure 4.4B,C**). Further, the NAFLD activity score, a summation of steatosis, lobular inflammation, and ballooning degeneration, was higher in HFD relative to SD in both adult (P=0.0051, Kruskal-Wallis) and aged (P=0.0197) mice (**Figure 4.4D**). In addition to Kleiner scoring, macrosteatosis was quantified by droplet counts, demonstrating that HFD increased counts in both adult (P=0.0021, Kruskal-Wallis) and aged (P=0.042) mice (**Figure 4.4E**).

4.3.3 HFD increases plasma but not hippocampal inflammatory cytokines

To examine possible differences in inflammatory cytokine and chemokine production due to HFD in adult and aged mice, plasma and hippocampi were assessed via ELISA (**Figure 4.5 and Figure 4.6**; cohort 2). In plasma, there were elevated concentrations of the pro-inflammatory chemokine monocyte chemoattractant protein-1 (MCP-1) in aged HFD mice relative to aged SD animals (**Figure 4.5B**; P=0.0235, one-

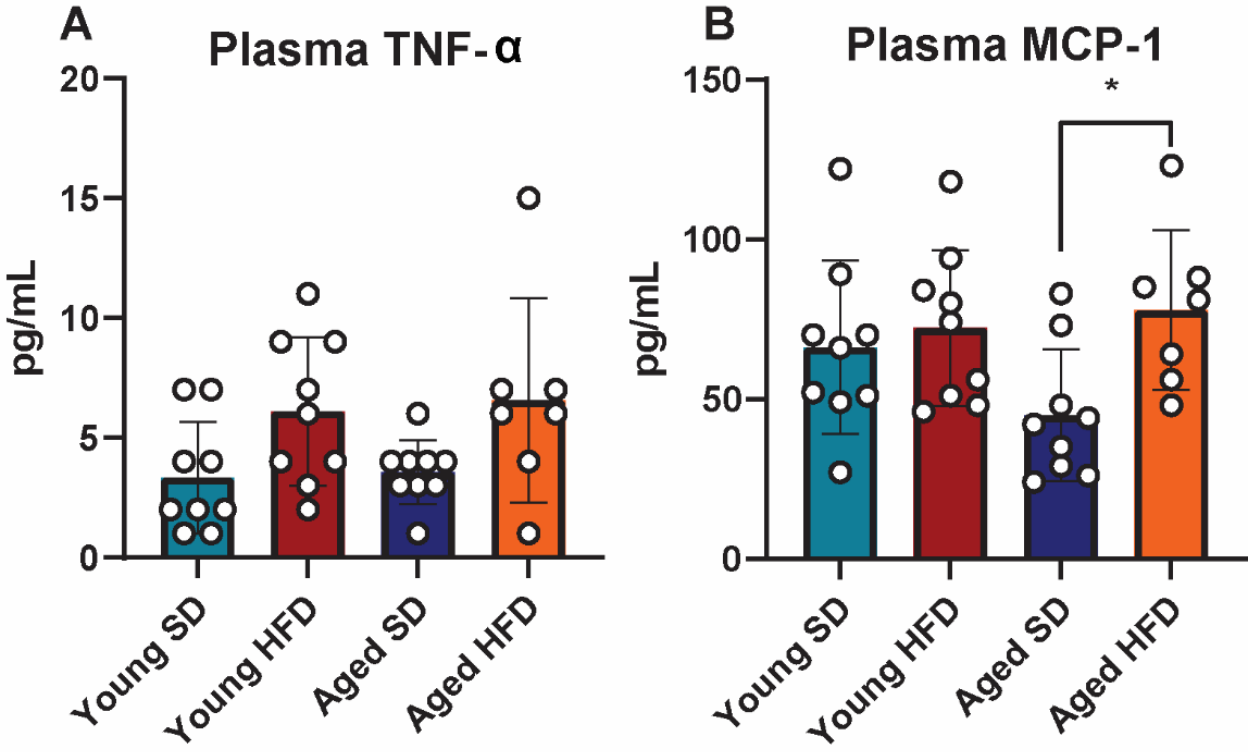

Figure 4.5 Terminal plasma cytokines.

Cohort 2 plasma cytokine protein concentrations via enzyme-linked immunosorbent assay (ELISA) for (A) TNF-α and (B) MCP-1; n=7-9 per group. For all bar plots, adult SD (teal), adult HFD (red), aged SD (blue), aged HFD (orange); *P<0.05 by one-way ANOVA; error bars represent mean ± standard deviation.

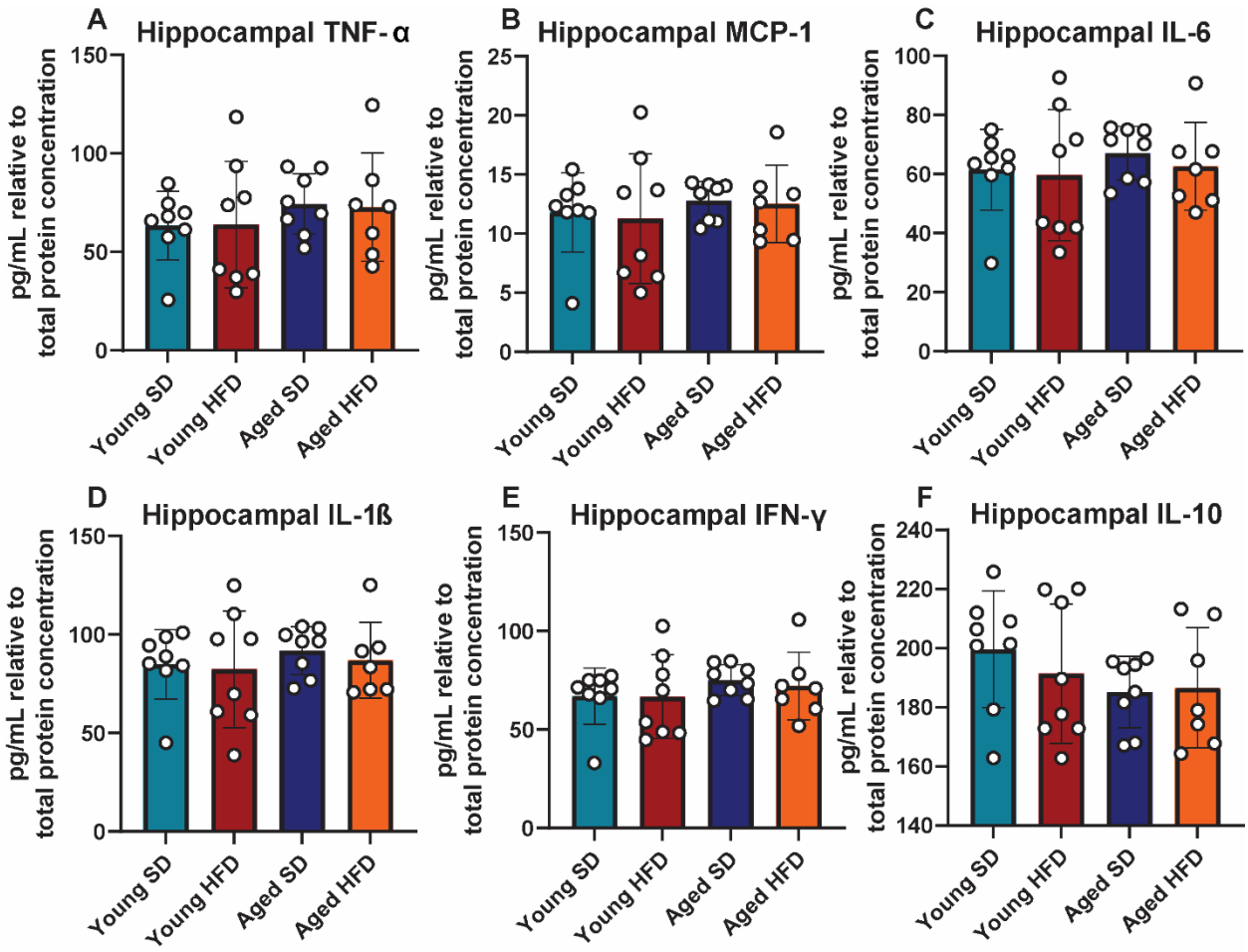

Figure 4.6 Terminal hippocampal cytokines.

Cohort 2 hippocampal cytokine protein concentrations via enzyme-linked immunosorbent assay (ELISA). Concentrations normalized to tissue lysate total protein for (A) TNF-α, (B) MCP-1, (C) IL-6, (D) IL-1β, (E) IFN-γ, and (F) IL-10; n=7-8 per group. For all bar plots, adult SD (teal), adult HFD (red), aged SD (blue), aged HFD (orange); *P<0.05 by one-way ANOVA; error bars represent mean ± standard deviation.

way ANOVA). Adult HFD and adult SD mice had similar plasma MCP-1 levels. Tumor necrosis factor alpha (TNF-α) plasma concentrations tended to be higher in HFD mice of both ages, although this did not reach statistical significance (**Figure 4.5A**). There were no differences in any of the measured hippocampal cytokines across the groups (**Figure 4.6A-F**).

4.3.4 HFD alters fear responses, particularly in aged mice

To assess the impact of HFD and aging on cognition, associative learning was evaluated using a Pavlovian fear conditioning paradigm (**Figure 4.7 and Figure 4.8**; cohort 2). After a baseline period and three tone-shock pairings in the conditioning chambers on day 1, mice were returned to the same chambers on day 2. Freezing was then measured as an index of associative memory between the chamber and the aversive foot shock. During the first 5 minutes in the training context on day 2, all mice exhibited robust freezing (**Figure 4.7A**; $P<0.0001$, 3-way RM ANOVA). However, HFD mice froze more than SD mice, regardless of age ($P=0.0001$, 3-way RM ANOVA). When placed in a novel context and exposed to the same tone used during training but in the absence of a foot-shock on day 5, all mice froze significantly more when compared to freezing during the pre-tone baseline period (**Figure 4.7B**; $P<0.0001$, 3-way RM ANOVA). Additionally, a main effect of diet was observed, where HFD mice froze more compared to SD mice ($P=0.0054$, 3-way RM ANOVA). When analyzing tone data, there was a compounding effect of age on diet, where aged HFD mice froze more compared to aged SD mice ($P=0.0141$, 1-way ANOVA). On days 2 through 4 when mice were returned to the original training context for 30 minutes/day (**Figure 4.7C**), HFD mice

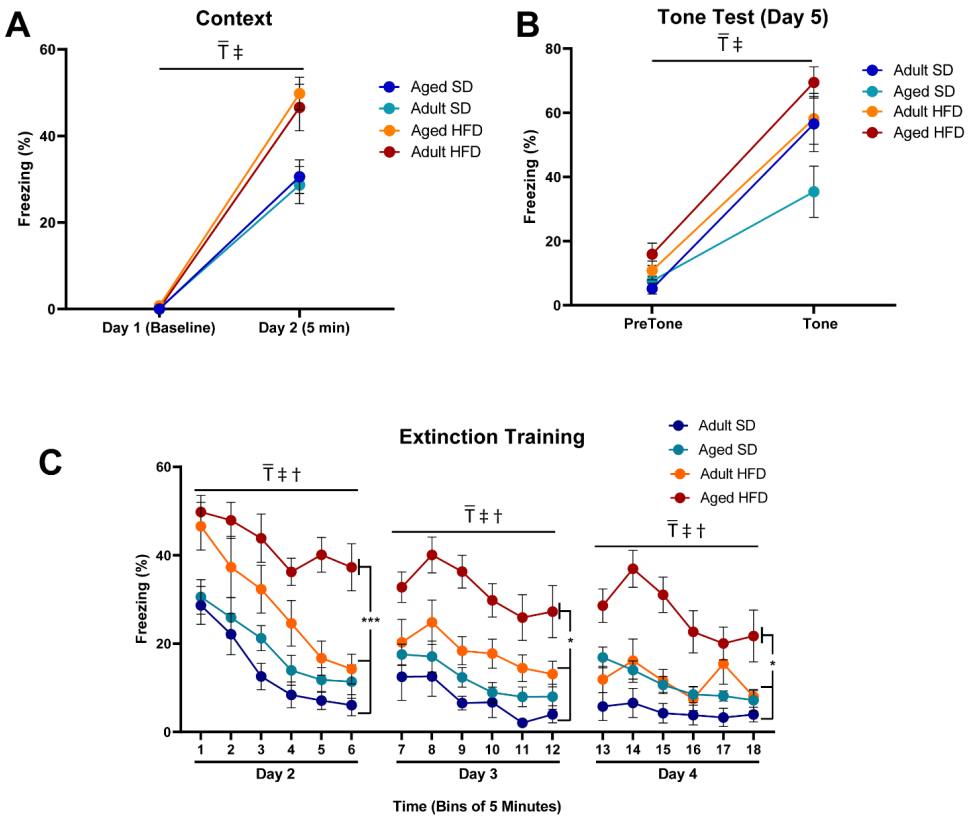

Figure 4.7 HFD increases fear responses, particularly in aged mice.

Aged HFD mice exhibit deficits in extinction learning. (A) Context test. Compared to baseline all mice displayed significant levels of freezing when returned to the training context on day 2 (3-way RM ANOVA; main effect of training F (1, 36) = 315.7; ₸, p<0.0001). Freezing levels appeared to be modulated by diet (3-way RM ANOVA; main effect of diet F (1, 36) = 18.8; ‡, p<0.0001) which was driven by the segregation of the two diet groups regardless of age at 24 hrs (1-way ANOVA F (3, 36) = 6.096, p=0.0018). (B) Tone test. Mice were placed in a novel context and after a 180 sec baseline period were exposed to the same tone used during training (the last 30 sec of baseline and first 30 sec of tone are presented. A 3-way repeated measures ANOVA revealed a main effect of training (F (1, 36) = 147.5 ₸, p<0.0001). Freezing levels appeared to be modulated by diet (3-way RM ANOVA; main effect of diet F (1, 36) = 18.8; ‡, p=0.0054) but this effect was not specific to group, although when freezing in response to tone was analyzed, there was a significant difference between mice in the Aged SD group and the Aged HFD group (1-way ANOVA F (3, 36) = 3.593, P=0.0228 followed by Tukey post hoc comparison: adjusted p=0.0141). (C) Extinction training. On days 2, 3 and 4 mice were returned to the original training context and freezing was measured for 30 minutes (presented here in 5 min bins). Across all three days there was a reduction in freezing in response to repeated context exposure (3-way RM ANOVA main effect of training: Day 2 F (1, 36) = 157.2, ₸, p<0.0001; Day 3: F (1, 36) = 14.17; ₸, p=0.0006; Day 4 F (1, 36) = 11.84; ₸, p=0.0015) which was likely influenced by diet (3-way RM ANOVA main effect of diet: Day 2 F (1, 36) = 22.46, ‡, p<0.0001; Day 3: F (1, 36) = 14.02; ‡, p=0.0006; Day 4 F (1, 36) = 10.63; ‡, p=0.0024) and age (3-way RM ANOVA main effect of age: Day 2 F (1, 36) = 4.963, †, p=0.0322; Day 3: F (1, 36) = 6.750; †, p=0.0135; Day 4 F (1, 36) = 16.03; † p=0.0003). This was especially evident on Day 2 where a training x diet x age interaction was observed (F (1, 36) = 4.963, p=0.0322). To more directly examine the effectiveness of extinction training a 1-way ANOVA was used to analyze freezing levels recorded in the final bin on each day. Across all three days there was a main effect of group (Day 2: F (3, 36) = 12.69, p<0.0001; Day 3: F (3, 36) = 7.524, p=0.0005; Day 4: F (3, 36) = 5.530 P=0.0032). This effect appears to be a function of mice in the Aged HFD group which exhibited significantly more freezing as compared to the other 3 groups (Tukey's multiple comparisons test *** p<0.001, * p<0.05). All data are presented as mean ± SEM.

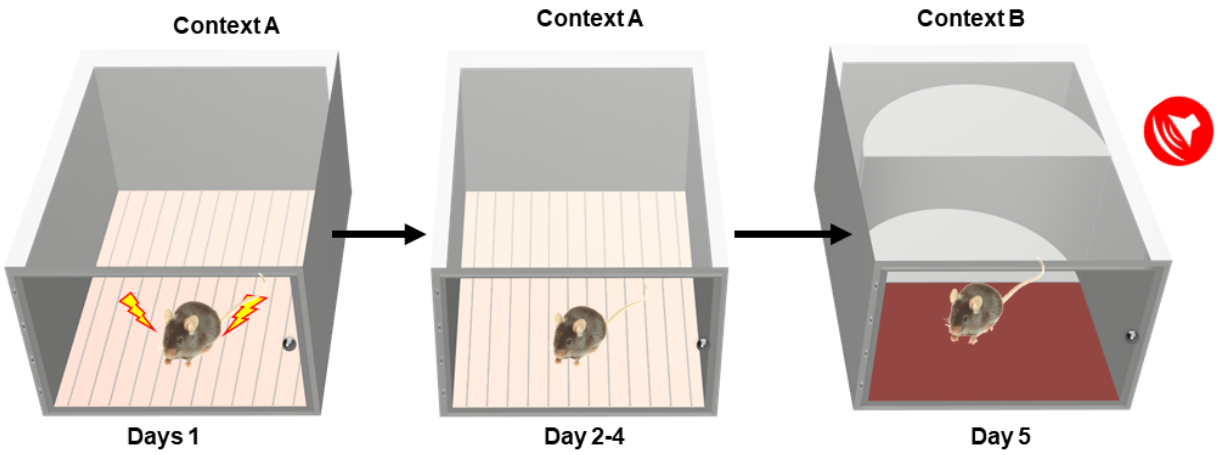

Figure 4.8 Fear conditioning training.

Fear conditioning paradigm. n=10 per group for all experimental groups.

initially displayed higher levels of freezing (Bin 1 in **Figure 4.7C** is the Day 2 data presented in **Figure 4.7A**). During the 30 min of extinction training on day 2, a main effect of extinction training was observed ($P<0.0001$, 3-way RM ANOVA). There were also main effects of both diet and age on extinction freezing, where HFD mice froze more compared to SD mice and aged mice froze more compared to adults (**Figure 4.7C**; P values dependent upon day and Bin and are detailed in figure legend). Furthermore, aged HFD mice froze more than all other groups, particularly for the final bin of each day (Day 2, $P<0.0001$; Day 3, $P=0.0005$; Day 4, $P=0.0032$; 1-way ANOVA).

4.3.5 Age determines hippocampal transcriptomic inflammatory response to HFD

Hippocampal inflammatory gene expression profiling by NanoString nCounter assay revealed a differential effect of diet dependent upon age (**Figure 4.9**; cohort 2). A pattern of relative gene expression emerged for many of the DEGs due to age and diet ($n=32$, $P<0.05$), with HFD-induced increased expression in adults versus SD adults, but decreased expression in aged HFD mice relative to age-matched SD controls. Specifically, HFD in adult animals frequently increased expression of inflammatory genes with a significant increase in 18% of DEGs. Age increased gene expression even further, with aged SD animals exhibiting significantly higher expression in 60% of inflammatory DEGs. However, HFD in aged animals decreased the mean expression of many of these same genes, with significant decrease in 60% of DEGs. These results indicate bi-directional effects from HFD; HFD increased expression of inflammatory genes in adults, but decreased expression in aged mice relative to age-matched SD controls. Of these genes, many were related to either lymphocyte differentiation or

function (**Table 4.2**). Additionally, a large proportion were also involved in chemotaxis or inflammation, and innate immune cell activation or pattern recognition. Genes of interest within these broad functions included C-X-C motif chemokine 11 (*CxCl11*), zinc finger E-box-binding homeobox 1 (*Zeb1*), and interferon regulatory factor-4 (*Irf4*). Altogether, these data indicate that HFD impacts expression of genes involved in immune cell recruitment, activation, and function, in an age-dependent manner.

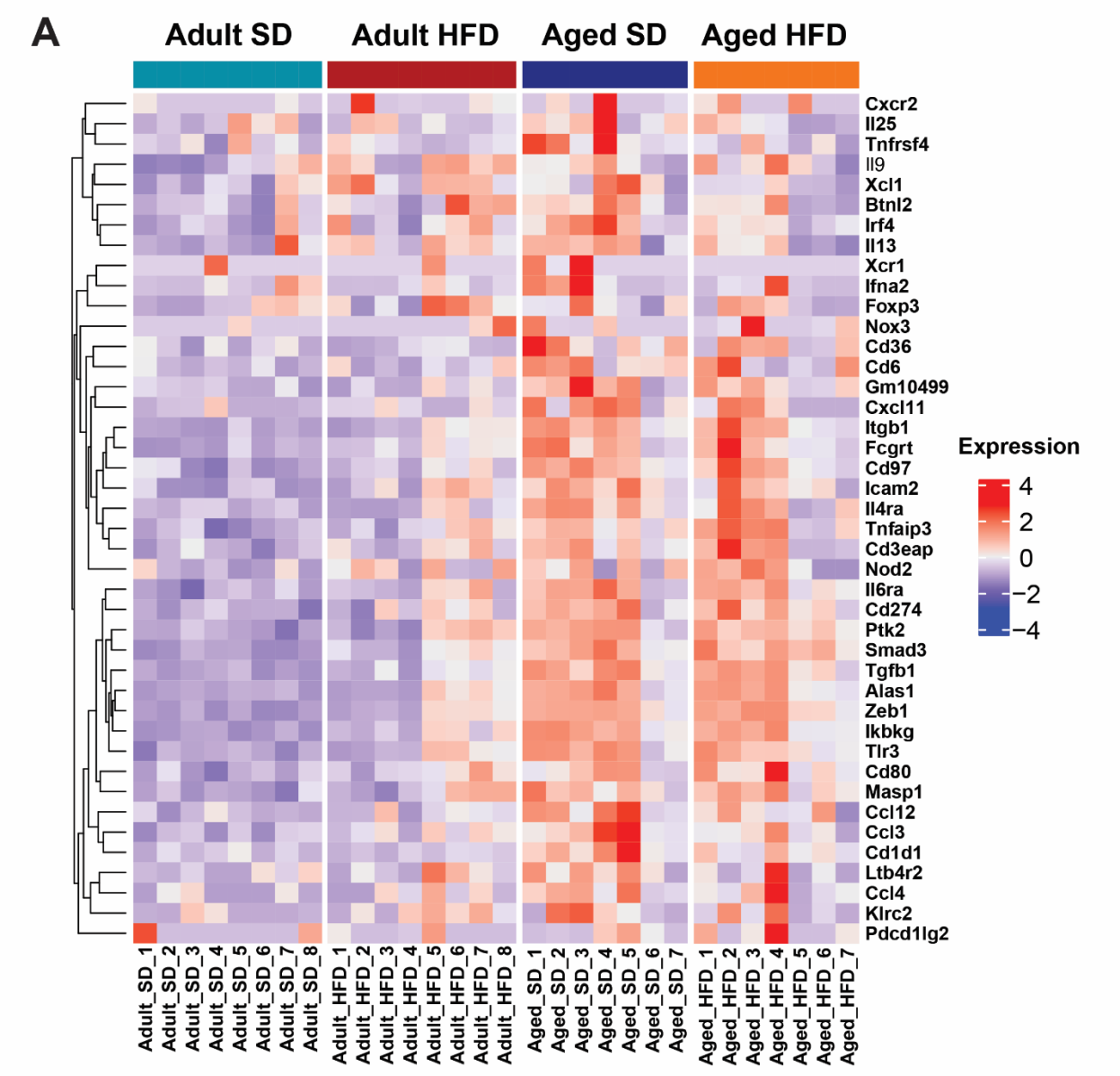

Figure 4.9 Age determines hippocampal transcriptomic response to obesity.

Heat map of hippocampal gene expression counts measured by NanoString nCounter for differentially expressed genes (diet*age interaction by mixed-effects model, P-value<0.05); adult standard diet (SD; teal, first column), adult high-fat diet (HFD; red, second column), aged SD (blue, third column), and aged HFD (orange, fourth column). Genes (rows) were hierarchically clustered, while columns include animals ordered by replicate number (n=7-8 per group). Color represents relative expression levels of normalized counts for each gene across all samples from low expression (blue) to high expression (red).

Table 4.2 Hippocampal gene expression characterization after 14 wk of high-fat diet (HFD) versus standard diet (SD).

Hippocampal inflammatory gene expression by NanoString for cohort 2; adult SD (n=8), adult HFD (n=8), aged SD (n=7), and aged HFD (n=7) mice. Genes with a significant interaction between diet and age are shown. Data are expressed as mean counts and clustered into broad gene functions, with a summary of individual gene functions. * Indicates P<0.05 SD versus HFD within the same age group, and $ indicates P<0.05 adult versus aged within the same dietary group.

Gene	SD adult	HFD adult	SD aged	HFD aged	Broad function	Function
Btnl2	8.0	10.3$	9.6	6.8	T-cells/lymphocytes	Immunoregulatory major histocompatibility complex II transmembrane protein involved in immune surveillance by negatively regulating T-cells.
Cd1d1	4.4	4.4	6.8*$	4.7		Invovlved in T-cell receptor binding (particularly of lipids), differentiation, activation, and proliferation.
Cd274	6.1	8$	8.8*	5.1		Inhibitory ligand for T-cells and B-cells.
Cd3eap	4.3	4.3	6.8*$	4.5		Has a role in RNA binding and one isoform is a component of the T-cell receptor complex.
Cxcl11	7.2	10.9	23.3*$	13.6		Antimicrobial chemokine superfamily chemotactic for activated T-cells.
Foxp3	4.1	6.0	6.8$	5.6		Transcriptional regulator of regulatory T-cells.
Il13	5.7	9.3	14.4*$	8.6		Th2 cell produced immunoregulatory cytokine with roles in B-cell maturation and differentiation, and downregulation of macrophage activity.
IL6ra	9.9	11.4	15.1*	10.6		Part of the interleukin-6 (IL-6) receptor complex, which is critical for T-helper 17 cell differentiation and Il-6 signaling.
Il9	14.9	20.6*$	15.8	14.5		Regulatory cytokine for hematopoietic cells which promotes proliferation as well as supporting helper T-cell growth.
Pdcd1lg2	7.7	6.1	10.0	11.8$		Co-stimulatory ligand involved in the negative regulation of activated T-cells.
Tnfrsf4	28.2	32.6	50.3$	42.5$		Receptor which interacts with TRAF2/5 to activate NF-kappaB and may have a roles in CD4+ T-cell responses and T-cell mediated B-cell proliferation/differentiation.
Xcl1	2965.9*$	2381.4	2367.1	2261.3		Antimicrobial chemokine which is chemotactic for T-cells and may have a role in promoting self-tolerance.
Ccl12	12.2	12.7$	10.7*	5.7	Chemotaxis/inflammation	Chemotactic cytokine for monocytes and basophils.
Ccl4	20.7	25.9	35.2$	27.2		Inflammatory and chemokinetic monokine produced by CD8+ T-cells that acts as a major HIV-suppressive factor.
Cd97	3.8	5.4	6.3$	5.5		G protein-coupled receptor involved in cellular adhesion as well as recruitment/migration and activation of leukocytes.
Ifna2	4.0	4.6	7*$	4.3		Type I interferon family antiviral cytokine which decreases proliferation and has immunomodulatory properties.
Il25	5.0	5.2	6.8*	4.3		Proinflammatory cytokine that can activate NF-kappaB activation.
Itgb1	12.9	18.7*	22$	19.0		An integrin family members (beta subunit) involved in cell adhesion.
Ltb4r2	7.6	9.9$	9.8*	6.1		Predicted functions; assist G protein-coupled peptide receptor and leukotriene B4 receptor activity, and assist granulocyte and macrophage chemotaxis.
Smad3	5.6	6.2	8.5*$	5.1		Part of the transforming growth factor-beta signaling pathway involved in genetic regulation and cell proliferation, it also plays a role in monocyte chemotaxis.
Zeb1	88.7	90.7	125*$	102.9		Zinc finger transcription factor involved in repression of interleukin 2 gene expression and positively impacts neuronal differentiation.
Cxcr2	7.1	8.5	10.1*	6.3	Innate immunity	Interleukin 8 receptor which also binds to CXCL1 to promote neutrophil migration and activation, and may play a role in oligodendrocyte precursor positioning.
Ikbkg	12.0	17.1*	18.7	16.4		Inhibitor of kappaB kinase (IKK) complex regulatory subunit which is critical for IRF3 activation and is involved in antiviral responses via TLR3- and IFIH1.
Il4ra	4.0	4.4	5.3*$	4.4		Predicted functions; upregulation of chemokine production and macrophage activation.
Irf4	11.9	16.9*	18.2$	16.1		Lymphocyte transcription factor that regulates toll-like-receptor (TLR) signaling and has a role in differentiation of CD8(+) dendritic cells.

Klrc2	4.4	4.6	6*	3.9		Calcium-dependent lectin that aids in the regulation of natural killer cells, and may aid in the response of natural killer cells to viruses.
Nod2	31.1	35.5	46$	39.5		Leukocyte protein in the Nod1/Apaf-1 family which plays a role in intracellular bacterial lipopolysaccharides (LPS) and ssRNA recognition.
Tlr3	8.4	9.8	18.7* $	13.2		Dendritic intracellular receptor involved in viral dsRNA responses, primarily via NFκβ.
Xcr1	8.5	13.5*	12.3	9.1		Dendritic chemokine receptor that may have a role in antigen cross-presentation to NK cells or CD8 T-cells.
Alas1	7.8	10.6	16.7* $	13.0	Other	Mitochondrial enzyme involved in the regulation of iron-protoporphyrin biosynthesis.
Fcgrt	6.1	6.9	14.9* $	9.4		Monomeric immunoglobulin G (IgG) receptor which also protects IgG from degradation.
Nox3	5.2	5.3	7.4*$	4.9		NADPH oxidases in the NOX family involved in gravity perception.
* indicates p<0.05 SD vs HFD within the same age group, $ indicates p<0.05 adult vs aged within the same dietary group						

4.4 Discussion

Immune dysregulation is a common feature in obesity and aging, which contributes to pathological CNS changes, including cognitive impairment. Here, in a mouse model of obesity and cognitive impairment [20,31], HFD promoted a premature hippocampal aging signature and led us to examine differential effects of HFD with age. Age exacerbated HFD effects on cognition, as well as body weight and glucose tolerance. However, most metabolic phenotyping parameters (body composition, plasma insulin, adipocyte hypertrophy, NAFLD liver pathology) appeared to reach a 'ceiling' where HFD produced similar effects in both adult and aged mice. Additionally, HFD induced bi-directional hippocampal inflammatory gene expression changes; increased in adults but decreased in aged animals. Overall, our data indicate that age plays an important role in obesity-induced hippocampal inflammatory response and cognitive impairment.

Here, HFD promoted a premature hippocampal aging phenotype. Many DEGs in 16 wk old HFD versus SD were also DEGs arising from aging (SD mice, 24 wk vs 16 wk). These overlapping genes were enriched in pathways related to metabolism, ribosome, oxidative phosphorylation, and neurodegenerative diseases, including Alzheimer's Disease. In the brain, ribosome and oxidative phosphorylation pathways are aging signatures in multiple cell types [43]. Our findings align with existing studies exploring consequences of obesity and metabolic dysfunction during aging, *i.e.* inflammaging, cellular senescence, and genomic damage [19,44]. Others have similarly shown that obesity induces an aging phenotype [45], particularly in adipose [46]. Both classically dysregulated during aging, immune function and metabolism are intrinsically linked. For example, saturated fatty acids activate pattern recognition receptors [47,48],

creating a pro-inflammatory state. In turn, this directly impacts insulin signaling, promoting insulin resistance [48,49].

Regardless of age, HFD mice had greater fat mass and lower lean mass, fewer small adipocytes, and increased liver steatosis, macrosteatosis, and NAFLD score. Although not significant, aged HFD mice also had higher plasma insulin concentrations. We [20,30,31] and others [50,51] have shown that HFD consistently causes obesity, dysregulated glucose metabolism, liver pathology, and adipocyte hypertrophy. Interestingly, for weight and glucose tolerance, age compounded dietary effects; HFD and age worsened the metabolic phenotype relative to adult controls, and HFD aged mice displayed the most severe phenotype. However, for all other parameters, aged and adult HFD mice were similar, possibly due to a 'ceiling effect' with HFD, which older age could not worsen past a certain point.

Chronic HFD impairs cognition in mice [20,51]. To examine the impact of age, we assessed cognitive function by training mice to associate a context and tone with a foot-shock. All mice were capable of learning and remembering this relationship. However, HFD mice, particularly aged HFD mice, exhibited higher levels of freezing when returned to the training context but in the absence of the tone. As the levels of freezing in response to the tone were similar between groups, this enhanced freezing is likely not due to a generalized increase in fear. While aged HFD mice exhibited extinction learning, their freezing levels remained elevated compared to all other groups. This deficit appears to be specific to extinction learning and are consistent with others suggesting that inflammation within the hippocampus [52] and increased cytokine levels [53] produce similar impairments in fear extinction.

Few studies have assessed cognitive effects of HFD in an age dependent manner. In rats [54], similar to here, age exacerbated negative cognitive outcomes in animals fed HFD for 3 days. However, aged HFD rats froze less compared to their SD counterparts [54], whereas HFD increased freezing here. In mice, there are conflicting results regarding HFD and age on cognitive function [23,24]. One study reported age worsened HFD learning deficits assessed by elevated plus maze [24]. However, another study showed increased anxiety in adults due to HFD, and spatial cognitive deficits due to age, which diet did not affect [23]. These conflicting results may be due to multiple factors, *e.g.*, different age of diet initiation, diet duration, model system, cognitive testing modalities. Normal age-related cognitive changes also could mask subtle HFD effects in older mice. Additionally, behavioral testing is susceptible to variability from multiple factors, such as season, lighting, and light-dark cycles [55,56].

To investigate underlying neuroinflammatory changes contributing to fear conditioning deficits, we measured hippocampal cytokines and inflammatory gene expression. While many report increased hippocampal inflammatory cytokines in response to age or HFD [12,14,57], we found no changes, which is aligned with another study [58]. Failure to detect differences may be due to the high degree of regulation for maintaining homeostasis or inherent individual variation in inflammatory measures. Immune challenge with lipopolysaccharide robustly increases cytokine production, which is impacted by age and HFD [59]. Thus, although we detected no differences in baseline hippocampal cytokines, immune challenge might reveal differential responses.

Many classic aging hallmarks, including inflammaging and senescence [60–63], are also associated with obesity and metabolic dysfunction [19,44]. Here, HFD induced a

premature aging phenotype by hippocampal RNA-seq. Similarly, hippocampal inflammatory gene expression was age and diet dependent. Specifically, HFD upregulated inflammatory gene expression in adults. Age further increased expression, but HFD had the opposite effect in aged mice, decreasing expression of many of the same inflammatory DEGs. Broadly, DEGs fell into categories related to lymphocyte differentiation or function, chemotaxis or inflammation, and innate immune cell activation or pattern recognition. Furthermore, several DEGs of interest were identified; C-X-C motif chemokine 11 (CxCl11), Zinc finger E-box-binding homeobox 1 (Zeb1), and interferon regulatory factor-4 (Irf4).

CxCl11 is a chemokine involved in lymphocyte differentiation or function, which attracts activated T-cells [64]. CxCl11 brain levels increase in response to trauma [65] and in neurological diseases [6667]. Inflammaging and immunosenescence [68] impact lymphocyte differentiation or function, especially T-cell function, and CxCl11 levels rise in parallel with senescent T-cells in hypertensive patients [69]. The second gene of interest, *Zeb1*, is involved in chemotaxis or inflammation [70 71], both cornerstones [16–19,72] of inflammaging and immunosenescence. Zeb1 may regulate adipocyte differentiation in obesity [73,74], and plays a role in insulin resistance in adipose tissue [73] and apoptosis in pancreatic beta cell during diabetes [75]. Furthermore, Zeb1 regulates IL-2, which activates natural killer cells, whose numbers and function decrease with age [76].

The innate immune system is the first line of defense against injury, insult, or infection, and participates in inflammaging and immunosenescence upon continued activation [68]. Irf4, a key player in innate immunity [77], was the final identified gene of interest. Irf4 helps regulate PGC-1α, a metabolic co-factor that promotes fatty acid

oxidation, mitochondrial biogenesis, and brown fat differentiation [78]. Irf4 is expressed by multiple brain cell types, including neurons and microglia, and plays a protective role in response to stroke [79,80]. Furthermore, and similar to our results, ischemia was associated with a lower IRF4 expression in aged vs younger animals [81], indicating an age-dependent response to insult or injury.

Our study has limitations. First, fear conditioning experiments may be impacted by known hearing loss in aged C57BL/6 mice, which may affect their ability to perform the task. However, the 28 kHz, 85 dB tone used can likely be sensed via vibration. This, combined with similar performances between SD adult and SD aged animals indicates hearing loss likely did not prevent mice from generating fear memory. Secondly, this study used only male animals. Sex is an important variable in metabolic, immune, and cognitive studies [58,82,83]. Given the differences observed here, future studies are vital to understand the impact of sex on mechanisms leading to cognitive impairment in obesity and metabolic dysfunction.

Overall, our data demonstrate that age significantly impacts the effects of HFD on hippocampal inflammatory responses and cognitive phenotype, with older aged associated with worse outcomes. HFD-induced metabolic dysfunction is also impacted by age but to a lesser extent, with a potential ‘ceiling effect’ for some parameters. Hippocampal gene expression supports an age-dependent regulation, indicating that HFD promotes an early aging phenotype.

4.5 Methods

4.5.1 Animals and experimental design

Experiments were performed on two cohorts of mice. Cohort 1 comprised young C57BL/6J males, 5 weeks (wk) of age (strain # 000664; Jackson Laboratory, Bar Harbor, ME), whose peripheral metabolic data and neurological tissues were analyzed in a previously published study [30]. Cohort 1 animals were fed *ad libitum* 10% fat standard diet or 60% high-fat diet (standard diet, SD, D12450B; high-fat diet, HFD, D12492; Research diets, New Brunswick, NJ), and used in this study only to obtain hippocampal tissue for RNA-seq analysis. Cohort 2 included C57BL/6J males at both 5 wk of age (strain # 000664; Jackson Laboratory, Bar Harbor, ME) and 1 yr of age (National Institute of Aging aged rodent colony). Cohort 2 animals were used for all other results reported here. Cohort 2 young and aged mice were fed *ad libitum* either 10% fat SD or 60% HFD (SD, D12450J; HFD, D12492; Research diets, New Brunswick, NJ). All animals were acclimated at the University of Michigan for at least 1 wk prior to dietary changes. Mice were also provided water *ad libitum* in a pathogen-free room maintained under a 14:10 light:dark cycle at 20 ± 2 °C and monitored daily by veterinary staff at the University of Michigan's Unit for Laboratory Animal Medicine.

The two cohorts differed in diet duration (SD or HFD) and experiment. Cohort 1 young mice were fed SD or HFD for 11 wk or 19 wk for two terminal timepoints to perform hippocampal RNA-seq. All cohort 2 young and aged mice were fed SD or HFD for 14 wk for a single terminal timepoint. At terminal timepoints in all cohorts, animals were sacrificed using an intraperitoneal injection of 150 mg/kg sodium pentobarbital (Fatal-Plus, Vortech Pharmaceuticals, Dearborn, MI). At sacrifice, cohort 1 mice were

16 wk of age after 11 wk on diet, or 24 wk of age after 19 wk on diet; cohort 2 mice were 19 wk of age after 14 wk on diet, or 66 wk of age after 14 wk on diet. Following sacrifice for all animals, plasma was taken for metabolic phenotyping and mice were then perfused with phosphate-buffered saline and tissues harvested. Cohort 1 hippocampal tissue was isolated and snap frozen and stored at -80° C for later RNA extraction and RNA-seq. Cohort 2 terminal plasma was isolated to measure insulin and cytokine levels, hippocampal tissue was isolated, snap frozen, and stored for later cytokine measures or RNA extraction for NanoString inflammatory gene expression analysis, and liver and epididymal fat tissues were formalin fixed for histological analysis. All procedures were carried out per the University of Michigan's Committee on Use and Care of Animals under protocol numbers PRO0010039, PRO00010247, PRO00006140, and PRO00008116.

4.5.2 Metabolic phenotyping

Cohort 1 mice underwent metabolic phenotyping as previously reported [30]. Cohort 2 young and aged mice underwent terminal metabolic phenotyping after 14 wk on diet. Metabolic phenotyping was performed on all animals according to the Diabetic Complications Consortium guidelines (https://www.diacomp.org/share/protocols.aspx) and as previously published [30,31]. At terminal, animals were weighed and glucose tolerance tests were performed, as previously published [31]. Briefly, mice underwent an intraperitoneal injection of 1 g glucose per 1 kg body weight and blood glucose readings were recorded prior to injection and at 15, 30, 60, and 120 minutes (min) post injection.

Additional metabolic phenotyping for cohort 2 included body composition quantification, plasma insulin concentration, liver pathology scoring, and adipose tissue histomorphometry. Body composition analysis was performed after cognitive phenotyping and immediately prior to study termination at 14 wk using a EcoMRI 4in1-900 (EcchoMRI LLC, Houston, TX) at the Metabolism, Bariatric Surgery and Behavior core as part of the University of Michigan Mouse Metabolic Phenotyping core. Terminal plasma insulin concentrations were measured using a rat/mouse insulin ELISA (catalog # EZRMI-13k, Millipore Sigma-Aldrich, St. Louis, MO) by the University of Michigan Mouse Metabolic Phenotyping core. Formalin fixed liver tissue samples collected at study endpoint after 14 wk of diet were processed by the University of Michigan *in vivo* animal core and assessed for liver pathology, which included measures of macrosteatosis (droplet counts within 100-1000 μm^2 in area, normalized to tissue area) and Kleiner scoring [32–34]. Kleiner scoring included measures of lobular inflammation (scale of 0-3), ballooning degeneration (scale of 0-2), steatosis (scale of 0-3), and a summed non-alcoholic fatty liver disease (NAFLD) activity score (NAS) (scale of 0-8).

Formalin fixed epididymal white adipose tissues collected at study endpoint after 14 wk of diet were paraffin embedded, sectioned, stained with hematoxylin and eosin, and assessed for fat histomorphometry, as previously published [35,36]. Briefly, four representative images were taken per animal at a 10X magnification, and histomorphological analysis was performed using Metamorph software version 7.10.3.279. Images were thresholded to include adipocytes with a shape factor between 0.35 and 1 (shape factor of 0 being a straight line, shape factor of 1 being a perfect circle), an equivalent sphere surface area between 5,000 μm^2 and $1x10^6$ μm^2, and

areas between 10 μm^2 and $1.5x10^3$ μm^2. Objects bordering the edge of the image were excluded. Following initial thresholding, manual adjustments were made to add, remove, cut, or join adipocytes. For each image, adipocytes were binned from 0 to $2x10^4$ μm^2 at 250 μm^2 increments. Using the frequency for each binned adipocyte size, the percentage of adipocytes belonging to each bin was calculated for each image and the images for each experimental group were averaged to determine differences for each binned adipocyte size between groups.

4.5.3 Cognitive phenotyping

Cohort 2 young and aged mice on SD and HFD underwent fear conditioning prior to study termination after 14 wk on diet. Fear conditioning was carried out as previously published [37,38]. In brief, mice were trained to anticipate a foot shock by training with a 180 sec baseline, a tone (28 kHz, 85 dB, 30 sec), followed by the 0.75 mA foot shock. Tone/shock pairings were completed 2 additional times, for a total of 3 pairings with a 120 sec gap following each tone. On days 2, 3, and 4, mice were placed into the chamber for a total of 30 min, with no tones or shocks to assess fear extinction. The first 5 min of time in the chamber on day 2 was used to assess contextual memory. On day 5, animals were assessed for cued (tone) memory. The chamber was re-configured to represent a different context, *i.e.*, different flooring type and wall shape. In addition, the background odor, noise, and lighting were altered [37,38]. The mice were placed into the reconfigured chamber and given a 180 sec baseline, followed by a 28 kHz tone (30 sec). Freezing behavior, *i.e.*, the absence of movement, excluding breathing, was measured and used to calculate percent freezing, *i.e.*, the amount of time spent freezing

out of the total amount of time while in the chamber. Percent freezing was used to assess fear extinction, cued memory, and contextual memory.

4.5.4 Gene expression

Hippocampi from mice on SD and HFD from cohorts 1 and 2 underwent RNA extraction and gene expression analysis. Cohort 1 hippocampal tissues were collected at study endpoint after 11 wk or 19 wk of diet and processed for RNA-seq, as previously published [30]. Cohort 2 hippocampi were collected at study endpoint after 14 wk of diet and RNA extracted for NanoString nCounter transcriptomics analysis (NanoString Technologies, Seattle, WA). For both cohorts, RNA was isolated using an RNAeasy kit (Qiagen, Germantown, MD), per the manufacturer's instructions.

Briefly, for RNA-seq on cohort 1 hippocampi, RNA quality was assessed using a 2100 Bioanalyzer at the University of Michigan's Advanced Genomics Core and used to construct a library, which was sequenced using the NovaSeq 6000 (Illumina, San Diego, CA) to obtain approximately 60 million 50 bp paired-end reads per sample. The raw FASTQ files were first cleaned by removing low quality reads (Q<30) and adapters with Trimmomatic [39]. All clean reads were mapped to the mouse reference genome mm10 (GRCm38) using HISAT2 mapper [40]. FeatureCounts [41] was used to summarize the reads mapped to mouse genes. Fragments per kilobase of transcript per million mapped reads values were calculated for all genes to represent their expression levels.

For NanoString on cohort 2 hippocampi, RNA samples were sent to Michigan State University for nCounter analysis using NanoString's mouse immunology panel

(catalog # PLS PPL M IMM) with 19 spike-in genes (Iba1, Aim2, Atf6, Cd200r, cGAS, Decaf1, Chop, Dgat2, Perk, Elovl6, Ire1a, Gfap, Jnk, Mapt, Mmp12, Nlrp3, Asc, Scd1, Tmem119). NanoString data were processed using nSolver 4.0 software. Any samples not passing quality control were removed and background thresholding was performed so that any samples with counts below the lowest negative control (a relative gene expression level of 4 counts) were set to that value for analysis. Data were then normalized to the positive controls and to the housekeeping genes provided within the panel. Normalized data were then used for subsequent statistical analysis of relative gene expression (counts).

4.5.5 Immunological phenotyping

Terminal plasma and hippocampal lysates from cohort 2 young and aged mice on SD and HFD were used to measure cytokine concentrations via enzyme-linked immunosorbent assay (ELISA). Plasma was analyzed for tumor necrosis factor alpha (TNF-α), monocyte chemoattractant protein-1 (MCP-1), interleukin 6 (IL-6), and interleukin 1 beta (IL-1β). Hippocampal lysates were analyzed for TNF-α, MCP-1, IL-6, IL-1β, interferon gamma (IFN-γ), and interleukin 10 (IL-10). ELISA was performed by the University of Michigan Immune Monitoring Core of the Rogel Cancer Center.

4.5.6 Bioinformatics and statistical analysis

Differentially expressed gene analysis for RNA-seq data was performed with DESeq2 package [42]. Differentially expressed genes (DEGs) were identified with an

adjusted P-value<0.05. To identify the overrepresented biological functions, the Kyoto Encyclopedia of Genes and Genomes (KEGG) pathways and Gene Ontology (GO) enrichment analysis were performed using a hypergeometric test with our in-house R analysis package richR (http://github.com/hurlab/richR). The terms with Benjamini-Hochberg corrected P-values<0.05 were deemed as significantly overrepresented biological functions in each DEG set.

Statistical analysis of all other data was performed using either Prism (version 9; GraphPad Software, La Jolla, CA, USA) or SAS 9.4 software (SAS Institute, Cary, NC). GraphPad analyses were performed using either t-test or analysis of variance (ANOVA) and significance of multiple comparisons determined using Tukey's test. SAS analyses were performed using the Proc Mixed function, and for NanoString data cartridge was set as a random effect to account for potential differences between batches. Normality was established using Anderson-Darling, D'Agostino-Pearson omnibus, Shapiro-Wilk, and Kolmogorov-Smirnov tests. Non-normal data were log transformed and if log transformation did not result in normality, non-parametric analysis was performed using Kruskal-Wallis test. Data are presented as either means or least square means ± standard deviation or as mean ± SEM and are indicated as such in the figure legends.

4.6 Bibliography

1. Blüher M. Obesity: global epidemiology and pathogenesis. *Nat Rev Endocrinol 2019 155*. 2019;15(5):288-298. doi:10.1038/s41574-019-0176-8
2. Larsson U, Karlsson J, Sullivan M. PAPER Impact of overweight and obesity on health-related quality of life-a Swedish population study. *Int J Obes*. 2002;26:417-424. doi:10.1038=sj=ijo=0801919
3. Friedlander SL, Larkin EK, Rosen CL, Palermo TM, Redline S. Decreased Quality of Life Associated With Obesity in School-aged Children. *Arch Pediatr Adolesc Med*. 2003;157(12):1206-1211. doi:10.1001/ARCHPEDI.157.12.1206
4. Stephenson J, Smith CM, Kearns B, Haywood A, Bissell P. The association between obesity and quality of life: a retrospective analysis of a large-scale population-based cohort study. *BMC Public Health*. 2021;21(1):1-9. doi:10.1186/S12889-021-12009-8/TABLES/5
5. Pedditizi E, Peters R, Beckett N. The risk of overweight/obesity in mid-life and late life for the development of dementia: a systematic review and meta-analysis of longitudinal studies. *Age Ageing*. 2016;45(1):14-21. doi:10.1093/AGEING/AFV151
6. Callaghan BC, Reynolds EL, Banerjee M, et al. The prevalence and determinants of cognitive deficits and traditional diabetic complications in the severely obese. *Diabetes Care*. 2020;43(3):683-690. doi:10.2337/dc19-1642
7. Hruby A, Manson JAE, Qi L, et al. Determinants and consequences of obesity. *Am J Public Health*. 2016;106(9):1656-1662. doi:10.2105/AJPH.2016.303326
8. Xu WL, Atti AR, Gatz M, Pedersen NL, Johansson B, Fratiglioni L. Midlife overweight and obesity increase late-life dementia risk A population-based twin study. Published online 2011.
9. Pérez De Heredia F, Gómez-Martínez S, Marcos A. Chronic and degenerative diseases Obesity, inflammation and the immune system. Published online 2000. doi:10.1017/S0029665112000092
10. Van Eldik LJ, Carrillo MC, Cole PE, et al. The roles of inflammation and immune mechanisms in Alzheimer's disease. *Alzheimer's Dement Transl Res Clin Interv*. 2016;2(2):99. doi:10.1016/J.TRCI.2016.05.001
11. Cope EC, LaMarca EA, Monari PK, et al. Microglia Play an Active Role in Obesity-Associated Cognitive Decline. *J Neurosci*. 2018;38(41):8889-8904. doi:10.1523/JNEUROSCI.0789-18.2018
12. Hao S, Dey A, Yu X, Stranahan AM. Dietary obesity reversibly induces synaptic stripping by microglia and impairs hippocampal plasticity. *Brain Behav Immun*. 2016;51:230-239. doi:10.1016/J.BBI.2015.08.023
13. Rohm T V., Meier DT, Olefsky JM, Donath MY. Inflammation in obesity, diabetes, and related disorders. *Immunity*. 2022;55(1):31-55. doi:10.1016/J.IMMUNI.2021.12.013
14. Nakandakari SCBR, Muñoz VR, Kuga GK, et al. Short-term high-fat diet

modulates several inflammatory, ER stress, and apoptosis markers in the hippocampus of young mice. *Brain Behav Immun*. 2019;79:284-293. doi:10.1016/j.bbi.2019.02.016

15. Halliday G. Pathology and hippocampal atrophy in Alzheimer's disease. *Lancet Neurol*. 2017;16(11):862-864. doi:10.1016/S1474-4422(17)30343-5
16. Weyand CM, Goronzy JJ. Aging of the immune system: Mechanisms and therapeutic targets. *Ann Am Thorac Soc*. 2016;13(Suppl 5):S422-S428. doi:10.1513/ANNALSATS.201602-095AW/SUPPL_FILE/DISCLOSURES.PDF
17. Haynes L. Aging of the Immune System: Research Challenges to Enhance the Health Span of Older Adults. *Front Aging*. 2020;0:2. doi:10.3389/FRAGI.2020.602108
18. Nikolich-Žugich J. The twilight of immunity: emerging concepts in aging of the immune system. *Nat Immunol 2017 191*. 2017;19(1):10-19. doi:10.1038/s41590-017-0006-x
19. Franceschi C, Garagnani P, Parini P, Giuliani C, Santoro A. Inflammaging: a new immune-metabolic viewpoint for age-related diseases. *Nat Rev Endocrinol*. 2018;14(10):576-590. doi:10.1038/S41574-018-0059-4
20. Sims-Robinson C, Bakeman A, Bruno E, et al. Dietary reversal ameliorates short- and long-term memory deficits induced by high-fat diet early in life. *PLoS One*. 2016;11(9). doi:10.1371/journal.pone.0163883
21. Watson LS, Stone TD, Williams D, Williams AS, Sims-Robinson C. High-Fat Diet Impairs Tactile Discrimination Memory in the Mouse. *Behav Brain Res*. 2020;382. doi:10.1016/j.bbr.2019.112454
22. Zhuang H, Yao X, Li H, et al. Long-term high-fat diet consumption by mice throughout adulthood induces neurobehavioral alterations and hippocampal neuronal remodeling accompanied by augmented microglial lipid accumulation. *Brain Behav Immun*. 2022;100:155-171. doi:10.1016/J.BBI.2021.11.018
23. Kesby JP, Kim JJ, Scadeng M, et al. Spatial Cognition in Adult and Aged Mice Exposed to High-Fat Diet. *PLoS One*. 2015;10(10):e0140034. doi:10.1371/JOURNAL.PONE.0140034
24. Tucsek Z, Toth P, Tarantini S, et al. Aging exacerbates obesity-induced cerebromicrovascular rarefaction, neurovascular uncoupling, and cognitive decline in mice. *J Gerontol A Biol Sci Med Sci*. 2014;69(11):1339-1352. doi:10.1093/GERONA/GLU080
25. Julien C, Tremblay C, Phivilay A, et al. High-fat diet aggravates amyloid-beta and tau pathologies in the 3xTg-AD mouse model. *Neurobiol Aging*. 2010;31(9):1516-1531. doi:10.1016/J.NEUROBIOLAGING.2008.08.022
26. Gannon OJ, Robison LS, Salinero AE, et al. High-fat diet exacerbates cognitive decline in mouse models of Alzheimer's disease and mixed dementia in a sex-dependent manner. *J Neuroinflammation 2022 191*. 2022;19(1):1-20. doi:10.1186/S12974-022-02466-2

27. Moser VA, Pike CJ. Obesity Accelerates Alzheimer-Related Pathology in APOE4 but not APOE3 Mice. *eNeuro*. 2017;4(3). doi:10.1523/ENEURO.0077-17.2017

28. Spencer SJ, Basri B, Sominsky L, et al. High-fat diet worsens the impact of aging on microglial function and morphology in a region-specific manner. *Neurobiol Aging*. 2019;74:121-134. doi:10.1016/J.NEUROBIOLAGING.2018.10.018

29. Valcarcel-Ares MN, Tucsek Z, Kiss T, et al. Obesity in Aging Exacerbates Neuroinflammation, Dysregulating Synaptic Function-Related Genes and Altering Eicosanoid Synthesis in the Mouse Hippocampus: Potential Role in Impaired Synaptic Plasticity and Cognitive Decline. *Journals Gerontol Ser A*. 2019;74(3):290-298. doi:10.1093/GERONA/GLY127

30. O'Brien PD, Guo K, Eid SA, et al. Integrated lipidomic and transcriptomic analyses identify altered nerve triglycerides in mouse models of prediabetes and type 2 diabetes. *DMM Dis Model Mech*. 2020;13(2). doi:10.1242/dmm.042101

31. O'Brien PD, Hinder LM, Rumora AE, et al. Juvenile murine models of prediabetes and type 2 diabetes develop neuropathy. *Dis Model Mech*. 2018;11(12). doi:10.1242/dmm.037374

32. Kleiner DE, Brunt EM, Van Natta M, et al. Design and validation of a histological scoring system for nonalcoholic fatty liver disease. *Hepatology*. 2005;41(6):1313-1321. doi:10.1002/HEP.20701

33. Brunt EM, Kleiner DE, Carpenter DH, et al. NAFLD: Reporting Histologic Findings in Clinical Practice. *Hepatology*. 2021;73(5):2028-2038. doi:10.1002/HEP.31599

34. Liang W, Menke AL, Driessen A, et al. Establishment of a general NAFLD scoring system for rodent models and comparison to human liver pathology. *PLoS One*. 2014;9(12). doi:10.1371/JOURNAL.PONE.0115922

35. Hinder LM, O'Brien PD, Hayes JM, et al. Dietary reversal of neuropathy in a murine model of prediabetes and metabolic syndrome. *Dis Model Mech*. 2017;10(6):717. doi:10.1242/DMM.028530

36. Parlee SD, Lentz SI, Mori H, MacDougald OA. Quantifying size and number of adipocytes in adipose tissue. *Methods Enzymol*. 2014;537:93-122. doi:10.1016/B978-0-12-411619-1.00006-9

37. Cazares VA, Rodriguez G, Parent R, et al. Environmental variables that ameliorate extinction learning deficits in the 129S1/SvImJ mouse strain. *Genes Brain Behav*. 2019;18(7). doi:10.1111/GBB.12575

38. Temme SJ, Murphy GG. The L-type voltage-gated calcium channel CaV1.2 mediates fear extinction and modulates synaptic tone in the lateral amygdale. *Learn Mem*. 2017;24(11):580-588. doi:10.1101/LM.045773.117

39. Bolger AM, Lohse M, Usadel B. Trimmomatic: a flexible trimmer for Illumina sequence data. *Bioinformatics*. 2014;30(15):2114-2120. doi:10.1093/BIOINFORMATICS/BTU170

40. Kim D, Paggi JM, Park C, Bennett C, Salzberg SL. Graph-based genome alignment and genotyping with HISAT2 and HISAT-genotype. *Nat Biotechnol*

2019 378. 2019;37(8):907-915. doi:10.1038/s41587-019-0201-4

41. Liao Y, Smyth GK, Shi W. Sequence analysis featureCounts: an efficient general purpose program for assigning sequence reads to genomic features. 2014;30(7):923-930. doi:10.1093/bioinformatics/btt656

42. Love MI, Huber W, Anders S. Moderated estimation of fold change and dispersion for RNA-seq data with DESeq2. *Genome Biol*. 2014;15(12):1-21. doi:10.1186/S13059-014-0550-8/FIGURES/9

43. Ximerakis M, Lipnick SL, Innes BT, et al. Single-cell transcriptomic profiling of the aging mouse brain. *Nat Neurosci*. 2019;22(10):1696-1708. doi:10.1038/S41593-019-0491-3

44. Ahima RS. *Connecting Obesity, Aging and Diabetes*.; 2009. doi:10.1038/nm0909-996

45. Chen G, Yung R. Meta-inflammaging at the crossroad of geroscience. *Aging Med (milt*. 2019;2(3):157-161. doi:10.1002/AGM2.12078

46. Hotamisligil GS. Inflammation, metaflammation and immunometabolic disorders. *Nat Publ Gr*. 2017;542. doi:10.1038/nature21363

47. Fessler MB, Rudel LL, Brown M. Toll-like receptor signaling links dietary fatty acids to the metabolic syndrome. Published online 2009. doi:10.1097/MOL.0b013e32832fa5c4

48. Li B, Leung JCK, Chan LYY, Yiu WH, Tang SCW. A global perspective on the crosstalk between saturated fatty acids and Toll-like receptor 4 in the etiology of inflammation and insulin resistance. *Prog Lipid Res*. 2020;77. doi:10.1016/J.PLIPRES.2019.101020

49. Arkan MC, Hevener AL, Greten FR, et al. *IKK-β Links Inflammation to Obesity-Induced Insulin Resistance*. Vol 11.; 2005. http://www.nature.com/naturemedicine

50. Vanani AR, Kalantari H, Mahdavinia M, Rashno M, Khorsandi L, Khodayar MJ. Dimethyl fumarate reduces oxidative stress, inflammation and fat deposition by modulation of Nrf2, SREBP-1c and NF-κB signaling in HFD fed mice. *Life Sci*. 2021;283. doi:10.1016/J.LFS.2021.119852

51. Jeon BT, Jeong EA, Shin HJ, et al. Resveratrol Attenuates Obesity-Associated Peripheral and Central Inflammation and Improves Memory Deficit in Mice Fed a High-Fat Diet. *Diabetes*. 2012;61(6):1444-1454. doi:10.2337/DB11-1498

52. Dong Y, Li S, Lu Y, et al. Stress-induced NLRP3 inflammasome activation negatively regulates fear memory in mice. *J Neuroinflammation*. 2020;17(1):1-16. doi:10.1186/S12974-020-01842-0/FIGURES/6

53. Singer BH, Newstead MW, Zeng X, et al. Cecal Ligation and Puncture Results in Long-Term Central Nervous System Myeloid Inflammation. *PLoS One*. 2016;11(2):e0149136. doi:10.1371/JOURNAL.PONE.0149136

54. Spencer SJ, D'Angelo H, Soch A, Watkins LR, Maier SF, Barrientos RM. High-fat diet and aging interact to produce neuroinflammation and impair hippocampal-

and amygdalar-dependent memory. *Neurobiol Aging*. 2017;58:88-101. doi:10.1016/J.NEUROBIOLAGING.2017.06.014

55. Schellinck HM, Cyr DP, Brown RE. How Many Ways Can Mouse Behavioral Experiments Go Wrong? Confounding Variables in Mouse Models of Neurodegenerative Diseases and How to Control Them. *Adv Study Behav*. 2010;41(C):255-366. doi:10.1016/S0065-3454(10)41007-4

56. Roedel A, Storch C, Holsboer F, Ohl F. Effects of light or dark phase testing on behavioural and cognitive performance in DBA mice. *Lab Anim*. 2006;40(4):371-381. doi:10.1258/002367706778476343

57. Kang EB, Koo JH, Jang YC, et al. Neuroprotective Effects of Endurance Exercise Against High-Fat Diet-Induced Hippocampal Neuroinflammation. *J Neuroendocrinol*. 2016;28(5). doi:10.1111/JNE.12385

58. Church JS, Renzelman ML, Schwartzer JJ. Ten-week high fat and high sugar diets in mice alter gut-brain axis cytokines in a sex-dependent manner. *J Nutr Biochem*. 2022;100. doi:10.1016/J.JNUTBIO.2021.108903

59. Boitard C, Cavaroc A, Sauvant J, et al. Impairment of hippocampal-dependent memory induced by juvenile high-fat diet intake is associated with enhanced hippocampal inflammation in rats. *Brain Behav Immun*. 2014;40:9-17. doi:10.1016/J.BBI.2014.03.005

60. Chalan P, Berg A van den, Kroesen B-J, Brouwer L, Boots A. Rheumatoid Arthritis, Immunosenescence and the Hallmarks of Aging. *Curr Aging Sci*. 2015;8(2):131. doi:10.2174/1874609808666150727110744

61. De Martinis M, Franceschi C, Monti D, Ginaldi L. Inflamm-ageing and lifelong antigenic load as major determinants of ageing rate and longevity. *FEBS Lett*. 2005;579(10):2035-2039. doi:10.1016/J.FEBSLET.2005.02.055

62. Freund A, Orjalo A V., Desprez PY, Campisi J. Inflammatory networks during cellular senescence: causes and consequences. *Trends Mol Med*. 2010;16(5):238-246. doi:10.1016/J.MOLMED.2010.03.003

63. Tchkonia T, Zhu Y, Van Deursen J, Campisi J, Kirkland JL. Cellular senescence and the senescent secretory phenotype: therapeutic opportunities. *J Clin Invest*. 2013;123(3):966-972. doi:10.1172/JCI64098

64. Cole KE, Strick CA, Paradis TJ, et al. Interferon-inducible T Cell Alpha Chemoattractant (I-TAC): A Novel Non-ELR CXC Chemokine with Potent Activity on Activated T Cells through Selective High Affinity Binding to CXCR3. *J Exp Med*. 1998;187. Accessed June 27, 2022. http://www.jem.org

65. Mousessian AS, Nunes da Silva CP, Oba-Shinjo SM, Kolias AG, Paiva WS, Nagahashi Marie SK. CXCR7, CXCR4, and Their Ligand Expression Profile in Traumatic Brain Injury. *World Neurosurg*. 2021;147:e16-e24. doi:10.1016/J.WNEU.2020.11.022

66. Mccoll SR, Mahalingam S, Staykova M, et al. Expression of rat I-TAC/CXCL11/SCYA11 during central nervous system inflammation: comparison

with other CXCR3 ligands. *Lab Investig*. 2004;84:1418-1429. doi:10.1038/labinvest.3700155

67. Rupprecht TA, Koedel U, Muhlberger B, Wilske B, Fontana A, Pfister H-W. ORIGINAL COMMUNICATION. *J Neurol*. 2005;252:820-823. doi:10.1007/s00415-005-0752-9

68. Thomas R, Wang W, Su DM. Contributions of Age-Related Thymic Involution to Immunosenescence and Inflammaging. *Immun Ageing 2020 171*. 2020;17(1):1-17. doi:10.1186/S12979-020-0173-8

69. Yu HT, Park S, Shin EC, Lee WW. T cell senescence and cardiovascular diseases. *Clin Exp Med*. 2016;16(3):257-263. doi:10.1007/S10238-015-0376-Z/FIGURES/1

70. Wang J, Lee S, Teh CEY, Bunting K, Ma L, Shannon MF. The transcription repressor, ZEB1, cooperates with CtBP2 and HDAC1 to suppress IL-2 gene activation in T cells. *Int Immunol*. 2009;21(3):227-235. doi:10.1093/INTIMM/DXN143

71. Romero-Pérez L, Ló pez-Garcıá ngeles, Dıáz-Martı J, et al. ZEB1 overexpression associated with E-cadherin and microRNA-200 downregulation is characteristic of undifferentiated endometrial carcinoma. *Mod Pathol*. 2013;26:1514-1524. doi:10.1038/modpathol.2013.93

72. Bleve A, Motta F, Durante B, Pandolfo C, Selmi C, Sica A. Immunosenescence, Inflammaging, and Frailty: Role of Myeloid Cells in Age-Related Diseases. 2016;1:3. doi:10.1007/s12016-021-08909-7

73. Becker-Greene D, Li H, Daniel Perez-Cremades ·, et al. MiR-409-3p targets a MAP4K3-ZEB1-PLGF signaling axis and controls brown adipose tissue angiogenesis and insulin resistance. 2021;78:7663-7679. doi:10.1007/s00018-021-03960-1

74. Gubelmann C, Schwalie PC, Raghav SK, et al. Identification of the transcription factor ZEB1 as a central component of the adipogenic gene regulatory network. *Elife*. 2014;3(August2014):1-30. doi:10.7554/ELIFE.03346

75. Filios SR, Xu G, Chen J, Hong K, Jing G, Shalev A. MicroRNA-200 is induced by thioredoxin-interacting protein and regulates Zeb1 protein signaling and beta cell. *J Biol Chem*. 2014;289(52):36275-36283. doi:10.1074/JBC.M114.592360

76. Panda A, Arjona A, Sapey E, et al. Human innate immunosenescence: causes and consequences for immunity in old age. *Trends Immunol*. 2009;30(7):325-333. doi:10.1016/J.IT.2009.05.004

77. Klein U, Casola S, Cattoretti G, et al. Transcription factor IRF4 controls plasma cell differentiation and class-switch recombination. Published online 2006. doi:10.1038/ni1357

78. Kong X, Banks A, Liu T, et al. IRF4 is a key thermogenic transcriptional partner of PGC-1α. *Cell*. 2014;158(1):69-83. doi:10.1016/J.CELL.2014.04.049

79. Guo S, Li ZZ, Jiang DS, et al. IRF4 is a novel mediator for neuronal survival in

ischaemic stroke. *Cell Death Differ*. 2014;21(6):888-903. doi:10.1038/CDD.2014.9

80. Al Mamun A, Chauhan A, Qi S, et al. Microglial IRF5-IRF4 regulatory axis regulates neuroinflammation after cerebral ischemia and impacts stroke outcomes. *Proc Natl Acad Sci U S A*. 2020;117(3):1742-1752. doi:10.1073/PNAS.1914742117/SUPPL_FILE/PNAS.1914742117.SAPP.PDF
81. Zhao SC, Wang C, Xu H, et al. Age-related differences in interferon regulatory factor-4 and -5 signaling in ischemic brains of mice. *Acta Pharmacol Sin*. 2017;38(11):1425-1434. doi:10.1038/APS.2017.122
82. Barron AM, Rosario ER, Elteriefi R, Pike CJ. Sex-specific effects of high fat diet on indices of metabolic syndrome in 3xTg-AD mice: implications for Alzheimer's disease. *PLoS One*. 2013;8(10). doi:10.1371/JOURNAL.PONE.0078554
83. Elzinga SE, Savelieff MG, O'Brien PD, Mendelson FE, Hayes JM, Feldman EL. Sex differences in insulin resistance, but not peripheral neuropathy, in a diet-induced prediabetes mouse model. *Dis Model Mech*. 2021;14(4). doi:10.1242/DMM.048909

Chapter 5 Preliminary Data on the Role of Endoplasmic Reticulum Stress in Hippocampal Microglial Activation in Obesity

5.1 Abstract

Obesity is an established risk factor for developing cognitive impairment and dementia. Despite decades of research, Alzheimer's disease (AD) lacks disease-modifying therapies, possibly because current therapeutics target pathways too late in the disease process. Understanding early events that set off the cascade of pathological changes may lead to potentially disease-modifying therapies, preventing progression of disease. Obesity induces brain inflammation and activates microglia in brain regions responsible for cognition, such as the hippocampus. In the periphery, high-fat diet (HFD) mediates a macrophage endoplasmic reticulum (ER) stress response, including through the IRE1α-XBP1 stress response pathway, and inflammation in obesity. However, the role of SFA-induced ER stress on microglial activation is unclear. Herein, we devised experiments to address our hypothesis that a saturated-fat-enriched HFD activates microglia through the ER stress response, contributing cognitive impairment. **Chapter 5** outlines the preliminary results currently available for **Aim 4** of the dissertation, and we propose future experiments to address unanswered questions.

5.2 Introduction

The prevalence of global obesity continues to rise [1,2], placing a great burden on

patients and healthcare systems. Unfortunately, obesity is an established risk factor for developing cognitive impairment and dementia [3,4]. Despite decades of research, disease-modifying therapies for dementia and AD are lacking. Reasons are manifold, but among them is the possibility that current therapeutics target pathways too late in the disease process. Thus, understanding early events that set off the cascade of pathological changes may constitute a potential therapeutic path forward. Obesity along the continuum of the life span, from childhood to midlife, predisposes individuals to cognitive deficits [4–7]. However, mechanisms linking obesity to cognitive dysfunction are not well characterized. Rodent models of diet-induced obesity demonstrate an inflammatory response to a saturated fatty acid-enriched HFD feeding in the hippocampus, a brain region critical for declarative memory, alongside hippocampal-dependent cognitive dysfunction [8–10]. Researchers suggest a contributory role for microglial activation in obesity-associated cognitive impairment [8]. Thus, understanding how and when microglial become activated over the course of obesity in the lifespan will clarify appropriate therapeutic opportunities. However, there is a gap in our understanding of the pathological mechanisms mediating obesogenic diet-induced hippocampal microglial activation.

Drawing on observations from peripheral macrophages in obesity, the endoplasmic reticulum stress response may be a potential mechanism mediating microglial activation. SFA-enriched HFD induces a macrophage endoplasmic reticulum (ER) stress response, which leads to a pro-inflammatory macrophage phenotype [11]. The inositol requiring enzyme 1-α (IRE1α) branch of the ER stress response (**Fig 5.1**) plays a role in this process in macrophages [11], and SFAs activate the IRE1α-XBP1 pathway

in macrophages *in vitro* [12]. IRE1α is a transmembrane ER protein with ribonuclease and kinase catalytic activity [13]. IRE1α splices X-box binding protein 1 (XBP1) mRNA into spliced XBP1 (sXBP1), which is translated into a transcription factor involved in an adaptive response to stress, and IRE1α activation can also induce apoptosis [14,15]. As an 'immunometabolic' hub, the ER senses metabolic disturbances and responds by inducing the transcription of adaptive genes, or if stress is chronic and excessive, apoptosis [14,15]. ER stress also contributes to insulin resistance (IR) in obesity models [16,17]. IRE1α can activate TNF receptor-associated factor 2 (TRAF2), leading to JNK phosphorylation (pJNK), which induces IR by phosphorylating insulin receptor substrate 1 (pIRS1) [16,17]. The ER stress response thus contributes to both inflammation and insulin resistance in obesity, but its role in microglia is unclear.

In contrast to macrophages, the role of SFA-induced ER stress on microglial activation is less well-established, but SFAs can induce a pro-inflammatory state in microglia *in vitro* [18]. We previously found elevated spliced XBP1 (sXBP1) and heat shock protein 5 (Hsp5) in the hippocampus of HFD mice following 20 wk of diet [19]. In **Chapter 3** of this dissertation, single-cell RNA-seq identified a signature of dysregulated protein processing in the ER across microglia from HFD versus control diet mice. Nevertheless, studies of SFA- and/or HFD-induced ER stress in microglia are lacking. Herein, we devised two sets of experiments (**Fig 5.1**, overview) to address our hypothesis that a SFA-enriched HFD activates microglia through the ER stress response, contributing to cognitive impairment. We leveraged a microglia cell line for *in*

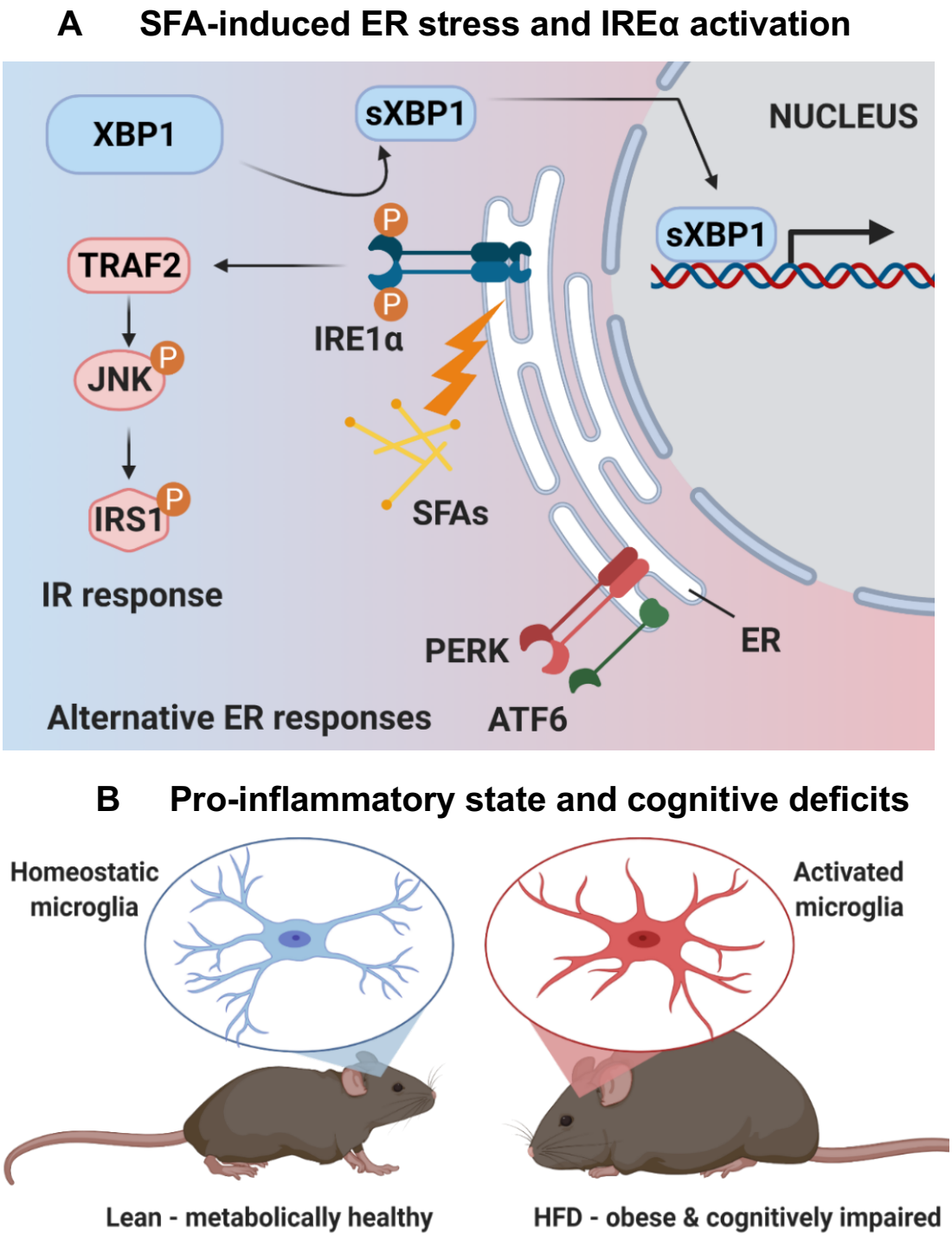

Figure 5.1 Study overview.

(A) Schematic of IRE1α signaling. SFAs (yellow rods) activate IRE1α (lightening), which splices XBP1 to sXBP1. IRE1α activation also activates TRAF2/JNK signaling, which can lead to IRS1 phosphorylation and IR. In vitro work in microglia will determine if this pathway is activated by the SFA palmitate. (B) In vivo SFA-rich HFD triggers ER stress, microglial activation, and cognitive impairment. We aim to determine whether the microglial ER stress response contributes to inflammatory activation.

vitro experiments and an ER stress-reporter mice for *in vivo* experiments. This **Chapter 5** of the thesis presents preliminary data and proposes future experiments to address **Aim 4** of the dissertation.

5.3 Results

5.3.1 Preliminary data suggests that the SFA palmitate activates the IRE1α-XBP1 pathway in microglia *in vitro*

Our prior work demonstrates that sXBP1 and pJNK, which can be activated by multiple mechanisms, including downstream of IRE1α (see **Fig 5.1**) are elevated in the hippocampus of obese mice [19]. Our analysis of hippocampal gene expression in obese mice also demonstrated dysregulation of XBP1 gene expression (unpublished, **Fig 5.2**). Because SFAs are known to activate the IRE1α-XBP1 ER stress response in macrophages [12], and IRE1α is activated in macrophages in obese mice [11], we asked whether SFAs can also activate this ER stress response pathway in microglia. We treated human immortalized microglia with the SFA palmitate, and preliminary results suggest that palmitate increases both total IRE1α and phospho-IRE1α protein levels in microglia (**Fig 5.3**). Further, we performed quantitative RT-PCR of total XBP1, spliced XBP1, and unspliced XBP1 in control or palmitate treated microglia, and preliminary findings show that palmitate increases spliced, unspliced, and total XBP1 RNA, and increases the ratio of spliced to unspliced XBP1 relative to controls (data not shown). Further work is required to confirm these preliminary results.

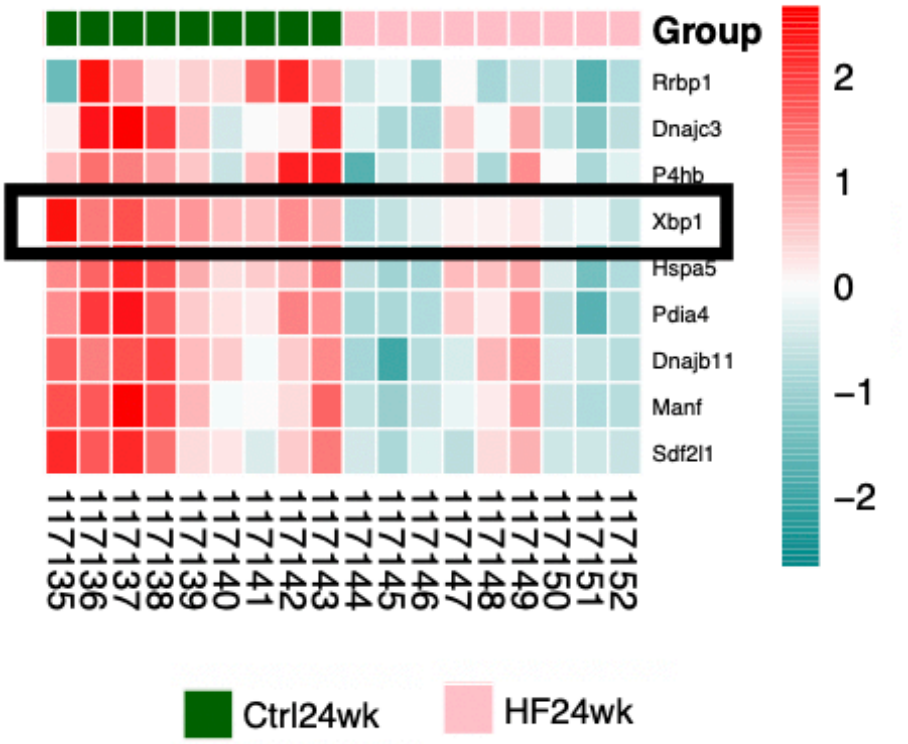

Figure 5.2 XBP1 expression in the hippocampus of obese mice.

Heat map of gene expression in mice fed control (Green, left) or HFD (pink, right) diets from 5 wk of age for a total of 19 wk. Individual animals are plotted on the x-axis, genes on the y-axis, and color represents relative gene expression from low (blue) to high (red).

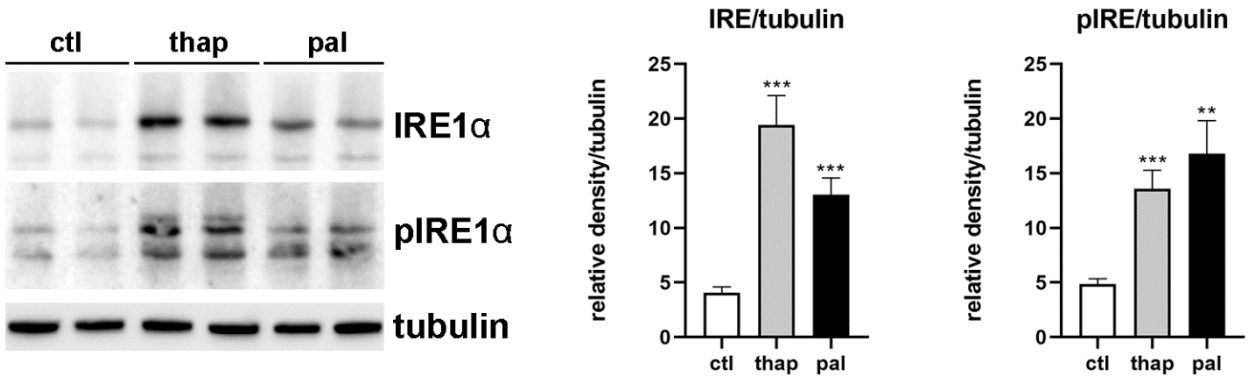

Figure 5.3 Palmitate increase protein and phosphorylation of IRE1α.

SV40 microglia cells are treated with thapsigargin (thap, positive control) or 62.5 μM palmitate (pal) for 18-24 hours and cells lysates are analyzed for IRE1α and pIRE1α level. Equal protein loading is confirmed with tubulin. *** $p<0.005$, ** $p<0.01$ by Student t-test, 2 experiments.

5.3.2 Preliminary data suggests that microglia are insulin responsive but do not develop insulin resistance *in vitro*

To our knowledge, there are no reports examining insulin resistance in microglia. One research group demonstrated that microglia respond to insulin *in vitro*, and that this response counteracts pro-inflammatory activation [20]. This effect suggests that if IR were to develop in microglia, as might occur through SFA-induced ER stress, or independently of ER stress, IR may promote a pro-inflammatory phenotype. We demonstrated IR in the hippocampus of our diet-induced obesity model [19], and in neurons using an *in vitro* model of IR [21,22]. Here we used immortalized human microglia *in vitro* to determine whether microglia develop insulin resistance in response to glucose or palmitate using our established *in vitro* model of insulin resistance [21,22]. Preliminary results suggest that microglia are responsive to insulin, demonstrated by an increase in phospho-AKT, phospho-ERK, and phospho-IRS1 (pS612) following insulin stimulation (**Fig 5.4**). However, when microglia are pre-treated with palmitate or glucose for 24 hours, we did not observe a blunted response to insulin stimulation compared to controls (**Fig 5.5**). These preliminary data suggest that although microglia are responsive to insulin, they are able to maintain responses in the context of metabolic stress, unlike neurons [21,22].

5.3.3 Ongoing studies will determine the role of microglial XBP1 activation using an *in vivo* model of diet-induced obesity

We utilized endoplasmic reticulum stress activated-indicator (ERAI) [23] transgenic mice, which display a Venus fluorescence reporter of XBP1 splicing, to examine

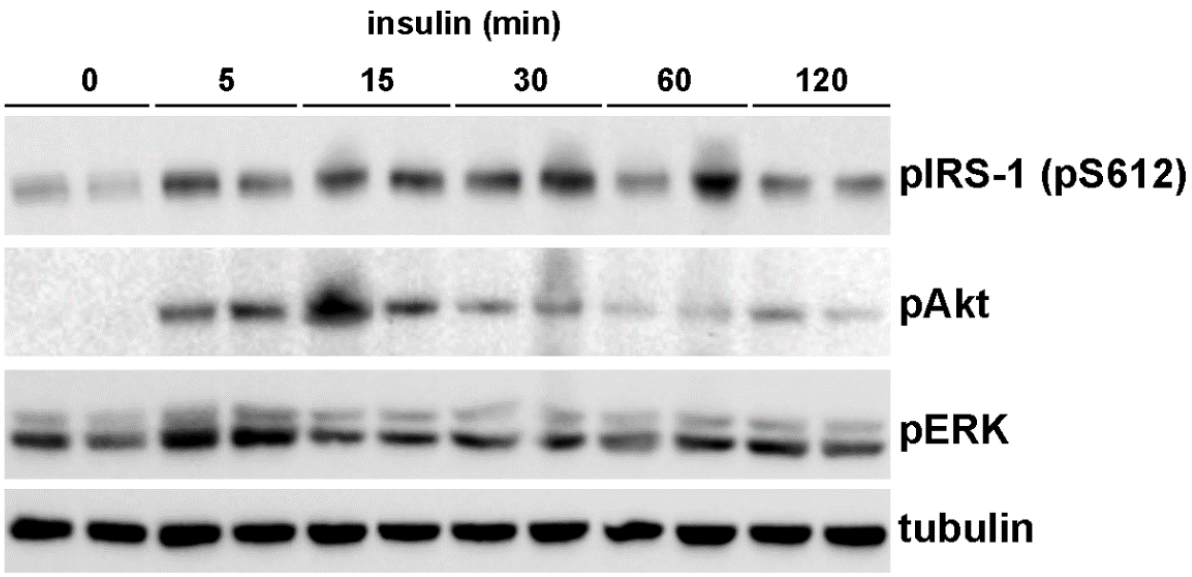

Figure 5.4 SV40 microglia cells respond to insulin treatment.

SV40 cells are treated with 20 nM insulin for the indicated times. Cells lysates are analyzed by Western blotting with the indicated antibodies. Equal protein loading is confirmed with tubulin.

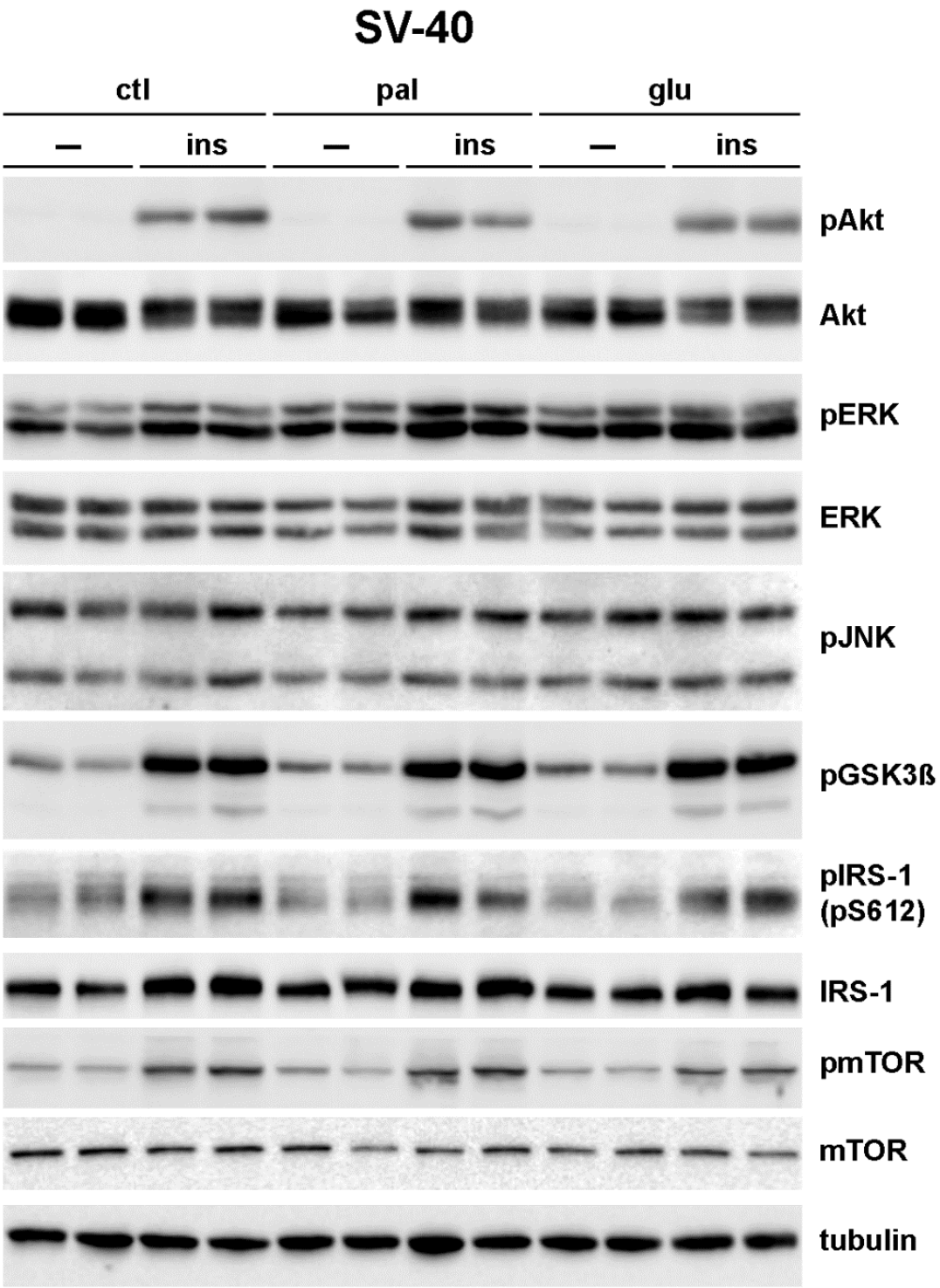

Figure 5.5 Palmitate or glucose do not induce insulin resistance in SV40 microglia cells.

SV40 cells are treated with 62.5 μM palmitate (pal) or 50 mM glucose (glu) for 24 h and then treated with 20 nM insulin (ins) for 30 min. Cells lysates are analyzed by Western blotting with the indicated antibodies. Equal protein loading is confirmed with tubulin.

activation of the IRE1α-XBP1 pathway *in vivo*. We fed ERAI transgenic and wild-type littermates HFD or control diet starting at 5 wk age for 1 wk, 1 mo, or 6 mo to longitudinally measure XBP1 pathway activation in the brain. Mice in the 1 wk and 1 mo cohorts have been sacrificed at their respective terminal time points, and the 6 mo cohorts are underway. Brains were processed for immunohistochemical analysis. Brain sections of the hippocampus will be stained for Iba1 and NeuN to identify cellular co-localization of XBP1-splicing Venus signal. An anti-GFP antibody that binds to the Venus protein, a variant of GFP, will be used to effectively visualize the Venus signal. We will quantify the percentage of microglia and neurons that are positive for the Venus reporter signal. Further, we will measure 3-D morphology of microglia using our established protocol, to determine whether the ER stress response associates with measures of microglial activation, as determined by microglial morphology, using a linear mixed effects regression model. Based on our findings in **Chapter 2**, we do not expect differences in microglial morphology between HFD and controls in the CA1 region before 6 mo. However, we will also examine the dentate gyrus molecular layer, and measure soma size as an additional morphology measure. Further, we will supplement with additional methods of determining microglial activation, such as spatial transcriptomics.

5.4 Discussion

5.4.1 Summary

Obesity is associated with deficits in cognitive function throughout the lifespan, however, how obesity elevates risk for cognitive dysfunction is not well understood. Mouse models of diet-induced obesity suggest that microglial activation may play a role in mediating hippocampal cognitive impairment. The mechanisms mediating obesity induced microglial activation in the hippocampus remain unclear. The IRE1α ER stress response plays a role in macrophage mediated inflammation in obesity [11], and represents a potential mechanism mediating microglial activation in the hippocampus. In this preliminary *in vitro* work, we found evidence that the SFA palmitate activates the IRE1α-XBP1 pathway in microglia, quantified by increased IRE1α and pIRE1α proteins, and increased RNA levels of total, spliced, and unspliced XBP1. Our preliminary results suggest that microglia respond to insulin, but do not develop insulin resistance in response to palmitate or glucose pre-treatment. Our study aimed at quantifying hippocampal microglial XBP1 splicing *in vivo* and correlating pathway activation with morphology in the ERAI mice is underway. We expect that microglial in HFD mice will demonstrate an elevated sXBP1 signal relative to controls. It is possible that our study may demonstrate an initial elevation in IRE1α/XBP1 signaling, followed by a reduction in some components of the ER stress response over time. A loss of appropriate ER stress response after chronic stress, or 'stress response failure,' has been reported in metabolic disease and aging models [24]. Our single cell RNA-sequencing results in **Chapter 3** demonstrated dysregulation of ER heat shock proteins in microglia from obese mice, and this microglial ER response has been proposed to be anti-inflammatory in this context [25]. Quantifying the longitudinal progression of XBP1 activation, and correlating this ER stress response with the microglial activation

phenotype, will help determine whether an ER response is protective, pro-inflammatory, or both, over time.

5.4.2 Future directions

To assess the effects of potential IRE1α-XBP1 pathway activation on hippocampal microglial pro-inflammatory activation and cognition, studies using pharmacological inhibition of IRE1α ribonuclease activity, or genetic ablation of microglial-specific IRE1α, would prove useful. Inhibiting activation of this pathway in a diet-induced obesity mouse model would help determine whether activation of this stress response pathway contributes to hippocampal microglial activation. Further, by performing tests of hippocampal-dependent cognition, these future studies could determine whether this ER stress response pathway contributes to cognitive impairment.

5.5 Methods

5.5.1 Microglial cell culture

Immortalized human microglia cells were obtained for *in vitro* experiments (abm, catalog # T0251) and maintained in high glucose DMEM (Thermo, catolog # 11965092) with 10% fetal bovine serum (Gibco, catalog # 10437-028). Cells were passaged with 0.25% trypsin-EDTA (Thermo, catalog # 25200056).

5.5.2 SFA treatments for ER stress

Sodium palmitate (Sigma, catalog # P9767 or NuCheckPrep INC) fatty acid treatment was prepared by conjugation to fatty-acid free bovine serum albumin (BSA) (Fischer, catalog # BP9704). Treatment conditions included treatment media (negative control), BSA only vehicle (negative control), thapsigargin (positive control, Tocris, catalog # 1138), and BSA-conjugated palmitate (PA) for 18-24 h. Per lab protocol [26], palmitate dose response curves using physiological concentrations (31.25, 62.5, 125, and 250 μM) were generated. ER stress was induced using thapsigargin as a positive control for comparison to SFA treated cells. IRE1α signaling was quantified by Western blot (WB) (outlined below) for IRE1α (Novus Biologicals, catalog # NB100-2324SS) and phospho-IRE1α (Novus Biologicals, catalog # NB100-2323SS).

5.5.3 Insulin resistance induction treatments

Insulin response was evaluated *in vitro* by treating SV40-microglia with 20 nM insulin and collecting cell lysates for Western blotting after 0, 5, 15, 30, 60, and 120 minutes post stimulation. Phospho-IRS-1 (pS612, Cell Signaling, catalog # 2386), phospho-AKT (Cells Signaling, catalog # 4060), and phospho-ERK (Cell Signaling, catalog # 4370) protein levels were evaluated by Western blots to determine downstream activation of insulin stimulation. To evaluate insulin resistance, SV40 microglia were incubated for 24 h with either 62.5 μM palmitate, 50 mM glucose, or control media plus BSA vehicle (positive control for insulin response) and then treated for 30 minutes with 20 nM insulin. Insulin response was evaluated by Western blot using

antibodies against phospho-AKT, total AKT (catalog # 4691), phospho-ERK, total ERK (catalog # 4695), phospho-JNK (catalog # 4668), phoshpo-GSK3β (catalog # 9315), pospho-IRS-1 (pS612), phospho-mTOR (catalog # 5536), total mTOR (catalog # 2983), and tubulin (catalog # 3873) for loading control. All antibodies are from Cell Signaling unless otherwise indicated.

5.5.4 Western blotting

Cell culture lysates were prepared on ice in RIPA lysis buffer (Thermo, catalog # 89901) containing protease inhibitor cocktail (Roche, catalog # 11836170001). Lysates were sonicated and centrifuged at 17,000 rpm at 4 degrees and the supernatant was collected. Protein concentration was measured using the Pierce 660 Protein Assay Reagent (Thermo, catalog #22660), and lysates were resolved by SDS-PAGE. Protein was transferred to nitrocellulose membranes, which were incubated in blocking solution (3% BSA in TBS with 0.1% Tween-20) for 2 h at room temperature. Nitrocellulose membranes were then incubated with primary antibodies overnight at 4 degrees: Primary antibodies were diluted 1:1000-1:3000 in blocking buffer. Membranes were washed with TBST and then incubated with horseradish peroxidase-conjugated secondary antibodies for 2 hr at room temperature. Secondary antibodies were diluted 1:2000 in 5% non-fat dry milk in TBS with 0.1% Tween-20. Membranes were washed again and incubated in Clarity (Bio-Rad cat#: 102031794) or Clarity Max (Bio-Rad cat#: 1705062) Western ECL substrate depending on signal strength. Bands were imaged on the ChemiDoc Imaging system, quantified by Image Lab 6.1 software (Bio-Rad) and analyzed by Prism (GraphPad Software, San Diego, CA).

5.5.5 XBP1 Quantitative RT-PCR

Following treatment, SV-40 microglia cell pellets were collected and frozen at -80 degrees Celsius. Total RNA was isolated using Trizol and the RNA Cleanup and Concentration kit (Norgen Biotek, catalog # 43200). Quantitative real-time PCR was performed using universal species primers, which were custom made according to published universal sequences [27].

5.5.6 Animal study design

Microglial activation *in vivo* will be quantified in ERAI-Venus mice. ERAI-Venus mice were provided by Dr. Iwawaki (Kanazawa Medical University) via Dr. Sheng (NINDS). Mice were maintained in the Unit for Laboratory Animal Medicine (ULAM) at the University of Michigan and housed with a 12/12-h light/dark cycle in specific-pathogen-free facility kept at 20 ± 2 °C. 5-wk-old ERAI-Venus or WT littermate control male mice were placed on a HFD (60% fat, Research Diets, D12492) or control diet (10% fat, D12450J) (n=6-7/group). To determine the temporal progression and association between hippocampal microglial activation and XBP1 splicing, and if ER stress precedes microglial activation, mice are sacrificed at 3 time points: after 1 wk diet (late acute), after 1 mo diet (intermediate), and after 6 mo diet (chronic). Chow and water were available *ad libitum*. Intraperitoneal injection of pentobarbital (Fatal-Plus, Vortech Pharmaceuticals) was administered for sacrifice at the terminal time points. Mice were perfused with phosphate buffered saline and the following tissues were

collected for later analyses: flash frozen cortex, flash frozen hippocampus, a 4% paraformaldehyde fixed brain hemisphere, fixed liver, fixed visceral fat, flash frozen visceral fat, flash frozen spleen, blood, and plasma. The University of Michigan's Institutional Animal Care and Use Committee (IACUC; protocol numbers PRO00010039 and PRO00010247) approved all procedures.

5.5.7 Metabolic phenotyping

All mice are will be phenotyped according to our well-established protocols [26,28], including: baseline and weekly body weights, fasting glucose (glucometer reading from tail blood draw), and glucose tolerance tests, as well as terminal fasting plasma insulin (ELISA) and lipid profiles (triglycerides, cholesterol, HDL).

5.5.8 Immunohistochemistry

One brain hemisphere from each mouse was dissected and fixed in 4% paraformaldehyde. Floating tissue sections will be cut to 50 μm thickness and immunohistochemistry will be performed using rabbit anti-Iba1 (Wako, cat# 019-19741), anti-NeuN (Abcam, catalog # ab279297), and anti-GFP (Rockland, catalog # 600-901-215) at 4 °C overnight. Incubation in secondary antibodies (Invitrogen, catalog #s A11039, A21096, and A32740) will be at room temperature for 2 h and nuclei will be stained with Hoechst (1mg/ml; Sigma-Aldrich, catalog # 861405) for 8 min. ProLong Gold Antifade Mountant (Thermo, catalog # P36930) will be used for mounting.

5.5.9 RNA-sequencing

RNA-sequencing data presented here was generated from cohort 1 in **Chapter 4**. Please refer to **Chapter 4** for methods.

5.6 Bibliography

1. Di Cesare M, Bentham J, Stevens GA, et al. Trends in adult body-mass index in 200 countries from 1975 to 2014: a pooled analysis of 1698 population-based measurement studies with 19·2 million participants. *Lancet (London, England)*. 2016;387(10026):1377-1396. doi:10.1016/S0140-6736(16)30054-X
2. Blüher M. Obesity: global epidemiology and pathogenesis. *Nat Rev Endocrinol 2019 155*. 2019;15(5):288-298. doi:10.1038/s41574-019-0176-8
3. Whitmer RA, Gustafson DR, Barrett-Connor E, Haan MN, Gunderson EP, Yaffe K. Central obesity and increased risk of dementia more than three decades later. *Neurology*. 2008;71(14):1057-1064. doi:10.1212/01.wnl.0000306313.89165.ef
4. Pedditizi E, Peters R, Beckett N. The risk of overweight/obesity in mid-life and late life for the development of dementia: a systematic review and meta-analysis of longitudinal studies. *Age Ageing*. 2016;45(1):14-21. doi:10.1093/AGEING/AFV151
5. Fitzpatrick AL, Kuller LH, Lopez OL, et al. Midlife and late-life obesity and the risk of dementia: Cardiovascular health study. *Arch Neurol*. 2009;66(3):336-342. doi:10.1001/archneurol.2008.582
6. Khan NA, Baym CL, Monti JM, et al. Central adiposity is negatively associated with hippocampal-dependent relational memory among overweight and obese children. *J Pediatr*. 2015;166(2):302-308.e1. doi:10.1016/J.JPEDS.2014.10.008
7. Liang J, Matheson BE, Kaye WH, Boutelle KN. Neurocognitive correlates of obesity and obesity-related behaviors in children and adolescents. *Int J Obes 2014 384*. 2013;38(4):494-506. doi:10.1038/ijo.2013.142
8. Cope EC, LaMarca EA, Monari PK, et al. Microglia Play an Active Role in Obesity-Associated Cognitive Decline. *J Neurosci*. 2018;38(41):8889-8904. doi:10.1523/JNEUROSCI.0789-18.2018
9. Hao S, Dey A, Yu X, Stranahan AM. Dietary obesity reversibly induces synaptic stripping by microglia and impairs hippocampal plasticity. *Brain Behav Immun*. 2016;51:230-239. doi:10.1016/J.BBI.2015.08.023
10. Vinuesa A, Bentivegna M, Calfa G, et al. Early Exposure to a High-Fat Diet Impacts on Hippocampal Plasticity: Implication of Microglia-Derived Exosome-like Extracellular Vesicles. *Mol Neurobiol*. Published online November 24, 2018:1-20. doi:10.1007/s12035-018-1435-8
11. Shan B, Wang X, Wu Y, et al. The metabolic ER stress sensor IRE1α suppresses alternative activation of macrophages and impairs energy expenditure in obesity. *Nat Immunol 2017 185*. 2017;18(5):519-529. doi:10.1038/ni.3709
12. Robblee MM, Kim CC, Abate JP, et al. Saturated Fatty Acids Engage an IRE1α-Dependent Pathway to Activate the NLRP3 Inflammasome in Myeloid Cells. *Cell Rep*. 2016;14(11):2611-2623. doi:10.1016/j.celrep.2016.02.053
13. Lee KPK, Dey M, Neculai D, Cao C, Dever TE, Sicheri F. Structure of the Dual Enzyme Ire1 Reveals the Basis for Catalysis and Regulation in Nonconventional

RNA Splicing. *Cell*. 2008;132(1):89-100. doi:10.1016/j.cell.2007.10.057

14. Maurel M, Chevet E, Tavernier J, Gerlo S. Getting RIDD of RNA: IRE1 in cell fate regulation. *Trends Biochem Sci*. 2014;39(5):245-254. doi:10.1016/j.tibs.2014.02.008
15. Chen Y, Brandizzi F. IRE1: ER stress sensor and cell fate executor. *Trends Cell Biol*. 2013;23(11):547-555. doi:10.1016/j.tcb.2013.06.005
16. Salvadó L, Palomer X, Barroso E, Vá Zquez-Carrera M. Targeting endoplasmic reticulum stress in insulin resistance. doi:10.1016/j.tem.2015.05.007
17. Zcan UO¨, Cao Q, Yilmaz E, et al. *Endoplasmic Reticulum Stress Links Obesity, Insulin Action, and Type 2 Diabetes*. Accessed April 4, 2021. http://science.sciencemag.org/
18. Wang Z, Liu D, Wang F, et al. Saturated fatty acids activate microglia via Toll-like receptor 4/NF-κB signalling. *Br J Nutr*. 2012;107(2):229-241. doi:10.1017/S0007114511002868
19. Sims-Robinson C, Bakeman A, Glasser R, Boggs J, Pacut C, Feldman EL. The role of endoplasmic reticulum stress in hippocampal insulin resistance. *Exp Neurol*. 2016;277:261-267. doi:10.1016/j.expneurol.2016.01.007
20. Brabazon F, Bermudez S, Shaughness M, Khayrullina G, Byrnes KR. The effects of insulin on the inflammatory activity of BV2 microglia. *PLoS One*. 2018;13(8). doi:10.1371/journal.pone.0201878
21. Kim B, Elzinga SE, Henn RE, McGinley LM, Feldman EL. The effects of insulin and insulin-like growth factor I on amyloid precursor protein phosphorylation in in vitro and in vivo models of Alzheimer's disease. *Neurobiol Dis*. 2019;132:104541. doi:10.1016/j.nbd.2019.104541
22. Kim B, McLean LL, Philip SS, Feldman EL. Hyperinsulinemia Induces Insulin Resistance in Dorsal Root Ganglion Neurons. *Endocrinology*. 2011;152(10):3638-3647. doi:10.1210/en.2011-0029
23. Iwawaki T, Akai R, Kohno K, Miura M. A transgenic mouse model for monitoring endoplasmic reticulum stress. *Nat Med*. 2004;10(1):98-102. doi:10.1038/nm970
24. Bhattarai KR, Chaudhary M, Kim HR, Chae HJ. Endoplasmic Reticulum (ER) Stress Response Failure in Diseases. *Trends Cell Biol*. 2020;0(0). doi:10.1016/j.tcb.2020.05.004
25. Brykczynska U, Geigges M, Wiedemann SJ, et al. Distinct Transcriptional Responses across Tissue-Resident Macrophages to Short-Term and Long-Term Metabolic Challenge. *Cell Rep*. 2020;30(5):1627-1643.e7. doi:10.1016/J.CELREP.2020.01.005
26. Rumora AE, LoGrasso G, Hayes JM, et al. The divergent roles of dietary saturated and monounsaturated fatty acids on nerve function in murine models of obesity. *J Neurosci*. 2019;39(19):3770-3781. doi:10.1523/JNEUROSCI.3173-18.2019

27. Yoon S Bin, Park YH, Choi SA, et al. Real-time PCR quantification of spliced X-box binding protein 1 (XBP1) using a universal primer method. *PLoS One*. 2019;14(7):e0219978. doi:10.1371/JOURNAL.PONE.0219978

28. O'Brien PD, Hinder LM, Rumora AE, et al. Juvenile murine models of prediabetes and type 2 diabetes develop neuropathy. *Dis Model Mech*. 2018;11(12). doi:10.1242/dmm.037374

Chapter 6 Conclusions and Future Directions

6.1 Summary

Rising rates of obesity in the last several decades have introduced a new health crisis, driven by the multitude of systemic complications that result from obesity and the resulting metabolic dysfunction. At the individual level, people with obesity face increased risk of co-morbidities including type 2 diabetes, cardiovascular disease, stroke, cancer, and as investigated in this dissertation work, cognitive impairment. At the national and international level, the obesity crisis creates a burden of chronic disease on the healthcare system, and results in exorbitant healthcare costs. Unfortunately, the obesity crisis is not limited to adults, but affects children and adolescents. These obese children go on to face increased morbidity in adulthood [1,2]. Chronic inflammation occurs in multiple tissues in obesity, and this inflammatory response contributes to sequelae of obesity, such as insulin resistance [3], cardiovascular disease, and retinopathy [4].

Inflammation in the brain may play a role in the pathophysiology of obesity induced cognitive impairment and dementia, as it does in Alzheimer's disease pathology [5,6]. Indeed, microglia, the resident innate immune cells of the CNS, are activated in rodent models of HFD feeding and obesity [7–9], and microglia have been proposed to contribute to hippocampal-dependent cognitive impairment [10]. Mechanisms mediating hippocampal microglia activation in this context, as well as the evolution of microglial activation over time are unclear. Elucidation of drivers of this activation, as well as an

understanding of temporal progression, will aid in the development of interventions to prevent, reverse, or treat obesity-induced cognitive impairment. In this dissertation, we used a mouse model of obesity to quantify morphological measures of hippocampal microglial activation longitudinally and performed single-cell RNA-sequencing to identify dysregulated intra- and inter-cellular processes and potential mechanisms of activation. We focused on the effects of HFD and subsequent obesity in the hippocampus during the adolescent period of development and compared inflammatory responses and cognitive performance in young versus middle-aged mice. Finally, we began to determine the role of endoplasmic reticulum stress in the phenotype of hippocampal microglia in obesity.

In addressing **Aim 1**, we found that HFD feeding induced obesity and progressive metabolic dysfunction in our established mouse model. We initially fed 5-week-old animals a HFD for 2 wk, 1 mo, or 3 mo, mirroring equivalent human age of adolescence through early adulthood. We quantified three-dimensional microglial morphology using metrics including cell territorial volume, cell volume, number of endpoints per cell, number of branchpoints per cell, and average branch length. We did not observe an effect of HFD on morphology metrics in the CA1 region of the hippocampus at any time point over the longitudinal course. To address **Aim 2**, we asked the same research question using a more sensitive technique, single cell RNA-seq, to elucidate effects of HFD on intercellular signaling and intracellular processes in this heterogeneous population of cells. Although morphology as an indicator of activation state did not reveal an effect of HFD in our model, transcriptomics at the single-cell level demonstrated that HFD dysregulates microglia-to-microglia immune

signaling and endoplasmic reticulum homeostasis at as early as 1 mo diet. Based on our scRNA-seq results, we propose a model where an early ER protein folding chaperone and co-chaperone response may reflect an attempt to maintain ER homeostasis, and potentially prevent microglial activation at 1 mo, followed by a transition to a more inflammatory microglial state by 3 mo. In parallel to studies of microglial activation in HFD-fed young mice, we asked whether age impacts the effect of obesity on cognition in our model, **Aim 3**. Performance in the fear conditioning task, which measures associative learning and relies on multiple brain regions including the amygdala and hippocampus, demonstrated that HFD-fed mice had elevated fear responses relative to controls, and deficits in this task were worse in middle-aged versus young HFD mice. Collectively, our data suggest that in a model of adolescent, early-life obesity, hippocampal microglial dysfunction can be measured at the single cell transcriptomic level, but not by changes in microglia morphology in the CA1 region. We anticipate more overt pro-inflammatory morphological changes indicating microglial activation may occur in aged obese mice, or in young mice after an even longer period of chronic obesity than 3 mo, and these findings may parallel changes in cognitive function. A microglial response to burden on the endoplasmic reticulum may be adaptive, or may contribute to an ER stress response that leads to a pro-inflammatory phenotype. The role of ER stress in microglial activation was explored in **Aim 4** and discussed in future directions section **6.2** below. Dissertation results and our proposed model are summarized in **Fig 6.1**.

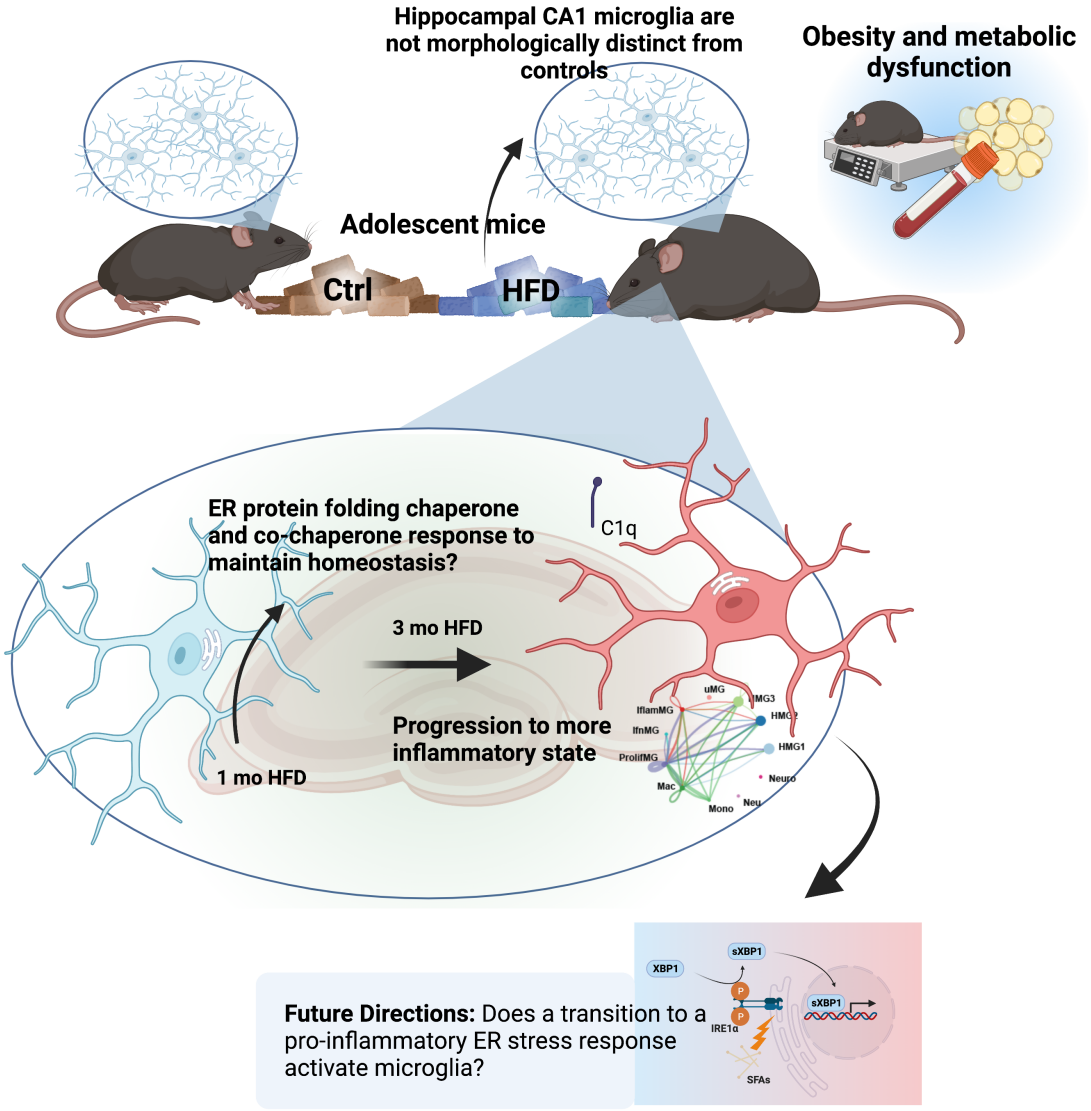

Figure 6.1 Summary and proposed model of HFD effects on hippocampal microglia in young mice.

This model integrates findings resulting from the dissertation. In adolescent mice, HFD feeding induces obesity and metabolic dysfunction, but does not alter microglial morphology in the CA1 region of the hippocampus by 3 mo. scRNA-seq results demonstrate a signature of dysregulation of genes involved in the endoplasmic reticulum, particularly at 1 mo. Cell signaling communication analysis reveals a greater effect of HFD on microglia-to-microglia immune signaling at 3 mo, and differentially expressed gene analysis suggests an upregulation of inflammatory genes such as complement at 3 mo. Future work will determine the role of a potential ER stress response in microglial activation.

6.2 Determining the role of endoplasmic reticulum stress in obesity-induced hippocampal microglial responses

Our single-cell RNA-sequencing data demonstrated dysregulation of endoplasmic reticulum heat shock proteins in hippocampal microglia. These findings align with those of Brykczynska et al (2020), who suggest a potential anti-inflammatory effect of microglial upregulation of heat shock proteins in response to HFD [11]. We previously reported elevated spliced XBP1, a mediator of the ER stress response, in the hippocampus of HFD mice [12], and our preliminary *in vitro* data suggests that the SFA palmitate activates the microglial IRE1α/XBP1 stress response. SFA-induced IRE1α pathway activation contributes to a pro-inflammatory phenotype in macrophages [13], but its function in microglia is unclear. We began feeding HFD to a transgenic mouse strain exhibiting fluorescence reporting of XBP1 splicing, allowing us to monitor the activation of this ER stress response in an *in vivo* model of obesity. Using this model and examining a longitudinal time course of 1 wk, 1 mo, and 6 mo of diet, we will determine whether the XBP1 pathway is activated in hippocampal microglia in response to HFD. Further, we will employ measures of morphological activation to determine whether potential XBP1 splicing correlates with microglial morphological measures. Future work administering an IRE1α ribonuclease inhibitor will allow us to begin to assess the effects of potential microglial XBP1 pathway activation on microglial phenotype (anti- or pro-inflammatory) and on cognitive performance.

6.3 Identifying obesity-induced cognitive deficits in alternative cognitive domains

Clinical studies on the association of childhood obesity with cognitive function have demonstrated deficits in hippocampal function [14], but also in cognitive domains that rely on regions of the brain outside of the hippocampus [15,16]. For example, a systematic review reported an association between obesity and deficits in cognition including in executive function and attention [16], which involve cortical function [17,18]. These findings in humans suggest that studies must expand beyond the hippocampus to examine the potential role of inflammation and microglial activation in cognitive deficits resulting from other brain regions. Perhaps the mid-life obesity risk for late-life dementia, which reflects deficits in hippocampal function, is more specific to the adult and aging brain. Potentially, in this childhood or adolescent period, other brain regions are more susceptible to obesity induced inflammation. For testing executive function, the attentional set shifting task has been used to demonstrate cognitive flexibility deficits in adolescent mice compared to adults, and this task could be employed to determine whether obesity impacts this adolescent developmental function [19]. Additionally, obesity in pre-adolescent children is associated with inhibitory control deficits [20,21], and the go/no-go task could be employed in mice to test inhibitory control. Future work could determine the effect of HFD and obesity on microglia in brain regions contributing to these executive function tasks, and cortical structures known to develop during adolescence [22].

6.4 Longitudinal cognition in obesity across the lifespan

In the work presented in this dissertation, we examined HFD feeding starting in adolescence at 5 wk of age and continuing to early, mature adulthood at around 4 mo of age. We investigated effects of adolescent obesity on hippocampal microglial activation and cognition, using the fear conditioning task. However, we did not yet determine whether adolescent obesity affects inflammatory status or cognition later in life, and data in this area in both humans and rodent models is lacking. One study feeding HFD to adolescent mice for 33 wk (over 8 mo) found impaired cognition in adulthood and increased total microglia numbers, and increased proportion of MHCII co-expressing microglia in the dentate gyrus [23]. Evidence suggests that childhood and adolescent obesity raise the risk for morbidity in adulthood [1,2,24]. Further, a recent longitudinal clinical report following children to mid-life, measured childhood fitness and waist-to-hip ratio and found an association between poor fitness and anthropometry in childhood and lower mid-life psychomotor attention and global cognition [25]. Our laboratory has begun to model longitudinal obesity across the lifespan in our mouse model of obesity. By performing repeated measures of cognitive function in adolescence, mid-life, and late life, we can define the onset and progression of cognitive impairment. Additionally, by measuring cognitive performance in adult mice started on HFD either in adolescence or later in adulthood, we can compare temporal windows of HFD and the risk of later life cognitive dysfunction. Further, a dietary reversal paradigm would enable us to determine whether weight loss following adolescent obesity can restore potential deficits that may be present later in life.

6.5 Conclusion

In summary, this dissertation work has demonstrated that obesity alters the hippocampal microglial phenotype in young mice transitioning through adolescence to early adulthood, without overt changes to morphology. In this age group, we showed that prolonged HFD feeding dysregulates endoplasmic reticulum homeostasis and inter-cellular immune signaling pathways in hippocampal microglia. Ongoing experiments will determine whether an ER response mitigates HFD-induced stressors on microglia, or leads to a pro-inflammatory and injurious microglial activation state. Finally, we found that aged obese mice demonstrated greater cognitive dysfunction than young obese mice using the fear conditioning test. Results arising from this work will provide an understanding of critical temporal windows in the lifespan for preventing or treating cognitive deficits in obesity. Further, an understanding of the microglial contribution to pathology will uncover avenues for targeted therapeutic intervention.

6.6 Bibliography

1. Barton M. Childhood obesity: a life-long health risk. *Acta Pharmacol Sin 2012 332*. 2012;33(2):189-193. doi:10.1038/aps.2011.204

2. Maffeis C, Tatò L. Long-Term Effects of Childhood Obesity on Morbidity and Mortality. *Horm Res Paediatr*. 2001;55(Suppl. 1):42-45. doi:10.1159/000063462

3. Wu H, Ballantyne CM. Metabolic Inflammation and Insulin Resistance in Obesity. *Circ Res*. Published online 2020:1549-1564. doi:10.1161/CIRCRESAHA.119.315896/FORMAT/EPUB

4. Rohm T V., Meier DT, Olefsky JM, Donath MY. Inflammation in obesity, diabetes, and related disorders. *Immunity*. 2022;55(1):31-55. doi:10.1016/J.IMMUNI.2021.12.013

5. Hong S, Beja-Glasser VF, Nfonoyim BM, et al. Complement and microglia mediate early synapse loss in Alzheimer mouse models. *Science (80-)*. 2016;352(6286):712-716. doi:10.1126/SCIENCE.AAD8373/SUPPL_FILE/HONG.SM.PDF

6. Hansen D V, Hanson JE, Sheng M. Microglia in Alzheimer's disease. *J Cell Biol*. 2018;217(2):459-472. doi:10.1083/jcb.201709069

7. Hao S, Dey A, Yu X, Stranahan AM. Dietary obesity reversibly induces synaptic stripping by microglia and impairs hippocampal plasticity. *Brain Behav Immun*. 2016;51:230-239. doi:10.1016/J.BBI.2015.08.023

8. Vinuesa A, Bentivegna M, Calfa G, et al. Early Exposure to a High-Fat Diet Impacts on Hippocampal Plasticity: Implication of Microglia-Derived Exosome-like Extracellular Vesicles. *Mol Neurobiol*. Published online November 24, 2018:1-20. doi:10.1007/s12035-018-1435-8

9. Valdearcos M, Douglass JD, Robblee MM, et al. Microglial Inflammatory Signaling Orchestrates the Hypothalamic Immune Response to Dietary Excess and Mediates Obesity Susceptibility. *Cell Metab*. 2017;26(1):185-197.e3. doi:10.1016/j.cmet.2017.05.015

10. Cope EC, LaMarca EA, Monari PK, et al. Microglia Play an Active Role in Obesity-Associated Cognitive Decline. *J Neurosci*. 2018;38(41):8889-8904. doi:10.1523/JNEUROSCI.0789-18.2018

11. Brykczynska U, Geigges M, Wiedemann SJ, et al. Distinct Transcriptional Responses across Tissue-Resident Macrophages to Short-Term and Long-Term Metabolic Challenge. *Cell Rep*. 2020;30(5):1627-1643.e7. doi:10.1016/J.CELREP.2020.01.005

12. Sims-Robinson C, Bakeman A, Glasser R, Boggs J, Pacut C, Feldman EL. The role of endoplasmic reticulum stress in hippocampal insulin resistance. *Exp Neurol*. 2016;277:261-267. doi:10.1016/j.expneurol.2016.01.007

13. Robblee MM, Kim CC, Abate JP, et al. Saturated Fatty Acids Engage an IRE1α-Dependent Pathway to Activate the NLRP3 Inflammasome in Myeloid Cells. *Cell Rep*. 2016;14(11):2611-2623. doi:10.1016/j.celrep.2016.02.053

14. Khan NA, Baym CL, Monti JM, et al. Central adiposity is negatively associated with hippocampal-dependent relational memory among overweight and obese children. *J Pediatr*. 2015;166(2):302-308.e1. doi:10.1016/J.JPEDS.2014.10.008

15. Kamijo K, Khan NA, Pontifex MB, et al. The relation of adiposity to cognitive control and scholastic achievement in preadolescent children. *Obesity (Silver Spring)*. 2012;20(12):2406-2411. doi:10.1038/OBY.2012.112

16. Liang J, Matheson BE, Kaye WH, Boutelle KN. Neurocognitive correlates of obesity and obesity-related behaviors in children and adolescents. *Int J Obes 2014 384*. 2013;38(4):494-506. doi:10.1038/ijo.2013.142

17. Nowrangi MA, Lyketsos C, Rao V, Munro CA. Systematic Review of Neuroimaging Correlates of Executive Functioning: Converging Evidence From Different Clinical Populations. *https://doi.org/101176/appi.neuropsych12070176*. 2014;26(2):114-125. doi:10.1176/APPI.NEUROPSYCH.12070176

18. Friedman NP, Robbins TW. The role of prefrontal cortex in cognitive control and executive function. *Neuropsychopharmacol 2021 471*. 2021;47(1):72-89. doi:10.1038/s41386-021-01132-0

19. Shepard R, Beckett E, Coutellier L. Assessment of the acquisition of executive function during the transition from adolescence to adulthood in male and female mice. *Dev Cogn Neurosci*. 2017;28:29-40. doi:10.1016/J.DCN.2017.10.009

20. Reyes S, Peirano P, Peigneux P, Lozoff B, Algarin C. Inhibitory control in otherwise healthy overweight 10-year-old children. *Int J Obes 2015 398*. 2015;39(8):1230-1235. doi:10.1038/ijo.2015.49

21. Alatorre-Cruz GC, Downs H, Hagood D, Sorensen ST, Williams DK, Larson-Prior L. Effect of obesity on inhibitory control in preadolescents during stop-signal task. An event-related potentials study. *Int J Psychophysiol*. 2021;165:56-67. doi:10.1016/J.IJPSYCHO.2021.04.003

22. Fuhrmann D, Knoll LJ, Blakemore SJ. Adolescence as a Sensitive Period of Brain Development. *Trends Cogn Sci*. 2015;19(10):558-566. doi:10.1016/J.TICS.2015.07.008

23. Wang Q, Yuan J, Yu Z, et al. FGF21 Attenuates High-Fat Diet-Induced Cognitive Impairment via Metabolic Regulation and Anti-inflammation of Obese Mice HHS Public Access Author manuscript. *Mol Neurobiol*. 2018;55(6):4702-4717. doi:10.1007/s12035-017-0663-7

24. Reilly JJ, Kelly J. PEDIATRIC REVIEW Long-term impact of overweight and obesity in childhood and adolescence on morbidity and premature mortality in adulthood: systematic review. *Int J Obes*. 2011;35:891-898. doi:10.1038/ijo.2010.222

25. Tait JL, Collyer TA, Gall SL, et al. Longitudinal associations of childhood fitness and obesity profiles with midlife cognitive function: an Australian cohort study. *J Sci Med Sport*. 2022;25(8). doi:10.1016/J.JSAMS.2022.05.009